PREPARATION, CHARACTERIZATION AND ADSORPTION STUDIES OF HEAVY METALS ONTO ACTIVATED ADSORBENT MATERIALS DERIVED FROM AGRICULTURAL RESIDUES

ZAIRA ZAMAN CHOWDHURY

**THESIS SUBMITTED IN FULFILMENT
OF THE REQUIREMENTS
FOR THE DEGREE OF DOCTOR OF
PHILOSOPHY**

**DEPARTMENT OF CHEMISTRY
FACULTY OF SCIENCE
UNIVERSITY OF MALAYA
KUALA LUMPUR**

2013

ABSTRACT

The extensive use of commercial activated carbon as an adsorbent for the purification of industrial effluent is not economically feasible due its high operational cost. Therefore, this research has been undertaken to explore the potential of certain agro based residues to produce suitable adsorbent for scavenging divalent cations of lead (Pb), copper (Cu) and manganese (Mn) from waste water to meet specific industrial requirements. In this regard, powdered activated carbons (PAC) were produced from cellulosic precursors namely kenaf core (KC) and kenaf fiber (KF) and granular activated carbon (GAC) from mangostene fruit shell (MFS) by physio-chemical activation. Their performance of the prepared activated carbons (KCAC, KFAC and MFSAC) was compared with activated oil palm ash (AOPA) sample in batch sorption system.

Design of experiment (DOE) based on central composite design (CCD) was used to study the effect of activation temperature, time and impregnation ration (IR) on adsorption performance along with maximum possible yield for powered activated carbon (PAC) from KC and KF. The results demonstrated that the optimum condition to obtain highest removal percentage and yield were different depending on the characteristics of the raw materials and the adsorbate under investigation. MFS was used to prepare granular activated carbon (GAC) due to its hard texture. It was used for batch as well as fixed bed sorption system.

The adsorption mechanisms of activated carbon and activated oil palm ash towards the divalent cations used for this study were completely different. This is expected owing to their different inherent surface morphological features. To prepare activated adsorbent

(AOPA) from natural oil palm ash (OPA), activation reaction by using sodium hydroxide has been carried out by using predefined reaction condition of temperature, time and impregnation ratio (IR) suggested by the software (DOE).

The surface characteristics of these powdered and granular adsorbent were determined in terms of their BET surface area, FTIR analysis, SEM analysis, bulk density and iodine number measurement. Chemical composition of activated carbons (KCAC, KFAC and MFSAC) were analyzed by ultimate (C, H, N, others) and proximate analysis (C, moisture volatile materials and ash). X-ray analysis (XRF) analysis was carried out to determine the chemical constituents of natural oil palm ash (OPA) and activated palm ash (AOPA).

The effect of initial metal ion concentration (50- 100 mg/l), contact time, pH of the solution and temperature (30 °C, 50 °C and 70 °C) were determined in this work. Equilibrium data were further analyzed to evaluate kinetics, isotherm and thermodynamic behavior of the adsorbate - adsorbent system. The fixed bed column showed better performance with lower influent concentration, less flow rate of the influent and higher bed height of the adsorbent. Desorption by using mineral acid was suitable for regenerating the spent adsorbent for further use. It can be concluded that the overall performance of the prepared activated carbons are better than the activated ash sample.

ABSTRAK

Penggunaan secara meluas karbon komersil yang diaktifkan sebagai bahan penjerap bagi penulenan bahan efluen industri adalah tidak begitu sesuai secara ekonomi kerana kos operasinya yang tinggi. Oleh itu, kajian ini telah dijalankan bagi meneroka potensi sisa pertanian tertentu untuk menghasilkan bahan penjerap yang bersesuaian bagi menjerap kation dwivalens plumbum (Pb), kuprum (Cu) dan mangan (Mn) daripada air sisa sebagai memenuhi keperluan industri yang khusus. Bagi penyelidikan ini, serbuk karbon yang diaktifkan telah dihasilkan dari prekursor cellulosic iaitu teras kenaf (KC) dan serat kenaf (KF) dan prestasi bahan-bahan tersebut untuk menyingkirkan logam berat tersebut telah dibandingkan dengan abu kelapa sawit teraktif (AOPA) dalam sistem berkelompok.

Reka bentuk eksperimen (DOE) berdasarkan reka bentuk pusat komposit (CCD) telah digunakan untuk mengkaji kesan suhu pengaktifan, masa dan nisbah pengisitepuan (IR) mengenai prestasi penjerapan bersama-sama dengan hasil maksimum yang mungkin bagi karbon teraktif berkuasa (PAC) dari KC dan KF . Keputusan menunjukkan bahawa, keadaan optimum untuk mendapatkan peratusan penyingkiran tertinggi dan hasil adalah berbeza bergantung kepada ciri-ciri bahan mentah dan bahan terjerap yang diuji dalam eksperimen. MFS digunakan bagi menyediakan butiran karbon teraktif (GAC) kerana teksturnya yang keras. Ia telah digunakan untuk sistem penyerapan secara berkelompok serta sistem penyerapan yang tetap.

Mekanisme penjerapan karbon dan abu kelapa sawit teraktif terhadap kation dwivalens yang digunakan dalam kajian ini adalah berbeza sama sekali. Ini dijangka berdasarkan kepada ciri-ciri morfologi permukaan yang berbeza. Bagi menyediakan penjerap teraktif

(AOPA) dari abu kelapa sawit semulajadi (OPA); tindak balas pengaktifan dengan menggunakan natrium hidroksida telah dijalankan dengan menggunakan kaedah tindak balas yang ditentukan secara nisbah bagi suhu, masa dan pengisitepuan (IR) yang dicadangkan oleh perisian (DOE).

Pencirian permukaan serbuk dan butiran penjerap secara terperinci telah dilakukan dari segi luas permukaan BET, analisis FTIR, SEM, ketumpatan pukal dan penentuan nombor iodin. Penentuan komposisi kimia karbon teraktif telah dijalankan melalui analisis muktamad (C, H, N, lain-lain) dan analisis proksimat (C, bahan meruap dan abu). Analisis sinar-X (XRF) analisis telah dijalankan bagi menentukan juzuk kimia AOPA.

Kesan kepekatan ion logam awal (50 - 100 mg / l), masa sentuhan, pH medium dan suhu (30 ° C, 50 ° C, 70 ° C) telah ditentukan. Data keseimbangan yang telah dianalisis untuk menilai kinetik, isoterma dan kelakuan termodinamik bahan terjerap dan sistem penjerap. Sistem penyerapan yang tetap menunjukkan prestasi yang lebih baik dengan kepekatan influen yang lebih rendah, kadar aliran influen yang berkurangan dan aras bahan penjerap yang lebih tinggi. Penyahjerapan dengan menggunakan asid mineral adalah sesuai bagi proses kitaran semula penjerap untuk kegunaan selanjutnya. Dapat disimpulkan bahawa prestasi keseluruhan karbon teraktif yang dihasilkan adalah lebih baik berbanding sampel abu teraktif.

ACKNOWLEDGEMENT

First of all I wish to express my deep gratitude towards almighty Allah who has given me the ability to pursue my studies abroad. I would like to thank my first supervisor Professor & Head of the Department Dr. Sharifuddin Mohd. Zain for giving me the opportunity to work on this project as well as for his helpful supervision, support and persistent tolerance. I am also grateful to Associate Professor Dr. Rashid Atta Khan for his regular observation and important suggestions throughout this study. My sincere thanks go to Dr. Abdul Bari and Mr. Arash who have helped me a lot for designing the project.

I would also extend my earnest gratitude to Engineering faculties and COMBICAT of University Malaya and institutions (MARDI), Malaysia related to my research. I would like to thank all of my friends, colleagues and laboratory personnel who have given their time, know-how, kind advise and technical assistance and support during my research. My special thanks go to Mr. Rostom, Mr. Zahari, Mr. Fandi, Mr. Yazeed, Ms. Jariany, and Ms Afzalena. I am very pleased to get some MSc. and PhD students namely Mr. Khalissani Khalid and Dr. Esam in our laboratory who were very much helpful. I will remember them in all sphere of my life. I would also express my gratitude to all other staffs in the Department of Chemistry, University Malaya, Malaysia.I owe gratitude to my all family members, my father, mother, brother and sister for their kind consideration and help without which I would be unable to continue my study here.

Finally I would like to acknowledge University of Malaya for the financial support and for providing me the excellent research environment to complete my studies. I would also acknowledge the financial support from the research grant (UMRG 056-09SUS).

TABLE OF CONTENTS

LIST OF APPENDICES

LIST OF TABLES

LIST OF FIGURES

LIST OF PLATES

LIST OF SYMBOLS

Symbols	Description	Unit
A	Arrhenius Factor	-
E_a	Activation energy of desorption	-
K	Boltzmann constant	-
K_T	Temkin Isotherm constant	(l/g)
B	Temkin Isotherm constant	-
A	Initial sorption rate for Elovich equation	mg/g h
B	Extent of surface coverage for Elovich equation	g/mg
1/b ln(ab)	Constant for Elovich equation	-
1/b	Constant for Elovich equation	mg/g
C_e	Equilibrium concentration in liquid phase	mg/l
C_t	concentration at any time t in liquid phase	mg/l
C_0	Initial adsorbate concentration	mg/l
C_{ad}	Adsorbed concentration of the solute by the adsorbent	mg/l
C_{de}	Desorbed concentration of the solute by eluting agent	mg/l
h	Initial rate of sorption in pseudo first and second order kinetics	mg/g-min
K_F	Freundlich constant	$(mg/g(l/mg)^{1/n})$
K_L	Langmuir constant	(l/mg)
k_{dif}	Intra-particle diffusion constant	mg/g h
k_1	Pseudo first order rate constant	min^{-1}
k_2	Pseudo second order rate constant	min^{-1}
k_{th}	Thomas Rate constant	(ml/min-mg)
k_{YN}	Yoon Nelson model constant	(l/min)
k_{AB}	Bohart Adams model constant	(L/mg-min)
N	Total number of experimental data points	
N_0	Bohart Adams model constant	(mg/l)

N	Intensity factor in Freundlich Isotherm	-
n_c	Number of data points at center	-
q_e	Equilibrium uptake by the adsorbent	mg/g
q_t	Uptake at any time t by the adsorbent	mg/g
$q_{e,\ exp}$	Experimental equilibrium uptake by the adsorbent	mg/g
$q_{e,\ cal}$	Calculated equilibrium uptake by the adsorbent	mg/g
q_{max}	Maximum monolayer adsorption capacity	mg/g
$q_{t,0.5}$	Bed capacity at 50 % breakthrough of the column	mg/g
q_0	Thomas constant for bed capacity	mg/g
q_{reg}	Adsorptive capacity of the regenerated column	mg/g
q_{org}	Original capacity of the column	mg/g
R	Rate of Desorption	min^{-1}
R	Universal gas constant	8.314 J/mol-K
R_L	Separation Factor	-
R^2	Correlation coefficient	-
T	Absolute temperature	°K
T	Time	Minute/hour
W_1	Dry weight (g) of the precursor before pyrolysis	g
W_2	Dry weight (g) after activation	g
W_{KOH}	Dry weight (g) of potassium	g
W_{char}	Dry weight (g) of char	g
W_{OPA}	Dry weight (g) of natural oil palm	g
W_{NaOH}	Dry weight (g) of caustic soda	g
X	Activated carbon preparation variables	-
Y	Predicted Responses	-

Greek Letters

$\Delta G°$	Change in standard free energy	(kJ/mol)
$\Delta H°$	Change in standard enthalpy	(kJ/mol)
$\Delta S°$	Change in standard entropy	(j/mol-K)
Δq_t	Normalized standard deviation	-
λ	Wavelength	nm
ζ	Time determined from Yoon Nelson model for 50 % Breakthrough of the column	minute

LIST OF ABBREVIATIONS

AC	Activated carbon
ANOVA	Analysis of variance
AOPA	Activated oil palm ash
BET	Brunauer-Emmett- Teller
BJH	Barrett-Joyner-Halenda
CCD	Central Composite Design
EBCT	Empty Bed Contact time
EFB	Empty Fruit bunch
PF	Palm Fiber
EPA	Environmental Protection Agency
DOE	Department of Environment
DOE	Design of Experiment
FTIR	Fourier Transform Infrared Spectroscopy
GAC	Granular Activated carbon
IR	Impregnation Ratio
IUPAC	International Union of Pure and Applied Chemistry
KC	Kenaf Core
KCAC	Kenaf Core based activated carbon
KF	Kenaf Fiber
KFAC	Kenaf Fiber based activated carbon
MFS	Mangostene Fruit Shell
MFSAC	Mangostene Fruit Shell based activated carbon
OPA	Oil palm ash
PS	Palm Shell
PAC	Powdered activated carbon
RSM	Response surface methodology
Rpm	Rotation per minute
SEM	Scanning electron microscopy

TGA	Thermo gravimetric analyzer
UK	United Kingdom
US	United States of America
XRF	X-ray Fluorescence
2FI	Two Factor interaction

CHAPTER ONE
INTRODUCTION

1.1 Overview of the Research

This chapter provides relevant information about environmental issues concerning water pollution created by release of heavy metals and the strategies so far taken for abatement of this problem. The contamination of ground and surface water in Malaysia, focusing mostly on aqueous effluent emanating from different types of industries has been described. The need for implementation of appropriate technique by applying adsorption onto suitable adsorbent is provided. The concluding phase of this chapter presents the problem statement, scope and objectives along with organization of the thesis.

1.2 Research Background – Current Scenario and Water Pollution problem in Malaysia

For the last few decades, phenomenal economical development has been observed throughout Malaysia. Urbanization, agricultural expansion and industrialization have resulted in increased usage of water and the use of different toxic chemicals. This rapid development has resulted in widespread contamination of soil, vegetables and above all fouling of water bodies up to a greater extent (Adil, 2006). Water pollution is a very persistent problem. This situation has evolved gradually over time. Recognition of these sorts of problem usually takes a long time and application of necessary preventive measures takes even longer time (Adil, 2006). Different reports and complaints about industrial waste disposal, stinking water courses within overcrowded cities were an early manifestation of water pollution.

It was reported earlier that industries- related to mining discharge toxic metallic waste into freshwater bodies which contaminates the surface water as well as causes soil pollution also (Ashraf *et al.,* 2010). Besides that, some agro based industries namely rubber and oil palm mills, domestic and animal farming, sewage treatment plants are also releasing harmful chemicals.

To put more emphasis, the Department of Environment (DOE) has made rigorous effort through implementation of Environmental quality Act in 1974. The statistical report showed that, a total of 17991 water pollution point sources were monitored and it was observed that 54% of the pollutants come from sewage treatment plants, 38% from manufacturing industries, 5% from animal farms and 3% from Agricultural industries; namely rubber and oil palm mills (WEPA-2010). It is reported that some manmade factors such as unplanned urbanization, industrialization, deforestation, agricultural runoff along with anthropogenic sources of weathering of rocks and volcanic activities are the major causes for enriching water reservoirs with heavy metals (Ong and Kamruzzaman, 2009; Farkas *et al.*, 2007).

In Malaysia, surface water quality is degrading due to disposal of waste water containing pesticides and herbicides of high toxicity. The quality of fresh water of some major rivers in Malaysia is further declined drastically due to discharge of heavy metals from different factories; especially in industrial zone (Ashraf *et al.*, 2010). The report showed that, 36 rivers of the country had already exceeded the lead (Pb) limit of 0.01 mg/l (Chan, 2003). A recent study reported that, Mamut river situated at the interior of Sabah, in Malaysia is highly contaminated by metal rich wastes (Ali *et al*., 2004). This acute pollution has been resulted from open pit copper

mining activities carried out in 1975. The runoff from this mining operation contains high level of several metals; notably copper which originates from flotation process used for preparation of copper concentrates (Ali *et al.*, 2004).

Tin mining is another oldest industry of Malaysia which is contributing significant amount of metallic sludge of lead, copper and manganese in surface water and soil. According to a recent investigation in ex-mining area of Bestari Jaya, Peninsular Malaysia; the presence of these metallic contaminants in the river water of Sungai Ayer Hitam has exceeded the maximum permissible limits fixed by Interim National Water Quality Standards for Malaysia (Ashraf *et al.*, 2010).

In 2006, 340 water samples were collected from 48 locations of Peninsular Malaysia. The water from 19 wells from the city of Sarawak and 15 wells from Sabah were collected to analyze the purity of ground water in Malaysia (WEPA-2011). The sampling showed that; around 15% to 100% of the sample obtained from all the respective area contains elevated level of manganese greater than the bench mark (WEPA-2011) set by the Government of Malaysia. Table 1.1 listed the major sources of heavy metals (lead, copper and manganese).

Table 1.1 Major sources of lead, copper and manganese from different industries (Kudesia, 2000)

Industrial Effluents	**Pb**	**Cu**	**Mn**
Pulp and paper mills	✓	✓	-
Fertilizers	✓	✓	✓
Inorganic chemicals, alkali, chlorine	✓	-	-
Petroleum refining	✓	✓	-
Organic chemicals, petrochemicals	✓	-	-
Basic Steel works foundries, iron-steel refining	✓	✓	✓
Basic non ferrous metal works foundries	✓	✓	✓
Motor vehicle, aircraft and metal plating	-	✓	-

Aqueous stream contaminated by divalent cations of lead and copper is regarded as one of the most common problem found in Malaysia (Ashraf *et al.*, 2010). Furthermore removal of manganese is of special interest due to the availability of limited research reported on adsorption of this micro pollutant using activated carbon or ash despite its potential toxicity, widespread application as plant nutrients, bio accumulating tendency and persistence in the environment. The statistics clearly reveals that, extensive research is needed to provide better understanding regarding their sorption mechanisms and to reduce these pollutants level within the purview of safe drinking water regulations or any other types of domestic or industrial consumption (Ashraf *et al.*, 2010, Ali *et al.*, 2004). In this context, the present research deals with the removal of divalent cations of lead Pb(II), copper Cu(II) and manganese Mn(II) from synthetic waste water by using some inexpensive indigenous agricultural biomass.

1.3 Wastewater Treatment Technology

There are three methods for treating waste water, namely physical, chemical and biological.

1.3.1 Physical Methods

Physical methods are the widely used method and comprises of membrane filtration and adsorption technique. The major disadvantage of membrane technology is its high cost of periodic replacement. Moreover it has limited life time as membrane fouling occurs very quickly. Filtration by using membrane was frequently used for exclusion of metallic contaminants from paper mill waste waters (Merrill *et al.*, 2001).

The perusal of literature reflects that, liquid-phase adsorption is one of the most popular methods for the purification of waste stream. This is an attractive alternative technique. By implementation of proper process design, high quality treated effluents can be produced. For this some inexpensive raw materials can be used. Thus, among the other methods, adsorption can be considered as an effective sequestration process for decontamination of process effluents (Dabrowski, 2001).

1.3.2 Chemical Methods

Chemical techniques for separation of toxic metals are rapid and efficient and no loss of sorbent is observed due to regeneration. But these methods are expensive. Accumulation and disposal of metal bearing sludge creates secondary pollution problem. Recently, advanced oxidation technique by generating hydroxyl radicals is used for degradation of pollutants but this is not economically feasible as high energy and chemical costs are involved (Mourao *et al.,* 2006). The advantage and disadvantage of these methods are summarized in Table 1.2.

Table 1.2 Advantage and Disadvantage of different method for waste water treatment (Adil, 2006)

Physical/Chemical Method	Advantages	Disadvantages
Ozonation	Applicable for gaseous phase	Half life is short (20 min)
Oxidation	Rapid Process	Byproduct formation and high energy cost
Photochemical	No sludge generation	Byproduct formation
Ion Exchange	No adsorbent loss	Not effective for all types of heavy metals
Membrane Filtration	Removes all contaminants	Concentrated sludge is produced
Coagulation	Economically viable	High sludge production
Activated Carbon	Highly effective	Very expensive, non renewable
Precipitation	Low cost	Byproduct formation
Adsorption	Good % Removal Percentage	Adsorbent requires regeneration and disposal

1.3.3 Biological Treatment

Biosorption is often considered as the most attractive alternative when compared with physical and chemical methods (Keskinkan *et al.,* 2003). Biological treatment involving microbial degradation of pollutants is a commonly used technique for waste water treatment. Due to some technical constrains, their application is restricted. The process is time consuming and requires a large area. Besides that it is constrained by lack of flexibility in design and operation (Bhattacharyya and Sarma, 2003).

1.4 Problem Statement

Among various pollutants present in surface water, inorganic species of heavy metals and metalloids are of major concern as they are difficult to remove owing to their smaller ionic size, complex state of existence, very low concentration in high volume and competition with non-toxic inorganic species (McLelland and Rock, 1988). In view of data from the literature, aqueous phase adsorption by utilizing different types of agro

residues are one of the most popular methods for treating inorganic as well as organic contaminants from waste effluents. US environmental protection agency has cited sorption onto activated carbon as an excellent treatment technology (Moreno- Castilla, 2004). It has a high adsorption capacity for metallic contaminants owing to its high surface area, adequate pore size and nucleophilic properties (Mohanty *et al.,* 2005). However, the use of commercially available activated carbon is expensive as it is obtained from non renewable starting materials such as lignite, coal and petroleum coke. This has initiated a growing research interest towards production of porous adsorbent which can be derived from renewable, abundant and low cost materials originated from agricultural biomass (Babel and Kurniawan, 2003; Boonamnuayvitaya *et al.,* 2005).

Agricultural biomass is obtained from organic origin; it can either be procured directly from plant species or indirectly from processing of commercial, domestic, industrial or agricultural products (Biofuels and Bioenergy Information, 2007). This biomass is considered very effective in producing adsorbent to be used for specific purposes by researchers due to its low ash and high volatile content which is essential to produce activated carbon having well developed pores inside the carbon matrix. The last residues obtained after burning of agricultural biomass in oxygenated atmosphere is ash particles which itself either in it's original form or after some simple chemical treatment can be used as efficient adsorbent having extended surface area and suitable mineral composition which is appropriate for surface complexation with divalent positive ions of lead, copper and manganese.

Agricultural Industry in Malaysia is producing enormous amount of agricultural residues every year. A recent statistics showed that, 70 million tones of agro residues are produced by Malaysia annually (Tan, 2008). Dumping of these agro residues are creating

a secondary environmental pollution of great concern. Limited studies have been carried out to convert these agro residues as suitable adsorbent for commercial application to remove inorganic species by using batch and fixed bed adsorption system (Tan, 2008). From the literature, it is observed that many studies have been conducted to convert this biomass into activated carbon for the removal of organic contaminants by applying either physical or chemical activation method. In most of the cases the above mentioned methods have yielded activated carbon having low surface area with microporous texture which is suitable for gas phase application. Recently, combination of both the methods has been given priority to produce activated carbon that has extended surface area with large amount of mesopores which is suitable for liquid phase application. Moreover, limited reports have been observed for design and process parameter optimization for the production of activated carbon with maximum possible yield along with adsorption performance which is essential for commercialization of the end products. Previous research trend showed that limited studies have been conducted on designing process parameters for preparing adsorbent from oil palm ash for the desulfurization process by carrying out pozzolanic reaction between palm ash and group two alkali metal hydroxide (Zainudin *et al.*, 2005).

In this research three types of lignocellulosic i.e., kenaf core (KC), kenaf fiber (KF) and mangostene fruit shell (MFS) and one type of mineral based i.e., oil palm ash (OPA) residues are taken to produce powdered and granular activated adsorbents for batch and fixed bed sorption system.

In Malaysia, the National Kenaf Research and Development Program has been started to produce kenaf crops due to its expanded application in different industrial sector. The government has allocated around RM 12 million (Aber *et al.*, 2009) for

further development of the kenaf-based industry under the 9th Malaysia Plan (2006–2010). Kenaf (*Hibiscus cannabinus L.*) is the common name given to a fiber collected from the stalks of the Kenaf plants. These plants belong to the genus *Hibiscus*, having family name of *Malvaceae*. It grows in tropic and subtropical regions abundantly. Kenaf (*Hibiscus cannabinus L.*) is one of the most fast growing herbaceous plants having similar morphological features like cotton and jute. Presently nine varieties of kenaf have been introduced in Malaysia as one of the potential plant to replace tobacco plantation. This plant contains branchless stalk. The stalk consists of a central wooden core. The bark is made up of fibrous materials and it surrounds the core. Kenaf fiber (KF) is extracted from the outer bark and the wooden core (KC) are taken in this research to prepare powdered activated carbon (PAC).

Mangostene (*Mangostana garcinia)* fruits are mainly cultivated in the tropical region. It grows abundantly in Thailand, Malaysia, Philippines, Indonesia, Brazil, Honduras, Panama and Hawaii. After consumption of the fruits, the peels are thrown without any potential applications. Compared to other two cellulosic precursors, it is relatively hard. Thus the dried fruit peels are taken to produce granular activated carbon (GAC). It was used to prepare fixed bed to design and assemble a lab scale column for treating synthetic water.

Malaysia produces a large amount of agro-based waste biomass-generated from oil palm industries which consists of empty fruit bunch (EFB), palm shell (PS) and mesocarp fiber (PF). The statistical report showed that, about 110 million tones of renewable non oil biological mass from palm oil industry is produced each year (Tan, 2008). Oil palm ash (OPA) is a kind of particulate material which is produced from combustion of this waste biomass (EFB, PS and PF) in boiler to obtain steam for

electricity generation. Oil palm ash has a very fine texture. Thus it has been considered to produce powdered activated adsorbent. Each year 4 million tones of palm ash is produced in Malaysia. It is a persistent and carcinogenic agent having bioaccumulation tendency (Foo and Hameed, 2009). The situation is quite alarming in terms of environmental stand point. The price of this ash disposal (either in landfills or ash ponds) is around $5/tones in developing countries and $50/tones in developed countries (Foo and Hameed, 2009). From one hectare of agricultural land of oil palm, about 50–70 tones of biomass residues are obtained. Oil palm industry is presently generating the largest amount of biomass in Malaysia which is 85.5% out of more than 70 million tones (Shuit *et al.*, 2009) as shown in Figure 1.1 (oil palm 85.5%, sugarcane 0.5%, rice 0.7 %, wood 3.7% and municipal waste 9.5%).

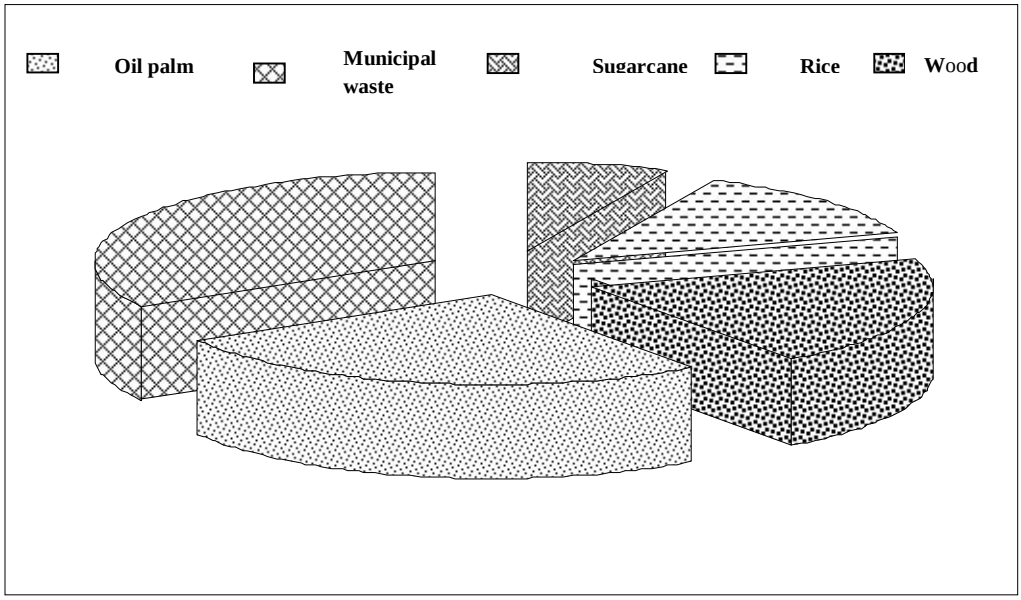

Figure 1.1 Biomass Productions in Malaysia

Until recently, no attempts have been made to produce activated adsorbent from natural oil palm ash (OPA) or activated carbon (AC) from different parts of kenaf crop

and mangostene fruit shell by physiochemical activation technique and optimize their preparation condition for industrial scale application. The utilization of these types cheap raw materials will not only purify the contaminated stream but it will simultaneously reduce waste disposal problem to a greater extent.

1.5 Objectives of the Research

The adsorption property of an adsorbent is highly influenced by its preparation conditions and the starting material. Preparation variables such as temperature, time and impregnation ratio will significantly change its surface area, pore size distribution and surface functional groups. Therefore, it is a challenge to produce specific types of adsorbent which are suitable for certain applications. For a commercial scale production, these points should be considered carefully to get maximum output of the process. The following objectives have been addressed in this work.

(i) To produce powdered and granular adsorbent from agro based residues of Kenaf core (KC), Kenaf fiber (KF) and Mangostene Fruit Shell (MFS) respectively, by converting them into activated carbon using the two step physio-chemical activation methods of alkali hydroxide impregnation and physical activation using carbon dioxide. Powdered activated adsorbent was prepared from siliceous raw materials of natural oil palm ash (OPA) by pretreatment with alkali metal hydroxide

(ii) To optimize the production condition to obtain maximum yield along with maximum removal percentage of divalent cations of lead, Pb (II), copper, Cu (II) and Mn (II) for powdered activated carbon (PAC) from KC and KF by using Design of Experiment (DOE). The production condition for oil palm ash samples were optimized also. However, the granular activated carbon (GAC) from mangostene fruit shell (MFSAC)

were prepared under identical condition to compare the sorption efficiency of three types of adsorbate (lead, copper and manganese) based on their chemical properties.

(iii) To characterize the surface of the adsorbents by physical and chemical tests.

(iv) To determine the effects of adsorbate (Pb, Cu and Mn) initial concentration, contact time, temperature and pH on adsorption performance through batch adsorption test. The kinetics, isotherm and thermodynamics parameters of different adsorbate adsorbent systems under investigation were determined.

(v) To analyze the breakthrough curve for adsorption of divalent cations of Pb, Cu and Mn by using granular adsorbent (MFSAC). The column dynamics studies are carried out by changing the initial concentration of the feed, flow rate of the adsorbate as well as the bed height of the prepared sorbent. The adsorbents used were regenerated by using eluting agents of distilled water, organic and mineral acids.

1.6 Outline of the Thesis

There are a total of 9 chapters in this thesis. Chapter One (Introduction) gives the overview of present situation of water pollution problem in Malaysia. This chapter briefly explains the research objectives and overall content of the thesis.

Chapter Two (Literature Review) provides important information about preparation of activated carbon from various precursors carried out by previous researchers. Important mechanism to convert ash materials as suitable adsorbent has been discussed also in terms of relevant literature. For producing both types of adsorbent,

selection of appropriate technique along with the importance for process parameters optimization has been explained in the last section.

Chapter Three (Theoretical Background of Batch and Fixed Bed Study) provides basic concepts of batch adsorption for different adsorbate adsorbent system. Basic phenomenon of fixed bed adsorption, it's importance in industrial scale and limitations are discussed in the second section. The third section summarizes the sorption dynamics of Fixed Bed in terms of Bohart-Adams, Thomas and Yoon-Nelson models.

Chapter Four (Materials and Methodology) deals with the experimental set up for production of powered and granular adsorbents. The detailed methodology and the reason to activate OPA by alkali treatment rather than converting it to activated carbon is discussed in the subsequent section. The experimental procedure by using response surface methodology (RSM), statistical analysis and model development, surface characterization, batch and fixed bed sorption techniques and regeneration of the prepared adsorbent is explained. The last section of the chapter comprises of schematic flow chart of all research activities in this project.

Chapter Five (Results and Discussion) presents results and discussion obtained from RSM technique to prepare activated carbon and activated oil palm ash together with ANOVA analysis and regression models for each adsorbate adsorbent system. Process parameters are optimized to get maximum removal percentage under the studied range of variable. The last section provides the necessary physio-chemical characteristics of the adsorbent's surface which is essential to understand sorption mechanisms in detail.

Chapter Six (Results and Discussion) presents the results obtained for surface characterization of the prepared adsorbents by different physical and chemical tests.

Chapter Seven (Results and Discussion) deals with the batch adsorption studies carried out for all types of powdered and granular adsorbents. Equilibrium isotherm, kinetics and thermodynamic parameters are evaluated. The last section provides the necessary information for regeneration of the metal loaded adsorbent by using different eluting agents. Overall performance of powder and granular activated carbons with activated oil palm ash towards the divalent cations under investigation are compared with other types of adsorbents.

Chapter Eight (Results and Discussion) presents the break through curve analysis and different process parameters related to fixed bed studies. The last section evaluates the model parameters necessary to understand sorption dynamics in continuous flow adsorption, regeneration and recycling of the fixed bed up to four cycles.

The conclusions of the overall findings of this research are given in Chapter Nine. The conclusion summarizes the extent of which the listed objectives are achieved throughout this study. The last section deals with some recommendations and their significance related to this study for future application.

CHAPTER TWO
LITERATURE REVIEW

2.1 Introduction

This chapter is subdivided into three sections. The first section describes the basic concept of adsorption, the forces governing the sorption process and general information regarding preparation and application of activated carbons in liquid phase adsorption. An overview of various types of ligno-cellulosic precursors and the methodology applied for them to produce activated carbons, characterization as well as the applications of these adsorbents for removal of contaminants from waste stream is then presented. The second section provides brief information about the physio-chemical characteristics of oil palm ash and relevant literature review to convert it as a suitable adsorbent for aqueous phase adsorption. The regeneration technologies for both types of adsorbents (activated carbon and activated ash) so far being adopted by previous researchers are then presented. A short summary of this chapter is given in the last section.

2.2 Adsorption

Adsorption is defined as the process of retaining atoms, molecules or ions of dissolved solids, liquids or gases on the surface having certain active sites (Paul, 1995). The phenomenon is observed due to the presence of unsaturated and unbalanced molecular forces that are present on every porous solid. When a porous adsorbent is in contact with a solution, it tends to accumulate a layer of adsorbate ions, molecules, gases or vapor to satisfy the residual surface forces (Eckenfelder, 2000) and forms a boundary layer. In the case of aqueous phase adsorption; the atoms, molecules or ions present in a liquid will diffuse inside the surface of the solid where they attach and retain themselves by weak intermolecular forces. For designing the adsorption processes, it is essential to optimize

the sorbent-sorbate ratio and the adsorption capacity of the targeted contaminants at constant temperature and pH for a fixed adsorbate concentration range.

2.2.1 Factors Affecting Adsorption

The factors on which the extent of adsorption depends are:

- The effective surface area including appropriate pore size distribution of the adsorbent.
- The solubility of the adsorbate in aqueous phase.
- The nature of the active sites or surface functional groups on the surface.
- The concentration of the liquid phase.
- The nature of adsorbent or adsorbate.
- The temperature of the surroundings.
- pH of the system in case of liquid phase applications.

2.2.2 Classification of Adsorption

Adsorption process can be classified into two main types; such as, physical adsorption (physisorption) and chemical adsorption (chemisorptions).

2.2.2.1 Physical Adsorption

Physisorption involves weak forces of van der walls, hydrogen bonding and dipole-dipole interactions between the sorbent and sorbate. It is reversible and resembles with condensation process. The process of physisorption is exothermic with a heat of adsorption analogous to that of latent heat of condensation (Cooney and David, 1999). Equilibrium is attained quickly, followed by the intra-particle diffusion process of the adsorbate molecules inside the capillary pores of the sorbent structure. The rate of

sorption varies reciprocally with the square of the particle diameter but increases usually with the increasing concentration of the adsorbate and the temperature of the surroundings. The rate of physisorption is inversely proportional with the molecular weight of the sorbate species (Eckenfelder, 2000). Physical adsorption represents comparatively weak adsorptive forces between sorbate and sorbent. It proceeds with almost zero or negligible activation energy (Mattson and Mark, 1971).

2.2.2.2 Chemical Adsorption

Chemical adsorption proceeds by exchange or sharing of electrons between the sorbate and sorbent (Allen and Koumanova, 2005). It is non reversible and occurs at high temperature with significant activation energy. Chemisorption is characterized by interaction between sorbate and specific functional groups attached on the surface of the sorbent (Mattson and Mark, 1971). It may be exothermic or endothermic depending on the magnitude of the energy changes during the sorption process. Table 2.1 shows a comparison of physical and chemical adsorption.

Table 2.1 Comparison of Physical and Chemical Adsorption (Ahmad, 2006).

Parameters	Physical Adsorption	Chemical Adsorption
Rate of adsorption	Controlled By Diffusion	Controlled by surface chemical reaction
Effect of temperature	Almost None	Positive
Enthalpy change (Kcal/mol)	<10	>20
Type of Interaction	Reversible	Irreversible
Surface Coverage	Complete	Incomplete
Sorption/mass ratio	Large	Small
Specifity	Low	High
Activation Energy	Small	Large

For removal of heavy metals, adsorption is considered as one of the most popular technique compared to other methods due to its low cost, abundant availability, simple process design with high removal efficiency, easy mode of operation and biodegradability. Moreover, it can treat pollutants in more concentrated form (Arami *et al*., 2005). It does not produce large amount of toxic sludge (Crini, 2006).

2.3 Adsorbate

The components present in ionic phases inside the solution that are adsorbed by the adsorbent are called adsorbate. In general, the higher the concentration of solute, the higher is the equilibrium uptake of the adsorbate on the surface of the adsorbent (Seader and Ernest, 1998). The elements of divalent cations of heavy metals (Pb, Cu and Mn) were taken here to prepare synthetic solution of adsorbate for bench scale adsorption studies in batch or continuous column in the laboratory. Heavy metals constitute a group of transition and post transition metals (IUPAC 2002). Heavy metals usually possess higher specific gravity, i.e more than five.

2.3.1 Properties of Adsorbate

The presence of maximum permissible limit of heavy metals including lead, copper and manganese in drinking as well as municipal and industrial waste water has been strictly regulated in most of the countries through legislation due to their potential toxicity.

2.3.1.1 Lead, Pb(II)

Lead is a soft, malleable, bluish gray heavy metal which belongs to the fourth column of the periodic table (Group IVB). Its maximum valency is IV but II is far more stable. Tetravalent lead forms few compounds of PbO_2, $PbCl_4$ and $Pb(SO_4)_2$ which are very powerful oxidizing agents. Combustion of coal generates lead into atmosphere. It is one

of the most widely used metals in piping, accumulators, lead chambers, anti-knock substances, soldering and colored pigments. In nature, lead occurs as galena, cerussite ($PbCl_2$) and sulphide. The earth's crust and ocean water contain 15 ppm and 5 ppb of lead respectively. It can diffuse inside the soft tissues and form metallothionein. About 500 mg of lead can create toxicity in human body (Kudesia, 2000). The toxicity symptoms are brain damage, uncoordinated body movement, convulsions, loss of appetite and after certain range it can cause coma and death.

2.3.1.2 Copper, Cu(II)

The name copper was derived from its Latin name cuprum which is a malleable and ductile metal. It is an excellent conductor of heat and electricity. Copper is an element of subgroup IB of the periodic table having valency II and I. It occurs in nature as sulphide. It inhibits the growth of root and shoot and production yield of the crops. The uptake of nutrient is adversely affected in presence of copper. It is frequently accumulated by different agricultural crops and from there it enters into the food chain causing potential danger to animal and human health. Copper is present in the waste effluents of several industries. It is an essential micronutrient for crops. Thus it can easily accumulate in surface waters. The excessive ingestion of copper than the desired limit can cause severe liver and gastrointestinal problems (Kudesia, 2000). Copper poisoning occurs due to consumption of acidic beverages stored in containers of copper. It can cause pathological changes in brain tissues. More than 470 mg of copper in human body will have toxic effects and can cause hypertension, sporadic fever, anemia, coma and even death (Kudesia, 2000).

2.3.1.3 Manganese, Mn(II)

Manganese occurs in nature as oxides, silicates and carbonates. Concentration greater than 100 ppm of manganese can cause growth retardation, fever, muscular fatigue and eye blindness. Inorganic species especially divalent cations of manganese and it's metalloids are commonly found in iron (Fe) bearing wastewater. The intake of manganese can cause neurological disorder in men when inhaled at concentration greater than 10 mg/day. Even at lower concentrations, it produces objectionable stains on fabric. Many industries, especially mining source discharge Mn (II) ions into natural freshwater bodies without sufficient prior treatment. It is very difficult to remove as this is the last member of Irving William series which has the least tendency to form stable surface complexes and thereby removed by sorption from waste water. Some physical and chemical properties including the electronic configuration of the selected cations are listed in Table 2.2.

Table 2.2 Properties of Lead Pb (II), Copper Cu (II) and Manganese Mn (II)

Chemical Properties	**Lead, Pb(II)**	**Copper, Cu(II)**	**Manganese, Mn(II)**
Ionic Radius	1.19°A	0.73°A	0.79°A
First Ionization Potential	7.416	7.726	7.435
Electronegativity	2.33	1.9	1.55
First Hydrolysis constant, $\log K_{OH}$	7.71	8.00	10.59
The softness parameter (ability to leave valence electrons), σ_P	0.131	0.104	0.125

2.3.2 Classification of Adsorbate

Metallic species exhibiting a net positive charge is classified as Lewis acid (Shriver, Atkins and Langford, 1991). Metallic cations of Pb(II), Cu(II) and Mn(II) are transition metals with incomplete d-orbital. They show Lewis-acid characteristics and their

electron clouds are easily deformed by the induction effect of electric field of other cationic or anionic species. Thus they can form stable inner sphere complexes by coordination with donor electrons from Lewis bases, organic and inorganic ligands in aqueous solution. They can act as electron acceptors and are known as 'soft' cations. However, alkali and alkali earth metals are poor Lewis acid as they have almost inert gas configuration. They form outer sphere complexes with ligands having oxygen donor atoms through coulombic force of attraction. Pearson (1968) developed HSAB principle to describe the strength of acid-base complexation of metals. Based on affinity towards different ligands, metallic species are classified as: Class A- Hard cations, Class B- Soft cations and Class AB- Borderline cations which are difficult to distinguish.

Class A Hard | **Class AB Borderline** | **Class B Soft**

1																
H	2											13	14	15	16	17
Li	Be											B	C	N	O	F
Na	Mg	3	4	5	6	7	8	9	10	11	12	Al	Si	P	S	Cl
K	Ca	Sc	Ti	V	Cr	Mn	Fe(III) Fe(II)	Co	Ni	Cu(II) Cu(I)	Zn			As	Se	Br
Rb	Sr	Y	Zr					Rh	Pd	Ag	Cd	In	Sn	Sb	Te	I
Cs	Ba	*	Hf					Ir	Pt	Au	Hg	Ti	Pb(IV) Pb(II)	Bi	Po	At
Fr	Ra	#	Rf	Db	Sg	Bh	Hs	Mt								

***Lanthanide**

La	Ce	Pr	Nd	Pm	Sm	Eu	Gd	Tb	Dy	Ho	Er	Tm	Yb	Lu

 # Actinide

Ac	Th	Pa	U	Np	Pu	Am	Cm	Bk	Cf	Es	Fm	Md	No	Lr

Figure 2.1 Classification of metal according to Lewis acidity (IUPAC 2002)

Metals having electronegativities above 1.45 is known as Class A, while metals with electronegativities below 1.88 belongs to Class B. Figure 2.1 shows the periodic table classifying the different class of metals (IUPAC 2002). The sorption of metallic species onto different types of adsorbent is dependent on their Lewis acidity. Thus the classification of metallic cations based on their Lewis acidity should be consistent for the preparation of adsorbents and subsequent remediation approach. However, the classification shown by the periodic table is empirical (Adil, 2006). In literature, the same metal ion is found to belong in different classes.

Hard cations exhibit fairly strong affinity towards hard (oxygen) donor ligands to form ionic complexes. Soft cations prefer nitrogenous and sulphurous species which have lone pair of electrons. The soft cations use this lone pair of electrons to form stable inner sphere surface complexes. The p-block metals show strong affinity towards sulphide or sulphur donor atoms to form covalent complexes. These metals are highly toxic for living organisms because once they enter, they form stable complexes with thiol (-SH) groups of protein. Thus they accumulate inside the organ. They are not readily excreted. The borderline metals are able to form stable surface complexes with both types of soft and hard donor ligands. However, the order of stability cannot be determined easily (Adil, 2006). The d-block transition metals in first row of the periodic table exhibits variable coordination chemistry. They are categorized as borderline metals.

Based on this principle, various types of chelating ion exchangers with covalently attached functional groups have been developed to remove heavy metals from waste water. The composition of functional groups in any types of ion exchange resins varies from hard oxygen donor atoms in carboxylate groups to soft nitrogenous donor atoms of bispicolylamine, $-CH_2-N.(CH_2-C_5H_9N)_2$. Chelating exchanger with thiol group, -SH

shows high affinity towards Hg(II) rather than Cu(II) and Zn(II) cations. However, the synthesis of polymeric chelating cation exchange resins is relatively difficult and expensive as organic functional groups needs to be attached covalently to the parent polymer beads. In addition to that, adsorption of metallic cations onto chelating ion exchangers exhibits slow kinetics. This is due to the slower intraparticle diffusion of metal ions through the rigid structure of the exchangers (SenGupta *et al.*, 2002). Consequently, the present scenario of water pollution demands the replacement of the chelating/polymeric cation exchangers with renewable naturally occurring low-cost agricultural residues. These materials contain hydroxide, carboxylate, carbonyl and phenolic groups which show moderate to high affinity towards heavy metal ions. The extent and composition of these functional groups can be judiciously modified to improve the specific affinities towards the target cations under investigation.

2.4 Adsorbent

The solid that captures the solute (adsorbate) is known as the adsorbent. On the surface of the adsorbent, large number of active centers is present which provides the necessary binding forces. Thus at these active sites, adsorption of adsorbate can take place. In an equilibrium system, adsorption and desorption occur simultaneously. Desorption is the process in which the solute is released back from or through the surface. The phenomenon is opposite of either adsorption or absorption. This occurs in an equilibrium system depending on the concentration gradient between bulk phase (fluid, i.e. gas or liquid solution) and the surface of the adsorbent (solid or boundary separating two fluids). When the concentration (or pressure) of solute in the bulk phase is reduced, some of the adsorbed substance tends to return back into the bulk state. As the temperature increases, some weak bonds start to break. The equation expressing the rate of desorption is:

$$R = rN^{x}$$

where; r is the rate constant for desorption, N is the concentration of the adsorbed materials, and x is the kinetic order of desorption.

The rate constant r may be expressed in the form:

$$r = Ae^{-Ea/kT}$$

where; A represents the "Arrhenius Factor", the chance of the adsorbed molecule overcoming its potential barrier to be desorbed, E_a is the activation energy of desorption, k is the Boltzmann constant, and T is the temperature. Figure 2.2 shows adsorbate-adsorbent interactions in the case of liquid phase adsorption (Henning and Degel, 1990).

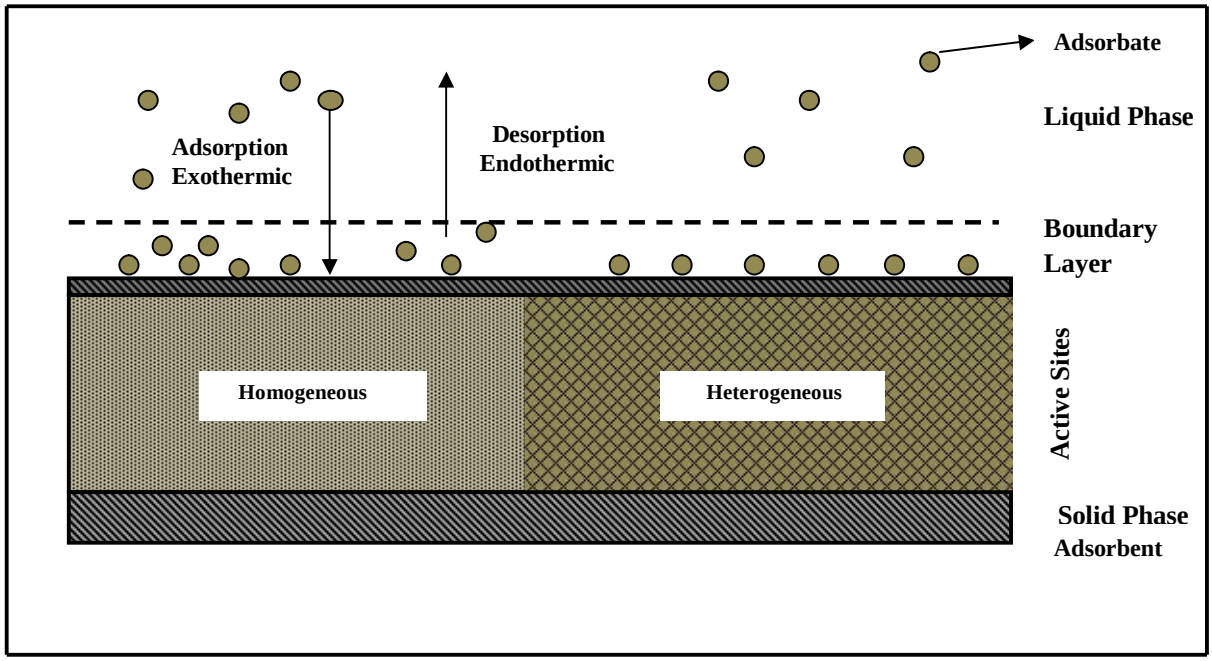

Figure 2.2 Adsorbate-Adsorbent interactions in liquid phase adsorption (Henning and Degel (1990)

2.4.1 Properties of Adsorbent

For Commercial applications, the adsorbent should have the following properties (Seader and Ernest, 1998):

- Reasonably high surface area with proper micropores mesopores distribution.
- Appropriate surface chemistry i.e., functional groups which can form surface complexes with the adsorbate.
- High selectivity to enable sharp separation.
- The amount of adsorbent should be small for economical feasibility of the process.
- Favorable kinetics i.e., rate of sorption and quick transportation properties for rapid sorption.
- Adequately stable both thermally and chemically.
- The adsorbent should have low solubility in the surrounding medium to prevent the weight loss of the adsorbent and retain its properties
- The adsorbent should have sufficient hardness and mechanical strength to prevent crushing and erosion.
- The aptitude of being regenerated.
- Relatively low cost.

2.4.2 Types of Adsorbent

Adsorbent can be divided into two major classes based on their application:

- Adsorbent used for gaseous phase applications such as solvent recovery, toxic gas separation or air purification.
- Adsorbent which are used for purification of liquid solutions. Following pie chart (Figure 2.3) reflects that majority of carbonaceous adsorbents are used for waste water treatment.

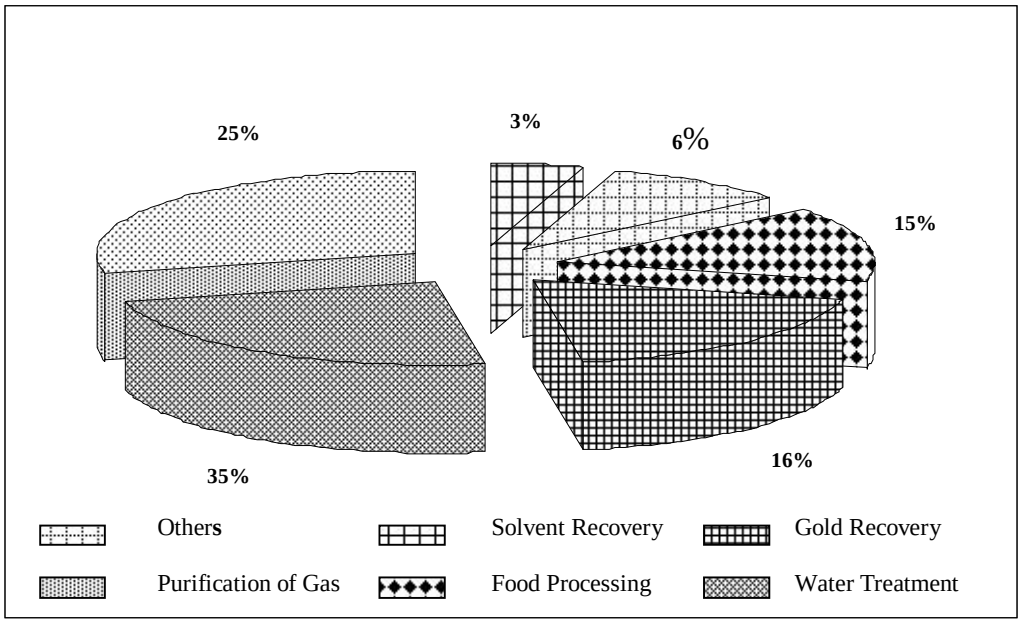

Figure 2.3 Applications of carbonaceous adsorbents (Qurishi, 2008)

The major difference between gas phase and liquid phase adsorbent is in their micro and meso pore size distribution. The pores are classified according to the International Union of Pure and Applied Chemistry (IUPAC 1972). Table 2.3 lists the classification of pores by their diameter (Perry and Green, 1997).

Table 2.3 Classification of pores (Perry and Green, 1997)

Type of pores	Diameter of the pore, D (°A)	Characteristics of pores
Micropore	D< 2 °A	Superimposed wall potential
Mesopore	2°A< D< 50°A	Capillary condensation
Macropore	D> 50°A	Effectively Flat walled

Adsorbents used for gaseous phase application usually have more micro pores and macro pores in their structure whereas liquid phase adsorbents have significant number of mesopores or transitional range of pores which allow easy access of aqueous solution to internal micro porous region through the macro pores and mesopores. This results in the rapid attainment of equilibrium contact time showing faster kinetics of adsorbate-adsorbent interactions. Different types of low cost adsorbent materials have

been reported for liquid phase applications. Table 2.4 summarizes the types of adsorbent used by previous researchers to remove organic and inorganic pollutants including heavy metals from aqueous solution.

Table 2.4 List of Low cost Adsorbents (Johnson *et al.,* 2008, Abia *et al.,* 2003, Ayyappan *et al.,* 2005)

Source of Adsorbents	Low cost Adsorbents
Activated carbon derived from agricultural by products or waste products	Activated carbon produced from palm shell, coconut husk, coconut shell, hazelnut shell, pecan shell, cotton seed hull carbon, almond husk activated carbon, banana pith carbon etc.
Modified agricultural biomass	Cassava waste, pecan shell, orange peel, banana peel, soyabean hull, tea waste, rice husk etc.
Industrial By products or waste products	Metal hydroxide sludge, paper mill sludge, red mud, Bagasse fly ash
Siliceous Materials	Dolomite, perlite, zeolite, clinoptilolite etc.
Natural Materials	Clays: Bentonite, diatomite, fullers earth etc.
Biosorbents	Chitin and chitosan, peat

2.5 Agricultural and Industrial Wastes for Preparation of Adsorbent

Natural materials and certain industrial wastes have the potential to be used as low cost adsorbent for decontaminating industrial or domestic waste water from toxic metal. Agricultural wastes are usually porous and lightweight and have carboxylic and hydroxyl functional groups on their surface. But the applicability of these materials has been found to be restricted up to a certain limit owing to their small surface area and leaching of some organic substances into the aqueous solution. Thus these residues can be converted to activated adsorbent either by producing activated carbon or by simple chemical treatment to enhance the surface area (Saravanane *et al.,* 2002). This improves their sorption performance to a greater extent which may compensate for the operating expense of additional processing. Many previous researchers have carried out studies to prepare low cost adsorbent from agricultural byproducts as listed in Table 2.5.

Table 2.5 Agricultural/Industrial waste used to prepare low cost activated carbons or chemically modified adsorbents

Precursor	**Reference**
Hazelnut Shell	Cimino *et al*., 2000
Maize Bran	Singh *et al*., 2006
Barley straw	Larsen and Schierup, 1981
Bengal gram husk	Saeed *et al*., 2005
Coir fiber	Conrad and Hansen, 2007
Olive	Stavropoulos and Zabaniotou, 2005; Martinez et al., 2006
Peanut hull	Girgis *et al*., 2002, Johnson *et al.*, 2002
Sago waste	Kadirvelu *et al*., 2004
Candlenut shell	Turmuzi *et al*., 2004
Corn cob	El-Hendawy, 2005; Tseng and Tseng, 2005; Cao *et al*.,2006; Tseng *et al.*, 2006
Jute fibre	Senthilkumaar *et al.*, 2005
Pistachio shell	Yang and Lua, 2003; Wu *et al.*, 2005
Nutshell	Aygun *et al.*, 2003
Rubber wood sawdust	Kalavathy *et al.*, 2005; Karthikeyan *et al.*, 2005
Date pit	Girgis and El-hendawy, 2002
seed/stone/kernel	Zabaniotou *et al.*, 2008; Spahis *et al.*, 2008; Kula *et al.*, 2008
Coir pith	Kavitha and Namasivayam. 2007; Namasivayam and Sangeetha, 2008
Pecan shell	Guo and Rockstraw, 2007
Chickpea husk	Hayashi *et al.*, 2002
Mango pit	Elizalde-Gonzalez and Hernandez-Montoya, 2007
Oil palm empty fruit bunch	Alam *et al*.. 2007a; Alam *et al*.. 2007b
Rice bran	Suzuki *el al*., 2007
Wheat bran	Ozer and Dursun, 2007
Apricot shell	Karagozoglu *et al.*, 2007
Peach stone	Attia *et al.*, 2008
Sunflower oil cake	Karagoz *et al.*, 2008
Coconut shell	Azavedo *et al*., 2007
Rice straw	Yun *et al.*, 2001; Oh and Park, 2002
Sugarcane bagasse	Tsai *et al*., 2001
Rice husk	Yalqin and Sevinc, 2000; Ahmedna *et al.*, 2000: Guo *et al*.. 2005: Kennedy *et al*.. 2007, Khalid *et al.*, 1998
Tea Wastes	Cay *et al.*, 2004
Sugar Beet pulp	Pehlivan *et al.*, 2006; Reddad *et al.*, 2002
Soybean hull	Marshall *et al.*, 1999
Cocoa Shell	Meunier *et al.*, 2003
Orange peel	Annadurai *et al.*, 2003
Sewage sludge ash	Pan *et al.*, 2003
Coal fly ash	Sharma *et al.*, 2007
Bagasse fly ash	Gupta and Ali, 2004
Grape Seed and chest nut shell	Didem *et al.*, 2009

Petroleum residues of bituminous coal, lignite, peat, wood and coconut shells are some of the widely used precursors to produce powdered (PAC) and granular (GAC) activated sorbent (Ahmenda *et al.,* 2000). The choice of starting materials is mainly dependent on its abundant availability and consistency in quality and purity along with processing cost (Girgis and El-Hendawy, 2002, Ioannidou and Zabaniotou, 2007). Various agricultural residues are annually generated in large quantities and considered as solid pollutants to the environment (El-Hendawy, 2005; Fiol *et al.,* 2006). Thus from environmental point of view, innocuous disposal of these agro residues are immensely important. In fact any types of lignocellulosic precursors with high carbon content and industrial waste with elevated oxide content but less leaching tendency can be used for production of activated adsorbent.

2.6 Activated Carbon

Activated carbon comprises a wide range of amorphous carbonaceous materials having significant numbers of pores and widespread surface areas. It contains graphite like microcrystalline units linked together, similar to that of carbon black (Do, 1996). The effectiveness of activated carbon as an adsorbent is attributed to its unique properties, including highly developed internal surface area between 500-2000 m^2/g, adequate pore size distribution and high degree of surface reactivity due to presence of surface active sites, especially oxygen functional groups (Ismadji and Bhatia, 2001).Their structure is complex and heterogeneous due to presence of micropores, mesopores and macro pores of different size and shape. It is anticipated that by restricted oxidation or activation technique, presence of carboxylate and phenol groups onto the surface of activated carbon particles can be enhanced. These groups act as essential binding groups for divalent metal (Sen Gupta *et al.,* 2002). It has been observed by many researchers (Dastgheib and Rockstraw, 2001; Toles *et al.*,1999; Johns *et al.*, 1998; Toles *et al.*, 1998;

Toles *et al.*, 1997) that ligno cellulosic agricultural residues, specially nutshells, are very good raw material for production of granular activated carbons having suitable surface active sites for the removal of metallic contaminants from waste water.

From prehistoric times, the powdered charcoal has been used for medicinal purpose and it has been reported in an Egyptian papyrus as early as 1550 B.C. (Hassler, 1974). A Swedish chemist Karl Wilhelm Scheele first discovered the adsorption properties of charcoal in 1773. The power of charcoal in removing color from solution was first observed by the Russian academician Lovits in 1785. In 1794, wood char was used for purification of cane sugar in England. Two activation processes were discovered and patented to produce activated carbon from cellulosic precursor in 1900 and 1901 (Adil, 2006). These patents are the basic scheme followed until now for the production of activated carbon on commercial basis. Metallic chlorides and carbon dioxide were used as selective oxidizing agents for production of activated carbons. High carbonization temperature was needed for activation with carbon dioxide. Industrial scale powdered activated carbon was first prepared on 1909. Peat was activated by steam and a new kind of activated carbon was produced in 1911. Granular activated carbon was developed in 1915 by Germany as filtering medium in gas masks to protect the soldiers against chlorine gas during World War I (Yehaskel, 1978).

Nowadays, different kinds of activated carbons are available. It is widely used as adsorbents, catalyst or support of a catalyst. Thus it is considered as one of the most important adsorbent materials for industrial scale application. The beginning of more rigorous environmental legislation worldwide has increased the demand for production of activated carbon. It has been observed that almost 80% of world production of activated carbon is utilized for purification of aqueous effluents (Dias *et al.*, 2007). The

production of activated carbon is now changing from western countries to South-East Asia and China because the raw materials, energy and labour costs are comparatively lower in these countries (Roskill, 2007). Century Chemical Works Sdn Bhd. in Malaysia has increased its production from 3000 tonnes/year to 11000 tonnes/year after Asian financial crises in late 1990's (Mohd Din, 2005). World demand for activated carbon has expanded from 5% per year through 2009 to 1.2 million metric tonnes in 2010 (World Activated Carbon forecasts to 2010 & 2015). The statistics clearly reveals the importance of producing activated carbon adsorbent for several applications. The adsorption properties of an activated carbon are highly influenced by the preparation variables of temperature, time and impregnation ratio (IR) will significantly amend its surface area, pore size distribution and surface functional groups.

2.6.1 Types of Activated Carbon

Different physical forms of activated carbons are produced depending on their applications (Allen and Koumanova, 2005). Liquid phase activated carbons are available in the following two forms:

- Granular activated carbon (GAC) to be used in adsorption columns
- Powdered activated carbon (PAC) for use in batch adsorption followed by filtration.

Commercially available PAC and GAC can be produced from different types of coal and have total surface area in the range from 450 to 1500 m^2/g. The pore volumes of commercial activated carbons range from 0.5 to 1.5 cm^2/g (Yehaskel, 1978). Table 2.6 provides the list of some commercially available activated carbons.

Table 2.6 List and properties of some commercially available activated carbon (Lu and Sorial 2004, Martin *et al.*, 2003)

Properties	**Commercially available Activated Carbon obtained (Petroleum**					
	Chemviron GW	**Witco 517**	**Westvaco Nuchar WV-L**	**NORIT**	**Calgon Filtrasorb 300**	**Calgon Filtrasorb 400**
Starting Materials	Bituminous	Bituminous	Bituminous	Lignite	Bituminous	Bituminous
Iodine Number	810	1000	950	650	900	-
Apparent Density (g/cm^3)	-	0.48	0.48	0.43	0.48	-
Particle	-	0.92	1.40	1.40	1.30-1.40	-
BET Surface Area (m^2/g)	1026	1050	1000	600-650	950-1050	1100
Pore Volume(cm^3/g)	0.49	0.60	0.85	0.95	0.85	0.84

GAC has a larger particle size than the powdered one; consequently it possesses smaller external surface area. It is commonly used as column filter bed for gas or liquid treatments and can be regenerated after use. The major disadvantage of using GAC is its slow intra particular diffusion rate. GAC is often prepared from hard precursors of coconut shell, palm shell etc.

On the other hand, PAC is obtained in smaller particles sizes and after treatment it can be disposed of (Dias *et al.*, 2007). PAC has larger external surface and a smaller diffusion distance between the layers. Thus faster adsorption velocities are observed and it is preferred for batch adsorption in liquid phase.

2.6.2 Properties and Structures of Activated Carbon

The surface areas of activated carbon can be up to 3000 m^2g^{-1}. The surface area of commonly available activated carbon is about 1000 m^2g^{-1}.These high surface area results from development of mainly micro- and meso pores of different size and shape. Macro pores have little contribution to the development of surface area (Sudaryanto *el al.*, 2006) as illustrated by Figure 2.4. The adsorption capacity of an activated carbon for a specific adsorbate is dependent on its physico-chemical properties such as effective surface area, pore volume and pore size distribution and surface functional groups. The development of micropores and mesopores is vital as they entrap and retain various types of adsorbate either from gas or liquid phases (Wu *et al*. 2005, Eckenfelder, 2000).

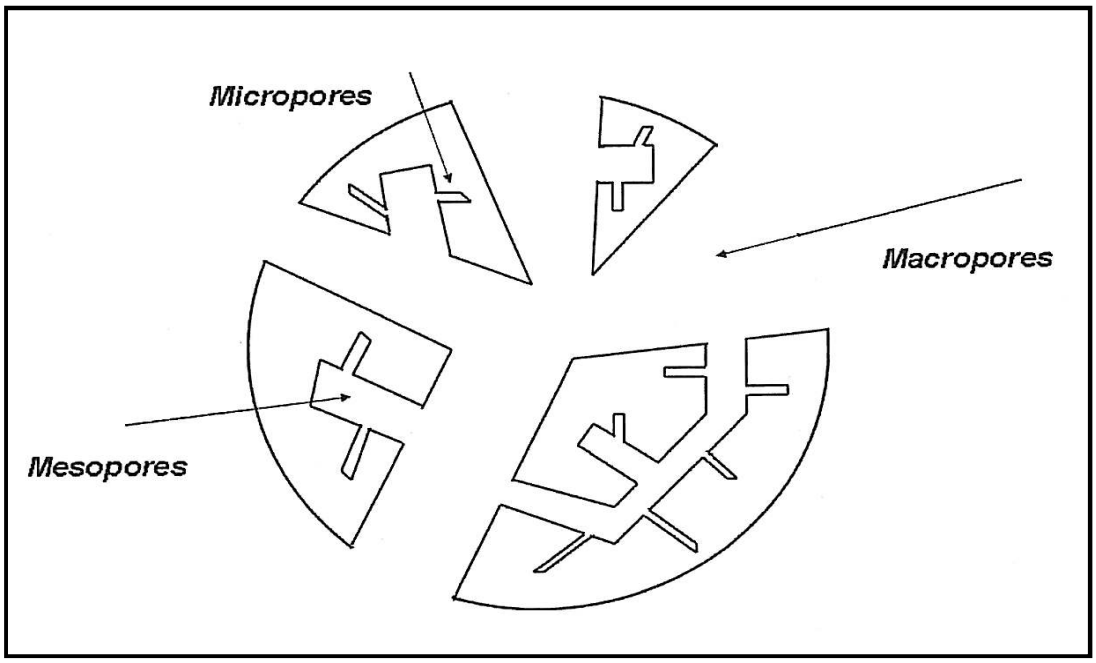

Figure 2.4 Schematic representation of pore structure (Azargohar, 2009)

Activated carbons along with coke and chars are often called amorphous carbon. X-ray diffraction and electron microscopic analysis revealed that these materials

have crystalline structure, although certain features of crystal angles and faces are not visible clearly. The microcrystal structure of activated carbon is known as crystallites. The amorphous carbon consists of hexagonal graphite flat plates in which each carbon atom, except those at the edge, is held by covalent linkages to three other neighboring carbon atoms. Two or more of these plate-structures with an interlayer distance of 3.6 Å (Hassler, 1974) are stacked together to form crystallites. Some hetero atoms including oxygen, hydrogen, nitrogen and others are incorporated in the carbon matrix in the form of single atoms and/or functional groups (El-Hendawy, 2005). The structure of activated carbon is almost similar like Turbostatic carbon containing micro crystallites having thickness less than 100 °A (Balachandran, 2004).

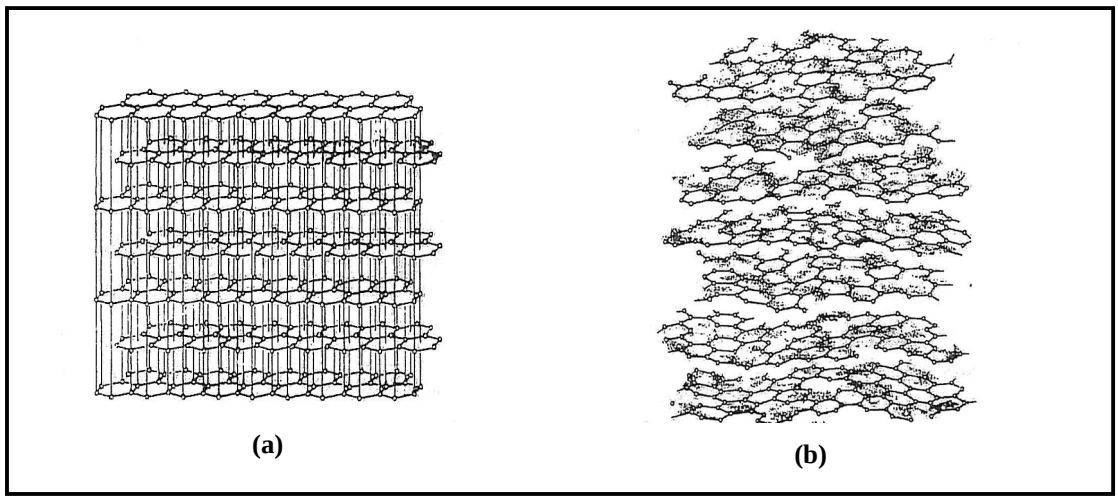

Figure 2.5 (a) Three dimensional structure of Graphite (b) Turbostatic Structure of Carbon

The presence of delocalized π-electrons in activated carbon is almost similar to that of aromatic hydrocarbons. Each basal layer acts as a unique macromolecule. These basal layers in the lattice, having delocalized electronic structures are noticeably separated from one another. The comparatively large distance between layers and the

weak forces that hold the layers together make it possible for atoms, ions or molecules to enter into the interlayer spaces. The adsorbate makes space for diffusion and enters inside by forcing the sheets farther apart.

2.6.3 Preparation of Activated carbon

There are two main steps involved for the production of activated carbon. The first step is known as carbonization of the carbonaceous precursors in the absence of oxygen to break down the cross-linkage between carbon matrixes. The second step is the activation of the carbonized product, known as char, for additional improvement of the porous texture of the activated carbon (Ioannidou and Zabaniotou, 2007).

2.6.3.1 Carbonization

Carbonization is carried out by pyrolysis of the precursors in an inert atmosphere. This will enhance the carbon content from the organic substances. The pores formed during the carbonization process are usually narrow and in some cases blocked by tarry substances. The deposition of tarry substances takes place when volatile components from carbon matrix diffuse out of the pore structure into the gas main stream. Some substances may collide with the walls of the pores resulting in hydrocracking and carbon deposition (Kamishita, 1977). This phenomenon was observed in preparing activated carbon from guava seed which yielded a poor adsorbing activated carbon due to the partial disintegration of organic constituents as the pores were blocked by carbonization byproducts (Rahman and Saad, 2003).

Carbonization process is divided into four main stages, based on the temperature reached in each stage (Wereko-Brobby and Hagen, 1996). The steps involved in carbonization process are summarized in Table 2.7.

Table 2.7 Steps and range of temperature in carbonization process (Wereko-Brobby and Hagen, 1996)

Stage	Temperature (^oC)	Type of Reaction	Process
1.	≤200	Endothermic	Initial drying of precursors
2.	170<300	Endothermic	Pre-carbonization stage, producing some pyroligneous liquids (methanol and acetic acid), small quantities of noncondensable gases (CO and CO_2)
3.	250<300	Exothermic	Greater proportion of the light tars and pyroligneous acids produced in the second stage are released steadily from precursors to produce charcoal
4.	>300	-	Increasing the carbon content of the charcoal by driven off the remaining volatile components of the charcoal

2.6.3.1 Activation

The properties of activated carbons are basically dependent on the process of activation. Technical know how about different parameters involved for activation process is very important in developing suitable activated carbon adsorbent required for a specified application. Activation step is necessary to enhance the porosity and burning off the deposited tars during carbonization (Turmuzi *et al.*, 2004). Activation process can be sub-divided into three major stages based on the individual activity of different parts of the carbon configuration. At the preliminary stage, tarry substances that cause pore clogging are eliminated to facilitate the surface of the elementary carbon crystal to come in contact with the activating agent for reaction. During the second stage elementary crystals of carbon will burn. The final stage involves oxidation of the carbon particles (Tan, 2008). This results in the reduction of the total micro pore volume due to the burning of the walls between the adjacent pores. The consequence of damaging the walls will create pores with large diameters. There are mainly two different methods for activation, namely physical and chemical.

2.6.3.1 (a) Physical Activation

Physical activation comprises of two-step process. After carbonization of carbonaceous materials, char is produced. The activation of the char is carried out in the presence of activating agents (oxidizing gases) such as CO_2, steam, air or their mixtures at an elevated temperature. Physical activation is carried out by the oxidation of the raw precursors or char using oxidizing gas at 800-1100°C to obtain a certain percentage of burn-off (El-Hendawy, 2005). The porous texture of the activated carbon is observed due to the exclusion of volatile matters present on the char. The main purpose of gasification is to expand the pores, resulting in meso porosity inside the carbon structure. However, the temperature must be selected carefully. At lower temperature, the reactions are too slow. Initially at lower temperature, reactions take place at the interior surface of carbon. At higher temperature, reactions become diffusion controlled at the outside of carbon particles. The following reaction takes place between CO_2 and carbon matrix (Qureshi, 2008):

$$CO_2 + C \longrightarrow 2\,CO \qquad \Delta H = +159\ kJ$$

Activation temperature and activation time are the two important parameters in determining the pore structure and surface functional groups of activated carbons. Sentorun-Shalaby *et al*. (2006) has reported that the increase in activation temperature and activation time were inversely proportional with the solid yield but directly proportional with the pore volume for activated carbon prepared from apricot stones. In the case of preparing activated carbon from pistachio-nut shell using CO_2 activation, it was observed that an increase in activation time or temperature increased the carbon-CO_2 reaction, resulting in the development of new pores together with the expansion of previously developed pores. Nevertheless, there is a precise limit after which increasing

the activation time or temperature might cause the destruction of the pores by collapsing some of the pore walls with the formation of ash residues.

Steam and air have been exhibited to react 8 times and 100 times faster respectively with carbon than CO_2. It is comparatively difficult to use steam or air mixture containing oxygen for activation step. Steam and air react with carbon particles to produce CO and CO_2 by the following reactions:

$$H_2O + C \longrightarrow CO + H_2 \qquad \Delta H = + 117 \text{ kJ}$$

$$2H_2O + C \longrightarrow CO_2 + 2H_2 \qquad \Delta H = + 117 \text{ kJ}$$

$$CO + 0.5\ O_2 \longrightarrow CO_2 \qquad \Delta H = - 285 \text{ kJ}$$

Due to the aggressive reaction of air (oxygen) with carbon, burn out occurs not only inside the pores but also on the external surface of the carbon resulting poor yield (Ullmann, 2002). Thus, from economical aspect, utilization of CO_2 is more preferable. CO_2 is the most frequently used activating gas as it is easy to handle, clean and it ensures overall control of the activation process due to the slow reaction rate at temperatures around 800°C (Ioannidou and Zabaniotou, 2007; Tseng *et al.*, 2006). Some of the previous works carried out on physical activation of various agricultural by-products are shown in Table 2.8.

Table 2.8 Production of Activated Carbon by Physical activation of Agricultural Residues

Agricultural Residues	Carbonization Temperature (^oC)	Carbonization Time (h)	Activating agent	Activation Temperature (^oC)	Activation Time (h)	Steps of Production	Referances
Jute fiber & Coconut fiber	-	-	CO_2	950	0.5	One-stage	Phan *et al.*, 2000
Date stone	500-800	1	Steam	500-800	0.5-9	Two-stage	Bouchelta *et al.*, 2009
Oil palm shell	400-900	0.5-3	CO_2	900	0.5	Two-stage	Lua *et al.*, 2006
coconut shell	325	2.5	Steam	800	2	Two-stage	Achaw and Afrane, 2007
Oil palm fiber and oil palm shell	600	2	CO_2	500-900	0.17-1	Two-stage	Gua and Lua, 2000
Rice straw	900	1	CO_2	700-900	1-6	One and Two-stage	Yun *et al.*, 2001
Pistachio-nut Shell	500	2	CO_2	725-825	0.5-3	Two-stage	Yang and Lua, 2003
Pecan Shell	700	1	Steam	850	2	Two-stage	Ng *et al.*, 2003
Candlenut shell	700	1	CO_2	800	0.5-6	Two-stage	Turmuzi *et al.*, 2004
Palm shell, coconut shell	850	1	CO_2	700-900	1	Two-stage	Daud and Ali, 2004
Corncob	550	3	Air Steam	350	0.08-1.33	Two-stage	El-Hendawy, 2005
Pistachio Shell	550	2	Steam	890	3	Two-stage	Wu *et al.*, 2005
Apricot stone	-	-	Steam	650-800	1-4	One-stage	Sentorun-Shalaby *et al* , 2006
Oil palm empty fruit Bunch	-	-	Steam	300-800	0.5-6	One-stage	Alam et al. 2007a

2.6.3.1 (b) Chemical Activation

For chemical activation, the two steps of carbonization and activation are carried out. It case of first step, the carbonaceous precursors is impregnated with predefined ratio of chemical activating agents for dehydrating purposes. The oxidants used are phosphoric acid, potassium carbonate, zinc chloride, sodium hydroxide and potassium hydroxide. Chemical activation is usually conducted at a temperature lower than that used in physical activation. The reaction between the chemicals and the carbon residues degrade the cellulosic backbone. It can improve the pore development in the carbon structure due to the effect of different chemicals that is by dehydration and oxidation reactions of the chemicals. The carbon yields of chemical activation are relatively higher (Sudaryanto *et al*., 2006, Mohanty et al., 2005). However, one disadvantage of chemical activation is that further washing stage is required for complete removal of the chemical agent.

The degree of development of surface area and porosity increased with increasing carbonization temperature in chemical activation (Olivares-Marin *et. al.*, 2006). Chemical activation by using phosphoric acid was reported to be more suitable to produce fibrous activated carbons from cellulose fiber compared to physical activation by CO_2. This is because; it could create a highly porous structure, enabling a high adsorption capacity for micro pollutants like phenol (Phan *et al.*, 2006). KOH was found to be a better activating agent compared to $ZnCl_2$ and H_3PO_4 because KOH not only requires less energy than water vapor, but it also has the least impact on the environment (Cao *et al*., 2006). KOH activation of peanut hull produced activated carbon having low surface area similar to steam pyrolysis (Girgis *et al*., 2002). Some of the previous studies reported on the chemical activation of various agricultural by-products are shown in Table 2.9**.**

Table 2.9 Production of Activated Carbon by Chemical activation of Agricultural Residues

Agricultural Residues	**Carbonization Temperature (°C)**	**Carbonization Time (h)**	**Activating agent**	**Activation Temperature (°C)**	**Activation Time (h)**	**Steps of Production**	**Referances**
Acorn, olive seed	400-800	1	H_3PO_4	-	-	One Stage	Lafi, 2001
Sugarcane bagasse	500	0.5	$ZnCl_2$	-	-	One Stage	Tsai *et al*., 2001
Rice straw	700-1000	1	KOH	600-950	1	One Stage and Two Stage	Oh and Park, 2001
Chickpea husk	500-900	1	K_2CO_3	-	-	One Stage	Hayashi *et al.*. 2002
Date pit	300-700	2	H_3PO_4	-	-	One Stage	Girgis and El-Hendawy, 2002
Palm shell	200-600	2	H_3PO_4	-	-	One Stage	Guo and Lua, 2003
Guava seed	200-750	1	$ZnCl_2$	700	1	Two Stage	Rahman and Saad, 2003
Pistachio-nut shell	500	2	KOH	500-900	2	Two Stage	Lua and Yang, 2004
Sago waste	105	3	H_3SO_4	-	0.75	One Stage	Kadirvelu *et al.,* 2004
Rabber wood sawdust	200	0.25	H_3PO_4	500	-	Two Stage	Srinivasakannan and Bakar, 2004
Rice husk	450	-	KOH, NaOH	400	0.3-1	Two Stage	*Guo et al.*, 2005
Olive-seed waste reduce	800	1	KOH	800-900	1-4	Two Stage	Stavropoulos and Zabaniotou, 2005
Rabber wood sawdust	400	1	H_3PO_4	-	-	One Stage	Kalavathy *et al*.. 2005; Karthikeyan *et al.*, 2005
Tectona grandis sawdust	300-600	1-3	$ZnCl_2$	-	-	One Stage	Mohanty *et al.*, 2005
pistachio Shell	550/2	2	KOH	780	1	Two Stage	Wu *et al.*, 2005

Table 2.9 Continue

Agricultural Residues	Carbonization Temperature (^oC)	Carbonization Time (h)	Activating agent	Activation Temperature (^oC)	Activation Time (h)	Steps of production	Referances
Corn cob	450	4	KOH	850	1.2	Two Stage	Cao *et al*.. 2006
Cassava peel	450-750	1-3	KOH	-	1	One Stage	Sudaryanto *et al.*, 2006
Olive stone, walnut shell	600	1	KOH	900	1	Two Stage	Martinez *et al.*, 2006
Jute Fiber,	900	2	H_3PO_4	-	-	One Stage	Phan *et al.*, 2006
Coconut fiber	600	2	KOH, NaOH, $CaCO_3$, H_3PO_4,$ZnCl_2$	800	1	Two Stage	Radhika and Palanivelu, 2006
Palm shell	600-1000	2	K_2CO_3	-	-	One Stage	Adinata *el al*.. 2007
Pecan shell	300-500	1	H_3PO_4	-	-	One Stage	Gua and Rockstraw, 2007
Olive kernel	270-600	-	KOH	800-900	1-4	Two Stage	Zabaniolou *et al*.. 2008
Olive stone	700	1	$ZnCl_2$	-	-	One Stage	Spahis *et al.*, 2008
Peach stone	500	2	H_3PO_4	-	-	One Stage	Attia *et al.*, 2008
Sunflower oil cake	600	0	H_3SO_4	-	-	One Stage	Karagoz *et al* ., 2008
Jute fiber	100	12	H_3PO_4	-	-	One Stage	Senthilkumaar *et al*., 2005
Corncob	550	3	KOH	700	1	Two Stage	El-Hendawy, 2005
Corncob	450	1.5	KOH	780	1	Two Stage	Tseng and Tseng, 2005

(-): Not Available

Different types of activating agent are added to the raw materials to produce activated carbons with different specific surface area. It is observed that some times, one step process for producing activated carbon is not efficient. In one step process, a great deal of activating agent can not penetrate inside the raw materials and break down the cross linkages or react with the carbon sufficiently to generate abundant pores. In this context, if the chemical activating agent is added with the previously carbonized materials or char containing a certain amount of porosity that would allow the activating agent to diffuse into the pores and react with the carbon easily. Therefore, it can be concluded that, addition of the activating agent after the raw material is carbonized would be better (Cao *et al.*, 2006). From the literature, it was observed that the two-stage chemical activation process was much more effective to obtain activated carbons with higher porosity and surface area (Tan, 2008).

2.6.3.1 (c) Physiochemical Activation

The majority of the research conducted by previous researchers used either physical or chemical activation method alone. This yielded activated carbons either having low surface area and/or mainly microporous in nature (Daud and Ali, 2004; Stavropoulos and Zabanjotou, 2005; Banerjee and Dastidar. 2005; Sudaryanto *et al*.. 2006; Lua *et al*, 2006). In the case of physiochemical activation method, physical and chemical activations are performed after carbonization of precursors. The combination of the chemical and physical activating agent can produce activated carbon having specific surface properties (Khalili *et al.*, 2000). This method has been employed by Hu and Srinivasan (2001) to obtain high surface area, granular, mesoporous activated carbons with mesopores volume above 70%.

Several activating agents, mainly phosphoric acid, zinc chloride and alkaline metal compounds have been used previously. However, the use of zinc chloride is not preferable because the activated carbon produced by zinc chloride cannot be used in pharmaceutical and food industries as it may contaminate the product due to liberation of toxic zinc (Srinivasakannan and Bakar, 2004). El-Hendawy (2005) had described that KOH is more efficient on the precursor while its effect on the char having developed porosity is not too prominent. Corncob fiber can strongly adsorb KOH during impregnation while on carbonization, KOH shows a very limited effect on the produced carbon. The strongly adsorbed KOH does not disappear by washing with distilled water and still remains on the surface, causing partial blockage of the existing pores. Therefore, activation with KOH may need subsequent gasification with CO_2 or steam. The combined activation procedure will impinge on pore cavity thus leading to a well developed porous structure (El-Hendawy, 2005). Tseng *et al*. (2006) found that KOH activation alone could only produce micro porous type of activated carbon. However, the process of KOH impregnation along with CO_2 gasification had produced activated carbon having higher ratio of macrospores and meso pores. This improves mass transfer within the activated carbon matrix.

Table 2.10 lists some of the previous researches done on the activation of various agricultural by products using physiochemical activation method.

Table 2.10 Physiochemical Activation method to produce Activated Carbon

Agricultural Residues	Carbonization Temperature (^oC)	Carbonization Time (h)	Activating agent	Activation Temperature (^oC)	Activation Time (h)	Steps of production	Referances
Pistachio Shell	-	-	Steam	450	1.5	Two Stage	Wu *et al.*, 2005
Coconut Shell	500	3	$ZnCl_2$/steam	900	0.5	One Stage	Azevedo *et al.*, 2007
Coconut Shell & Palm Seed	-	-	$ZnCl_2/CO_2$	800	2-3	One Stage	Hu and Srivastava, 2001
Coir Pith	-	-	H_2SO_4/CO_2	900	0.5	One Stage	Santhi and Silvapathi, 2006
Rice Husk	-	-	$ZnCl_2/CO_2$	600	1	One Stage	Yalcin and Sevnic 2000
Corncob	450	1.5	KOH/CO_2	780	1	Two Stage	Tseng *et al.*, 2006

(-): Not Available

2.7 Fly Ash Adsorbent

Fly ash is a finely divided mineral residues which results from the incineration of ground or powdered coal, municipal or solid wastes, sugar cane bagasse, tea dust, palm waste, rice husk mainly at power generating plants (Iyer and Scott, 2001). Depending on the origin, fly ash can be categorized as two types: coal fly ash and biomass ash. Biomass ash is reported to have no toxic metals like coal fly ash (Ahmaruzzaman, 2010). The biomass ash of palm is a pozzolanic material (substances with silica and alumina) which in the presence of $Ca(OH)_2$ and water can produce calcium silicate hydrate at ambient temperature (Zainuddin *et al.,* 2008). The waste biomass of palm tree namely palm shell, palm fiber, empty fruit bunch are burnt to generate electricity. The resultant ash residues are solidified and it is suspended in the exhaust gases. Afterwards it is collected by electrostatic precipitators. Since the particles coagulate while suspended in the exhaust gases; palm ash particles are generally very fine.

2.7.1 Types of Ash Adsorbent

Based on chemical composition, fly ash can be classified as Class F, Class C and Class N pozzolanic materials. Class F is obtained from burning of anthracite and bituminous coal and Class C fly ash originates from lignite and sub bituminous coal. The major constituent of palm ash is SiO_2. The total amount of SiO_2, Al_2O_3 and Fe_2O_3 in palm ash is less than 70%, loss of ignition less than 10% and SO_2 is below 4% (Sata *et al.,* 2004). Based on these findings, palm ash can be classified as Class N pozzolanic materials (Sata *et al.,* 2007). In another literature, the sum of SiO_2, Al_2O_3 and Fe_2O_3 was found to be lower than the minimum requirement of Class N pozzolanic materials in ASTM C618-08a (2008) (Saifuddin *et al.,* 2011; Tangchirapat *et al.,* 2009) method. Abdullah *et al.,* 2006 found 4.12% of CaO in palm ash. Based on this finding, it has been classified

as Class F ash. The chemical constituent in palm ash reported by previous researchers is summarized in Table 2.11.

Table 2.11 Chemical Constituent of Natural Palm Ash (Saifuddin *et al.*, 2011)

% of Chemical Constituent	**Weight %**	**Requirements by ASTM C618-08a (2008)**		
		Class F	**Class C**	**Class N**
SiO_2	44-46	-	-	-
Al_2O_3	1.5-11.5	-	-	-
Fe_2O_3	1.5-5.5	-	-	-
SiO_2+Fe_2O_3+ Al_2O_3	55-70	70	50	70
CaO	4-8.5	-	-	-
MgO	2-6.5	-	-	-
K_2O	2-8.5	-	-	-
Na_2O	0.10-3.50	1.5	1.5	1.5
SO_2	0.2-3.0	5	5	4
Loss on Ignition	1-3	6	6	10

(-): Not Available

2.7.2 Properties and Structure of Palm Ash Adsorbent

The chemical constituent of biomass ash varies due to temperature, types of biomass, soil, harvesting and duration of burning time. The ash residues have hydrophilic properties with porous structure. Based on the main chemical constituent, an empirical formula for fly ash has been proposed (Iyer and Scott, 2001):

$$Si_{1.0}\ Al_{0.45}Ca_{0.51}\ Na_{0.047}Fe_{0.039}Mg_{0.02}K_{0.013}\ Ti_{0.011}$$

The major metallic elements present in oil palm ash are Ca, Na and K. Some biomass ash such as rice husk ash contains large proportion of silica whereas wood ash contains higher percentage of alumina. Previous literature revealed that palm ash exhibits comparable pozzolanic characteristics like coal fly ash and other biomass ash of

rice husk, wheat straw, sugar cane straw and wood (Martirena *et al.,* 2006; Yu *et al*., 1999). Table 2.12 summarizes some physical properties of unground and ground palm ash.

Table 2.12 Properties of Natural Oil Palm Ash (Saifuddin *et al*., 2011)

Physical Properties	**Unground Oil Palm Ash**	**Ground Palm Ash**
Specific Surface area m^2/kg	796	882-1244
Color	Light Grey/whitish	Dark Grey
Specific Gravity	1.78-1.97	2.22-2.78
Median Particle size d_{50} (µm)	54.3-183	7.2-10.1
% passing through 45 µm sieve	5.6-58.8	97-99

2.7.3 Preparation of Ash Adsorbent

The applicability of fly ash as low cost adsorbents for waste water treatment depends strongly on its origin, percentage of unburnt SiO_2 and Al_2O_3. The promising approach of utilizing ash residues is to convert them into low grade zeolite. Zeoites are crystalline form of aluminium silicate incorporated with group I or Group II metallic cations incorporated within it. The structure contains framework of $[SiO_4]^{-4}$ and $[AlO_4]^{-5}$ tetrahedral units which forms a three dimensional network (Figure 2.6).

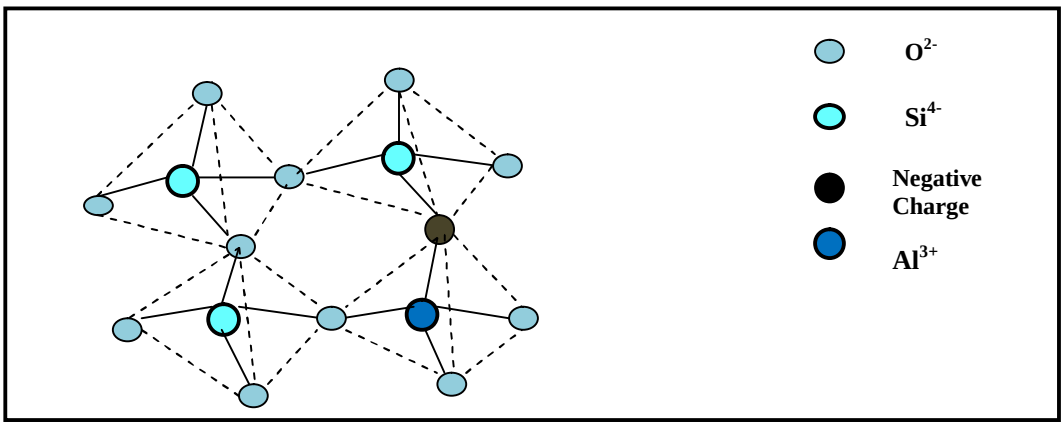

Figure 2.6 Structure of Zeolite Frame in Activated Ash (Ahmaruzzaman 2010)

The structure contains lots of void and open system. The substitutions of Si (IV) and Al (III) in the structure for a negative charge enhance its cation exchange capacity. However, there are two main methods for preparing activated ash adsorbent; direct synthesis and indirect synthesis of zeolite.

2.7.3.1 Direct Synthesis of Zeolite from Ash

For direct synthesis, the fly ash is treated with alkaline solution at temperature below 100℃. The concentration of NaOH used is 2-4 M to prepare zeolite P, X and Na-P1 whereas hydroxyl sodalite and zeolite Y are obtained by using 4-10 M NaOH.

2.7.3.2 Indirect Synthesis of Zeolite from Ash

For indirect synthesis, silica and alumina are extracted from ash with hot alkaline solution. To produce faujasite, the mixture of silicate and aluminate extracts are used at 60-90°C and it takes 2-5 days to complete the reaction. The compositional similarity of coal fly ash or biomass fly ash with volcanic materials material to synthesize zeolite is the main reason to produce synthetic zeolite from ash residues. Hydrothermal treatment of fly ash can also give rise to synthetic zeolite. Holman *et al.,* (1999) proposed a two step hydrothermal activation method to produce zeolite from coal fly ash. However, the reaction of hydration is very slow. Thus, to expedite the reaction, high temperature (125-200°C) is proposed. Shigemoto *et al.,* (1995) has reported to improve the properties of Na-X zeolite by fusion of NaOH with coal fly ash prior to hydrothermal reaction. The conversion of ash to different types of zeolite depends on the activation solution/fly ash residues, hydration temperature, pressure and reaction time. The time of activation can be reduced by using microwave assisted digestion system. However, similar types of fly ash has been used with NaOH and KOH with different molarity at temperature 80-200 °C and 3-48 hours to produce 13 different types of zeolite having

different adsorptive properties. The resultant mixture contains 40-75% of active zeolite mixture depending on the ratio of activated solution/ash and hydration period. The main limitation of producing zeolite by the above mentioned two processes is the generation of large amount of waste water. Park *et al.,* (2000) developed a method to overcome this disadvantage by using salt mixture instead of aqueous solution. However, the cation exchange capacities of these types of zeolites were very less. Table 2.13 summarizes the list of zeolite which has been synthesized from coal fly ash until now for commercial application.

Table 2.13 Zeolites Produced from Ash Residues

Synthetic Zeolite	Chemical Formula
NaP1 Zeolites	$Na_6Al_6Si_{10}O_{32}.12H_2O$
NaP Zeolites	$Na_{3.6}Al_{3.6}Si_{12.4}O_{32}.12H_2O$
Phillipsite	$K_2Al_2Si_3O_{10}.H_2O$
Zeolite A	$NaAlSi_{1.1}O_{4.2}.2.25H_2O$
Zeolite X	$NaAlSi_{1.23}O_{4.46}.3.07H_2O$
Zeolite Y	$NaAlSi_{2.43}O_{6.86}.1.8H_2O$
Hydroxy Sodalite	$Na_{1.08}Al_2Si_{1.68}O_{7.44}.1.8H_2O$
Hydroxy cancrinite	$Na_{14}Al_{12}Si_{13}O_{51}.6H_2O$

2.8 Applications of Activated carbon

The adsorptions of metal ions from the single, binary and multi-solute solutions onto mostly commercial and some noncommercial, laboratory prepared activated carbons have been investigated. These studies are described by the following paragraphs.

The adsorption characteristics of some heavy metals, namely Cu (II) and Pb (II) onto the hydrous surface of 14 different types of activated carbons obtained from various commercial brands were studied by Corapcioglu and Huang (1987). The

adsorption properties were evaluated based on the carbon type, pH and surface loading. They observed that the adsorption is favorable for the removal of metal ions for pH less than neutral region. The equilibrium data were calculated at varying pH, from 2.5 to 10.5, in a single-solute solution. The initial concentrations of Cu (II) and Pb (II) were kept constant at 6.4, and 20.7 mg/L respectively. The amount of adsorbent was kept constant at 10 g/L. The highest adsorption capacity for the above mentioned metal ions were exhibited by the activated carbons having acidic properties because the ashes of these acidic carbons contain higher level of phosphorus. From the trend of sorption, they speculated that heavy metals were removed through the formation of organometallic complexes with phosphoryl groups rather than hydroxo complexes. Within the pH range of 3 to 5, the acid activated carbon had removed above 90% of the metal ions of Cu (II) and Pb (II). However, in the alkaline pH region, the metal ions removal capacities of all activated carbons were impossible to differentiate due to cumulative effect of adsorption and precipitation. With increasing surface loading, the removal percentages of heavy metals were decreasing. The optimum adsorption for Cu (II) and Pb (II) were found at a pH range of 3 to 5 and 3 to 6 respectively (Corapcioglu and Huang, 1987). The adsorption properties of Pb (II) onto activated carbon were calculated (Tan and Teo 1987). They observed that adsorption is dependent significantly on the pH, carbon dosage and initial cation concentration.

The single and competitive adsorption of Cu (II) and Pb(II) in single and multi-solute solutions were studied onto various granular activated carbons (John *et al.*1998). According to their study, physically activated and controlled air oxidized activated carbons have higher Cu (II) adsorption capacities of 41-51 mgg^{-1}. But the drawback of this study is that they determined the equilibrium adsorption data from the single point concentration which is not enough to comprehend the adsorption characteristics. The

highest adsorption of the total solutes by one of the prepared activated carbon was observed at 510 $\mu molg^{-1}$ and the selectivity order was reported as Pb > Cu > Cd > Zn >Ni. All granular activated carbons adsorbed Pb (II) and Cu (II) to a much higher extent than the other cations such as Cd, Zn and Ni.

The adsorption of Cu (II) onto commercial activated carbon was investigated as a function of pH, metal ion and carbon concentrations (Seco *et al.*,1999). They also observed that the removal percentage was increased with the increase of pH and carbon concentration. They found that an increase of initial metal ion concentration reduced the metal removal percentage. They successfully interpreted the stronger affinity of Cu (II) than Cd (II) towards carbon from their electronegativities, as 2.00 and 1.69 and the first hydrolysis equilibrium constants (pK values), as 8.00 and 10.08 respectively. They applied a mechanistic model, the Triple Layer surface complex formation (SCF) model, to predict the adsorption behavior of Cd (II) and Cu (II) on carbon. The experimental data were calculated by Langmuir and Freundlich models where the Langmuir model failed to estimate the parameters, demonstrating a multi-layer adsorption.

The adsorption properties of Cu (II) and Pb (II) in their single and binary solution in a fixed-bed column were observed by (Chen and Wang 2000). They observed that; the breakthrough capacity increases with the increase of inlet pH and the lowering of flow rate. The selectivity order for the adsorption of metal ions in single solution was shown to be: Cu > Pb. The multi solute adsorption indicated that activated carbon has a higher affinity towards Cu (II). The adsorption capacity for Cu (II) was slightly suppressed by the presence of competing ions of Pb (II) in binary solute solution. Chen and Wang's (2000) assumption of Pb (II) and Cu (II) on a same functional group may not be correct. Nevertheless, Pb (II) might be assumed to be

adsorbed onto both harder and softer active sites on carbon. Thus they anticipated another mechanism for sorption of ion-exchange and surface complexation of metal ions with oxygen- and phosphorous-containing functional groups. They did not illustrate any substantiation or offer any explanation for this supposition.

The HSAB theory was applied to understand the adsorption behavior of metal ions on activated carbon by considering surface groups of activated carbon as their hard sites and the surface of basal planes as soft sites (Alfarra *et al.*, 2004). In an IUPAC report (2002), Pb (II) was classified as soft cation whereas some literature had identified Pb (II) and Cu (II) as borderline cations (Ahrland *et al.*,1958).

The adsorption of Pb (II) on the prepared sulphurized steam activated carbon with respect to contact time, initial concentration, pH, and temperature was studied (Krishnan and Anirudhan 2002). The kinetic data were well fitted to the pseudo-second order kinetic model. Carbon nanotubes-iron oxides magnetic composites were developed as an effective adsorbent for the removal of Pb (II) and Cu (II) (Peng *et al.*, 2005). They premeditated the effect of pH on the removal percentage as well as on the constructed isotherms. They obtained the adsorption capacities at pH 5 for Pb (II) and Cu (II) cations as 103 mg/g and 45 mg/g respectively. Some previous studies also reported to remove Mn (II) ions by using granular activated carbon (41%), lignite (25.84%) and palm fruit bunch (50%) (Emmanuel and Rao, 2009).

2.9 Application of Ash Residues

Ash residues have been utilized to remove divalent cations of copper. The kinetics of adsorption indicated diffusion controlled mechanisms (Lin and Chang, 2001). Presence of different quantities of carbon and mineral were used to remove the copper. It was

found that carbon in fly ash removed 2.2 mg/gm to 2.8 mg/g of copper and minerals removed 0.63 to 0.81 mg/g of copper. Pelletized fly ash removed 20.92 mg/g of copper (Papandreou *et al.,* 2007). Rice husk ash was used to remove Pb (II) from waste water where the kinetics were controlled by Bangham's equation (Feng *et al.,* 2004). Raw and modified coal fly ashes absorb copper effectively from waste water (Hsu *et al.,* 2008). The reaction was endothermic and the activation energy were 1.3 and 9.6 kJ/mol. The researchers have found that coal fly ash (CFA), CFA-600 and CFA-NaOH followed pseudo second order rate kinetics. The adsorption capability was not improved by changing the type of fly ash. Bagasse fly ash was used to remove lead from waste water (Gupta and Ali, 2004). The adsorption properties of sewage sludge ash were determined and maximum sorption capacity was observed to be 3.2 mg/g to 4.1 mg/g (Pan *et al.,* 2003). Sorption of copper onto sewage sludge ash followed Langmuir isotherm. A mixture of lime and fly ash had been utilized to remove lead and copper from waste water (Apak *et al.,* 1998). The reactive species of calcium silicate hydrate was found to be responsible for enhanced removal percentage and less desorption. It was discovered that removal of manganese onto fly ash is exothermic and spontaneous (Sharma *et al.,* 2007).

2.10 Optimization of Operating Conditions for Adsorbent Preparation

The most significant properties of an adsorbent are its adsorption capacity which is highly subjective by the preparation variables. For producing activated carbon specially powdered one (PAC) on commercial basis, yield is a major concern along with removal percentage for economical feasibility of the entire process. In order to prepare an optimum activated carbon for a specific purpose, the effects of the parameters influencing its surface characteristics must be studied. Similarly, to prepare efficient adsorbent from natural palm ash, process parameters should be optimized to obtain

active surface with maximum removal percentage. Nevertheless, for assessing the effect of each preparation variables on the quality of the end product, the application of an adequate experimental design is predominantly essential.

Response surface methodology (RSM) has been used by several researchers to study the interactions of two or more variables. RSM is a compilation of statistical and arithmetical techniques which are inevitable for developing regression model, improving and optimizing processes. Generally it contains three stages: (i) Process design and experimental lay out in different operating condition, (ii) Response surface analyzing through model development and regression and (iii) optimization of the process (Myers and Montgomery, l995). The main benefit of RSM is the application of the reduced number of experimental run to evaluate the effect of multiple parameters and their interactions (Lee *et al.*, 2009). RSM is applied for developing models and analyzing problems in which a response of concern is prejudiced by numerous factors. By employing RSM, it is possible to study many processes systematically as it is considered as a single-factor-at-a-time method (Myers and Montgomery, l995). According to this method, it is possible to study the trend of the process by changing one factor while keeping other factors constant (Karacan *et al.*, 2007). However, the effect of each variable does not necessarily have significant impact on the responses. Therefore, it is compulsory to analyze the influence of each factor and also the interaction between these factors which may be synergistic that is directly proportional or antagonistic that is inversely proportional (Karacan *et al.*, 2007). In the case of standard RSM technique, a central composite design (CCD) is well appropriate for fitting a quadratic surface, which is commonly employed for process optimization (Montgomery, 2001).

RSM has been used by many researchers in process optimization for different fields, such as in biodiesel production (Vicente *et al.*, 1998), photo degradation of dye (Lizaman *et al.*, 2002), extracellular lipase production (Burkert *et al.*, 2004) and removal of 2, 4-dichlorophenol by activated carbon (Alam *et al.*, 2007b). However, its application in adsorbent preparation for liquid phase decontamination of waste water is still very rare. Some of the previous studies found in applying RSM in the preparation of activated carbons using rattan saw dust (Ahmad *et al.*, 2009), olive-waste cakes (Bacaoui *et al*., 2001), Luscar char (Azargohar and Dalai, 2005), and bamboo (Ahmad *et al.*, 2010a) and Turkish lignite (Karacan *et al*., 2007). The influence of activation temperature, mass ratio of steam to char and activation time on the yield and BET surface area of activated carbon prepared from Luscar char was studied by using RSM technique (Azargohar and Dalai, 2005). Bacaoui *et al*., (2001) found that the most influential factors affecting the preparation of activated carbon were activation time and activation temperature. Karacan *et al*.,(2006) also applied RSM so study the effect of K_2CO_3 ratio and activation temperature on the carbon yield, BET surface area, total pore volume and micropore fraction of the activated carbon prepared from Turkish lignite.

The surface of palm ash was activated by CaO and $Ca(OH)_2$ by using RSM technique for flue gas desulfurization (Zainuddin *et al*., 2005). Activated adsorbent from rice husk ash was prepared by CaO for gaseous phase adsorption for the removal of SO_2 and NO gas and the process parameters were optimized by using RSM technique (Dahlan *et al*., 2010). As far as is known, no study has been conducted on activation of natural oil palm ash for preparing effective sorbent for heavy metals and different parts of kenaf crops to prepare powdered activated carbon by using RSM approach.

2.11 Regeneration of Adsorbent

The feasibility of prepared sorbent depends on several factors together with the expenditure of regeneration and disposal of spent sorbent. Therefore, the cation loaded spent adsorbent should have high regeneration efficiency for wider application of the process. Thermal volatilization, chemical extraction and bio-regeneration are frequently used for regeneration of activated carbon. However 5-l0% of the activated carbon is lost by attrition and burn-off during each cycle of thermal regeneration. Moreover, thermal regeneration needs high energy consumption (Hamdaoui *et al.,* 2005, Lim and Okada, 2005, Tanthapanichakoon *et al.,* 2005).

Bio-regeneration may be considered as the most economical process but this method suffers from several limitations due to non-biodegradability and toxicity of the sorbents towards microorganisms. The entire process is time-consuming since most biological activities are significantly slow (Lim and Okada, 2005; Hamdaoui *et al.,* 2005).

In this regard, solvent regeneration can be considered as the best option in which carbon loss by attrition is negligible. According to the surface complexation reaction, it was found that lowering the pH of the exhausted carbon below the zero point charge (P_{ZPC}) will protonate the surface. This leads to the repulsive force between adsorbed cation and the surface of the adsorbent (Adil, 2006). This is the basic principal for which mineral acids are used as eluting agent for cation loaded adsorbent. About 97.4 % Cu (II) was regenerated from palm shell based activated carbon by using 10% HCl (Adil, 2006). Dastgheib and Rockstraw (2001) recovered above 98% of adsorbed Cu (II) through regeneration of the exhausted carbon using 10% HCl. About 65.49% Cd (II) was desorbed from bagasse fly ash by using HCl (Srivastava *et al.*, 2008) but in the

case of rice husk ash only 25.76% of Cd (II) was desorbed by using HCl (Srivastava *et al.*, 2008).

2.12 Summary

Recently, special emphasis has been given to the preparation of adsorbent from renewable, abundant and low cost starting materials, especially agricultural biomass. However, there are limited studies carried out on the utilization of agricultural biomass such as by-products from kenaf (Kenaf fiber and kenaf core), mangostene fruit shell and oil palm ash derived from burning of oil palm residues in oxygenated atmosphere (oil palm fiber, shell, empty fruit bunch).

Although a good number of researches have been conducted regarding preparation of activated adsorbent from agricultural waste, the publications concerning the effect of preparation variables, especially using response surface methodology and their application in removing metallic cations from aqueous solution are still rare. The literature study revealed that the characteristics of an adsorbent are depended on the type of starting materials and the process of activation used. So it would be our major focus to utilize low cost local agricultural residues for the preparation of powdered and granular activated adsorbents, characterize their surface morphological features and carry out subsequent adsorption studies for the removal of metal ions in batch as well as in fixed bed sorption system.

CHAPTER THREE
THEORETICAL ASPECTS

3.1 Introduction

This chapter describes the basic theories involved in analyzing experimental uptakes by batch and fixed bed sorption studies. The first section summarizes adsorption equilibrium process in terms of isotherm, kinetics and thermodynamics characterization of a specific adsorbate-adsorbent system (Sections 3.3-3.7). The last section (Section 3.8) describes the process parameters including the dynamics of fixed bed sorption onto granular adsorbent.

3.2 Adsorption Equilibrium

The design and characteristics of an adsorption system from an aqueous solution involves determination of the final amount of solute attached onto the surface of the sorbent and the residual amount left in the liquid phase. As the adsorption process proceeds, some fraction of the sorbed solute tends to desorb into the liquid phase depending on the nature of the sorption process. When equal amounts of solute adsorb and desorb simultaneously, then the system attains an equilibrium state which is called adsorption equilibrium. It is the most indispensable part to understand the adsorption process. Adsorption equilibrium gives elementary physiochemical statistics for determining the process parameters of an adsorption process for a specific adsorbent-adsorbate system as a unit operation under predetermined reaction condition (Vadivelan and Kumar, 2005).

The adsorption of a solute from the liquid phase to the surface of the sorbent proceeds by a thermodynamically defined allocation of that solute between the two phases. Eventually when the system reaches equilibrium, there is no further net

adsorption. This distribution is depicted as the amount of solute or sorbate adsorbed per unit weight of adsorbent and is denoted by q_e (mg/g). The remaining adsorbate left in the solution phase or failed to attach itself onto the surface of the sorbent is the residual equilibrium concentration and is denoted by C_e (mg/l).

3.3 Adsorption Isotherms

Adsorption is the collective phenomenon of a mass transfer process of an adsorbate at the boundary between solid and aqueous phases. Equilibrium relationships between sorbent and sorbate at constant temperature are described by adsorption isotherms, i.e., the ratio between the amount of solute adsorbed and the residual portion left in the solution at equilibrium. Experimental data is fitted with different isotherm models to evaluate suitability of the model which can be used for designing the process (Arami *et al.,* 2005). Adsorption isotherms parameters are usually evaluated to estimate the competence of different types of adsorbent for the adsorption of a particular adsorbate (Moreno-Castilla, 2004) under predefined reaction condition.

The shape of adsorption isotherms gives qualitative insight about the sorption process and the degree of surface coverage by the adsorbate which is useful for the assessment of the viability of the process for a particular application. It helps to choose the most suitable adsorbent and for the determination of sorbent dosage required for the process. Brunauer classified the shape of isotherm into five basic types for gaseous and liquid phase application and are given in Figure 3.1 (Brunauer *et. al.,* 1938).

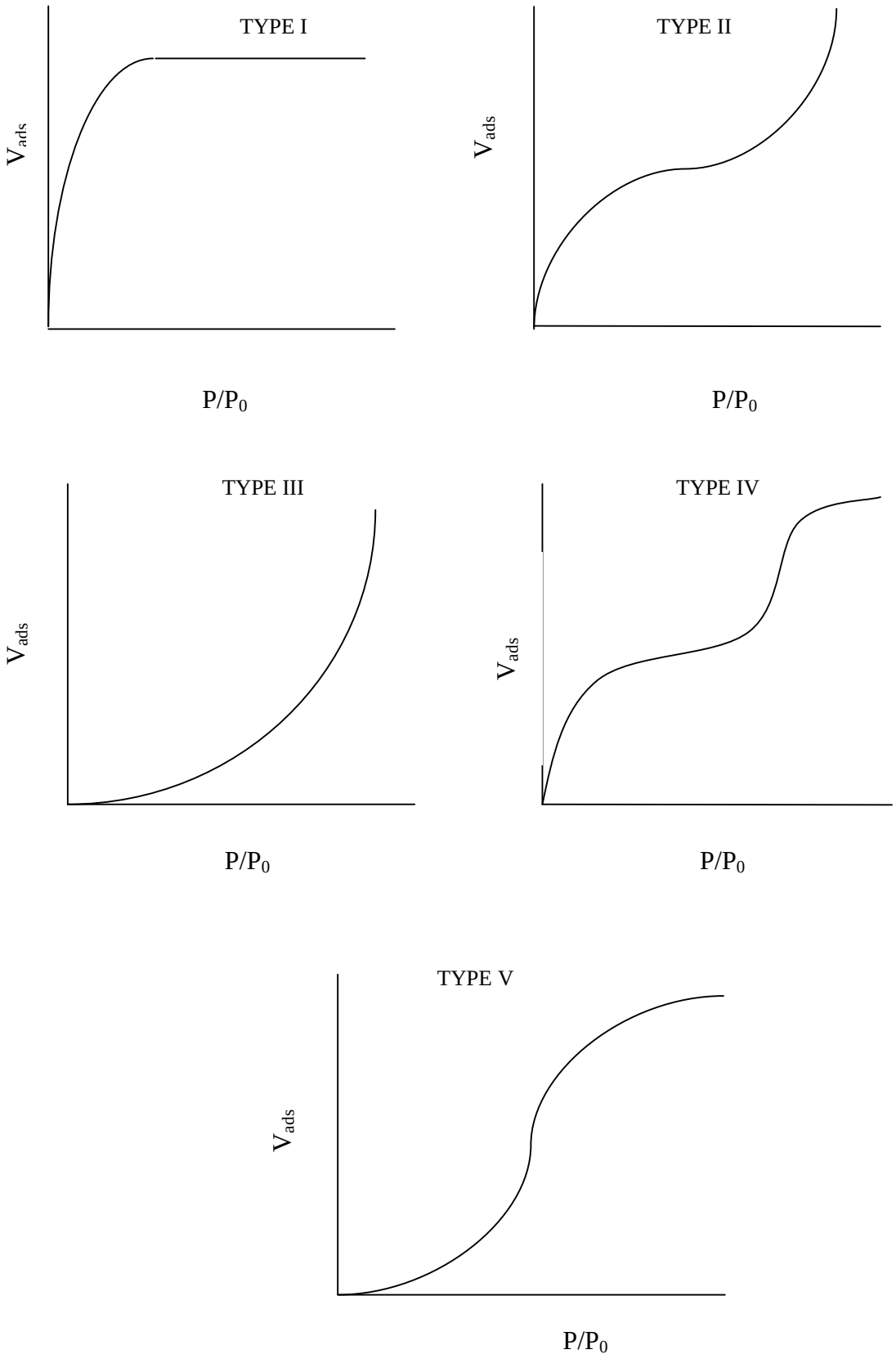

Figure 3.1 Brauner's Classification of Isotherm

From the literature, it is observed that different equilibrium systems show diverse sorption behaviors. Type I isotherm depicts the equilibrium process where sorption proceeds only with the formation of monolayer. This type of curve was exhibited by oxygen onto the surface of carbon black at -183 °C. It also indicates that the adsorbent contains extremely narrow micropores. Type II isotherm is characterized by an indefinite multilayer formation. This type of isotherm has been shown by water vapor onto carbon black at 30 °C. Type III isotherm is exhibited when gas sorption takes place without any limit. Adsorption of bromide onto silica gel at 20 °C yield this types of curve. Type IV is the variation of Type II isotherm which proceeds by finite multilayer formation. An example of this type of isotherm is sorption process of water vapor on the surface of activated carbon at 30 °C. Type V is another variation of Type III isotherm which is observed for sorption of water vapor onto the surface of activated carbon at 100 °C. Theoretically several types of sorption equations have been developed but none of them is able to generalize the sorption behaviors by all types of adsorption process.

3.3.1 Langmuir Isotherm

Langmuir model was initially developed for adsorption of gases onto solid adsorbent and is also known as the ideal localized monolayer model (Langmuir, 1918). The basic assumptions underlying this model are:

1. The adsorbate (molecules or ions) are adsorbed on definite sites of the sorbate.
2. Each and every site can contain only one cation, anion or molecule of the adsorbate.
3. The energy for sorption by each site is equal.

4. The area of each site is preset and determined exclusively by the geometry of the sorbate.

The Langmuir model is expressed as:

$$q_e = \frac{q_{max} K_L C_e}{1 + K_L C_e} \quad (3.1)$$

The linear form of Langmuir isotherm is given by Equation 3.2

$$\frac{C_e}{q_e} = \frac{1}{q_{max} K_L} + \frac{1}{q_{max}} C_e \quad (3.2)$$

where C_e is the equilibrium concentration of the adsorbate (mg/l), q_e is the amount of adsorbate adsorbed per unit mass of adsorbent (mg/g), q_{max}, (mg/g) and K_L (L/mg) are Langmuir constants related to maximum monolayer adsorption capacity and rate of adsorption, respectively (Tan *et al.*, 2007). When C_e/q_e is plotted against C_e, a straight line with slope of $1/q_{max}$ K_L and intercept of $1/q_{max}K_L$ is determined.

Langmuir equation assumes that the maximum adsorption of an adsorbate corresponds to a monolayer formation by the adsorbate molecules on the adsorbent surface that is energetically homogeneous (Namane *et al.*, 2005; Senthilkumaar *et al.*, 2005). This isotherm predicts that intermolecular forces decrease rapidly with the distance and consequently forecast the subsistence of monolayer of adsorbate at the outer surface of the adsorbent. It is implicit that once the adsorbate attaches itself onto the site, no additional sorption can take place at that site (Wang *et al.*, 2005). The different shapes of the adsorption isotherms result from the dissimilar porous structures

of adsorbent and the different sorbate-sorbent interactions. Isotherms containing a step increase in adsorption capacity in lower concentration range and an apparent plateau on achievement of a monolayer of molecules are related to a very high sorption affinity and comparatively strong adsorbent-adsorbate interactions (Martin *et al*., 2003).

The essential characteristic of the Langmuir isotherm is defined by Weber and Chakkravorti (1974) as:

$$R_L = \frac{1}{1+K_L C_o} \tag{3.3}$$

where, K_L (L/mg) is the Langmuir constant and C_0 is the adsorbate initial concentration (mg/l). The parameter R_L which is called separation factor indicates the nature of the adsorption process, as explained in Table 3.1.

Table 3.1 Separation factor (Weber and Chakkravorti, 1974)

R_L value	Nature of Adsorption Process
$R_L>1$	Unfavorable
$R_L=1$	Linear
$0<R_L<1$	Favorable
$R_L= 0$	Irreversible

3.3.2 Freundlich Isotherm

Freundlich model is an empirical equation which encompasses the heterogeneity of the surface or surface sustaining sites of wide-ranging affinities. It is based on the exponential distribution of active sites and their energies. It is implicit that the stronger binding sites are engaged first for sorption and the binding force decreases with the

increasing degree of site occupation (Freundlich, 1906). Freundlich isotherm is expressed as:

$$q_e = K_F C_e^{1/n} \quad (3.4)$$

The well-known logarithmic form of Freundlich isotherm is given by the following equation:

$$\ln q_e = \ln K_F + (1/n) \quad (3.5)$$

where C_e (mg/L) is the equilibrium concentration of the adsorbate, q_e (mg/g) is the amount of adsorbate adsorbed per unit mass of adsorbent, K_F and n are Freundlich constants with n giving an indication of how favorable the adsorption process is, and K_F (mg/g (L/mg)) can be defined as the adsorption or distribution coefficient and represents the quantity of adsorbate adsorbed onto the adsorbent for a unit equilibrium concentration (Freundlich, 1906). The slope $1/n$ is the surface heterogeneity factor ranging between 0 and 1 and is a measure of adsorption intensity or surface heterogeneity, becoming more heterogeneous as its value gets closer to zero (Hagliseresht and Lu, 1998). Steep slope that is value of 1/n close to 1 reflects high sorption capacity at high equilibrium concentration which diminishes rapidly at lower equilibrium concentration. A flat slope whith 1/n<< 1 represents that the sorption capacity is slightly reduced at lower equilibrium concentration. A value for $1/n$ below one designates a normal Langmuir isotherm while $1/n$ above one is a reflection of cooperative adsorption (Fytianos *et al.,* 2000). The plot of log q_e versus log C_e gives a straight line with slope of $1/n$ and intercept of ln K_F. Table 3.2 summarizes the list of sorbate-sorbent systems based on divalent cations of lead, copper and manganese for following different isotherm models.

Table 3.2 Adsorption Isotherms of lead, copper and manganese onto various adsorbents

Adsorbate/ species	Type of Adsorbent	Isotherm	References
Lead Pb (II)	Bengal gram husk	Langmuir	Saeed *et al.*, 2005
	Coir	Langmuir & Freundlich	Quek *et al.*, 1998
	Coir Fiber	Langmuir & Freundlich	Conrad and Hansen, 2008
	Hazelnut shell	Langmuir & Freundlich	Cimino *et al.*, 2000
	Maize Bran	Langmuir	Singh *et al.*, 2006
	Bagasse fly ash	Langmuir & Freundlich	Gupta and Ali, 2004
	Lawny grass modified with 0.6mol/l Citric acid after saponification with 0.1mol/l NaOH	Langmuir & Freundlich	Lua *et al.*, 2009
Copper Cu(II)	Banana pill	Freundlich	Annadurai *et al*., 2003
	Banana pith carbon	Langmuir	Low *et al*., 1995
	Bengal gram husk	Langmuir & Freundlich	Saeed *et al.*, 2005
	Coir activated	Langmuir	Baes *et al.*, 1996
	Orange peel	Freundlich	Annadurai *et al*., 2003
	Peanut hull carbon	Langmuir	Periasamy *et al*., 1996
	Pecan shell carbon(H_3PO_4 activated)	Freundlich	Bansode *et al.*, 2003
	Pecan shell carbon(CO_2 activated)	Freundlich	Bansode *et al.*, 2003
	Pecan shell carbon(steam activated)	Freundlich	Bansode *et al.*, 2003

Table 3.2 Continued

Adsorbate/ species	Type of Adsorbent	Isotherm	References
Copper Cu(II)	Sugar beet pulp	Langmuir & Freundlich	Pehlivan *et al*., 2006
	Tea waste	Freundlich	Cay *et al*., 2004
	Tea waste (Binary system)	Freundlich	Cay *et al*., 2004
	Sawdust	Langmuir & Freundlich	Azmal *et al*., 1998
	Rubber wood sawdust activated carbon	Langmuir, Temkin & Freundlich	Kalavathy *et al*., 2005
	Sewage sludge ash	Langmuir	Pan *et al*., 2003
Manganese Mn (II)	Electric Arc Furnace Slag	Langmuir & Freundlich	Beh *et al*., 2010
	Raw and acid treated corncob biomass	Langmuir & Freundlich	Abideen *et al*., 2011
	Cow Bone Charcoal	Langmuir & Freundlich	Moreno *et al*., 2010
	C. papaya seeds	Freundlich	Egila *et al*., 2011
	A. Hybridus L stalk	Freundlich	Egila *et al*., 2011

3.3.3 Temkin Isotherm

Temkin isotherm is based on a factor that unambiguously describes the adsorbent-adsorbate interactions (Temkin and Pyzhev, 1940) which assumes that the heat of adsorption of all the molecules in the layer would decrease linearly with coverage. The adsorption is characterized by a standard distribution of binding energies, up to some maximum binding energy. The Temkin model is expressed as:

$$q_e = \left({}^{RT}/_{b}\right) ln(K_T C_e) \tag{3.6}$$

The linear form of Temkin Isotherm is:

$$q_e = B \ln K_T + B ln\, C_e \tag{3.7}$$

where,

$$B = \frac{RT}{b} \tag{3.8}$$

Here R is the gas constant (8.314 J/mol K), T is the absolute temperature (K) and RT/b=B. A plot of q_e versus C_e yields a linear line with B as the slope and B ($\ln K_T$) as the intercept. K_T (L/g) and B are Temkin isotherm constants.

3.4 Adsorption Kinetics

Adsorption of solutes from aqueous phase system onto the adsorbent is a time dependent process. In order to design an effective sorption system, investigations should be carried out to determine the rate of sorption. For determination of the rate of an adsorption process such as physical or chemical reaction, diffusion mechanism and mass transfer, several kinetic models are implemented to examine the experimental data

(Senthilkumaar *et al.,* 2005). The kinetics of sorption illustrates the rate of adsorbate uptake by the adsorbent at predetermined interval and equilibrium contact time. The kinetic parameters are essential for the calculation of adsorption rate, providing significant information for designing and modeling the process (Kalavathy *et al.,* 2005). Nevertheless, the characteristics of the sorption process will entirely depend on physical and chemical properties of the sorbate, sorbent and also on the operating variables (Vadivelan and Kumar, 2005).

Table 3.3 lists some of the works reported in the literature on adsorption kinetics of lead, copper and manganese using various adsorbents. It was observed that most of the equilibrium data fitted well with the pseudo-first-order or pseudo-second-order kinetic models. However, some other sorbent-sorbate systems were also found to follow intraparticle diffusion model and Elovich equation.

Table 3.3 Adsorption Kinetics of divalent lead, copper and manganese on different adsorbents

Adsorbate	Adsorbent	Kinetic Model	Reference
Lead Pb(II)	Peat	Second Order	Ho and McKay 1998
	Peanut Hull Carbon	First Order	Periasamy and Namasivayam 1995
	Biogas residual slurry	First Order	Namasivayam and Yasmuna 1995
	Kaolinite Clay	First Order	Orumwense 1996
	Biopolymers	First Order	Seki and Suzuki 1996
	Immobalized biomass	First Order	Ramelow *et al.*1994
	Bottom ash	Second Order	Kaur *et al.,* 1991
Copper Cu (II)	Peat	Second Order	Ho *et al*., 1994
	Peanut Hull Carbon	First Order	Periasamy and Namasivayam 1995
	Immobalized biomass	First Order	Ramelow *et al.*1994
	Fly ash	First Order	Panday *et al.*, 1985
	Bottom ash	Second Order	Kaur *et al.*, 1991
	Coir pith carbon	First Order	Namasivayam and Kadirvelu 1997
	H_3PO_4 treated Rubber wood Sawdust	First Order, Second Order and Intra Particle Diffusion	Kalavathy *et al.*, 2005
	Raw and Acid Treated Corn cob	First Order and Second Order	Abideen *et al.*, 2011
Manganese Mn (II)	Fly ash	First Order	Sharma *et al.*, 2007
	Electric Arc Furnace Slag	First Order and Second Order	Beh *et al.*, 2010
	Cow bone charcoal	First Order and Second Order	Moreno *et al.*, 2010

3. 4.1Pseudo-First-Order Kinetic Model

The pseudo-first-order kinetic model has been widely used to predict sorption kinetics (Baral *et al.,* 2009). The model is defined as (Langergren and Svenska, 1898):

$$\frac{dq}{dt} = k_1(q_e - q_t) \tag{3.9}$$

Integrating Equation (3.9) with respect to boundary conditions q=0 at t=0 and $q=q_t$ at t=t, yields Equation (3.10).

$$log(q_e - q_t) = logq_e - k_1 \frac{t}{2.303} \tag{3.10}$$

The initial rate of sorption, h is determined by following equation:

$$h = k_1 q_{e,cal} \tag{3.11}$$

where q_e and q_t are the amounts of adsorbate adsorbed (mg/g) at equilibrium and at time t (minute) respectively, h (mg/g-min) is the initial rate of sorption and k_1 (l/min.) is the adsorption rate constant. The plot of ln (q_e-q_t) versus t gives the slope of k_1, and intercept of Lnq_e. However, it is observed that the pseudo-first-order equation does not fit well with the complete range of contact time. It is commonly relevant for the initial stage of the sorption processes (Ho and McKay, 1999).

3.4.2 Pseudo-Second-Order Kinetic Model

The pseudo-second-order equation predicts the behavior over the whole range of the adsorption process and appears to be controlled by the chemical sorption mechanism as the rate controlling step. The pseudo-second-order equation based on equilibrium adsorption is expressed as (Ho and McKay, 1998):

$$\frac{dq}{dt} = k_2(q_e - q_t)^2 \quad (3.12)$$

Separating the variables in Equation 3.12 gives the following Equation of 3.13.

$$\frac{dq}{(q_e - q_t)^2} = k_2 dt \quad (3.13)$$

Integrating Equation (3.13) with respect to boundary conditions q=0 at t=0 and q=q_t, at t=t, yields Equation (3.14).

$$\frac{t}{qt} = \frac{1}{k_2 q_e^2} + \frac{1}{q_e} t \quad (3.14)$$

$$h = k_2 q_e^2 \quad (3.15)$$

where, k_2 (g/mg h) is the rate constant of second-order adsorption and h (mg/g-min) is the initial rate of sorption. The linear plot of t/q_t, versus t gives l/q_e as the slope and $1/k_2 q_e^2$ as the intercept.

3.4.3 Elovich Equation

Elovich equation is one of the most frequently used model for describing chemisorption. The Elovich equation is given as (Ozacar and Sengil, 2005):

$$\frac{dq_t}{dt} = ae^{-bq_t} \quad (3.16)$$

The integration of the rate equation with the same boundary conditions as the pseudo first- and second-order equations give Elovich equation:

$$q_t = \left(\frac{1}{b}\right) ln(ab) + \frac{1}{b} \ln t \qquad (3.17)$$

where, a (mg/g h) is the initial sorption rate and b (g/mg) is related to the extent of surface coverage and activation energy for chemisorption. The parameters (1/b) and (1/b) ln (ab) can be obtained respectively from the slope and intercept of the linear plots of q_t versus lnt. The value of (1/b) is indicative of the number of sites available for adsorption while the (l/b) ln (ab) is the adsorption quantity when lnt is equal to zero; i.e., the adsorption quantity when time t is 1. This value is helpful in understanding the adsorption behavior of the first step (Tseng, 2006; Wu and Tseng, 2006).

3.5 Adsorption Mechanism

The aforementioned models can not describe the diffusion mechanism of the solute into the interior of the sorbent. The experimental data is usually fitted with intra-particle diffusion equations to observe the diffusion process.

3.5.1 Intraparticle Diffusion Model

Intraparticle diffusion model is used to test the role of diffusion as the rate controlling step in the sorption process. It is an empirically found functional relationship. It is commonly observed for most of the sorption processes. It is anticipated that uptake varies almost proportionally with the square root of time, $t^{1/2}$ rather than with the contact time t. Based on the theory proposed, intraparticle diffusion model is defined as (Weber and Morris, 1962):

$$q_t = k_{id} t^{1/2} + C \quad (3.18)$$

where, k_{id} (mg/g h), the intraparticle diffusion rate constant, is obtained from the slope of the straight line of q_t versus $t^{1/2}$, C gives an idea about the thickness of boundary layer, i.e., the larger the intercept, the greater the boundary layer effect (Tan *et al.*, 2008). If intraparticle diffusion occurs, then q_t, versus $t^{1/2}$ will be linear. If the linear plots pass through the origin, then the rate limiting process is governed by the intraparticle diffusion that is particle diffusion is involved in the rate controlling step. Otherwise, some other mechanism along with intraparticle diffusion is also involved in the sorption process.

For intraparticle diffusion plots, the first, steeper region represents the immediate sorption or external surface sorption. The second region which is the gradual adsorption stage reflects that intraparticle diffusion is the rate limiting step. In few cases, the third region is present, which is the concluding part of sorption stage, where intraparticle diffusion starts to slow down due to low sorbate concentrations remaining in the solutions (Wu *et al*., 2005).

The three chronological steps in the adsorption are film diffusion, particle diffusion and absorption (Tan, 2008). At initial stage, the adsorbate ions travel towards the exterior surface of the adsorbent which is termed as film diffusion. After small fraction of adsorbate attaches onto the outside surface of the adsorbent, particle diffusion starts in which the adsorbate ions travel within the pores of the adsorbent. The final stage is termed as absorption where adsorbate ions attach themselves inside the

interior surface of the sorbent. The final stage or third step is generally very rapid thus it cannot be treated as rate limiting step.

If external transport> internal transport, rate is governed by particle diffusion. If external transport < internal transport, rate is governed by film diffusion and if external transport≈ internal transport, the transport of adsorbate ions to the boundary may not be promising at a noteworthy rate (Mittal *et al*., 2008). Overall the adsorption process can be depicted by following Figure 3.2 (Datchaneekul, 2005).

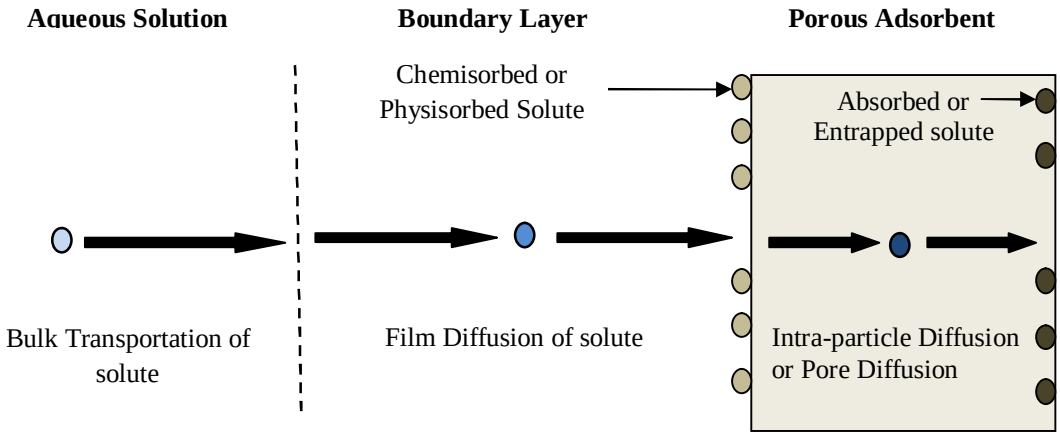

Figure 3.2 Steps in adsorption process

3.6 Validity of Kinetic Model

The applicability of the kinetic models to describe the adsorption process can be validated by both the correlation coefficient, R^2 value and also the normalized standard deviation, Δq (%), which is defined as:

$$\Delta q\ (\%) = 100 \sqrt{\frac{\sum[(q_{t,exp} - q_{t\ cal})/q_{t,exp}]^2}{(N-1)}} \quad (3.19)$$

where, N represents the number of data points, $q_{t,exp}$ and $q_{t,cal}$, (mg/g) are the experimental and calculated adsorption uptake at time t, respectively (Ahmad, 2006).

3.7 Adsorption Thermodynamics

The thermodynamic parameters including standard enthalpy (ΔH°), standard entropy (ΔS°) and standard Gibb's free energy (ΔG°) should be evaluated. According to the concept of thermodynamics, in an isolated system where the energy cannot be gained or lost, the entropy change is the driving force (Kumar and Kumaran, 2005) for sorption. The value of ΔH° and ΔS° can be calculated by using the following Equation:

$$\ln K_L = \frac{\Delta S^\circ}{R} - \frac{\Delta H^\circ}{RT} \quad (3.20)$$

Here, K_L (l/mg) is Langmuir Isotherm constant at different temperature; R is universal gas constant (8.314 J/mol-K) and T is the absolute temperature in Kelvin. The values of ΔH° and ΔS° can be determined from the graph of ln K_L versus 1/T) and T is the absolute temperature in Kelvin. The values of ΔH° and ΔS° can be determined from the slope and intercept of the graph of ln K_L versus 1/T (Wu, 2007). ΔG° can be calculated by using following Equation:

$$\Delta G^\circ = RT \ln K_L \quad (3.21)$$

Table 3.4 lists some previous works reporting thermodynamics of sorption of lead, copper and manganese on different types of adsorbent.

Table 3.4 Thermodynamics Characterization of lead, copper and manganese onto different types of adsorbent

Adsorbate	Type of Adsorbent	Temperature, °K	ΔH° (kJ/mol)	ΔG° (kJ/mol)	ΔS° (J/Kmol)	References
Lead Pb(II)	China Clay	293	-77.95	-8.08	-238.46	Yadava *et al*., 1991
		303		-4.53		
		313		-3.07		
	Wollastonite	293	-16.40	-2.36	-47.98	Yadava *et al*., 1991
		303		-1.58		
		313		-1.05		
	Bagasse fly Ash	303	+11.44	-3.43	48.30	Gupta and Ali, 2004
		313		-3.18		
		323		-3.20		
Copper Cu(II)	SDS-modified montmorillonite	Room Temperature	+7.05	-9.66	+9.09	Lin and Juang 2002
	Kaolinite	Room Temperature	+39.52	-4.61	+0.117	Yavuz *et al.*, 2003
	Sawdust	303	23.40	+21.37	+0.149	Azmal *et al*., 1998
		313		+23.54		
		323		+24.31		
Manganese Mn (II)	Kaolinite	Room Temperature	+36.73	-6.69	+0.101	Yavuz *et al.*, 2003

3.8 Fixed-Bed Adsorption

Batch adsorption studies are often complemented by dynamic continuous flow column sorption studies to determine the amount of adsorbent, system size requirements and contact time where these parameters can be obtained from the breakthrough curves. Batch reactors are easy to design and operate in laboratory scale study, but less convenient for large scale industrial applications.

The utilization of powdered (PAC) and granular (GAC) activated carbon depends on price, existing equipment, usage rate of carbon and contaminants level in the residual slurry. If the usage rate is 250 kg/day, then recycling and reuse of granular activated carbon is not feasible. In that scenario, powdered activated carbons (PAC) are suitable as the operating cost by using PAC in batch reactor is lower (Balachandran, 2004). For higher carbon usage rate, application of GAC with regeneration and recycling is effective. For different types of process industries where the flow rate, concentration of the contaminants and composition of the residual slurry varys significantly, GAC is preferable. In that case ample amount of GAC would be present to compensate the variations (Balachandran, 2004).

In static mode batch adsorption studies, the same solution remains in contact with a certain quantity of the adsorbent. The adsorption process continues until equilibrium is established between the solute present in liquid phase and the solute sorbed per unit weight of the sorbent. The equilibrium established is static in nature as it does not change significantly with time. In fixed bed adsorption, influent solution continuously enters and leaves the column packed with sorbent. Consequently, complete equilibrium is never established at any stage between the solute present in the solution and the amount adsorbed. It reflects that, equilibrium has to be continuously established for each time as it comes into contact with the fresh concentrations. That is why, equilibrium system in column mode/fixed bed is termed as dynamic equilibrium of sorption. The performance of continuous adsorption by using fixed bed packed with GAC is explained in terms of breakthrough curve. The time required for breakthrough and the shape of the breakthrough curves are very important characteristics for evaluating the dynamic response of an adsorption system (Malkoc *et al.*, 2006).

Figure 3.3(a) shows different steps in column sorption process whereas Figure 3.3(b) illustrates the breakthrough curve as a function of contact time.

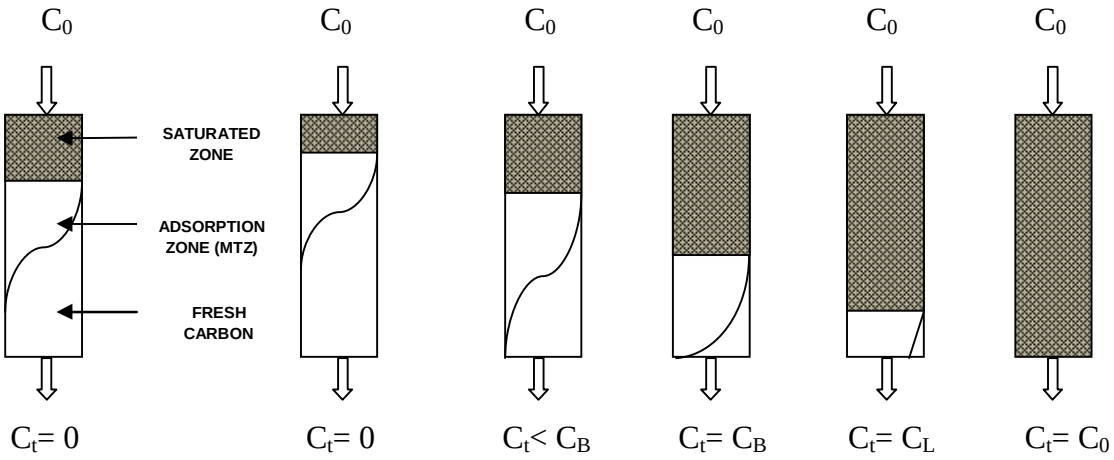

Figure 3.3 (a) Steps in column adsorption

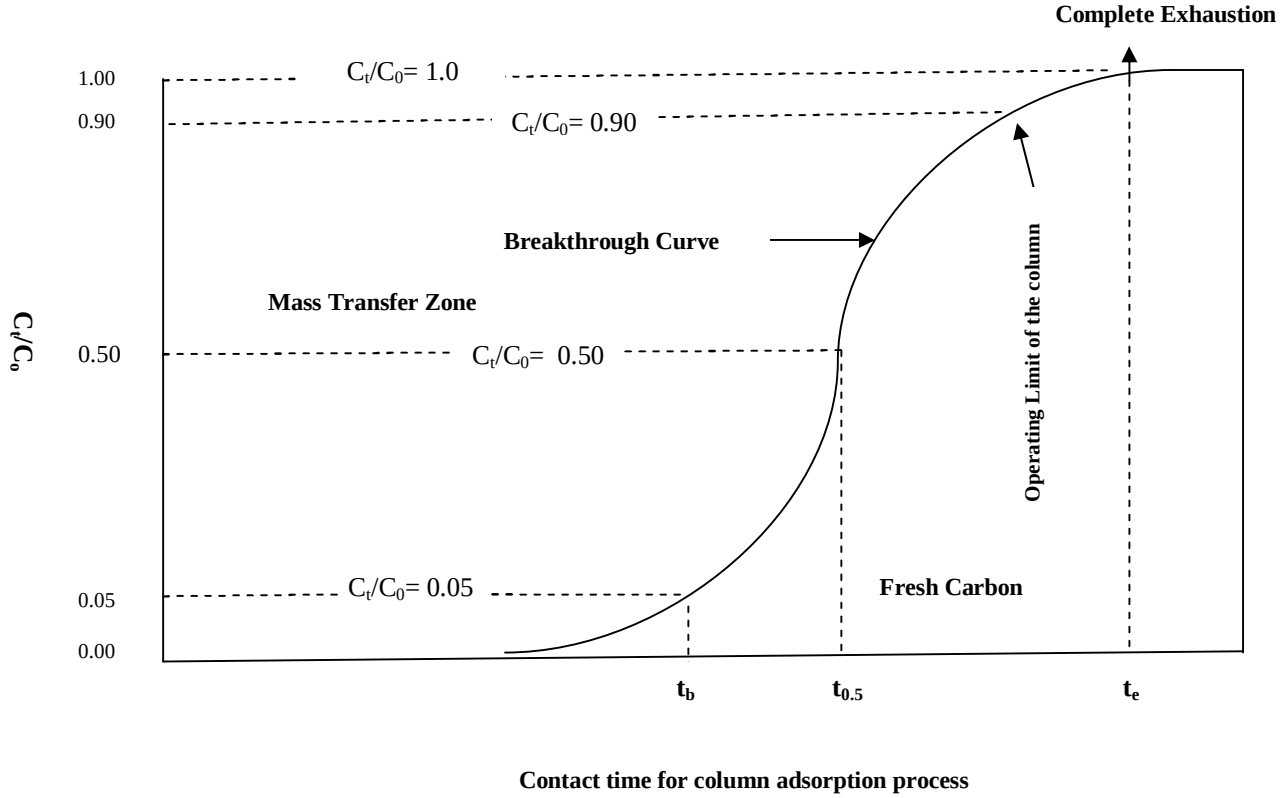

Figure 3.3 (b) Breakthrough Curve characteristics in column adsorption process with respect to time

In a fixed bed column, the flow of polluted water creates a wave front through the adsorbent bed (Figure 3.3 (a)). The wave front near the inlet side is known as mass transfer zone (MTZ). The sorption process takes place in mass transfer zone. As the activated adsorbent becomes exhausted with time, the mass transfer zone moves forward across the adsorbent bed. As the mass transfer zone travel forward, it leaves behind the portion of adsorbent bed which is saturated by the contaminants. When the edge of the mass transfer zone reaches the end of the column breakthrough occurs. The graphical representation for the movement of MTZ zone through the column is called breakthrough curve. However, the breakthrough point is usually defined as the point when the ratio between influent, C_0 (mg/l) or effluent and outlet concentration, C_t (mg/l) becomes 0.05-0.1 at time t_b (minutes) as illustrated by Figure 3.3(b).The adsorbent from the column is usually replaced when the ratio between the inlet and outlet concentration, C_t/C_0 becomes 0.50 at time $t_{0.5}$ (minutes) in case of industrial scale application i.e., 50% breakthrough of the column. The column sorption capacity is calculated at this point (Baral *et al.,* 2009). After 50% breakthrough point, the column can still operate until the ratio C_t/C_0 becomes 0.90. This point is termed as operating limit of the column (Figure 3.3 (b). The column will be completely exhausted when the pre-determined inlet concentration is almost equal to the outlet concentration i.e., $C_0 \approx C_t$ (Figure 3.3 (a)) at time t_e (minutes). In this study, the column sorption capacity for removal of adsorbate at 50% breakthrough (mg/g) was estimated using Treybal equation (Treybal, 1980; Baral *et al.,* 2009):

Adsorption column capacity at 50% breakthrough

= [Breakthrough time (at 50%) (min.) × flow rate (ml/min) × feed concentration (mg/l)]/mass of adsorbent in bed (g) (3.22)

3.9 Breakthrough Curve Modeling

3.9.1 Thomas Model

The hypothesis of Thomas or reaction model is based on the postulation that the sorption process follows Langmuir kinetics of adsorption-desorption. This model presumes that no axial dispersion is present for sorbate-sorbent interactions. The rate of column dynamics obeys 2nd order reversible reaction kinetics. The sorption phenomenon will have constant separation factor. This model is applicable to either favorable or unfavorable isotherm.

The linearized expression developed by Thomas (Thomas, 1944) model is given by:

$$\ln\left[\left(\frac{C_0}{C_t}\right)-1\right] = \left(\frac{k_{Th}q_0 m}{Q}\right)-\left(\frac{k_{Th}q_0 V_{eff}}{Q}\right) \quad (3.23)$$

where k_{Th}, (ml/mg-min) is the Thomas rate constant q_0 (mg/g) is the equilibrium adsorbate uptake, Q is flow rate (ml/min) and m is the amount of adsorbent in the column.

3.9.2. The Yoon-Nelson Model

Yoon and Nelson developed a relatively simple model to analyze the breakthrough performance of the column (Yoon and Nelson, 1984). Previous literature stated that, the rate of decrease in the probability of adsorption for each adsorbate molecule is proportional to the probability of adsorbate adsorption and the probability of adsorbate breakthrough on the adsorbent (Baral *et al.*, 2009).

The linearized model for a single component system is expressed as:

$$\ln\left[\frac{C_t}{C_0 - C_t}\right] = k_{YN}t - \tau k_{YN} \quad (3.24)$$

where k_{YN} (min^{-1}) is the rate constant and τ is the time required for 50% adsorbate breakthrough (Baral *et al.*, 2009).

3.9.3 Bohart-Adams model

Bohart and Adams proposed a basic equation relating the relationship between C_t/C_o and t (minute) in the case of column dynamics studies for the sorption of chlorine on charcoal (Bohart and Adams, 1980). This model is developed based on the surface reaction theory. It predicts that equilibrium is not instantaneous. Therefore, the rate of adsorption is proportional to both the remaining capacity of the adsorbent and the concentration of the adsorbate (Goel *et al.*, 2005). The initial part of the breakthrough curve can be analyzed by Bohart-Adams mode (Aksu and Gonen, 2004). The mathematical equation of the model can be written as:

$$In\left(\frac{C_t}{C_0}\right) = k_{AB}C_0 t - k_{AB}N_0\left(\frac{z}{U_0}\right) \quad (3.25)$$

where, C_0 and C_t are the inlet and outlet adsorbate concentrations respectively, z(cm) is the bed height, U_o (cm/min) is the superficial velocity. N_o (mg/l) is the situation concentration and k_{AB} (l/mg min) is the mass transfer coefficient (Baral *et al.*, 2009). The

range of time in this study was considered from the beginning to the end of the breakthrough curve.

3.10 Summary

Different adsorbent-adsorbate systems were reported to show divergent adsorption behaviors and mechanism as the performance of each adsorption system was significantly influenced by the physical and chemical properties of the adsorbent and the adsorbate as well as other operating parameters such as adsorbate initial concentration, contact time, solution pH and temperature. In this research attempts have been taken to prepare activated sorbent (Chapter 5) and consequently study their surface characteristics (Chapter 6) and performance (Chapter 7 and 8) for batch and fixed bed adsorption system. The theory explained in this chapter is used to estimate the process parameters in batch (Chapter 7) and fixed bed (Chapter 8) sorption system.

CHAPTER FOUR
MATERIALS AND METHODS

4.1 Introduction

This chapter provides the list of chemicals and reagents and the description of major equipments which were used to carry out the research. The chapter is subdivided into three sections. The first section contains the list of chemicals and reagent along with physio-chemical characteristics of the adsorbate; Pb (II), Cu (II) and Mn (II) ions whereas the second section gives the description of the structure and operational features of the major equipments used including the drawing of the experimental setup, surface characterization systems used for activated carbon and activated palm ash. The analysis systems for the adsorbate ions are described in section two also. The third section contains experimental procedure for preparing adsorbent by using design of experiment (DOE), model development and ANOVA analysis, batch sorption studies, kinetics and thermodynamics studies. Column dynamics for fixed-bed sorption system is explained. The process used for regeneration of the cations loaded sorbent in batch and fixed bed sorption system is described. The chapter ends with a schematic flow chart reflecting generally the experimental activities undertaken to carry out the project.

4.2 Materials

The materials used are divided into three main sub categories; comprises of the agricultural residues to prepare adsorbent, chemicals to prepare adsorbate solution, reagents and gases.

4.2.1 Raw materials to prepare powdered and granular adsorbent

The agro-based residues which were selected as the precursors for preparation of activated carbons were kenaf core (KC), Kenaf fibre (KF) and mangostene fruit shell (MFS). These residues were collected from MARDI (Malaysian Agricultural Research and Development Institute) and local markets in Malaysia. The above mentioned indigenous precursors were converted to activated carbon and their performance is compared with activated oil palm ash sample (AOPA).The natural oil palm ash (OPA) was collected from middle fraction of the flue tower from United Palm Ash Mill, Penang, Malaysia. Plate 4.1 shows the raw materials used in this work to prepare activated adsorbents.

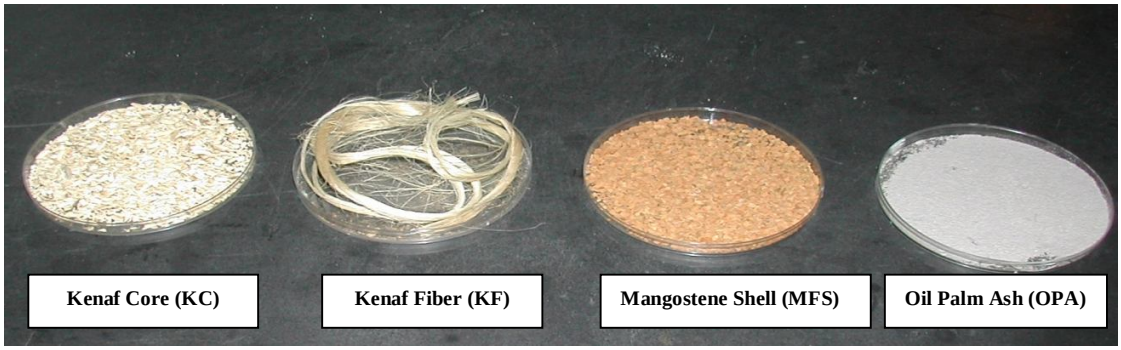

Plate 4.1 Agricultural Residues used for preparing activated adsorbent

4.2.2 Reagents and Chemicals

The list of reagents and chemicals used in this research as well as their respective suppliers, purity grade and applications are given in the Table 4.1. Before starting the experimental activities in the laboratories, the Material Safety Data Sheet (MSDS) of all the reagents and chemicals used in this research were examined and understood.

Table 4.1 List of Reagents and Chemicals

Chemicals/Reagent	Supplier	Purity Grade	Application
Anhydrous Lead Nitrate, $Pb(NO_3)_2$	Merck, Germany	98-99%	To prepare adsorbate solution
Copper sulfate penta hydrate,$CuSO_4.5H_2O$	Merck, Germany	98-99%	To prepare adsorbate solution
Manganese Chloride di hydrate,$MnCl_2.2H_2O$	Merck, Germany	98-99%	To prepare adsorbate solution
Sodium hydroxide	Merck, Germany	98-99%	As an activating agent & for pH adjustment
Hydrochloric acid	BDH Chemicals	Analytical Reagent	To adjust the pH
Potassium Hydroxide	Merck, Germany	98-99%	As an activating agent

Considering the eco toxic properties of Pb (II), Cu (II) and Mn (II) cations, these three cations were selected as the adsorbate in this research to evaluate the adsorption performance of the powdered (KCAC, KFAC and AOPA) and granular activated adsorbent (MFSAC).

4.2.3 Gases

In this study, nitrogen gas (N_2) and carbon dioxide (CO_2) gas in semi carbonization step and activation step were used for the preparation of powdered and granular activated carbon. Table 4.2 lists the suppliers and the purities of both the gases.

Table 4.2 List of Gases

Gases	Supplier	Application	% Purity Grade
Purified Nitrogen Gas	Mox Gases Berhad, Malaysia	Purging gas	99.99
Purified Carbon di oxide	Mox Gases Berhad, Malaysia	Physical activating agent	99.99

4.3 Preparation of Adsorbate Solution

Stock solution of single solute of Pb (II), Cu (II), and Mn (II) were prepared by dissolving requisite amount of lead nitrate, copper (II) sulfate pentahydrate, and manganese (II) chloride dihydrate, respectively in a 1000 ml volumetric flask followed by dilution up to the mark by addition of de-ionized water. The concentration of each single solute in the respective stock solution prepared was 1000 mg/l. The test solutions having concentrations of 50 mg/l, 60 mg/l, 70 mg/l, 80 mg/l, 90 mg/l and 100 mg/l were prepared through fresh dilution of the stock solution prior to each adsorption study by using equation (4.1).

$$M_1V_1 = M_2V_2 \tag{4.1}$$

4.4 Experimental set up for Adsorbent Preparation

The equipments used for this study were generally divided into powdered (KCAC and KFAC) and granular activated carbon (MFSAC) preparation system and refluxing system to activate natural oil palm ash (OPA). The surface characterization system including physical and chemical analysis of the prepared adsorbent, batch and continuous flow adsorption and water analysis system are described in the subsequent section.

4.4.1 Experimental Approach for Preparation of Activated Carbon

The production of all the activated carbons was carried out in a tubular reactor which consists of the following two major parts:

I. Gas transmitting section where the gas flow rates were controlled to the requisite levels.

II. The tubular reactor is made up of stainless steel with a tubular furnace placed outside it.

Plate 4.2 (Appendix B-1) shows the equipment used to prepare powdered (PAC) and granular activated carbon (GAC). At constant pressure, Nitrogen (N_2) and CO_2 gases were passed inside the furnace. The pressure of gas flow was adjusted by using pressure regulators and the flow rates of the gases were controlled by gas flow meters (Model Dwyer RMA-12-SSV, US). The two types of gas streams were combined by using a 3-way valve. The outlet from the valve was connected at the bottom of the reactor. The schematic diagram of the furnace (Figure 4.1) together with the measurement of their important parts is shown in Figure 4.2.

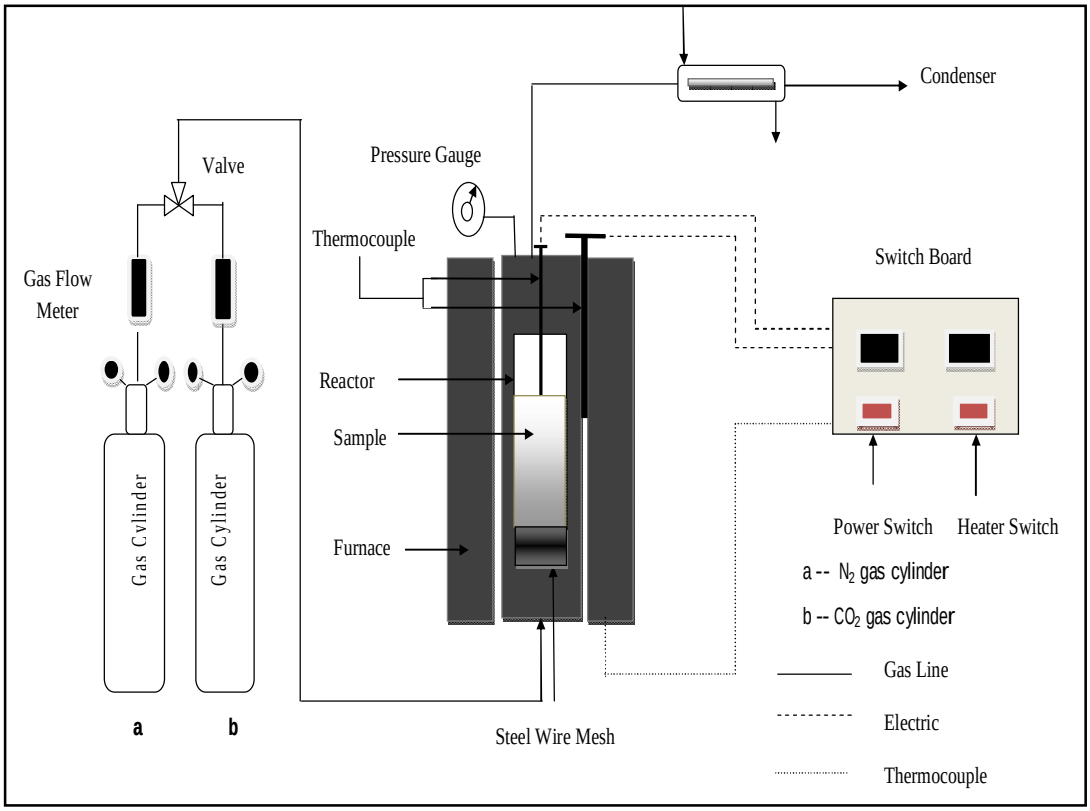

Figure 4.1 Schematic representation of activated carbon preparation unit

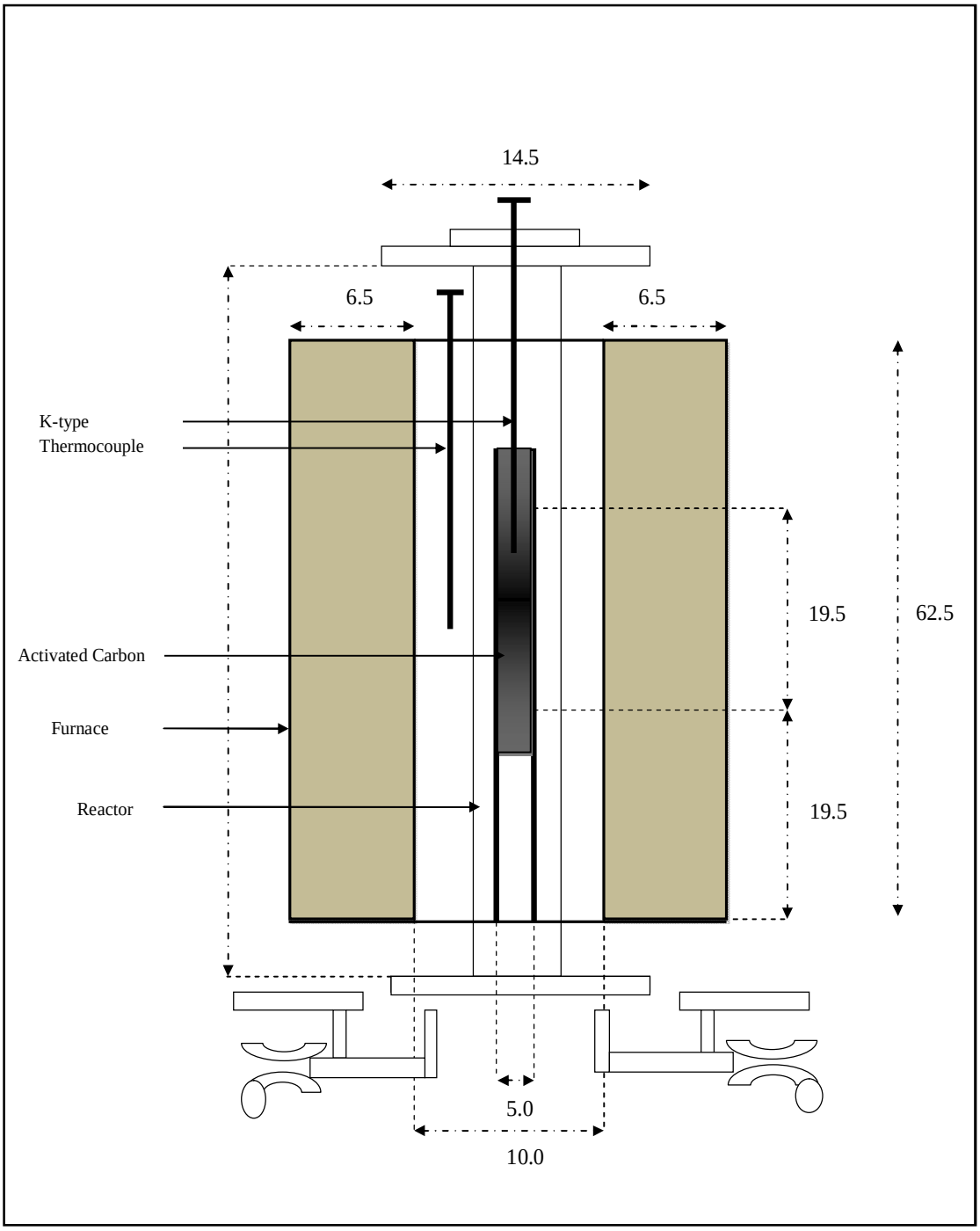

*All dimensions in cm

Figure 4.2 Schematic flow diagram of vertical Tubular Furnace with Reactor

All the connecting piping system inside and outside of the furnace was made up of stainless steel tubing (6.35 mm) which were joined by stainless steel fittings to withstand high temperature and pressure. The char after impregnated with required amount of KOH is placed inside the reactor for pyrolysis. A wire mesh made of stainless steel was placed at the bottom of the tubular reactor to protect the sample from falling outside. The reactor was kept inside the vertical tubular furnace.

The furnace was equipped with programmable system (Model Watlow Series 942, US) to control the rate of heating, desired temperature and residence time. The furnace was 625 mm long with 230 mm inner diameter. The reactor was kept in the centre of the furnace by a support of the same height and width as the reactor. A K-type thermocouple which can withstand maximum temperature limit of 1000 °C was placed inside the char. Another similar type of thermocouple was positioned outside the reactor to measure the temperature of the tubular furnace. The exhaust gas emitted from the reactor was condensed. After condensation, it is collected in a container.

It was reported earlier in the literature that soft precursor like rice husk activated with KOH had a surface area of more than 3000 m^2/g whereas the surface area of the carbon became 2500 m^2/g after NaOH activation (Yupeng *et al.*, 2003). It was concluded by the researcher that intercalation of metallic sodium inside the carbon matrix is less effective than potassium due to its higher boiling point (Yupeng *et al.*, 2003). Activated carbon was produced from red oak, wall nut shell and corncob by using LiOH, NaOH and KOH. It was found that the mass loss for activated carbon obtained by LiOH was highest. This made LiOH an unfavorable activated agent when compared to KOH and NaOH

(Leimkuehler, 2010). That is why in the present research KOH has been chosen as the chemical activating agent rather than NaOH or LiOH.

4.4.2 Experimental Set up for Activated Palm Ash

Previous literature reveals that fly ash type mineral based raw material contains a very small amount of carbon about 1 to 10% depending on the combustion rate (Ahmaruzzaman, 2010). Therefore, no methodological approach has been undertaken to prepare activated carbon from the ash. To prepare effective sorbent from oil palm ash, alkali activation is the best choice. It had been reported that NaOH was more active than KOH in preparing prepare adsorbent from coal fly ash with high surface area under the same temperature (Ahmaruzzaman, 2010). It was also observed that when KOH was added as an additive with rice husk ash (RHA) and CaO, it could not bring sufficient dissolution of silica and extend the surface area of RHA by the reaction between CaO/KOH and RHA (Dahlan *et al.*, 2009).

Based on previous literature (Ahmad, 2006), it was concluded that sodium hydroxide is a better alternative to prepare activated palm ash. Consequently, refluxing under boiling condition was employed to ensure sufficient hydration and to reduce water loss by evaporation over 100 °C of the natural oil palm ash (Ahmad, 2006). However, the optimum condition for refluxing had been determined by varying different operating parameters of temperature, hydration time and ratio of OPA: NaOH by using Design of Experiment (DOE). Plate 4.3 (Appendix B-2) shows the apparatus used to activate natural oil palm ash.

4.5 Experimental Methodology for Adsorbent Preparation

The experimental procedure consisted of preparation of activated carbons and activated oil palm ash, followed by batch adsorption studies of Pb (II), Cu (II) and Mn (II) cations on all the adsorbents prepared which include the equilibrium isotherm modeling and analysis of kinetics and thermodynamics behaviors of the adsorption processes. Fixed-bed adsorption studies were further carried out on the granular activated carbons derived from mangostene fruit shell (MFSAC). Regeneration of the spent adsorbent saturated with cations was done by using distilled water, organic acid (acetic acid), mineral acids (hydrochloric, sulfuric and nitric acid) each of 1M strength.

4.5.1 Preparation of Powdered (PAC) and granular activated (GAC) carbon

For preparation of activated carbon the following steps were undertaken.

4.5.1.1 Preparation of Lignocellulosic Precursors (KC, KF and MFS)

The selected agricultural by-products (KC, KF and MFS) were first washed thoroughly to eliminate dust and inorganic matters on their surfaces. The collected samples of agro residues were dried in an oven (Model Memmert 600, Germany) at a temperature of 105 °C for 24 h to remove all the moisture. The dried precursors were cut or ground into small pieces. They were sieved to the size of 1-2 mm. They were then stored in air-tight containers to avoid moisture build up and fungal infections.

4.5.1.2 Semi- Carbonization

A requisite amount of precursors (40-80 g depending on the category of the precursors) were placed on the metal mesh located at the bottom of the tubular reactor. Purified

nitrogen gas was used to evacuate oxygen and create the inert atmosphere through the reactor. The flow rate of nitrogen gas and the heating, rate was maintained at 150 cm^3/min and 10 °C/min, respectively. The temperature was ramped from room temperature to 400°C and held for 2 hrs. The chars thus produced were allowed to cool at room temperature by passing nitrogen gas over it and then stored in air-tight containers for further treatment.

4.5.1.3 Potassium Hydroxide Impregnation

The chars produced were impregnated with potassium hydroxide (KOH) at various impregnation ratios (IR). The dimensionless impregnation ratio was calculated as:

$$IR = \frac{W_{KOH}}{W_{char}} \quad (4.2)$$

where, W_{KOH} is the dry weight (g) of potassium hydroxide pellets and W_{char} is the dry weight (g) of char.

A specific amount of char and KOH pellets (depending on the IR) were mixed together with deionized water in a 500 ml beaker. The mixture was then stirred until the KOH pellets were completely dissolved. Then, the beaker was placed inside an oven (Model Memmert 600 Germany) overnight at temperature 105 °C. This would dehydrate the sample, leaving only KOH onto the samples. Based on the literature KOH has been chosen as the chemical activating agent as it can disrupt the graphite layer in presence of carbon dioxide and thereby increase the porosity of the activated carbon (Tan, 2008).

4.5.1.4 Carbon Dioxide Activation

The KOH-impregnated chars were placed inside the stainless steel tubular reactor for activation. The condition of heating rate and nitrogen gas flow was the same as the carbonization step. The temperature was ramped from room temperature to the desired activation temperature. When the required activation temperature was reached, the nitrogen gas flow was turned off and carbon dioxide (CO_2) gas flow at the same flow rate was started to initiate activation process. According to the experimental requirement preset by the software, the samples were kept inside for certain duration of time.

The activated products were washed with hot deionized water to recover unreacted KOH. Few drops of hydrochloric acid (0.1 molar) were used during washing the sample. The sample was washed several times with hot deionized water until the pH of the washing solutions reached around 6-7. The pH was measured using a pH meter. The washed activated carbons were then kept in an oven (Model Memmert 600, Germany) at 105°C until the activated carbons were totally dried. Prepared activated carbons were sieved through 200µm mesh size. The dried products were stored in air-tight containers for subsequent characterization and sorption studies.

4.5.1.5 Preparation of Granular Activated Carbon from Mangostene Fruit Shell

The fruit shell was used as the precursor to prepare granular activated carbon due to its hard and dense nature compared to other ligno-cellulosic precursors. The preparation condition was kept fixed in order to analyze and compare its performance for the different adsorbate. The following preparation conditions were used:

- Semi carbonization at 400 °C for 2 hours.
- CO_2 activation temperature: 750 °C
- CO_2 activation time: 2 hours
- KOH: char impregnation ratio: 1:1

The production conditions used to prepare this activated carbon was not optimized as it is known in general that powdered activated carbons (PAC) perform better than granular activated carbons (GAC) in liquid phase adsorption. It is reported earlier that utilization of powdered activated carbon (PAC) for batch adsorbtion system is less expensive compared to granular one (GAC) to fabricate filter bed in a column. The operating cost associated with the design of industrial scale column is also higher. Larger mass of granular activated carbon is used for the filter bed to ensure substantial removal of the adsorbate (Balachandran, 2004). However, this activated carbon was prepared, characterized and its adsorption ability was evaluated in this study for batch and fixed bed sorption for comparison purposes. Prepared activated carbons were sieved through 450-550 µm mesh size to maintain a homogeneous particle size.

Yield is the ratio of final activated carbon with the original precursor before pyrolysis. Yield can be calculated by using Equation 4.3.

$$Yield = \frac{W_2}{W_1} X100 \qquad (4.3)$$

Here,

W_2= Dry weight after activation (g)

W_1= Dry weight of the precursor before pyrolysis (g)

4.5.2 Activation of Oil Palm Ash (OPA)

For activation of natural palm ash, the following steps were undertaken.

4.5.2.1 Collection of natural oil palm ash (OPA)

The lump of natural oil palm ash (OPA) was collected from middle fraction of flue gas chamber and it was grounded to fine powder. It was washed with deionized water for several times to remove foreign particles and oven dried at 110 °C over night. The adsorbent thus obtained was sieved through sieve no 200µm. It was stored in desiccators over fresh silica gel before activation.

4.5.2.2 Activation

According to the preset condition provided by Design of experiment (DOE), the temperature, ratio of OPA: Caustic soda and time were varied to obtain maximum removal percentage. The ratio was calculated by using Equation (4.4).

$$Ratio = \frac{W_{OPA}}{W_{NaOH}} \tag{4.4}$$

where, W_{OPA} is the dry weight (g) of natural oil palm ash (OPA) and W_{NaOH} is the dry weight (g) of caustic soda.

The amount of OPA was changed with fixed amount of sodium hydroxide to obtain a different ratio preselected by the software as well as to maintain the pH level up to a certain desirable limit to develop high surface area of the adsorbent (Zainuddin *et al.*,

2005). The mixture of OPA and NaOH along with water was refluxed in a round bottom flask with a magnetic stirrer placed inside it. The slurry was allowed to cool at room temperature and filtered. The filter cake was repeatedly washed with deionized water until neutral pH of the filtrate was observed. Then it was dried in an oven at 110 °C for 12 hours before use and stored in desiccators over fresh silica gel for further use.

4.5.3 Process Parameter Optimization

Temperature, time and ratio between the starting material and alkali were optimized. The range of variables to develop the adsorbent was predetermined based on literature and physio-chemical characteristics of the raw materials.

4.5.3.1 Application of Central Composite Design for Preparation of Adsorbent

The parameters used for preparing powdered activated carbons (PAC) from KC and KF were studied by using a standard response surface methodology (RSM) based on central composite design (CCD). The activated carbon preparation variables studied were:

i) $x_1 - CO_2$ activation temperature $(°C)$

ii) $x_2 - CO_2$ activation time (h)

iii) $x_3 - KOH$ char impregnation ratio

Table 4.3 and 4.4 summarizes the coded and actual levels of process variables and complete design matrix of the experiments required to prepare powdered activated carbon.

Table 4.3 Independent variables and their coded and actual levels for the central composite design for preparation of PAC.

Variables	Code	Units	Coded Variable Levels				
			-α	**-1**	**0**	**+1**	**+α**
Temperature	x_1	°C	431.82	500	600	700	768.18
Activation Time	x_2	Hour	0.32	1	2	3	3.68
Impregnation Ratio	x_3	-	0.32	1	2	3	3.68

Table 4.4 Experimental Design matrix for preparation of powdered activated carbon (PAC)

		Activated Carbon Preparation variables		
Run No	**Point Type**	**Temperature (°C)**	**Time (Hour)**	**Impregnation Ratio (IR)**
1	Axial	600	3.68	2.00
2	Fact	500	3.00	3.00
3	Fact	700	3.00	3.00
4	Axial	431.82	2.00	2.00
5	Axial	600	2.00	3.68
6	Axial	600	2.00	0.32
7	Fact	500	3.00	1.00
8	Center	600	2.00	2.00
9	Fact	500	1.00	3.00
10	Axial	600	0.32	2.00
11	Center	600	2.00	2.00
12	Fact	700	1.00	3.00
13	Center	600	2.00	2.00
14	Axial	768.18	2.00	2.00
15	Center	600	2.00	2.00
16	Axial	600	2.00	2.00
17	Fact	700	1.00	1.00
18	Fact	700	3.00	1.00
19	Fact	500	1.00	1.00
20	Center	600	2.00	2.00

The activated Palm ash preparation Variables studied were:

i) $x_1 -$ activation temperature $(°C)$

ii) x_2 -- activation time (h)

iii) $x_3 - OPA: NaOH$, impregnation ratio

Table 4.5 and 4.6 summarizes the coded and actual levels of process variables and complete design matrix of the experiments required to prepare activated palm ash.

Table 4.5 Independent variables and their coded levels for the central composite design for preparation of AOPA

Variables	**Code**	**Units**	**Coded Variable Levels**				
			-α	**-1**	**0**	**+1**	**+α**
Temperature	x_1	°C	52.73	80	120	160	187.27
Ratio	x_2	-	2.32	3	4	5	5.68
Time	x_3	Hour	2.64	4	6	8	9.36

Table 4.6 Experimental Design matrix for preparation of activated palm ash (AOPA)

Run No	Point Type	Activated Palm Ash Preparation variables		
		Temperature(°C)	Ratio (IR)	Time (Hour)
1	Fact	80	5.00	4.00
2	Center	120	4.00	6.00
3	Axial	187.27	4.00	6.00
4	Center	120	4.00	6.00
5	Fact	160	5.00	8.00
6	Fact	80	5.00	8.00
7	Fact	160	3.00	4.00
8	Axial	120	5.68	6.00
9	Center	120	4.00	6.00
10	Center	120	4.00	6.00
11	Center	120	4.00	6.00
12	Fact	80	3.00	4.00
13	Fact	80	3.00	8.00
14	Axial	52.73	4.00	6.00
15	Axial	120	2.32	6.00
16	Center	120	4.00	6.00
17	Axial	120	4.00	9.36
18	Axial	120	4.00	2.64
19	Fact	160	5.00	4.00
20	Fact	160	3.00	8.00

According to basic principal of DOE, 20 experimental run were required for studying the effects of three variables to prepare the adsorbent. Equations 4.5 and 4.6 were used for regression analysis and evaluation of statistical parameters involved in the process.

4.5.3.2 Development of Regression Model Statistical Analysis

For each categorical variable, a 2^3 full factorial CCD for the three numerical variables, consisting of 8 factorial points (coded as -1 and +1), 6 axial points (coded as -1.682 and +1.682) and 6 replicates at the center points (coded as 0,0) were employed. This indicated that 20 experiments were required for this procedure for each precursor, as calculated from Equation 4.5.

$$N = 2^n + 2n + n_c = 2^3 + 2 * 3 + 6 = 20 \quad (4.5)$$

where, N is the total number of experiments required and n is the number of factors. The center points (n_c) were used to determine the experimental error and estimate the reproducibility of the data. The experimental sequence was randomized. This will minimize the effects of the uncontrolled factors.

In the design matrix, the low and high levels were coded as -1 and + 1 values respectively. Figure 4.3 illustrates the layout of the design matrix used in this research. The factorial points are forming the box whereas the axial points are placed at the end of the dotted lines which are coming out from the center point. ±α represents the distance between axial points and center point (0, 0). The coordinates of axial points are (±α, 0, 0), (0, ±α, 0) and (0, 0, ±α). The center points are considered as an indicator to elucidate the variability in the system.

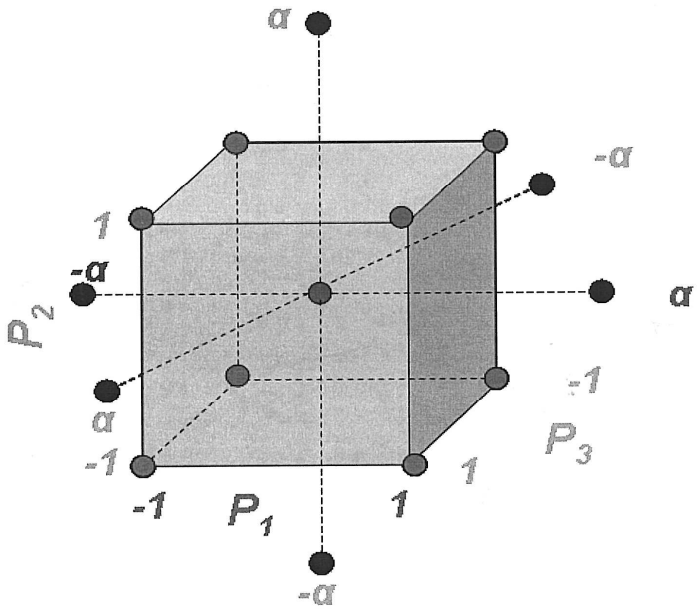

Figure 4.3 Design Layout of Central Composite design (CCD) to study 3-parameter process (Montgomery, 2001)

Each response of the removal percentage of lead (Y_1), copper (Y_2), manganese (Y_3) and activated carbon yield (Y_4) was used to develop an empirical model that correlates the responses to the preparation variables using a second-degree polynomial equation as given by Equations 4.6 and 4.7 (Zainudin *et al.,* 2005).

$$x_i = \frac{X_i - X_i^x}{\Delta X_i} \tag{4.6}$$

Where x_i is the coded value of the ith independent variable, X_i is the natural value of the ith independent variable, X_i^x denotes the natural value of the ith independent variable at the center point, and ΔX_i is the value of step change.

$$Y = b_o + \sum_{i=l}^{n} b_i x_i + (\sum_{i=l}^{n} b_{it} x_t)^2 + \sum_{i-l}^{n-l} \sum_{j=i=l}^{n} b_{ij} x_i x_j \quad (4.7)$$

where, Y denotes the predicted response, b_0 reflects the constant coefficient, b_i the linear coefficients, b_{ij} the interaction coefficients, b_{ii} the quadratic coefficients and $x_i x_j$ are the coded values of the activated carbon preparation variables (Zainudin *et al.,* 2005).

Design Expert software version 6.0.6 (STAT-EASE Inc. Minneapolis, US) was used to fit the experimental data and regression analysis of the developed model. The statistical significance of the model was observed. CCD was used to develop the correlation between the three activated carbon preparation variables to the four responses for each types of precursor.

4.6 Experimental set up for Batch Adsorption Studies

Batch equilibrium tests were carried out for adsorption of Pb (II), Cu (II) and Mn (II) on all types of adsorbent prepared. Adsorption studies were carried out using Erlenmeyer flasks (100 ml) with glass stoppers. The freshly prepared solutions of adsorbate having different initial concentrations were placed in these flasks. A definite amount of adsorbents were placed to the flasks and were kept inside an isothermal water-bath shaker (Haake Wia Model, Japan) for a definite period of contact time. The water-bath shaker was equipped with a temperature controller which could be set from 25 to 100 ±0.1 °C and agitation speed could be controlled up to 250 ±1 rpm. The shaker had a cover which could prevent heat loss to the surroundings. The effects of initial adsorbate concentration, contact time, solution temperature and solution pH at constant agitation speed of 150 rpm for adsorption

uptake and percentage removal were investigated. 0.2 gm of prepared adsorbent was added with 50 ml solution of different concentrated solutions at pH 5.5 to ensure true adsorption. The sample solutions were withdrawn at equilibrium to determine the residual concentrations. The solutions were filtered using syringe filter (Model Whattman 0.45 pm, UK) prior to analysis. The concentrations were measured using Atomic adsorption Spectrophotometer (Model Perkin Elmer- 3100, Japan). The amount of adsorbate adsorbed at equilibrium contact time, q_e (mg/g) was calculated according to Equation 4.8 whereas the percent removal of adsorbate was calculated using Equation 4.9.

$$q_e = \frac{(C_o - C_e)V}{W} \tag{4.8}$$

$$Removal\ (\%) = \frac{(C_o - C_e)}{C_o} x100 \tag{4.9}$$

where, C_o and C_e (mg/L) are the liquid-phase concentrations of adsorbate at initial and at equilibrium contact time, respectively. V is the volume of the solution (l) and W is the mass of adsorbent used (g) (Ahmad, 2006; Tan, 2008).

4.6.1 Effects of Initial Adsorbate Concentration and Contact Time

In order to study the effects of initial cation concentration and contact time on the adsorption uptake and percentage removal, 50 ml of adsorbate solutions with known initial concentrations (50-100 mg/l) were prepared in a series of 100 ml Erlenmeyer flasks. 0.2 g of adsorbent was placed inside the flask. The flasks were covered with stopper to prevent water loss by evaporation and the flasks were then placed in an isothermal water bath shaker at constant temperature of 30 ℃, with agitation speed of 150 rpm.

4.6.2 Effect of Solution Temperature

The effect of solution temperature on the adsorption process was studied by varying the adsorption temperature at 30, 50 and 70 °C by using the temperature control system of the water bath shaker **(**Haake Wia Model, Japan**)**, while other process parameters such as adsorbent dosage, agitation speed, pH 5.5 and volume of the solution remained constant.

4.6.3 Effect of Solution pH

The effect of solution pH was monitored by changing the initial pH of the solutions from 2 to 12. The pH was adjusted by using 0.1 M hydrochloric acid or 0.1 M sodium hydroxide and was measured using a pH meter (Mettles Toledo, Model: Ross FE 20, USA). The initial adsorbate concentration was fixed at 100 mg/l with adsorbent dosage of 0.2 g/50 ml and solution temperature of 30 °C.

4.6.4 Adsorption Isotherms

Adsorption isotherm study was carried out by fitting the equilibrium data to three isotherm models: the Langmuir, Freundlich and Temkin isotherm models. The applicability of the isotherm equation to the equilibrium data was explained by observing the values of the correlation coefficients, R^2. According to the regression analysis, the higher the R^2 value (closer to unity), the better is the model for depicting the isotherm parameters (Ahmad, 2006; Tan, 2008).

4.6.5 Batch Kinetic Studies

The methodology for evaluation of kinetic parameters was identical to that of batch equilibrium experiments. The aqueous samples were taken at predetermined time intervals

and the concentrations of the residual solute in the solutions were similarly measured. The amount of uptake at any time t, q_t, (mg/g), was calculated by Equation 4.10.

$$q_t = \frac{(C_o - C_t)V}{W} \quad (4.10)$$

where C_0 and C_t, (mg/'L) are the liquid-phase concentrations of adsorbate at initial and at any time t, respectively. V is the volume of the solution (L) and W is the mass of adsorbent used (g) (Tan *et al.*, 2008).

4.6.6 Adsorption Thermodynamics

In order to study the thermodynamic behaviors of the adsorption of lead, copper and manganese onto the prepared adsorbent in this study, the experimental data obtained from the batch adsorption experiment conducted earlier were analyzed using the thermodynamic equations expressed by Equations 3.20-3.21, The values of ΔH° and ΔS° were calculated respectively from the slope and intercept of the Vant's Hoff plot of In K_L versus l/T, where K_L (l/mg) is the Langmuir isotherm constant and T is absolute temperature in Kelvin.

4.7 Experimental Set up for Fixed Bed Adsorption

Figure 4.3 represents the schematic diagram of the fixed-bed adsorption system used for the granular adsorption system. Continuous flow adsorption studies were conducted in a column made of Pyrex glass tube of 3.5 cm inner diameter and 25 cm height. A sieve made up of stainless steel was placed at the bottom of the column. Over the sieve, a layer of glass wool was placed to prevent loss of adsorbent. A peristaltic pump (Model Masterfiex, Cole-Parmer Instrument Co., US) was used to pump the feed upward through the column at a

desired flow rate. The solution was pumped upward to avoid channeling due to gravity. It will provide uniform distribution of the solutions through the column. The stock solutions were placed in a tank and were connected with a pipe through which the water will pass through the column.

Fixed bed sorption studies were conducted for lead, copper and manganese on MFS based GAC by varying the adsorbate inlet/influent concentration, flow rate of the feed and adsorbent bed height. The effect of adsorbate inlet concentration was studied by changing the concentration from 50mg/l, 70 mg/l and 100 mg/l by keeping the bed height constant at 4.5 cm and feed flow rate of 1 ml/min.

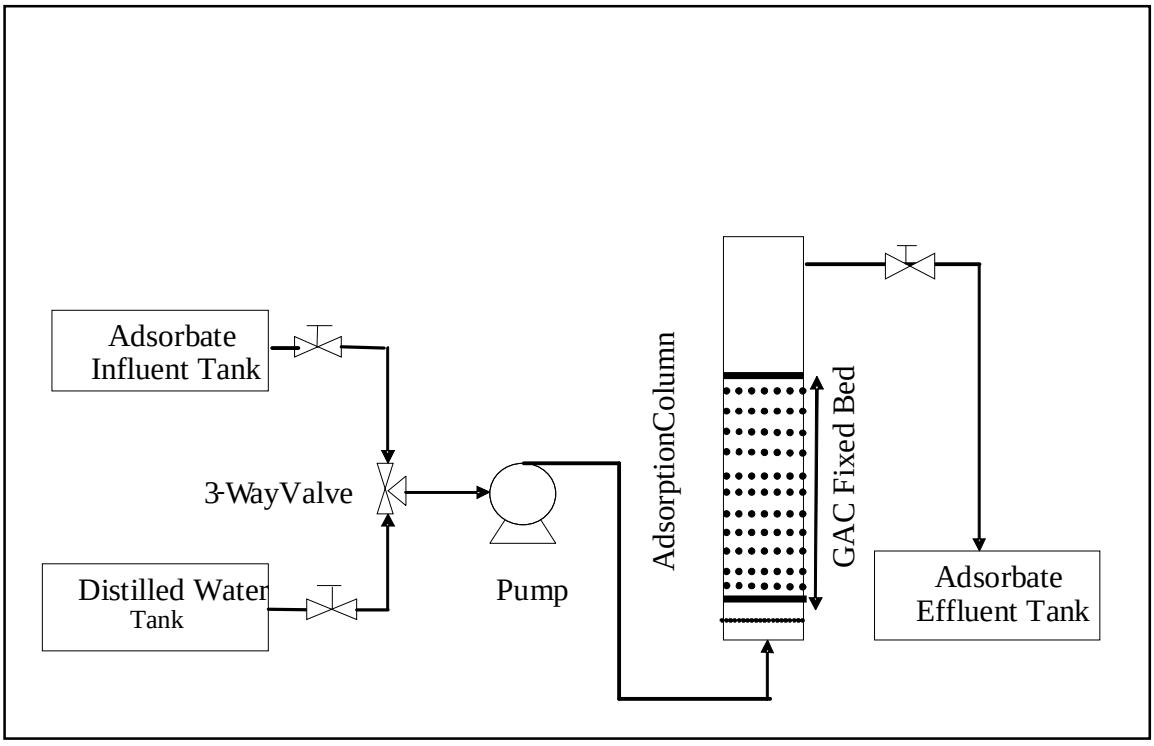

Figure 4.4 Schematic Flow diagram of Fixed Bed System onto GAC

In order to study the effect of activated carbon bed height, two bed height of 3 cm and 4.5 cm at constant flow rate of 1 ml/min and inlet concentration of 100 mg/l were used. The effect of feed flow rate of 1ml/min and 3 ml/min were observed by keeping constant bed height of 4.5 cm and an inlet concentration of 100 mg/l.

For each sorption test, after packing the column with activated carbon, the column was flushed with deionized water for 5 min. to ensure that the closely packed arrangement of GAC has no voids and channels. After a predetermined interval of time, the outlet concentration, C_t mg/l was measured. The breakthrough curves of C_t/C_0 were plotted against time. The maximum column capacity for a given inlet concentration and feed flow rate was calculated by using Equation 3.22.

4.8 Analysis System

The concentrations of the adsorbate under investigation were measured using an atomic adsorption spectrophotometer (Model Perkin Elmer 3100, Japan). The basic principle for single element quantitative analysis using atomic adsorption spectrophotometer is the Beer-Lambert or Beer's Law.

According to Beer – Lambert's Law-

$$A = -\log (I/I_\circ) = -\log T = abc \qquad (4.11)$$

where A = total absorption of light

a = absorptive co-efficient

b = light path

c = the concentration of the absorbing species in the light path, that is analyte concentration.

T = Transmittance

I_o = Incident light intensity

I = transmitted light intensity

The calibration curves were developed by using an Atomic Absorption Spectrophotometer (Perkin Elmer 3100, Japan). It was obtained by aspirating the standard solution into the flame; standard solutions containing known five concentrations; 1, 2, 3, 4 and 5 mg/l of Pb(II), Cu(II) and Mn(II) cations solutions respectively. The calibration curves are shown in Appendix A. The absorption of each solution was determined and the water samples were analyzed against the calibration curve prepared by the standard solutions of the metals (Pb, Cu, and Mn). A blank reagent, i.e., distilled water was also run before the development of the calibration curve and during the interval of each sample. Lead specific hollow cathode lamp (wavelength 283.3 nm), Copper specific hollow cathode lamp (wavelength 324.8 nm), and Manganese specific hollow cathode lamp (wavelength 279.8 nm) were used. The correlation coefficients are provided in Appendix A. Dilution of the samples was performed, and the results were accordingly evaluated using the appropriate dilution factor.

4.9 Surface Characterization System

The raw materials and the prepared adsorbents were characterized by using various techniques to analyze their individual physical and chemical properties. Owing to the different nature of the original starting material in preparing the adsorbent, some tests which were essential to characterize activated carbon were not at all appropriate for activated palm ash. Consequently the following section describes the surface

characterization for both the adsorbent which are necessary in order to understand its sorption mechanism in detail.

4.9.1 Physical Characterization

4.9.1.1 Nitrogen Adsorption-Desorption Isotherms

Surface area, pore volume and pore diameter of the prepared adsorbent was measured by Autosorb 6B, Quantachrome Autosorb Automated gas sorption system supplied by Quantachrome. Before performing the nitrogen gas adsorption-desorption at 77 K, the prepared adsorbent was outgassed under vacuum at 300°C for 4 hours to remove any moisture content from the solid surface. Surface area and pore volume were calculated by Brunauer Emmett Teller (BET). Above mentioned procedure was automatically performed by software (Micropore version 2.26) available within the instrument. The total pore volume was estimated by the liquid volume of nitrogen at a relative pressure of 0.98 cm^3/g. The pore size distribution was determined using the Barrett, Joyner and Halenda (BJH) model by the software (Micropore version 2.26) of the instrument.

4.9.1.2 Scanning Electron Microscopy

The surface morphology showing surface texture, pore structure and arrangements of the pores of prepared adsorbent samples (powdered and granular activated carbon and activated oil palm ash) were taken before preparation as well as after semi carbonization and activation by scanning electron microscopy (SEM) (Model Leo Supra 5OVP Field Emission, UK) . It was carried out by the bombardment of electrons on target sample particle which was spread earlier over an aluminum stub with the help of a doubled edged tape followed by coating of the surface with platinum film by using SEM instrument.

4.9.1.3 Determination of Bulk Density

1 gm of each type of adsorbent was accurately weighted. A measuring cylinder was filled up with water up to 500 ml. The adsorbent was placed inside it. The increased volume of water was measured by deducting the previous volume from the new volume after immersion of the adsorbent. This volume is the specific volume of 1 gm of the adsorbent itself. The mass is divided by the volume to get bulk density of the sorbent by using Equation 4.13 (Zahangir *et al.,* 2008).

$$Bulk\ Density = \frac{Dry\ weight\ of\ the\ adsorbent\ gm}{Volume\ of\ the\ sample\ ml} \quad (4.12)$$

4.9.2 Chemical Characterization

4.9.2.1 Determination of Iodine Number

Iodine number is one of the most fundamental parameter to characterize activated carbon.0.1 gm of activated carbon is mixed with 25 ml of iodine solution and was shaken for 1 minute. After that the solution was filtered and 10 ml of filtrate was put inside a conical flask. The solution is titrated with 0.04 N sodium thio-sulphate solutions until it becomes clear. The iodine number for both the activated carbon was determined by using Equation (4.13) which represents the number of milligrams of iodine adsorbed by one gram of activated carbon (Birbas, 2011).

$$\text{Iodine Number} = V(T_i - T_f)C_i M_i /(T_i g) \quad (4.13)$$

where,

V= Volume of iodine solution 25 ml

T_i = Volume of sodium thio-sulfate solution used for titration of 10 ml iodine solution

T_f = Volume of sodium thio-sulfate solution used for titration of 10 ml of filtrate

g = Weight of activated carbon= 0.1 gm

M_i = Molar weight of Iodine = 126.9044 g/mol

C_i= 0.045 N = Concentration of Iodine Solution

4.9.2.2 Elemental Analysis of the adsorbent

Activated carbon and activated palm ash possess different types of chemical constituents. The former is based on cellulosic materials enriched with carbon and the latter is mineral based starting material to produce effective sorbent for cations. Therefore the elemental analysis of both types of adsorbent is different. Elemental analysis of the prepared activated carbon along with the precursor was performed using Elemental Analyzer (PerkinElmer- Series II 2400, Japan) to investigate the presence of elements of carbon, hydrogen, nitrogen and others in the activated carbon sample; whereas X –ray fluorescence (XRF, Rigaku RIX, 3000, Japan) was used to identify the percentage chemical composition of the activated ash.

4.9.2.3 Proximate Analysis of activated carbon

Proximate analysis of the cellulosic agricultural biomass, semi carbonized sample and the finally prepared activated carbons were performed by using thermo gravimetric analyzer (TGA). This would help to determine the moisture content, volatile matter, fixed carbon and remaining ash contents of the sample. Due to the different physio-chemical features of activated palm ash, TGA analysis was not necessary for its surface. Approximately 5 mg

of activated carbon sample was loaded into a platinum pan of the TGA equipment (Model Perkin Elmer TGA7, US). The chamber of the furnace was then raised and the sample was degassed for ten minutes. At first stage of analysis, nitrogen gas was purged through the furnace to evacuate oxygen and create an inert atmosphere. The sample was heated from 30 °C temperature to 110 °C until complete dehydration was achieved. This was done for the determination of moisture content. The temperature was then increased to 850 ^{0}C and was kept static for 7 min. Then the temperature was decreased to 800 °C, and nitrogen gas was switched off and CO_2 gas was passed inside the chamber to obtain oxidizing atmosphere. After the dehydration stage, weight loss was due to the release of volatile matters. Fixed carbon content was obtained from the weight loss during the oxidation stage. Ash was the remaining mass obtained at the end of the analysis.

4.9.2.3 Fourier Transform Infrared Spectroscopy

Fourier transform infrared (FTIR) technique is an essential tool to analyze surface functional groups for both types of raw materials; semi carbonized sample and activated carbon and activated oil palm ash. The adsorbent samples were ground to very fine powder and dried overnight in the oven at 105 °C. For infrared analysis, potassium bromide (KBr) pellet was used.

The ground materials and KBr was used in 1:10 ratio and with the aid of manual bench press, translucent disks were prepared. These disks were directly placed in the middle of the paper holder inside the analysis chamber of spectrophotometer. The spectra were measured from 400 to 4000 cm^{-1} (Model Perkin Elmer FTIR-2000, US). The analysis was done automatically by the software (Spectrum version 6.0.2) attached to the system.

4.10 Regeneration of cation loaded adsorbent

The feasibility of regenerating spent adsorbent saturated with cations was performed by using five types of eluting agents; namely distilled water, 1M organic and mineral acids of hydrochloric, sulfuric and nitric acid. Initially batch adsorption was carried out between 0.2 g of fresh adsorbent of each type in a flask and 50 ml of adsorbate solution of 100 mg/l was added. The mixture were agitated in an isothermal water bath shaker at 30 °C and agitation speed of 150 rpm until equilibrium contact time was reached. The solution pH was kept at 5.5. After equilibrium is attained, the residual concentration of each type of adsorbate-adsorbent system was measured and C_{ad} (mg/l) was calculated as the difference between the initial and final equilibrium concentration ($C_0 - C_e$).

The spent adsorbent was separated from the solution and dried at 110 °C. The dried samples of each type of adsorbent were placed in the flask containing 50 ml of different eluting agents mentioned above. Flasks with stoppers were placed inside the thermal water bath shaker and agitated at the same agitation speed, time and temperature to identify the efficiency of regeneration by different eluting agents. After equilibrium time, the concentration of the desorbed adsorbate was measured. The percent desorption was calculated by using Equation 4.14:

$$Desorption\% = \frac{C_{de}}{C_{ad}} X100 \qquad (4.14)$$

From batch sorption/desorption study, it was observed that 1M HNO_3 acid acts as best eluting agent for activated carbon samples (KCAC, KFAC and MFSAC) whereas 1M

HCl was better for activated ash sample. Therefore, for column regeneration using MFSAC, 1M HNO_3 acid solution was used to regenerate and reuse the column up to four cycles. After each cycle, the adsorbent was washed with hot distilled water and then packed inside the column. The regeneration efficiency (RE%) was calculated for highest bed height (cm), flow rate (ml/min) and initial concentration of (mg/l) for all the cations by using following Equation 4.15.

$$RE(\%) = \frac{q_{reg}}{q_{org}} \times 100 \quad (4.15)$$

where, q_{reg} is the adsorptive capacity of the regenerated column and q_{org} is the original capacity (mg/g) of the adsorbent

4.11 Experimental Activities

The overall experimental activities carried out in this study are illustrated by following flow chart represented by Figure 4.5.

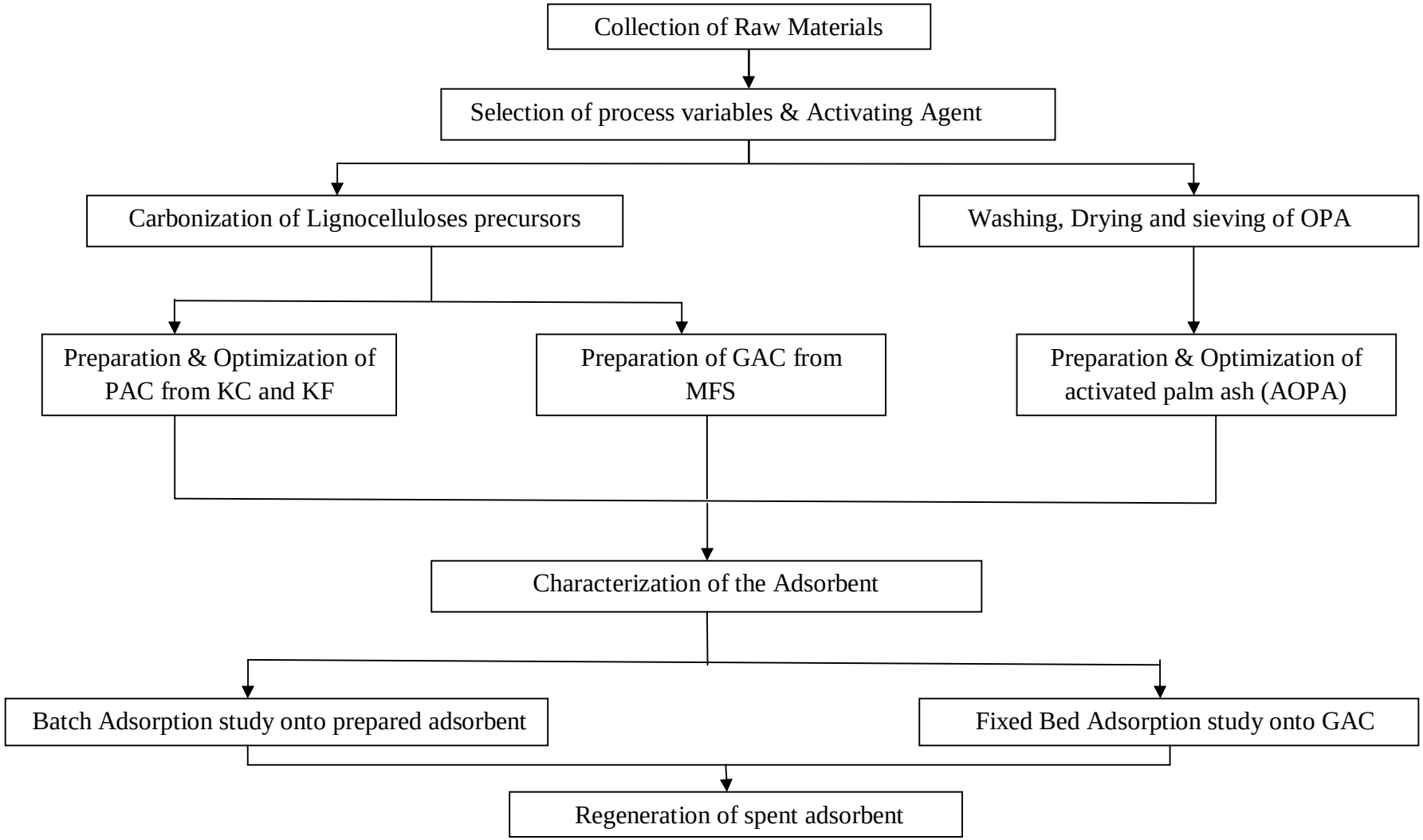

Figure 4.5 Schematic Flow Chart of Experimental Activities

CHAPTER FIVE
RESULTS AND DISCUSSION
Preparation of Powdered Activated Adsorbents

5.1 Introduction

This chapter illustrates the experimental results based on the Central Composite Design (CCD) for the preparation of powdered activated adsorbent derived from Kenaf core (KC), Kenaf fibre (KF) and natural oi1 palm ash (OPA). The last part summarizes the optimum parameters obtained to achieve maximum output of the entire process.

5.2 Preparation of Activated Carbon

In the first phase of this study, two sets of experimental design matrix were applied for preparing powdered activated carbon (PAC) from different agricultural residues of kenaf core (KC) and kenaf fiber (KF) by using response surface methodology (RSM). The preparation variables were changed according to the experimental run. However, the chemical and physical activating agents of CO_2 and KOH together with the range of variables (temperature-x_1, time-x_2 and impregnation ratio, IR-x_3) were preselected based on literature. The most important properties of an activated carbon is its adsorption capacity. Moreover, yield of powdered activated carbon is also a prime concern for economical viability of the process. Therefore, the responses which were considered in this study were :

(i) Y_1- adsorption capacity/ removal percentage of Lead, Pb (II)

(ii) Y_2- adsorption capacity/ removal percentage of Copper, Cu (II)

(iii) Y_3- adsorption capacity/ removal percentage of Manganese, Mn (II)

(iv) Y_4- activated carbon yield

Design Expert software version 6.0.6 (STAT-EASE Inc., Minneapolis, US) was used for evaluation of the statistical parameters obtained from the model regression analysis and also for the appraisal of the surface contour plots constructed based on preparation variables and responses for each adsorbete-adsorbent interction at identical condition.

5.2.1 Preparation of Kenaf Core Activated Carbons (KCAC) using Design of Experiment

The complete design matrix given by the software for preparing 20 samples of activated carbons are designated as sample S-1 to S-20 from Kenaf Core (KC). The results obtained for four responses from the experimental works are presented in Table 5.1. Sample S-15 to S-20 at the center point were prepared for the same set of variables to resolve experimental errors and reproducibiliy of the data. It is observed from Table 5.1 that,the highest removal effeciency for Pb(II) and Cu(II) cations were shown by sample S-10 (temperature (x_1)-768.18 °C, time (x_2)- 2h and impregnation ratio (x_3) -2), whereas highest removal effeciency for Mn(II) was obtained by S-8(temperature (x_1)-700.00 °C, time (x_2)- 3h and impregnation ratio (x_3) -3). This is expected due to different physio-chemical properties and affinity of the selected adsorbate and adsorbate-adsorbent interaction under identical condition. The highest yield was observed for sample S-9 when all the variables were at minimum range (temperature (x_1)-431.82 °C, time (x_2)-2h and impregnation ratio (x_3) -2). The design matrix clearly reveals that yield and removal percentages are inversely related to each other.

Table 5.1 Experimental Design Matrix for preparation of Kenaf Core (KCAC) based activated carbon

Sample ID	Run	Type of Point	Level (coded Factors)			Activated Carbon Preparation Variables (Actual Factors)			Percentage Removal, Pb (II) Y_1(mg/g)	Percentage Removal, Cu (II) Y_2(mg/g)	Percentage Removal, Mn (II) Y_3(mg/g)	Percentage Yield Y_4
						Temperature x_1, (°C)	Time, x_2,(Hour)	Ratio IR, x_3				
S-1	1	Fact	-1	-1	-1	500	1	1	69.98	60.03	53.44	32.87
S-2	2	Fact	+1	-1	-1	700	1	1	85.77	77.09	90.09	21.87
S-3	3	Fact	-1	+1	-1	500	3	1	68.89	66.65	55.09	27.99
S-4	4	Fact	+1	+1	-1	700	3	1	85.76	83.59	94.04	16.54
S-5	5	Fact	-1	-1	+1	500	1	3	69.09	64.09	59.89	24.66
S-6	6	Fact	+1	-1	+1	700	1	3	89.99	84.33	96.09	16.89
S-7	7	Fact	-1	+1	+1	500	3	3	79.99	76.87	64.98	23.22
S-8	8	Fact	+1	+1	+1	700	3	3	90.43	95.09	98.99	15.98
S-9	9	Axial	-1.682	0	0	431.82	2	2	68.09	59.78	48.77	33.09
S-10	10	Axial	+1.682	0	0	768.18	2	2	94.09	97.97	97.99	13.33
S-11	11	Axial	0	-1.682	0	600	0.32	2	74.09	69.09	67.77	26.76
S-12	12	Axial	0	+1.682	0	600	3.68	2	85.89	95.54	97.77	18.99
S-13	13	Axial	0	0	-1.682	600	2	0.32	75.09	75.58	60.09	24.66
S-14	14	Axial	0	0	+1.682	600	2	3.68	90.96	92.33	98.03	17.02
S-15	15	Center	0	0	0	600	2	2	83.09	93.08	96.99	21.09
S-16	16	Center	0	0	0	600	2	2	85.88	94.77	95.99	22.54
S-17	17	Center	0	0	0	600	2	2	85.09	93.99	94.56	23.01
S-18	18	Center	0	0	0	600	2	2	82.88	93.78	96.66	21.87
S-19	19	Center	0	0	0	600	2	2	84.65	94.09	96.87	22.88
S-20	20	Center	0	0	0	600	2	2	84.09	94.02	94.67	22.99

5.2.1.1 Development of Regression Model Equations for Preparation of Kenaf Core Activated Carbons

According to the sequential model sum of squares, the models were selected based on the highest order polynomials where the additional terms were significant and the models were not aliased (Montgomery, 2001). Model parameters were estimated and illustrated in Table 5.1. For adsorption capacity of Pb(II) and Cu (II), quadratic model was suggested by the software. However, for Mn(II), both linear and quadratic models were suggested by the software. In this case, quadratic models were selected due to the higher order of polynomials. On the contrary, 2FI model was selected as suggested by the software for yield. The final empirical models in terms of coded factors after excluding the insignificant terms for the above mentioned responses are represented by Equations 5.1, 5.2, 5.3 and 5.4 respectively.

$$Percentage\ removal\ of\ Pb(II), Y_1 = 84.32 + 7.89x_1 + 2.20x_2 + 3.35x_3 - 1.38x_1^2 - 1.77x_2^2 - 0.70x_3^2 - 1.17x_1x_2 - 0.16x_1x_3 + 1.56x_2x_3 \quad (5.1)$$

$$Percentage\ removal\ of\ Cu(II)\ \ Y_1 = 94.12 + 10.01x_1 + 5.94x_2 + 4.48x_3 - 6.39\ x_1^2 - 5.17x_2^2 - 4.59x_3^2 - 0.27\ x_1x_2 + 0.56x_1x_3 + 1.30\ x_2x_3 \quad (5.2)$$

$$Percentage\ removal\ of\ Mn(II), Y_3 = 95.98 + 16.74x_1 + 4.69x_2 + 6.67x_3 - 8.14x_1^2 - 4.82x_2^2 - 6.13x_3^2 + 0.014x_1x_2 - 0.67x_1x_3 + 0.30x_2x_3 \quad (5.3)$$

$$Activated\ Carbon\ yield, Y_4 = 22.41 - 5.18x_1 - 1.88x_2 - 2.30x_3 + 0.0013x_1x_2 + 0.93x_1x_3 + 0.98x_2x_3 \quad (5.4)$$

The coefficients with temperature (x_1), time (x_2) and impregnation ratio (x_3) represent the effect of that particular factor for the preparation of activated carbon. Coefficients with two factors (x_1x_2, x_2x_3 and x_3x_1) and others with second order terms (x_1^2, x_2^2 and x_3^2) show the interaction between the two variables and quadratic effect respectively. Positive sign in front of the terms indicates synergistic effect, whereas negative sign indicates antagonistic effect (Hameed *et al.*, 2008; Montgomery, 2001).

The quality of the model developed can be understood by the correlation coefficient, R^2 and standard deviation values. R^2 indicates the ratio between sum of squares (SSR) with total sum of squares (SST) and this depicts how well the models approximate the experimental data points. The R^2 values for Equations 5.1-5.4 were 0.95, 0.96, 0.94 and 0.97 respectively, which ensures satisfactory adjustment of developed models with the experimental data. Other statistical parameters used to analyze the suitability of the developed models are also listed in Table 5.2.

Table 5.2 Statistical parameters for ANOVA analysis for Model regression of removal percentage of Pb (II), Cu (II), Mn (II) and Yield for Kenaf Core based activated carbon (KCAC)

Statistical Parameters	**Responses**			
	Percentage Removal of Pb (II) Y_1	**Percentage Removal of Cu (II)** Y_2	**Percentage Removal of Mn(II)** Y_3	**Yield** Y_4
Standard Deviation, SD%	2.51	3.71	6.57	1.12
Correlation Coefficient, R^2	0.95	0.96	0.94	0.97
Adjusted R^2	0.90	0.92	0.88	0.95
Mean	81.69	83.09	82.94	22.41
Coefficient of Variation, CV	3.07	4.46	7.92	5.00
Adeq. Precision	15.23	15.58	12.89	30.13

The small values of standard deviations and co-efficient of variation, CV reflect reproducibility of the model. "Adeq Precision" measures the signal to noise ratio. A ratio greater than 4 is desirable (Montgomery, 2001). The ratio obtained for all the responses reflects that the models can be used to navigate the design space.

Diagnostic tests (residuals vs. predicted and outliers) were carried out in this study to determine the adequacy of the developed models. The linear plots obtained are shown in Appendix C (C1-C4). Figures C1 (a-b), C2 (a-b), C3 (a-b) and C4 (a-b) show outliers t plot and studentized residuals vs. predicted plots for removal percentage of Pb(II), Cu (II), Mn(II) ions and carbon yield, respectively. For successful resolution of designed experiments, the outliers should be carefully observed. Outlier *t* plots reflect a simple data recording error. Sometimes it shows the region of independent variables where the fitted model has showed poor approximation to the true response surface (Montgomery, 2001). From Figures C1 (a), C2(a), C3 (a) and C4 (a), it was observed that most of the data points lie between the intervals of ± 3.50 (Outliers t plots). This showed that the data approximation for the fitted models (Equations 5.1-5.4) to the response surface was fairly good and reflected no data recording error. However, there was only one data recorded below -3.50 for removal percentages of Pb(II) and over +3.50 for removal percentages of Cu(II). This might be due to the insignificant terms or nonlinear influence of the studied variables over the response. Similar observation has been reported for adsorption studies of Cu (II) ions onto a type of seaweed, *Enteromorpha prolifera* (Ozer *et al.* 2009).

The data points for studentized residuals vs. predicted plots (Figures C1 (b), C2 (b), C3 (b) and C4 (d)) were scattered. The data points in these plots should be randomly scattered, demonstrating that the variance of the experimental observations

were constant for all the values of response depicted by Table 5.1. The data points obtained were between ±3.00 which implied that no response transformation was needed for the experimental design of this study (Myers and Montgomery, 1995).

The competence of the developed models was further justified through analysis of variance (ANOVA) and the results obtained are depicted in Tables 5.3-5.6. The significance of the empirical models was investigated by the F-test value which is a statistical measure of how well the empirical model describes the variation in the data about the mean. The greater the F-value, the more certain it is, that the model explains adequately the variation in the data and the estimated significant terms of the adsorbent preparation variables are closer to the actual value. Based on 95% confidence level, the model F-value for removal percentage of lead, copper and manganese are 20.69, 25.97 and 16.21 respectively, which implied that these models were significant. Neverthless, the values of Prob > F for uptake of all the adsorbate were less than 0.05 indicating that the model terms are significant.

For Pb (II) activation temperature (x_1), activation time (x_2), impregnation ratio - IR (x_3) and quadratic terms of time (x_2^2) are significant model terms whereas the interaction terms of x_1x_2, x_1x_3 and x_2x_3 and quadratic terms of x_1^2 and x_3^2 are all insignificant to the response. For Mn(II) and Cu (II), activation temperature (x_1), activation ratio, IR (x_3) and activation time (x_2) as well as their quadratic terms of (x_1^2), (x_2^2) and (x_3^2) are significant whereas the interaction terms of x_1x_2, x_1x_3 and x_2x_3 are all insignificant to the response.

Table 5.3 ANOVA analysis and Lack of Fit test for Response Surface Model for removal percentage of Pb (II) from synthetic water by using Kenaf Core based activated carbon (KCAC)

Source	Sum of Squares	Degree of Freedom	Mean Square	F Value	Prob> F	Comments
Model	1168.79	9	129.87	20.69	<0.0001	*Significant*
x_1	849.65	1	849.65	135.35	<0.0001	
x_2	66.24	1	66.24	10.55	0.0087	
x_3	153.48	1	153.48	24.45	0.0006	
x_1^2	27.52	1	27.52	4.38	0.0627	
x_2^2	45.18	1	45.18	7.20	0.0230	
x_3^2	7.010	1	7.010	1.12	0.3154	
x_1x_2	10.98	1	10.98	1.75	0.2154	
x_1x_3	0.220	1	0.220	0.034	0.8567	
x_2x_3	19.37	1	19.37	3.08	0.1095	
Residuals	62.78	10	6.28			
Lack of Fit	56.01	5	11.20	8.28	0.0184	*Significant*
Pure Error	6.77	5	1.35			

Table 5.4 ANOVA analysis and Lack of Fit test for Response Surface Model for removal percentage of Cu (II) from synthetic water by using Kenaf Core based activated carbon (KCAC)

Source	Sum of Squares	Degree of Freedom	Mean Square	F Value	Prob> F	Comments
Model	3213.34	9	357.04	25.97	<0.0001	*Significant*
x_1	1368.07	1	1368.07	99.50	<0.0001	
x_2	482.12	1	395.48	35.06	<0.0001	
x_3	274.16	1	268.17	19.94	0.0012	
x_1^2	588.03	1	559.87	42.77	<0.0001	
x_2^2	385.43	1	488.32	28.03	0.0004	
x_3^2	303.85	1	274.73	22.10	0.0008	
x_1x_2	0.570	1	0.570	0.042	0.8424	
x_1x_3	2.490	1	2.490	0.18	0.6797	
x_2x_3	13.57	1	13.57	0.99	0.3439	
Residuals	137.50	10	13.75			
Lack of Fit	136.01	5	27.20	91.64	<0.0001	*Significant*
Pure Error	1.48	5	0.30			

Table 5.5 ANOVA analysis and Lack of Fit test for Response Surface Model for removal percentage of Mn (II) from synthetic water by using Kenaf Core based activated carbon (KCAC)

Source	Sum of Squares	Degree of Freedom	Mean Square	F Value	Prob> F	Comments
Model	6290.11	9	698.90	16.21	<0.0001	*Significant*
x_1	3826.09	1	3826.09	88.76	<0.0001	
x_2	300.33	1	300.33	6.97	0.0248	
x_3	607.66	1	607.66	14.10	0.0038	
x_1^2	955.57	1	955.57	22.17	0.0008	
x_2^2	335.23	1	335.23	7.78	0.0192	
x_3^2	542.37	1	542.37	12.58	0.0053	
x_1x_2	0.002	1	0.002	0.00004	0.9954	
x_1x_3	3.63	1	3.63	0.084	0.7776	
x_2x_3	0.71	1	0.71	0.017	0.9001	
Residuals	431.07	10	43.11			
Lack of Fit	425.07	5	85.01	70.80	0.0001	*Significant*
Pure Error	6.00	5	1.20			

Table 5.6 ANOVA analysis and Lack of Fit test for Response Surface Model for activated carbon yield by using Kenaf Core based activated carbon (KCAC)

Source	Sum of Squares	Degree of Freedom	Mean Square	F Value	Prob> F	Comments
Model	500.71	9	83.45	66.44	<0.0001	*Significant*
x_1	365.93	1	365.93	291.31	<0.0001	
x_2	48.09	1	48.09	38.29	<0.0001	
x_3	72.05	1	72.05	57.36	<0.0001	
x_1x_2	0.001	1	0.001	0.001	0.9802	
x_1x_3	6.92	1	6.92	5.51	0.0354	
x_2x_3	7.72	1	7.72	6.15	0.0276	
Residuals	16.33	13	1.26			
Lack of Fit	13.36	8	1.67	2.81	0.1347	*Not Significant*
Pure Error	2.97	5	0.59			

Referring to Table 5.6 for 2FI model for yield, the model F value of 66.44 and probable F value less than 0.0001 indicate the significance of the model. For yeild, x_1,

x_2, x_3 and interaction terms of x_2x_3 and x_1x_3 are significant model terms whereas other terms are all negligible to the response.

From the statistical results obtained, it can be seen that the above models (Equations 5.1-5.4) are adequate to predict the removal percentage and the carbon yield within the experimental range of variables selected. The performance of the model can be also visualized by observing the plots of predicted versus experimental percentage yield and removal as shown in Figures 5.1, 5.2, 5.3 and 5.4. As estimated, the predicted values for activated carbon yield are the closest to their experimental values as compared to the other three responses.

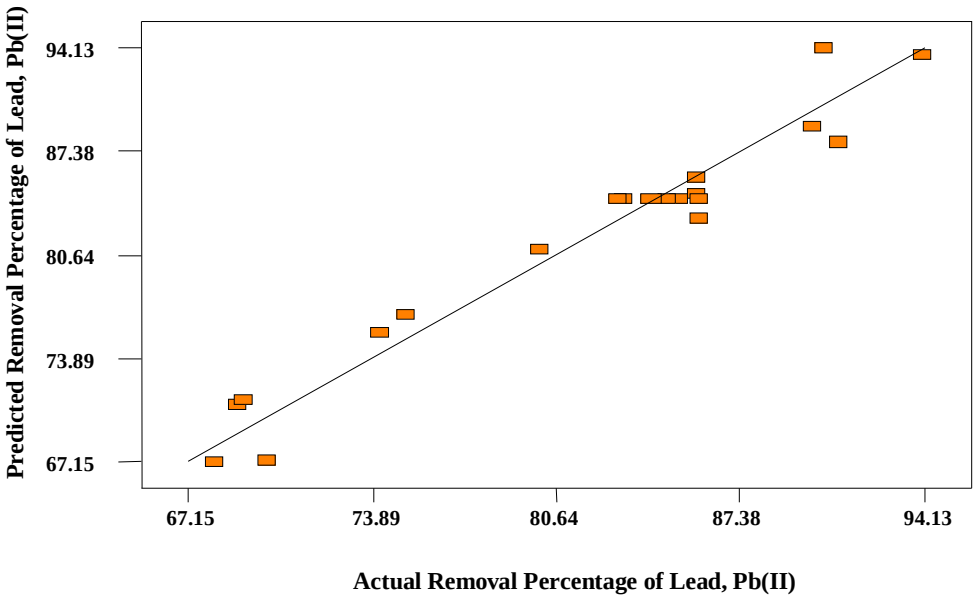

Figure 5.1 Predicted versus experimental removal percentage of lead onto Kenaf Core Activated carbon (KCAC)

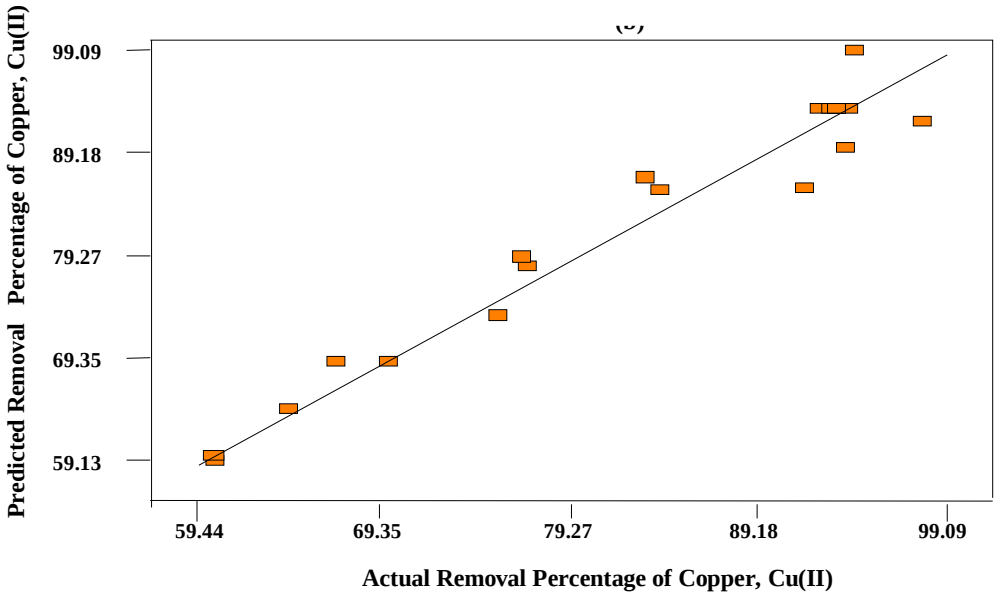

Figure 5.2 Predicted versus experimental removal percentage of copper onto Kenaf Core Activated carbon (KCAC)

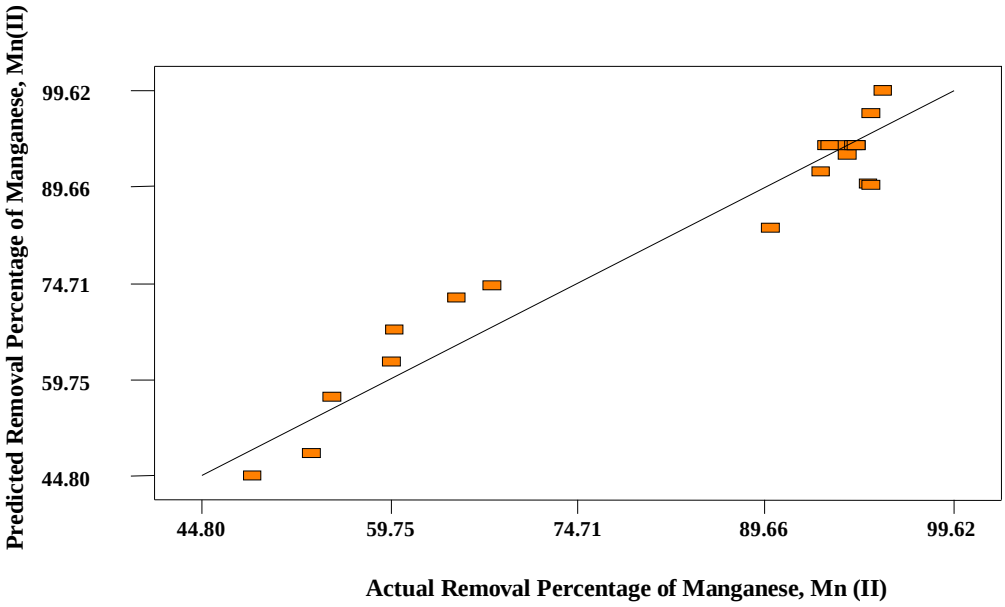

Figure 5.3 Predicted versus experimental removal percentage of manganese onto Kenaf Core Activated carbon (KCAC)

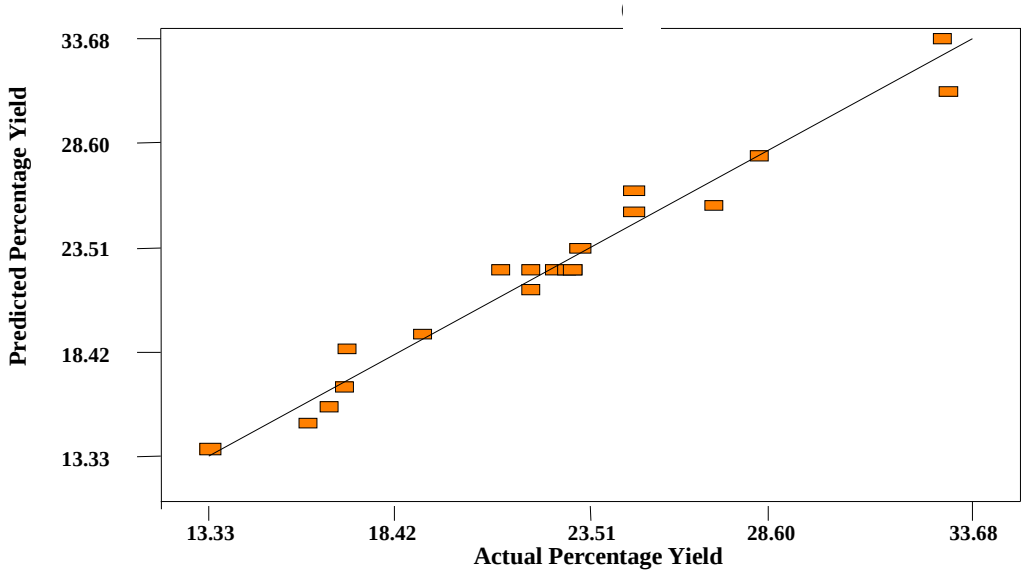

Figure 5.4 Predicted versus experimental Kenaf Core Activated carbon (KCAC) yield

5.2.1.1 Removal Efficiency of Kenaf Core Activated Carbons

Based on the F values as shown in Table 5.3-5.5, both the activation temperature and IR are found to have the greatest effects on the adsorption capacity of Pb(II) and Mn (II) ions onto the activated carbons prepared from KC, whereas activation temperature and activation time showed greatest effect on adsorption capacity of Cu(II). The interaction effect between the factors for Pb(II), and Cu(II) are moderate. In case of Mn(II) ions, interaction effect of activation temperature and activation ratio have the greatest impact. Figure 5.5- 5.7 depicts the three-dimensional response surfaces with contour plot which show the effects of the combined effects of two significant variables (activation temperature and IR) on the adsorption capacity of the adsorbate. In this case, the activation time was fixed at zero level, which was 2 h.

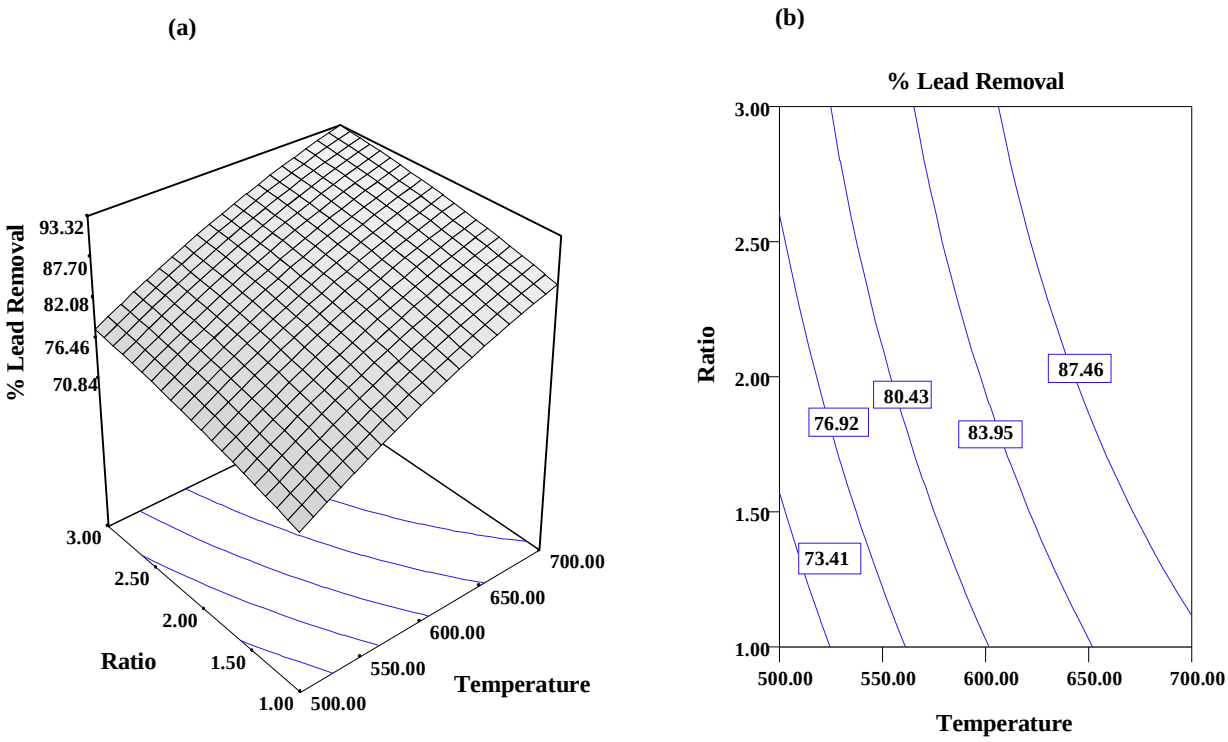

Figure 5.5 (a) Three Dimensional Response Surface (b) Surface contour plot of removal percentage of lead (II) (Effect of activation temperature and IR, Time, t=2 h) onto Kenaf Core activated carbon (KCAC)

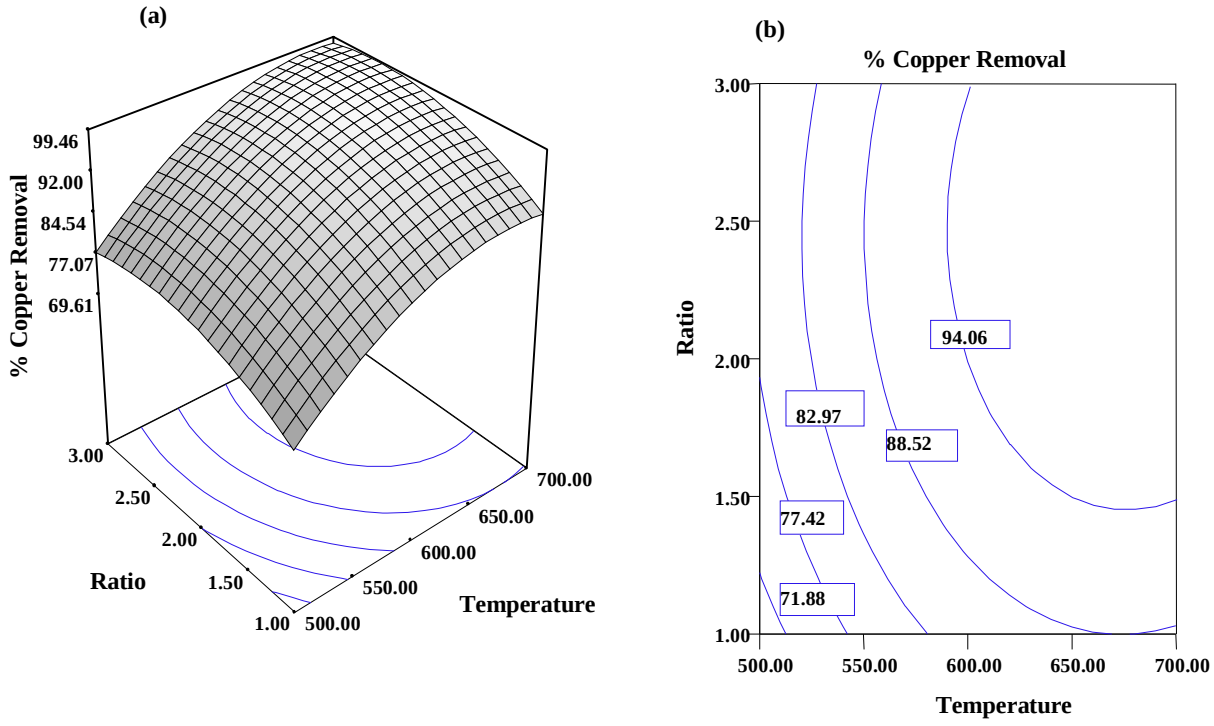

Figure 5.6 (a) Three Dimensional Response Surface (b) Surface contour plot of removal percentage of copper (II) (Effect of activation temperature and IR, Time, t=2 h) onto Kenaf Core activated carbon (KCAC)

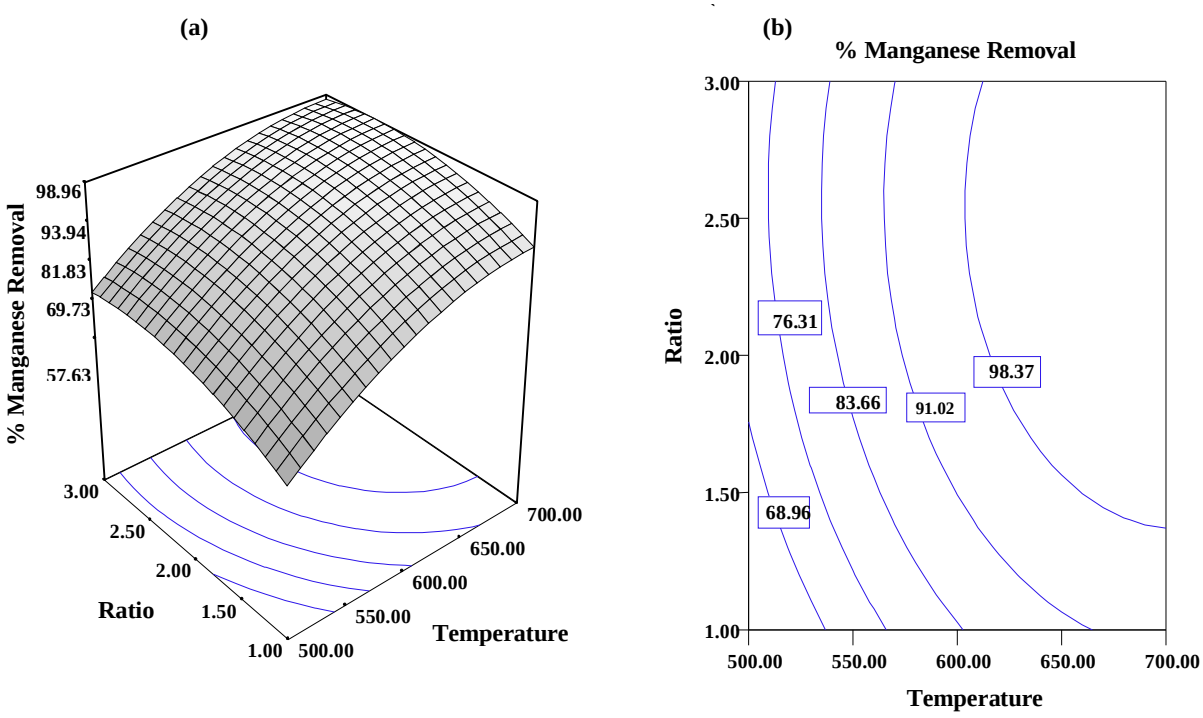

Figure 5.7 (a) Three Dimensional Response Surface (b) Surface contour plot of removal percentage of manganese (II) (Effect of activation temperature and IR, Time, t=2 h) onto Kenaf Core activated carbon (KCAC)

The 2D surface contour curve represents an infinite number of combinations of selected variables. The maximum possible response value is indicated by the surface confined by the smallest ellipse in the diagram. Elliptical contour obtained for removal efficiency of lead, copper and manganese demonstrate that there are interactions present between the independent variables. As can be seen from the surface contour plots, removal efficiency of the KC activated carbons generally increases with increase in activation temperature and IR. The highest adsorption capacity for Pb (II) ion is observed when both these variables are at the maximum point within the range studied. The results obtained are in agreement with the previous research reported by Sudaryanto *et al.,* (2006) which inferred that activation time gave no significant impact on the pore development of activated carbon produced from cassava peel, whereas the pore characteristics changed considerably with the activation temperature and KOH

impregnation ratio. It was reported earlier that activation time did not have much effect on the surface area obtained for activated carbons prepared from apricot stones using steam activation (Sentorun -Shalaby *et al.*, 2006). It was also observed for KOH treated oil palm fronds that activation time had least effect on pore development (Salman *et al.*, 2010).

It is observed for Cu (II) and Mn (II) ions that after certain limit of temperature and KOH ratio, the adsorption capacity reduced slightly. This is most probably due to the development of excess mesopore surface area or large pore diameter which failed to retain smaller cations like copper and manganese (Ahmenda *et al.*, 2000) but made easier for bulky cations of lead to penetrate inside the basal planes of activated carbon and adsorbed onto the soft site of the activated carbon (Chen and Wang, 2000). Another plausible explanation for this is that there may be a disruption or lessening of the intensity of some surface functional groups which could readily form surface complexes with the cations of copper and manganese.

However, in this work all the three variables studied were found to have synergistic effects on the adsorption capacity of the preselected cations. This was expected as the progressive increase of temperature and activation time would increase the reaction between char and KOH and char with CO_2. This would result in enhanced devolatilization which would further develop the existing rudimentary pore structure of the char and create new pores. The increase in activation temperature and time would ensure sufficient contact time between carbon matrix and physical and chemical activating agents of CO_2 and KOH for the dissolution of cellulosic structure (Baçaoui *et al.*, 2001; Stavropoulos and Zabaniotou, 2005; Lua and Yang, 2004).

Impregnation ratio, IR played a crucial role in the formation of pores. The increase in KOH would accelerate the reaction rate and therefore the quantity of the pores increased correspondingly (Adinata *et al.,* 2007; Zabaniotou *et al,* 2008). However, there was a maximum range for IR and time beyond which the uptake capacity of the adsorbate onto KC activated carbon is reduced. Since excessive quantity of KOH would cause additional reaction between KOH and carbon, it might obliterate the pore structure formed at previous stage (Cao *et al.,* 2006). The excessive KOH molecules might also be decomposed at higher temperature leading to the following gasification reactions (Guo and Lua, 2000).

$$2KOH \rightarrow K_2O + H_2O \qquad (5.5)$$

$$H_2O + C \rightarrow CO + H_2 \qquad (5.6)$$

5.2.1.3 Kenaf Core Activated Carbon Yield

For activated carbon yield, activation temperature was found to have the utmost effect on this response by showing the highest F value of 66.44, as shown by Table 5.6, whereas activation time and IR showed almost similar impact on the response, which were less noteworthy compared to activation temperature. The interaction effect of activation time and ratio was more pronounced than the other two interaction terms on the yield of KC activated carbon. Figures 5.8(a) and (b) show the three-dimensional response surfaces which were constructed to reveal the effects of the activated carbon preparation variables on the activated carbon yield. Figure 5.8(a) represents the combined effect of activation temperature and activation time on the response where IR was fixed at zero level (IR. = 2) whereas Figure 5.8(b) depicts the effect of activation temperature and IR on the same response where activation time was fixed at zero leve1 (t = 2 h).

In general, the KC activated carbon yield was found to decrease with activation temperature, activation time and IR. As can be seen from both the plots (Figures 5.8 (a) and (b), activation temperature was more dominant on the activated carbon yield as compared to the other two variables.

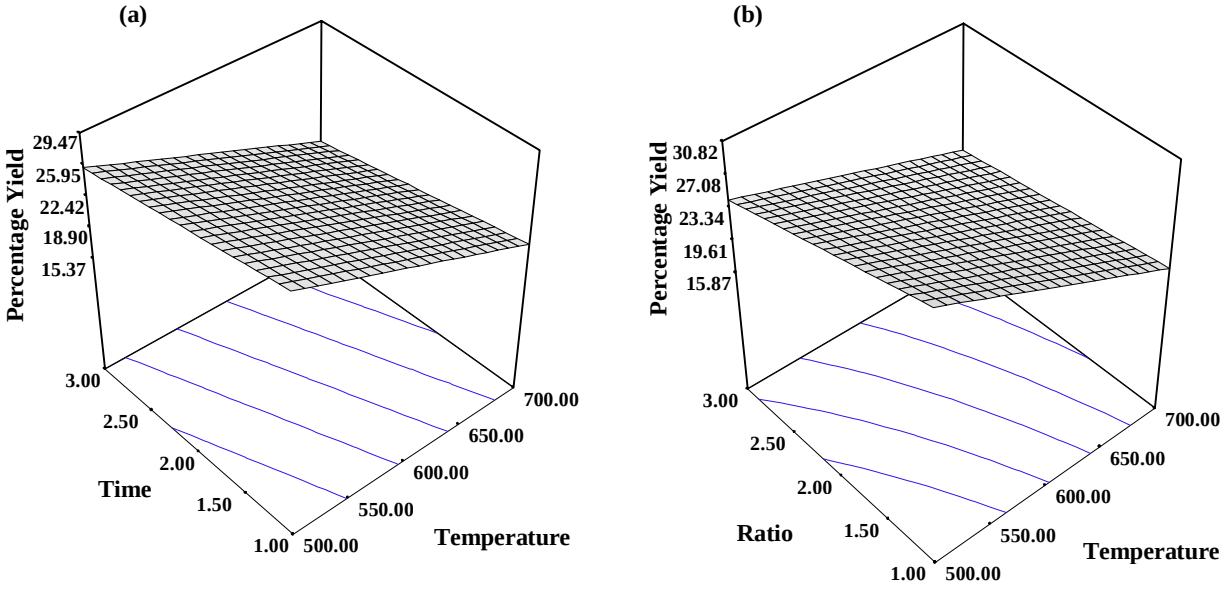

Figure 5.8 Three Dimensional Response Surface plot of Kenaf Core activated carbon (KCAC) yield (a) Effect of activation temperature and activation time, IR= 2 (b) Effect of activation temperature and IR, Time= 2 h)

Similar observation was reported for preparation of the activated carbon from coconut husk by using KOH (Tan, 2008). The lowest carbon yield was obtained for sample S-10, when temperature was at the maximum point within the range studied (temperature (x_1)-768.18 °C, time (x_2)- 2h and impregnation ratio (x_3) -2). This outcome was also in concurrence with the previous work carried out by Sudaryanto *et al.* (2006) where activation temperature was found to play a vital role on the yield of cassava peel based activated carbon whereas activation time did not show much effect on the carbon yield. However, for KC based activated carbon, the effect of activation time was moderate. The increase in temperature would release more volatile component as a result of intensifying dehydration and elimination reaction. This would increase the C-

KOH and C-CO_2 reaction rate thereby resulting in decreasing carbon yield (Bacaoui *et al.*, 2001, Lua and Yang, 2004; Adinata *et al*, 2007).

It was reported that for applying higher activation temperature, the yield of apricot stone became less (Sentorun-Shalaby *et al.*, 2006). The yield of fir wood based activated carbon was also found to reduce steadily with increase in extent of CO_2 gasification reaction with the carbon matrix (Wu and Tseng, 2006). This was probable as increasing activation time favored releasing of volatile matters, consequently producing less amount of activated carbon. However, materials with higher carbon content should be volatilized to a much lesser extent and undergo less weight loss (Suzuki *et al*, 2007).

The activated carbon yield from KC is strongly affected by ratio. It is observed that by increasing IR, carbon yield is decreased significantly and increased the burn-off. Adinata *et. al.*, 2007 reported for palm shell based activated carbon that at higher IR, the weight losses were due to extensive release of volatile products. KOH is a strong dehydrating agent which will increase the oxidation process resulting in increase in the weight loss of carbon (Sudaryanto *et al.*, 2006).

5.2.2 Preparation of Kenaf Fiber (KF) Activated Carbons (KFAC) using Design of Experiment

Table 5.7 lists the results obtained from a complete design matrix for preparing activated carbons (KFAC) from kenaf fiber (KF). The results again revealed that the properties of activated carbons prepared from different types of precursors have different characteristics although the same preparations conditions were used to produce the carbons.

Table 5.7 Experimental Design Matrix for preparation of Kenaf Fiber (KFAC) based activated carbon

Sample ID	Run	Type of Point	Level (coded Factors)			Activated Carbon Preparation Variables (Actual Factors)			Percentage Removal, Pb (II) Y_1(mg/g)	Percentage Removal, Cu (II) Y_2(mg/g)	Percentage Removal, Mn (II) Y_3(mg/g)	Percentage Yield Y_4
						Temperature x_1, (°C)	Time, x_2,(Hour)	Ratio IR, x_3				
S-1	1	Fact	-1	-1	-1	500	1	1	63.98	78.99	70.76	33.89
S-2	2	Fact	+1	-1	-1	700	1	1	87.98	81.99	70.23	23.98
S-3	3	Fact	-1	+1	-1	500	3	1	64.99	80.99	71.89	32.02
S-4	4	Fact	+1	+1	-1	700	3	1	86.89	94.99	78.99	14.99
S-5	5	Fact	-1	-1	+1	500	1	3	66.09	86.88	78.90	26.99
S-6	6	Fact	+1	-1	+1	700	1	3	89.99	82.22	89.11	19.99
S-7	7	Fact	-1	+1	+1	500	3	3	67.77	85.78	75.98	22.09
S-8	8	Fact	+1	+1	+1	700	3	3	93.99	93.99	90.95	5.77
S-9	9	Axial	-1.682	0	0	431.82	2	2	65.09	75.87	70.99	34.99
S-10	10	Axial	+1.682	0	0	768.18	2	2	94.56	91.65	82.89	9.98
S-11	11	Axial	0	-1.682	0	600	0.32	2	74.04	74.88	70.07	26.78
S-12	12	Axial	0	+1.682	0	600	3.68	2	72.09	86.78	74.78	14.88
S-13	13	Axial	0	0	-1.682	600	2	0.32	71.09	80.43	72.89	27.89
S-14	14	Axial	0	0	+1.682	600	2	3.68	78.99	95.77	91.09	13.99
S-15	15	Center	0	0	0	600	2	2	82.78	85.43	89.90	18.65
S-16	16	Center	0	0	0	600	2	2	85.45	88.45	88.10	17.99
S-17	17	Center	0	0	0	600	2	2	84.34	84.99	88.43	19.88
S-18	18	Center	0	0	0	600	2	2	86.54	86.90	87.89	17.78
S-19	19	Center	0	0	0	600	2	2	85.87	87.88	88.34	18.98
S-20	20	Center	0	0	0	600	2	2	83.99	87.99	90.00	16.67

5.2.2.1 Development of Regression Model Equation for Preparation of Kenaf Fiber (KF) Activated Carbons (KFAC)

As explained in the previous sections for preparation of activated carbons from KC, the same procedure was followed for the development of regression models based on the sequential model sum of squares and the models were selected according to the highest order polynomials where the additional terms were significant and the models were not aliased. For all the three responses of removal percentage of cations under analysis and activated carbon yield of KFAC, the quadratic models were suggested by the software to correlate the data to all the three responses. The design matrix with respective variables and responses are listed in Table- 5.7. It was observed that sample S-10 (temperature (x_1)-768.18 °C, time (x_2)- 2h and impregnation ratio (x_3) -2) for lead, and S-14 (temperature (x_1)-600.00 °C, time (x_2)- 2h and impregnation ratio (x_3) -3.68) showed the highest removal efficiency for copper and manganese.

The final empirical models in terms of coded factors after excluding the insignificant terms for the adsorption uptake of Pb(II) - Y_1,Cu(II) - Y_2, Mn(II) - Y_3 and carbon yield - Y_4 of the KFAC are represented by Equations 5.7, 5.8, 5.9 and 5.10 respectively.

$$Percentage\ removal\ of\ Pb(II), Y_1 = 84.76 + 10.66x_1 + 0.17x_2 + 2.00x_3 - 1.29x_1^2 - 3.68x_2^2 - 2.98x_3^2 + 0.027x_1x_2 + 0.53x_1x_3 + 0.72x_2x_3 \quad (5.7)$$

$$Percentage\ removal\ of\ Cu(II)\ \ Y_2 = 86.89 + 3.45x_1 + 3.35x_2 + 2.76x_3 - 0.77x_1^2 - 1.81x_2^2 + 0.76x_3^2 + 2.98\,x_1x_2 - 1.68x_1x_3 - 0.54x_2x_3 \quad (5.8)$$

$$Percentage\ removal\ of\ Mn(II), Y_3 = 88.71 + 3.78x_1 + 1.22x_2 + 5.40x_3 - 3.77x_1^2 - 5.37x_2^2 - 1.99x_3^2 + 1.56x_1x_2 + 2.32x_1x_3 - 1.38x_2x_3 \quad (5.9)$$

$$Activated\ Carbon\ yield, Y_4 = 18.30 - 6.76x_1 - 3.66x_2 - 3.91x_3 + 1.65x_1^2 + 1.07x_2^2 + 1.11x_3^2 - 2.05x_1x_2 + 0.45x_1x_3 - 1.03x_2x_3 \quad (5.10)$$

The R^2 values for Equations 5.7, 5.8, 5.9 and 5.10 are 0.964, 0.897, 0.985 and 0.987 respectively. As explained earlier, the quality of the model developed was evaluated based on the R^2 and standard deviation values. In this case, the R^2 values for all the above four models (Equations 5.7-5.10) are considered as relatively high, as they are all greater than 0.9. This indicated that there is a good agreement between experimental and predicted values for the responses obtained from these four models. The statistical parameters are listed below in Table 5.8.

Table 5.8 Statistical parameters for ANOVA analysis for Model regression of removal percentage of Pb (II), Cu (II), Mn (II) and Yield for Kenaf Fiber based activated carbon

Statistical Parameters	**Responses**			
	Percentage Removal of Pb (II) Y_1	**Percentage Removal of Cu (II)** Y_2	**Percentage Removal of Mn(II)** Y_3	**Yield** Y_4
Standard Deviation, SD%	2.64	2.57	1.35	1.19
Correlation Coefficient, R^2	0.96	0.89	0.98	0.98
Adjusted R^2	0.93	0.80	0.97	0.97
Mean	79.33	85.64	81.11	20.91
Coefficient of Variation, CV	3.33	3.00	1.67	5.68
Adeq. Precision	19.18	10.58	23.68	34.76

The linear plots obtained for dignostic tests are shown in Appendix C (C5-C8). Figures C5 (a-b), C6 (a-b), C7 (a-b) and C8 (a-b) show outliers t plot and studentized residuals vs. predicted plots for removal percentage of Pb(II), Cu (II), Mn(II) ions and carbon yield, respectively. From Figures C5 (a), C6(a), C7 (a) and C8 (a), it was observed, that only one data point is below -3.50 for removal percentage of Pb(II) and Cu(II). However the rest of the points are between ±3.50 (outlier t plots). Like Kenaf core based activated carbon, the studentized residuals vs. predicted plots for removal percentage of Pb(II), Cu (II), Mn(II) ions and carbon yield show no response transformation was needed for the experimental design of this study (Myers and Montgomery 2001).

The ANOVA for response surface quadratic models for all the responses are given in Table 5.9-5.12. The Prob> F value was less than 0.0001for all the models which implies that the models are significant. For the model terms in case of Pb(II) ions, the activation temperature (x_1), impregnation ratio IR (x_3), the quadratic effect of time (x_2^2) and ratio (x_3^2) are significant model terms where as the other terms are all insignificant. For Cu (II) ions, x_1, x_2, x_3, x_2^2 and interaction terms of x_1x_2 are significant model terms and for Mn(II) ions, x_1, x_2, x_3, x_1^2, x_2^2, x_3^2 and interaction terms of x_1x_2, x_1x_3, and x_2x_3 are significant model terms. For yield, x_1, x_2, x_3, x_1^2, x_2^2, x_3^2, x_1x_2 *and* x_2x_3 are all significant model terms.

Table 5.9 ANOVA analysis and Lack of Fit test for Response Surface Model for removal percentage of Pb (II) from Synthetic water by using Kenaf Fiber based activated carbon (KFAC)

Source	Sum of Squares	Degree of Freedom	Mean Square	F Value	Prob> F	Comments
Model	1914.93	9	212.77	30.45	<0.0001	*Significant*
x_1	1551.91	1	1551.91	222.13	<0.0001	
x_2	0.39	1	0.39	0.056	0.8170	
x_3	54.52	1	54.52	7.80	0.0190	
x_1^2	23.98	1	23.98	3.43	0.0937	
x_2^2	195.15	1	195.15	27.93	0.0004	
x_3^2	128.12	1	128.12	18.34	0.0016	
x_1x_2	0.0061	1	0.0061	0.009	0.9771	
x_1x_3	2.23	1	2.23	0.32	0.5849	
x_2x_3	4.15	1	4.15	0.59	0.4588	
Residuals	69.86	10	6.99			
Lack of Fit	60.33	5	12.07	6.32	0.0321	*Significant*
Pure Error	9.54	5	1.91			

Table 5.10 ANOVA analysis and Lack of Fit test for Response Surface Model for removal percentage of Cu (II) from Synthetic water by using Kenaf Fiber based activated carbon (KFAC)

Source	Sum of Squares	Degree of Freedom	Mean Square	F Value	Prob> F	Comments
Model	582.29	9	64.70	9.78	0.0007	*Significant*
x_1	162.36	1	162.36	24.53	0.0006	
x_2	152.81	1	152.81	23.09	0.0007	
x_3	104.12	1	104.12	15.73	0.0027	
x_1^2	8.62	1	8.62	1.30	0.2804	
x_2^2	47.17	1	47.17	7.13	0.0235	
x_3^2	8.35	1	8.35	1.26	0.2876	
x_1x_2	71.22	1	71.22	10.76	0.0083	
x_1x_3	22.61	1	22.61	3.42	0.0943	
x_2x_3	2.34	1	2.34	0.35	0.5650	
Residuals	66.18	10	6.62			
Lack of Fit	55.83	5	11.17	5.39	0.0440	*Significant*
Pure Error	10.35	5	2.07			

Table 5.11 ANOVA analysis and Lack of Fit test for Response Surface Model for removal percentage of Mn (II) from Synthetic water by using Kenaf Fiber based activated carbon (KFAC)

Source	Sum of Squares	Degree of Freedom	Mean Square	F Value	Prob> F	Comments
Model	1279.97	9	142.22	77.53	<0.0001	*Significant*
x_1	195.52	1	195.52	106.58	<0.0001	
x_2	20.28	1	20.28	11.05	0.0077	
x_3	398.47	1	398.47	217.22	<0.0001	
x_1^2	205.16	1	205.16	111.84	<0.0001	
x_2^2	415.48	1	415.48	226.50	<0.0001	
x_3^2	56.94	1	56.94	31.04	0.0002	
x_1x_2	19.47	1	19.47	10.61	0.0086	
x_1x_3	42.87	1	42.87	23.37	0.0007	
x_2x_3	15.29	1	15.29	8.34	0.0162	
Residuals	18.34	10	1.83			
Lack of Fit	14.03	5	2.81	3.25	0.1107	*Not Significant*
Pure Error	4.31	5	0.86			

Table 5.12 ANOVA analysis and Lack of Fit test for Response Surface Model for Activated carbon yield by using Kenaf Fiber based activated carbon (KFAC)

Source	Sum of Squares	Degree of Freedom	Mean Square	F Value	Prob> F	Comments
Model	1122.05	9	124.67	88.51	<0.0001	*Significant*
x_1	624.10	1	624.10	443.07	<0.0001	
x_2	183.01	1	183.01	129.92	<0.0001	
x_3	208.93	1	208.93	148.33	<0.0001	
x_1^2	39.33	1	39.33	27.92	0.0004	
x_2^2	16.40	1	16.40	11.65	0.0066	
x_2^2	17.62	1	17.62	12.51	0.0054	
x_1x_2	33.78	1	33.78	23.98	0.0006	
x_1x_3	1.64	1	1.64	1.16	0.3062	
x_2x_3	8.53	1	8.53	6.05	0.0336	
Residuals	14.09	10	1.41			
Lack of Fit	7.98	5	1.60	1.31	0.3875	*Not Significant*
Pure Error	6.10	5	1.22			

Figures 5.9, 5.10, 5.11 and 5.12 respectively show predicted values versus experimental values for the responses for KFAC. As can be seen from these plots, the predicted values obtained are quite close to the experimental values, indicating that the models developed are successful in capturing the correlation between the activated carbon preparation variables and the responses under investigation. As expected, the values predicted by the models are quite accurate with relatively small variation errors. However, some data points of copper show relatively large residual values, due to the lower R^2 values campared to the other three models. (Equations 5.7 - 5.10).

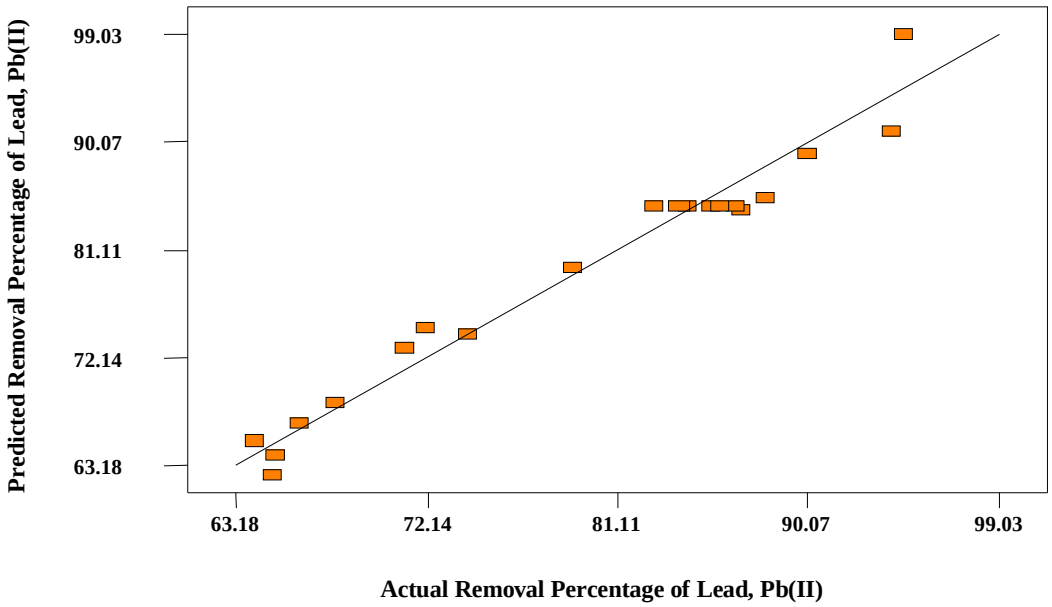

Figure 5.9 Predicted versus experimental removal percentage of lead onto Kenaf Fiber Activated carbon (KFAC)

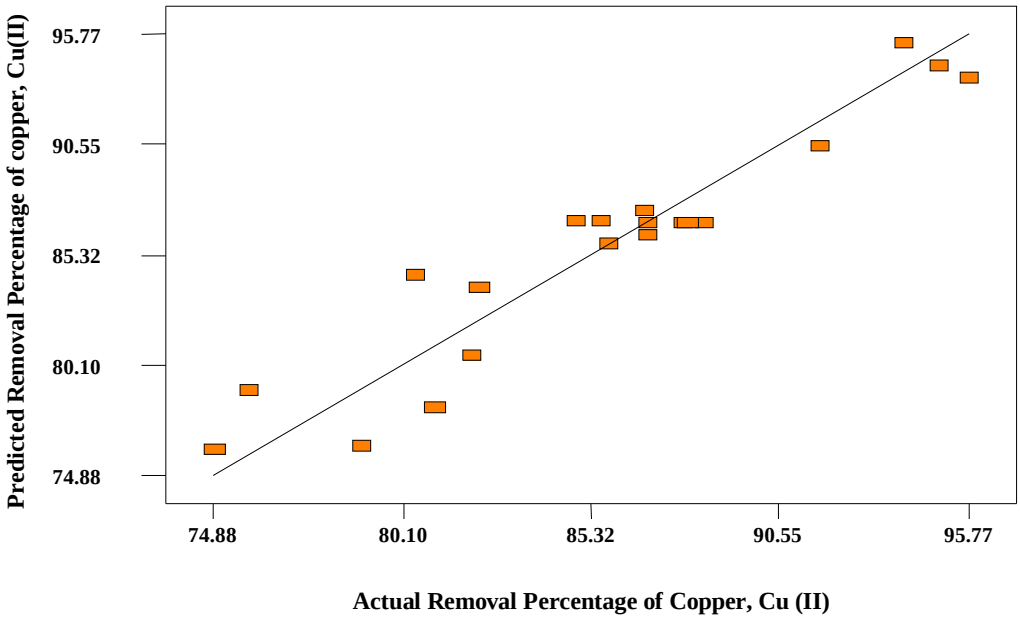

Figure 5.10 Predicted versus experimental removal percentage of copper onto Kenaf Fiber Activated carbon (KFAC)

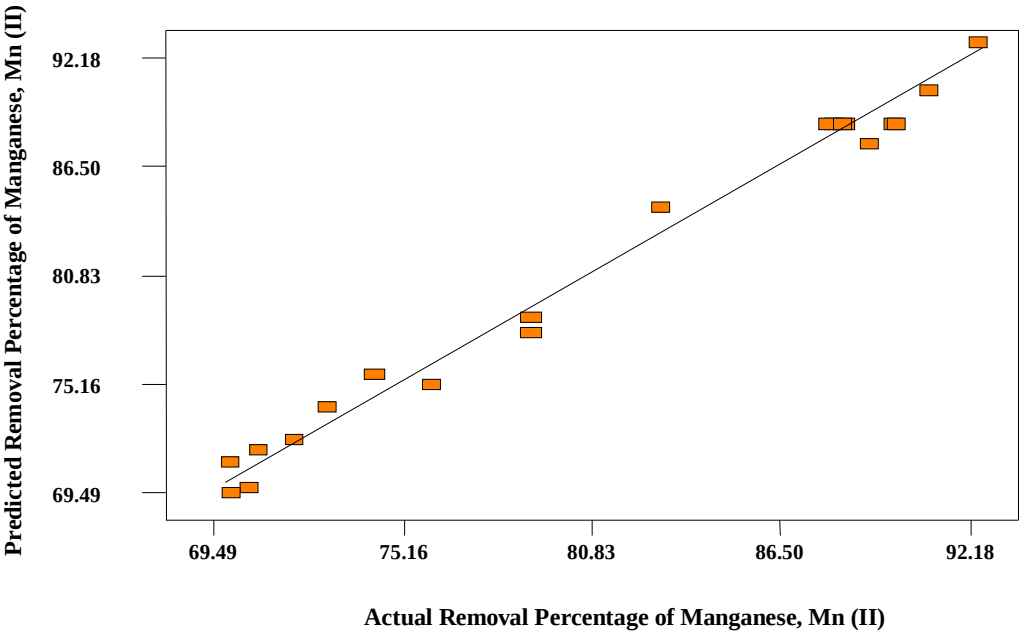

Figure 5.11 Predicted versus experimental removal percentage of manganese onto Kenaf Fiber Activated carbon (KFAC)

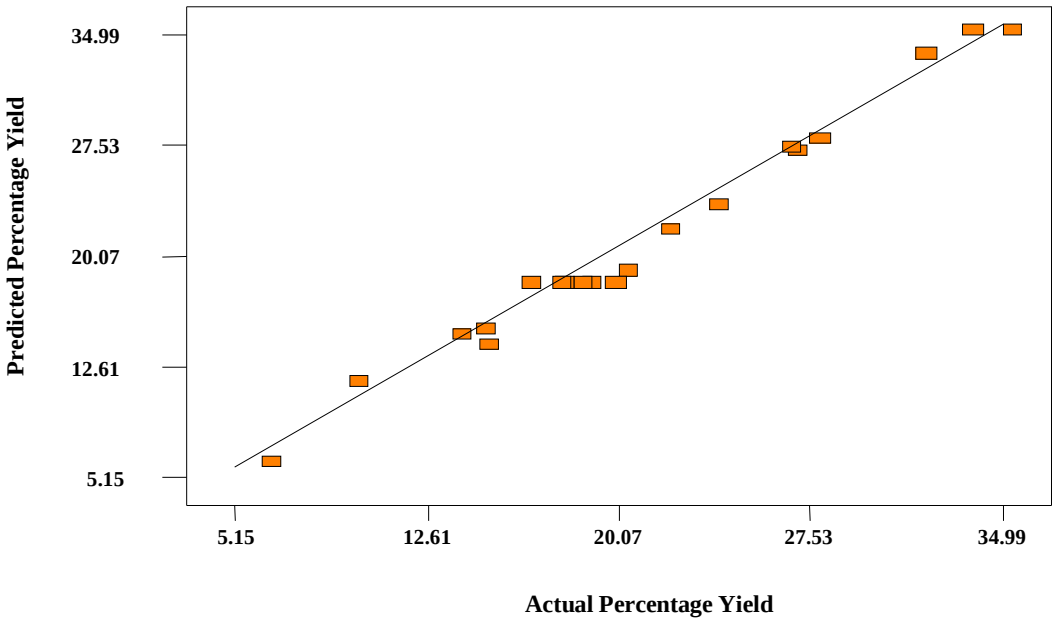

Figure 5.12 Predicted versus experimental Kenaf Fiber Activated carbon (KFAC) Yield

5.2.2.2 Removal Effeciency of Kenaf fiber based Activated Carbons

Based on the F values from Tables 5.9-5.12, both CO_2 activation temperature and IR are found to have significant effects on the adsorption uptake of Pb(II) cations with activation temperature showing the greater effect between these two factors. The effect of activation time on the other hand is not significant to the response, following the same trend for activated carbons prepared from KC. The quadratic effect of time and IR (x_2x_3) are as well significant whereas the other two quadratic effects of activation temperature and ratio (x_1x_3, x_1x_2) are considered moderate. For Mn(II) ions also, both CO_2 activation temperature (x_1) and IR (x_3) are found to have significant effects rather than activation time (x_2). Similar observation had been reported for H_3PO_4 treated rattan sawdust where activation temperature and ratio played vital role for development of surface area (Ahmad *et al.,* 2009). For adsorption of Cu(II) ions activation temperature (x_1) and time (x_2) showed almost similar impact.

Figures 5.13- 5.16 show three dimensional response surfaces with contour plot which was constructed to show the most important two variables (activation temperature and IR) on the adsorption uptake of KFAC based activated carbons. For this plot, the activation time was fixed at zero level (t = 2 h). As can be seen from Figure 5.13,5.14 and 5.15, the uptake of Pb(II), Cu(II) and Mn(II) cations increases with increase in activation temperature and IR. However, after a certain limit of activation time and ratio, the removal percentage is reduced slightly. This phenomena is explained earlier in terms of destruction of pore walls and degradation of surface functional groups.

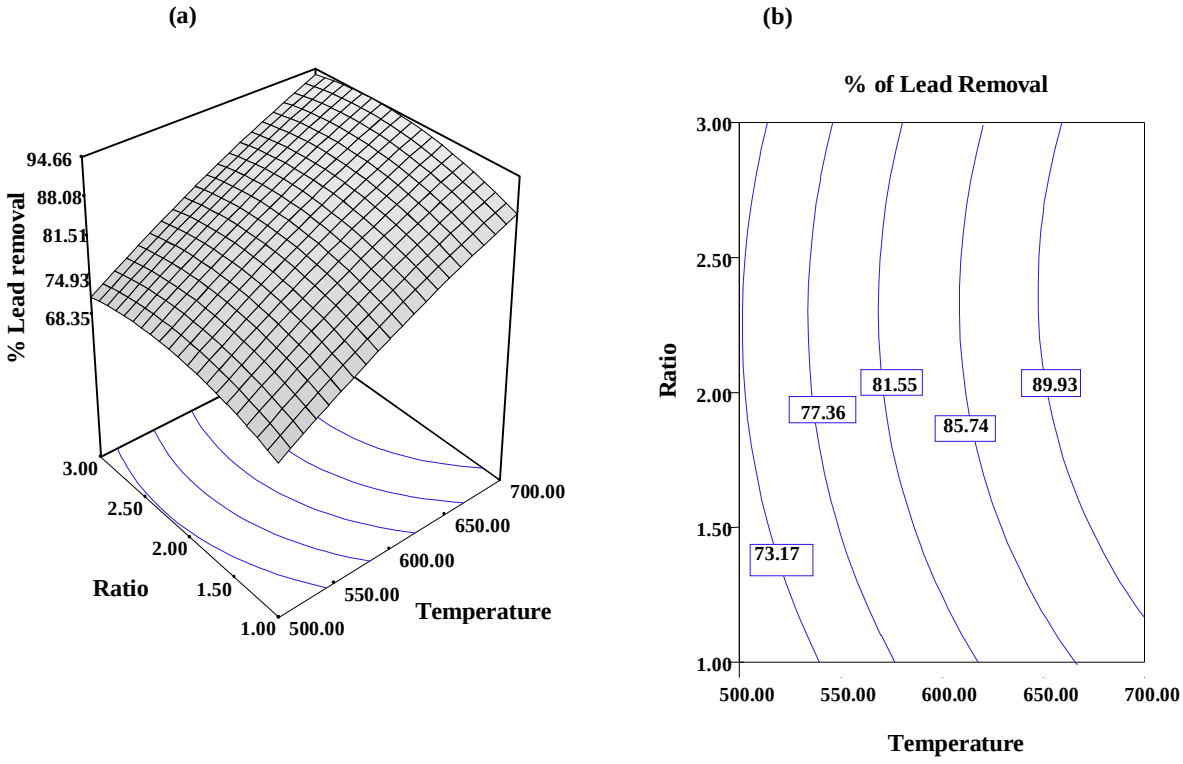

Figure 5.13 (a) Three Dimensional Response Surface (b) Surface contour plot of removal percentage of lead (II) (Effect of activation temperature and IR, Time, t=2 h) onto Kenaf Fiber activated carbon (KFAC)

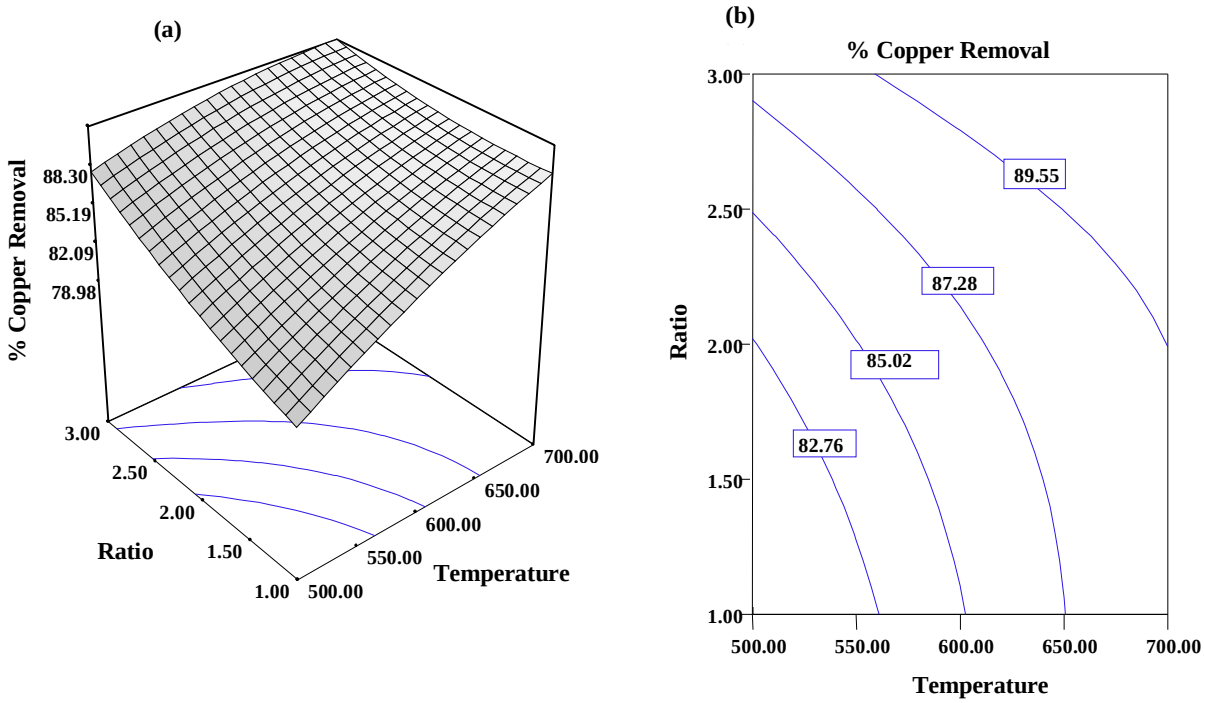

Figure 5.14 (a) Three Dimensional Response Surface (b) Surface contour plot of removal percentage of copper (II) (Effect of activation temperature and IR, Time, t=2 h) onto Kenaf Fiber activated carbon (KFAC)

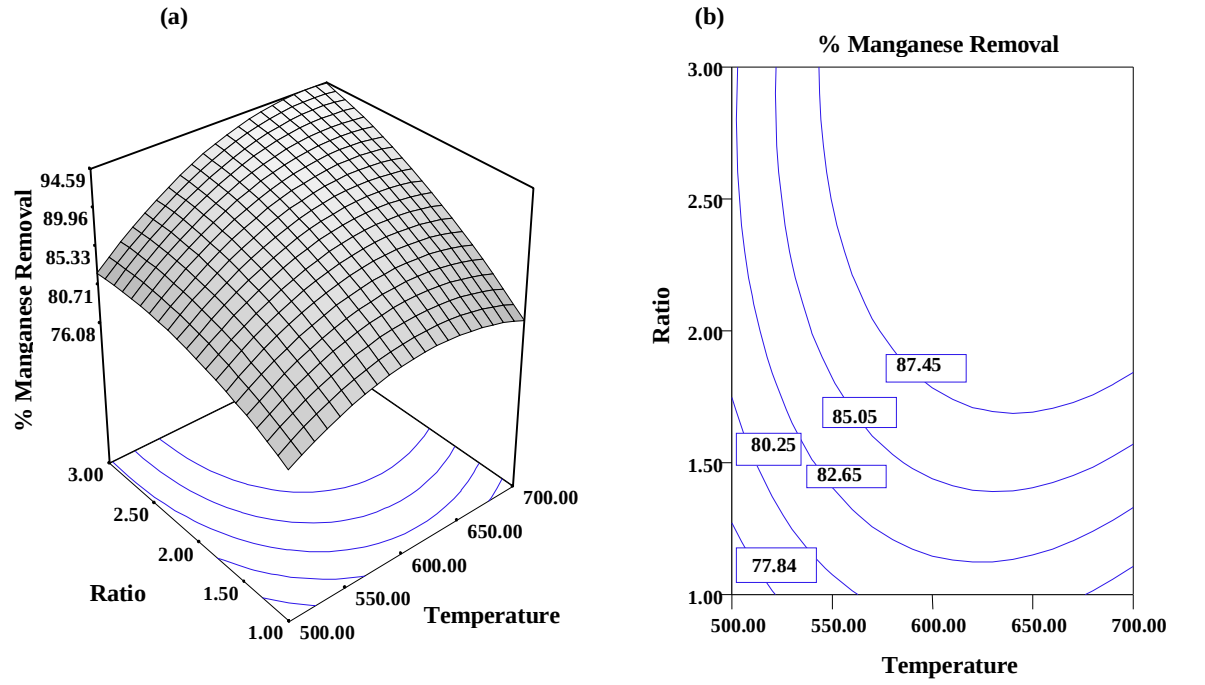

Figure 5.15 (a) Three Dimensional Response Surface (b) Surface contour plot of removal percentage of manganese (II) (Effect of activation temperature and IR, Time, t=2 h) onto Kenaf Fiber activated carbon (KFAC)

It was reported in the literature that too long or too short activation time and/or too high or too low activation temperature could reduce the surface area and the adsorption capacity of activated carbon. This is because longer activation time and/or higher activation temperature might destroy the pore structure formed previously whereas shorter activation time and/or lower activation temperature could not enhance the formation of porosity (Cao *et al.*, 2006). At very high temperatures, thermal annealing causes the walls of the micropore to collapse and form more mesopores which are helpful for carrying the adsorbate towards the interior of micropores for liquid phase adsorption but in some cases, inspite of high surface area, if the pore distribution is not suitable or pore diameter of those mesopores are larger, then they faile to capture and retain the smaller cations resulting in smaller removal effeciency. It was observed for these two adsorbates (copper and manganese) that after certain limit of temperature and KOH ratio, the adsorption capacity reduced slightly. This phenomenon had been explained earlier in terms of porosity and intensity or disruption of surface functional groups.

However, for preparing activated carbon from oil palm frond for the removal of zinc from aqueous solution by RSM technique similar observation was reported. Another pausible explanation for this observation may be due to the formation of more ash residues which can sinter and block the pores resulting in smaller removal effeciency (Zahangir *et al.*, 2005). However, it is well documented that ash residues which are regarded as impurities for activated carbon preparation may take part in sorption process of heavy metals due to the presence of oxide content (Ahmad, 2006).

5.2.2.3 Kenaf Fiber (KF) Activated Carbon Yield

For activated carbon yield, all the three variables are found to be significant on the response. However, activation temperature is found to have the greatest effect on it. The quadratic effect of activation temperature is the highest among all the factors being considered in this study whereas the interaction effect between activation temperature and ratio is insignificant to the response. Figure 5.16 (a) demonstrates the effect of activation temperature and activation time on the KF activated carbon yield, with IR fixed at zero level (IR = 2), and Figure 5.16(b) shows the effect of activation temperature and IR on the same response, with activation time fixed at zero level (t = 2 h).

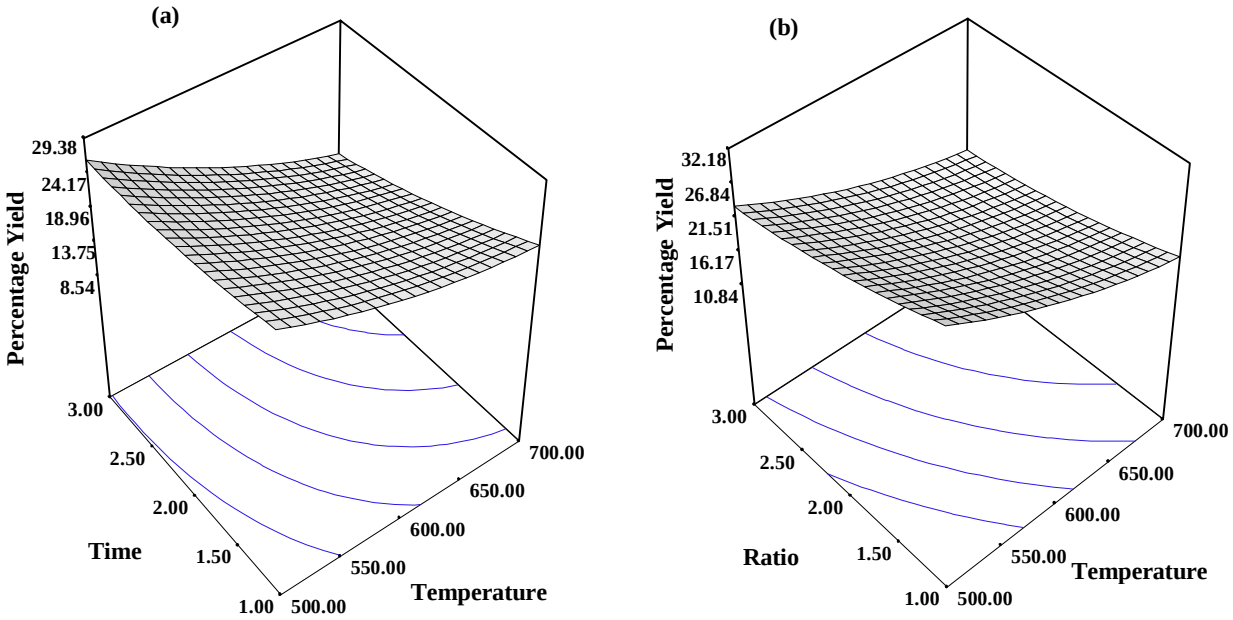

Figure 5.16 Three Dimensional Response Surface plot of Kenaf Core activated carbon (KCAC) yield (a) Effect of activation temperature and activation time, IR= 2 (b) Effect of activation temperature and IR, Time= 2 h)

Basically, the activated carbon yield was found to decrease with increasing activation temperature activation time and IR, following the same trend as the KC and KF activated carbon yields. As expected, the increase in activation temperature, time and IR would decrease the activated carbon yield due to higher carbon burn off (Bacaoui *et al.,* 2001; Yan and Lua, 2003; Lua and Yang 2004; Sentorun-Shalaby *et al.,* 2006; Wu and Tseng, 2006; Adinata *et al.,* 2007).

5.3 Preparation of Activated Ash

Activated ash was prepared by using three variables of activation temperature, (x_1), ratio between OPA and NaOH (x_2) and time, (x_3) based on the central composite design (CCD). The preparation variables were changed according to the experimental run and 20 sample of activated ash was prepared. However, the chemical activating agent together with the range of process variables (Temperature, time and ratio) were preselected based on the literature. The responses considered in this study are :

(i) Y_1 - adsorption capacity/ removal percentage of Lead (II)

(ii) Y_2 - adsorption capacity/ removal percentage of Copper (II)

(iii) Y_3 - adsorption capacity/ removal percentage of Manganese (II)

Model regression analysis of the experimental data was performed by using Design Expert software version 6.0.6 (STAT-EASE Inc., Minneapolis, US).

5.3.1 Preparation of Activated Oil Palm Ash (AOPA) using Design of Experiment

The complete design matrix for preparing activated palm ash is presented in Table 5.13 20 samples prepared at different experimental condition are designated as S-1 to S-20.

Table 5.13 Experimental Design Matrix for preparation of Activated palm ash (AOPA) from natural palm ash (OPA)

Sample ID	Run	Type of Point	Level (coded Factors)			Activated oil palm ash preparation Variables (Actual Factors)			Percentage Removal, Pb (II) Y_1(mg/g)	Percentage Removal, Cu (II) Y_2(mg/g)	Percentage Removal, Mn (II) Y_3(mg/g)
						Temperature x_1, (°C)	Ratio, x_2 OPA:NaOH,	Time, x_3,(Hour)			
S-1	1	Fact	-1	-1	-1	80.00	3.00	4.00	32.99	38.38	36.77
S-2	2	Fact	+1	-1	-1	160.00	3.00	4.00	48.89	59.09	46.67
S-3	3	Fact	-1	+1	-1	80.00	5.00	4.00	39.87	56.09	35.56
S-4	4	Fact	+1	+1	-1	160.00	5.00	4.00	53.45	60.22	51.09
S-5	5	Fact	-1	-1	+1	80.00	3.00	8.00	40.99	50.06	38.09
S-6	6	Fact	+1	-1	+1	160.00	3.00	8.00	46.66	69.09	52.06
S-7	7	Fact	-1	+1	+1	80.00	5.00	8.00	58.88	64.98	39.99
S-8	8	Fact	+1	+1	+1	160.00	5.00	8.00	63.33	71.99	53.22
S-9	9	Axial	-1.682	0	0	52.73	4.00	6.00	41.09	49.99	30.99
S-10	10	Axial	+1.682	0	0	187.27	4.00	6.00	60.32	64.55	49.99
S-11	11	Axial	0	-1.682	0	120.00	2.32	6.00	36.89	51.22	44.88
S-12	12	Axial	0	+1.682	0	120.00	5.68	6.00	42.88	66.55	52.78
S-13	13	Axial	0	0	-1.682	120.00	4.00	2.64	38.88	49.56	44.87
S-14	14	Axial	0	0	+1.682	120.00	4.00	9.34	62.09	65.09	49.89
S-15	15	Center	0	0	0	120.00	4.00	6.00	44.98	57.99	43.09
S-16	16	Center	0	0	0	120.00	4.00	6.00	45.44	54.09	47.09
S-17	17	Center	0	0	0	120.00	4.00	6.00	43.99	61.44	43.09
S-18	18	Center	0	0	0	120.00	4.00	6.00	45.48	58.88	48.77
S-19	19	Center	0	0	0	120.00	4.00	6.00	43.44	55.78	40.44
S-20	20	Center	0	0	0	120.00	4.00	6.00	44.77	55.03	45.09

As before, samples S-15 to S-20 at the center point were prepared under the same set of variables to determine experimental errors and reproducibiliy of data. S-8 prepared at factorial point (temperature x_1-160 °C, ratio x_2-5 and time x_3- 8 h) showed highest removal effeciency for all the cations.

5.3.1(a) Development of Regression Model Equations for Preparation of Activated Ash (AOPA)

The result obtained in Table 5.13 were correlated with the three preparation variables studied using second degree polynomial equation. The final empirical models in terms of coded factors after excluding the insignificant terms are presented by Equations 5.11-5.13.

$$Percentage\ removal\ of\ Pb(II), Y_1 = 44.65 + 5.27x_1 + 4.11x_2 + 5.40x_3 - 2.33\ x_1^2 - 1.49x_2^2 + 2.26x_3^2 - 0.44x_1x_2 - 2.42x_1x_3 + 2.89x_2x_3 \quad (5.11)$$

$$Percentage\ removal\ of\ Cu(II)\ \ Y_2 = 58.00 + 5.52x_1 + 4.57x_2 + 5.01x_3 - 3.57\ x_1x_2 + 0.15x_1x_3 - 0.13x_2x_3 \quad (5.12)$$

$$Percentage\ removal\ of\ Mn(II), Y_3 = 44.64 + 6.19x_1 + 1.43x_2 + 1.59x_3 - 1.76x_1^2 + 1.19x_2^2 + 0.68x_3^2 + 0.61x_1x_2 + 0.22x_1x_3 - 0.019x_2x_3 \quad (5.13)$$

The empirical models shown by equation 5.11-5.13 indicate that duration of reaction represented by hydration period, temperature and ratio have significant effect on the removal efficiency. For lead and copper, quadratic and 2FI models respectively,

had been suggested by the software. Apart from terms x_1, x_2 and x_3, quadratic terms of temperature x_1^2 and ratio x_3^2 and interaction terms of x_1x_3 x_2x_3 are significant model terms for removal percentage of lead. For copper, x_1, x_2 and x_3, and interaction terms of temperature and time x_1x_2 are significant model terms. However, for manganese uptake onto AOPA, both linear and quadratic models were suggested. Due to higher order polynomial, the data has been analyzed by using quadratic model. For manganese, x_1 and x_3 and quadratic term of temperature, x_1^2 is significant. The R^2 value for Equations 5.1-5.4 are 0.94, 0.95 and 0.91 respectively which ensures satisfactory adjustment of the developed models with the experimental data. The other statistical parameters used to analyze the suitability of the developed models are listed in Table 5.14.

Table 5.14 Statistical parameters for ANOVA analysis for Model regression of removal percentage of Pb (II), Cu (II) and Mn (II) for activated oil palm ash (AOPA)

Statistical Parameters	**Percentage Removal of Pb (II)** Y_1	**Percentage Removal of Cu (II)** Y_2	**Percentage Removal of Mn(II)** Y_3
Standard Deviation, SD%	2.86	2.28	2.62
Correlation Coefficient, R^2	0.94	0.95	0.91
Adjusted R^2	0.89	0.92	0.82
Mean	46.76	58.00	44.72
Coefficient of Variation, CV	6.14	3.92	5.85
Adeq. Precision	14.55	22.42	13.79

The small values of standard deviations and co-efficient of variation, CV reflected reproducibility of the model.

The values for "Adeq Precision" obtained for all the responses reflected that the models can be used to navigate the design space.

The linear plots obtained for diagnostic tests are shown in Appendix C (C9-C11). Figures C9 (a-b), C10 (a-b) and C11 (a-b) show outliers t plot and studentized residuals vs. predicted plots for removal percentage of Pb(II), Cu (II) and Mn(II) ions respectively. From Figures C9 (a), C10 (a) and C11 (a), it was observed, that all the data points are between ±3.50 (outlier t plots). Like Kenaf core and kenaf fiber based activated carbon (KCAC and KFAC), the studentized residuals vs. predicted plots for removal percentage of Pb(II), Cu (II) and Mn(II) ions show no response transformation was needed for the experimental design of this study (Myers and Montgomery, 1995).

The adequacy of the developed models were further justified through analysis of variance (ANOVA) and the results obtained are depicted in Tables 5.15-5.17. The model F-value for removal percentage of lead, copper and manganese are 17.69, 36.92 and 10.86 respectively which implied that these models are significant. Based on 99% confidence level, the model F- value indicated that the models are reliable in predicting the removal percentage of the divalent cations.

Table 5.15 ANOVA analysis and Lack of Fit test for Response Surface Model for removal percentage of lead, Pb (II) by using activated palm ash (AOPA)

Source	Sum of Squares	Degree of Freedom	Mean Square	F Value	Prob> F	Comments
Model	1313.21	9	145.91	17.69	<0.0001	*Significant*
x_1	378.86	1	378.86	45.94	<0.0001	
x_2	230.15	1	230.15	27.91	0.0004	
x_3	397.56	1	397.56	48.21	<0.0001	
x_1^2	78.44	1	78.44	9.51	0.0116	
x_2^2	32.10	1	32.10	3.89	0.0768	
x_3^3	73.30	1	73.30	8.89	0.0138	
x_1x_2	1.58	1	1.58	0.19	0.6714	
x_1x_3	46.90	1	46.90	5.69	0.0383	
x_2x_3	66.76	1	66.76	8.09	0.0174	
Residuals	82.47	10	8.25			
Lack of Fit	79.12	5	15.82	23.59	0.0017	*Significant*
Pure Error	3.35	5	0.67			

Table 5.16 ANOVA analysis and Lack of Fit test for Response Surface Model for removal percentage of copper, Cu (II) by using activated palm ash (AOPA)

Source	Sum of Squares	Degree of Freedom	Mean Square	F Value	Prob> F	Comments
Model	1147.14	6	191.19	36.92	<0.0001	*Significant*
x_1	415.92	1	415.92	80.31	<0.0001	
x_2	285.50	1	285.50	55.13	<0.0001	
x_3	343.16	1	343.16	66.26	<0.0001	
x_1x_2	102.24	1	102.24	19.74	0.0007	
x_1x_3	0.18	1	0.18	0.035	0.8550	
x_2x_3	0.13	1	0.13	0.025	0.8765	
Residuals	67.33	13	5.18			
Lack of Fit	29.50	8	3.69	0.49	0.8251	*Not Significant*
Pure Error	37.82	5	7.56			

Table 5.17 ANOVA analysis and Lack of Fit test for Response Surface Model for removal percentage of manganese, Mn (II) by using activated palm ash (AOPA)

Source	Sum of Squares	Degree of Freedom	Mean Square	F Value	Prob> F	Comments
Model	669.26	9	74.36	10.86	0.0004	*Significant*
x_1	523.87	1	523.87	76.47	<0.0001	
x_2	28.00	1	28.00	4.09	0.0708	
x_3	34.52	1	34.52	5.04	0.0486	
x_1^2	44.44	1	44.44	6.49	0.0290	
x_2^2	20.49	1	20.49	2.99	0.1144	
x_3^3	6.66	1	6.66	0.97	0.3474	
x_1x_2	2.99	1	2.99	0.44	0.5238	
x_1x_3	0.39	1	0.39	0.057	0.8159	
x_2x_3	0.003	1	0.003	0.0004	0.9842	
Residuals	68.50	10	6.85			
Lack of Fit	22.81	5	4.56	0.50	0.7680	*Not Significant*
Pure Error	45.69	5	9.14			

Referring to Table 5.15, it is observed that hydration temperature, x_1 and hydration period, x_3 have more impact on adsorbent development for the removal percentage of lead. The effect of OPA to NaOH ratio is less pronounced in this case. Similar trend has been observed for uptake of manganese.

From the statistical results obtained, it is shown that the above models (Equations 5.11-5.13) are adequate to predict the removal percentage within the experimental range of variables selected. The performance of the model can also be visualized by observing the linear plots of predicted versus experimental percentage removal as shown in Figures 5.17, 5.18, and 5.19 respectively.

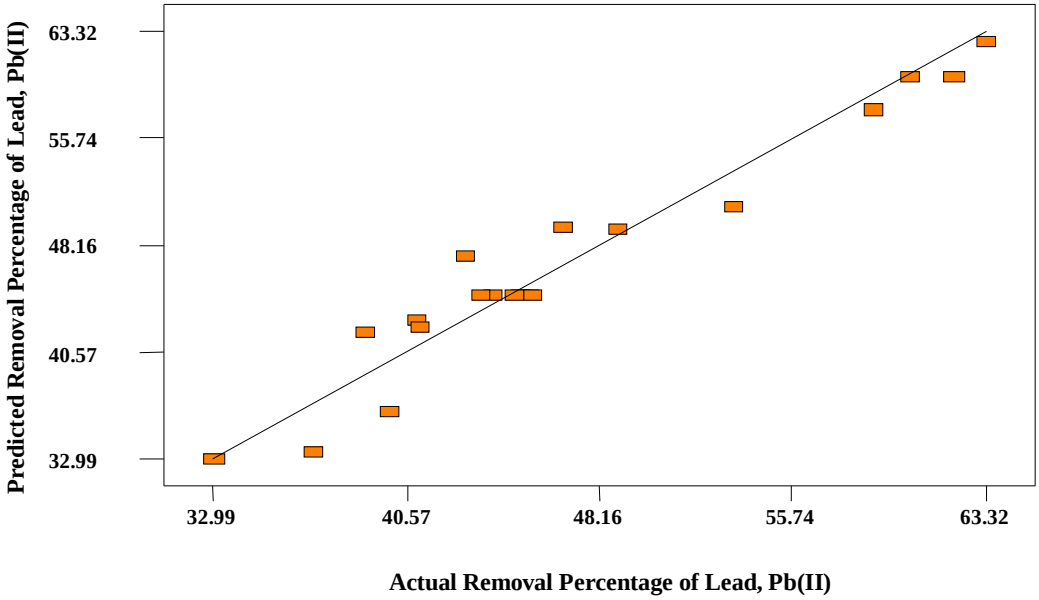

Figure 5.17 Predicted versus experimental removal percentage of lead onto AOPA

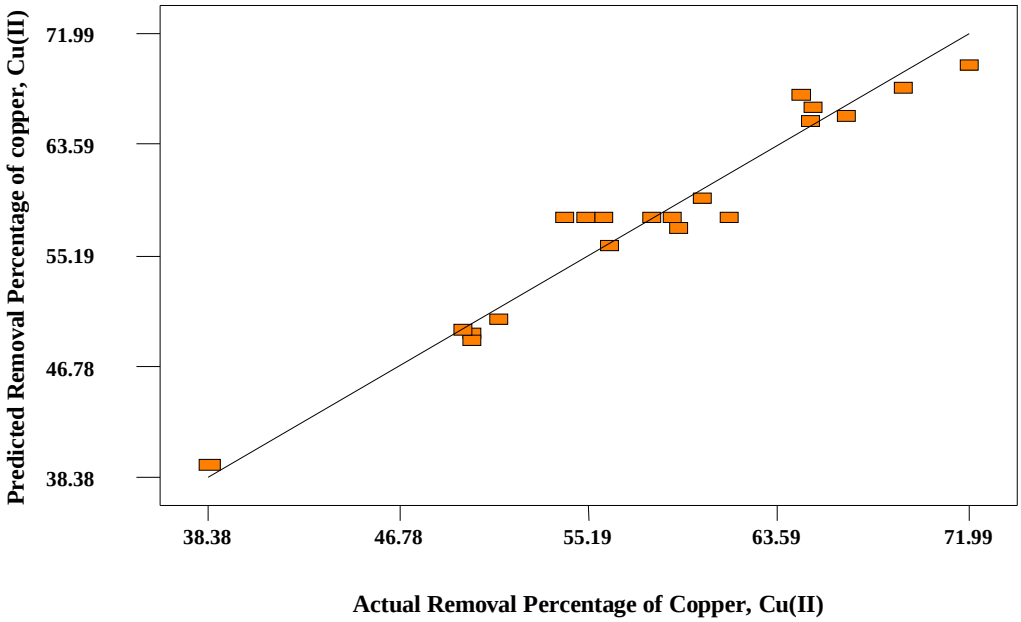

Figure 5.18 Predicted versus experimental removal percentage of copper onto AOPA

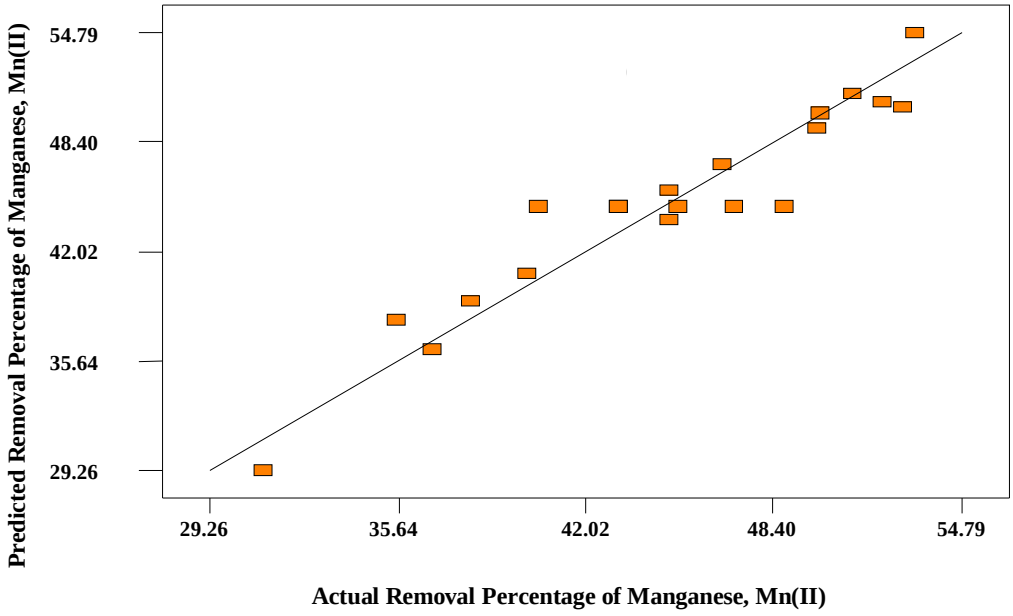

Figure 5.19 Predicted versus experimental removal percentage of manganese onto AOPA

5.3.1(b) Removal Efficiency of Activated Ash

Figures 5.20, 5.21 and 5.22 were constructed to depict the three-dimensional response surfaces which show the combined effects of activation temperature (x_1) and ratio (x_2) on the adsorption capacity of the adsorbate. In this case, the activation time was fixed at zero level, which was 4 h. As can be seen from the design matrix, removal efficiency of AOPA towards the cations increases successively with the increasing ratio between oil palm ash and NaOH. This is expected as at higher ratio, more ash would be available to react with sodium hydroxide to form active species (Zainudin *et al.*, 2005). However, applying too high ratio is not feasible as there will be a decrease in converted alkali per unit weight of sorbent (Davini *et al.*, 1994).

The plots showed that, maximum removal percentage is observed when all the preparation variables were set at maximum point. It is observed that increasing contact

time increases the removal efficiency. This is most probably due to the increase in surface area. However, it was reported earlier that dissolution of silica in presence of alkali-water is a time-consuming process (Zainudin *et al.*, 2005). Therefore, sufficient contact time should be given for the activation process to be completed. It was observed in the case of coal fly ash activated with NaOH that, prolonged contact time caused dissolution of more silica or alumina from ash particles to react with the activating agent resulting in extended surface area (Pretorius *et al.*, 2003).

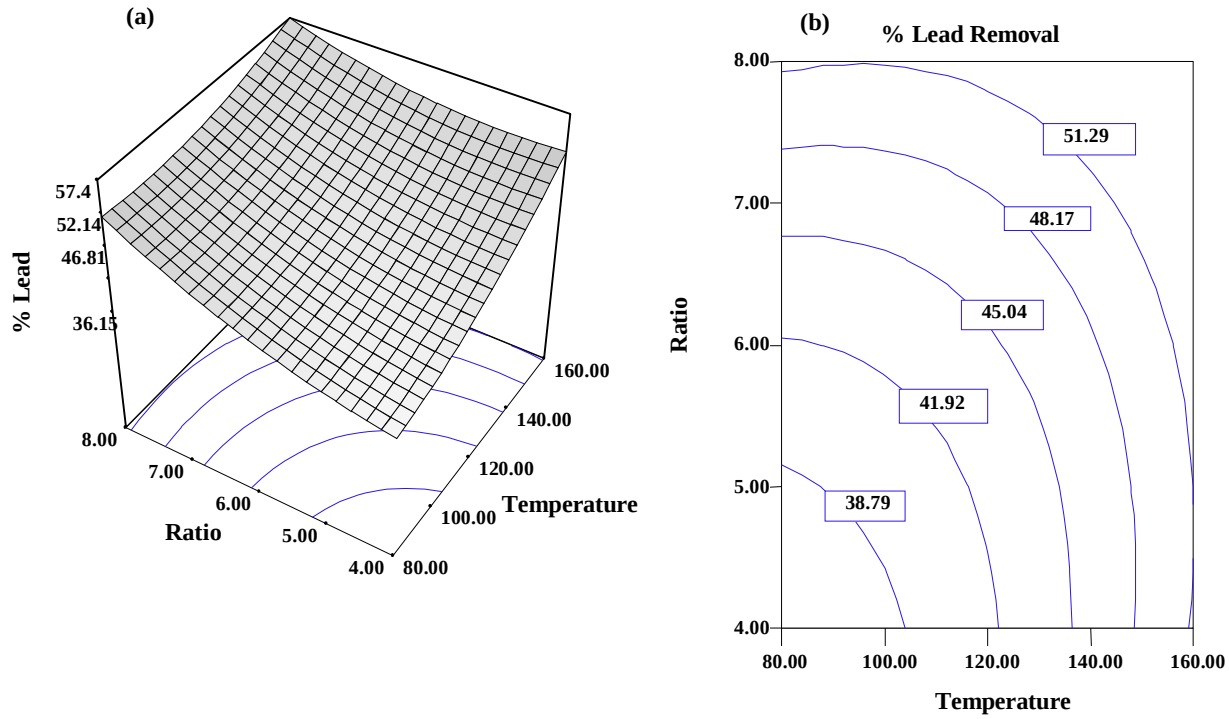

Figure 5.20 (a) Three Dimensional Response Surface (b) Surface contour plot of removal percentage of lead(II) (Effect of activation temperature and Time, IR=4) onto AOPA

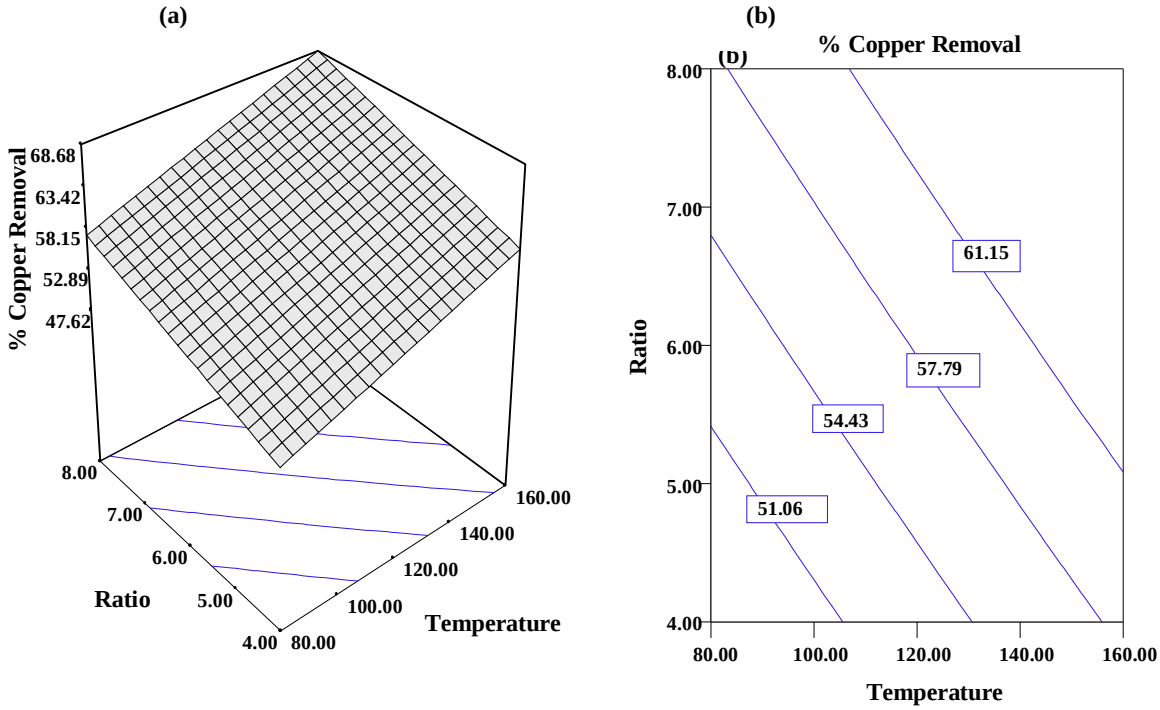

Figure 5.21 (a) Three Dimensional Response Surface (b) Surface contour plot of removal percentage of copper (II) (Effect of activation temperature and Time, IR=4) onto AOPA

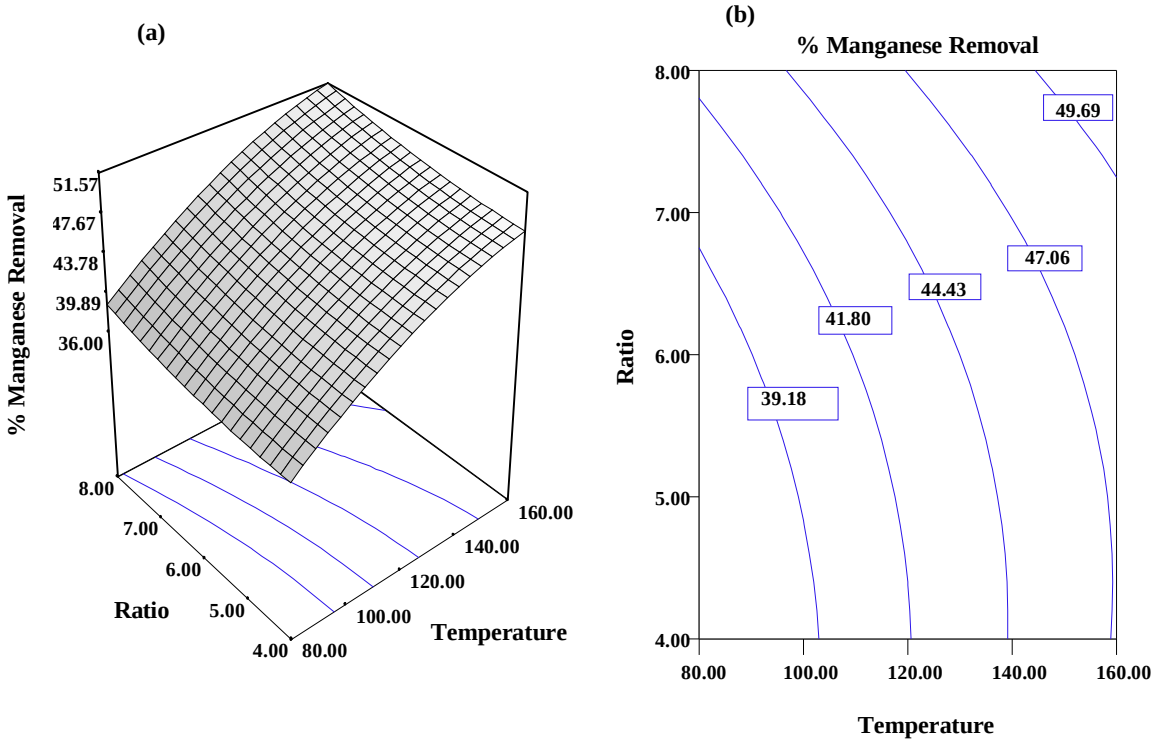

Figure 5.22 (a) Three Dimensional Response Surface (b) Surface contour plot of removal percentage of manganese (II) (Effect of activation temperature and Time, IR=4) onto AOPA

Present study shows that increasing temperature increases removal efficiency. Similar observation was reported for activation of coal fly ash by using CaOH, where it was observed that by changing reaction condition preset at 40 °C for 4 hours to 90 °C for 6 h, the BET surface area became almost double (Davini *et al*., 1994). It was observed that Amaga coal based ash after treated with NaOH of different concentration, time and temperature produced an activated adsorbent having adsorptive capacity equal to 70-80% of the commercially available zeolite (Mehta, 1989). However, bagasse fly ash treated with hydrogen peroxide was reported to remove 95% to 96% of lead and chromium from waste water (Gupta *et al*., 2004).

5.4 Optimization of Process Parameters

To produce powdered form of commercial activated carbons, relatively high product yields are expected. At the same time, the most important property of an activated carbon is its adsorption performance. Therefore, in a practical manufacturing process, a compromise should be made between the activated carbon yield and the adsorption performance of the prepared activated carbon. However, to optimize both these responses under the same condition is difficult because for the region of interest the factors are different. As observed from the basic design matrix for all the precursors, when adsorption performace was increasing, carbon yield was decreasing and vice versa.

In order to compromise between these two responses, the numerical optimization menu was selected using Design Expert software version 6.0.6 (STAT-EASE Inc., Minneapolis, LTS). In order to optimize the preparation conditions for all types of powdered activated carbons used for adsorption of Pb(II), Cu(II) and Mn(II) ions from aqueous solution, the targeted criteria were set as maximum values for all the

three responses along with yield and the values of the three variables (CO_2 activation temperature, CO_2 activation time and IR) were set in the ranges being studied. However, after model simulation, different operating conditions were suggested for different adsorbate-adsorbent system. The optimization ramp for KCAC and KFAC including exact design points estimated by the software is provided in Appendix D. Therefore, three optimum operating conditions must be determined for each adsorbate for powdered activated carbon (KCAC and KFAC). Since same sets of variables were preselected for adsorption studies of all the cations onto AOPA, sample-8 was considered for further surface charecterization and adsorption studies. Based on optimization ramp for KCAC and KFAC, the summary of the results including AOPA are tabulated in Tables 5.18, 5.19 and 5.20.

The experimental condition listed in Table 5.18-5.20 were applied to prepare the optimum activated adsorbent from KC, KF and AOPA for the adsorption of Pb(II), Cu(II) and Mn(II) ions. The predicted and experimental values for the responses obtained for each activited carbon prepared are also presented in the same Tables 5.18 - 5.20. The result revealed a trend showing that higher activation tempeature is needed to prepare activated carbon for lead compared to other two cations. This is due to the different characteristics and affinity of the three adsorbate towards the prepared adsorbents. However, for activation time and ratio, no consistent trend is observed on the responses. This could be explained based on the observation obtained earlier where the effect of these two variables on the uptake capacity are comparatively minor compared to temperature.

Table 5.18 Process Parameters optimization for adsorption of Lead Pb (II)

Activated Adsorbent	Activation Temperature (°C)	Activation Ratio -	Activation Time (Hour)	Lead Adsorption Capacity (%)			Activated Carbon Yield (%)		
				Predicted	Experimental	Error	Predicted	Experimental	Error
KCAC	651.53	1.00	1.00	82.24	93.59	12.14	24.42	22.59	8.05
KFAC	700.00	1.35	1.00	87.84	93.23	5.78	21.99	22.22	1.03
AOPA	160.00	5.00	8.00	-	63.22	-	-	-	-

Table 5.19 Process Parameters optimization for adsorption of Copper Cu (II)

Activated Adsorbent	Activation Temperature (°C)	Activation Ratio -	Activation Time (Hour)	Copper Adsorption Capacity (%)			Activated Carbon Yield (%)		
				Predicted	Experimental	Error	Predicted	Experimental	Error
KCAC	568.00	1.75	2.02	89.02	97.24	8.45	24.66	27.55	0.10
KFAC	500.00	3.00	1.25	86.99	96.54	9.89	26.02	26.99	3.59
AOPA	160.00	5.00	8.00	-	71.99	-	-	-	-

Table 5.20 Process Parameters optimization for adsorption of Manganese Mn (II)

Activated Adsorbent	Activation Temperature (°C)	Activation Ratio -	Activation Time (Hour)	Manganese Adsorption Capacity (%)			Activated Carbon Yield (%)		
				Predicted	Experimental	Error	Predicted	Experimental	Error
KCAC	584.27	1.74	1.68	88.99	90.01	1.13	24.54	23.51	4.38
KFAC	573.96	3.00	1.31	88.12	86.23	2.19	20.62	20.06	2.79
AOPA	160.00	5.00	8.00	-	53.22	-	-	-	-

It can be seen from the tabulated results in Tables 5.18-5.20 that the experimental and predicted values obtained for yield showed deviation errors less than removal percentage. However, the predicted result for removal effeciency deviated less than 10% except for lead using kenaf core activated carbon (KCAC). This indicates that the models are suitable and sufficient to determine the responses from the operating variables.

Process parameter optimization to produce activated adsorbent from oil palm ash (OPA) is less complicated compared to the production of powdered activated carbon because there is no need to consider two opposing responses. However, for preparing activated ash from natural oil palm ash, sample S-8 prepared at 160 °C, contact time 8 h and OPA to NaOH ratio of 5 is taken as the optimum as it shows maximum removal effeciency for all the adsorbates under investigation.

5.5 Summary

Based on this study, the effects of the operating variables are optimized for preparing powdered activated adsorbent from lignocellosic materials such as KC and KF together with a silaceous starting material of OPA. Although these two types of starting materials originate from agricultural biomass, they contain different, even zero proportion of carbon (OPA) as depicted earlier. In view of this, different range of process variables were preset to get maximum removal effeciency from oil palm ash (OPA) so as to compare it's performance with other powdered activated carbon obtained from KC and KF and commercial activated carbon.

The experimental design results for preparing activated carbon revealed that CO_2 activation temperature is the most important factor influencing the adsorption performance of the activated carbons prepared from KC and KF regardless of different adsorbates. However, all the three variables showed significant effects on the activated carbon yields, in spite of the different types of precursors used. It could be concluded that the variables investigated are important factors which must be taken into consideration in activated carbon production. The process optimization resulted in activated carbons with maximum possible yield and adsorption performance within the experimental ranges studied. This would help in minimizing the activated carbon production costs industrially. The experimental design matrix for activation of palm ash demonstrated that hydration temperature, time and ratio are important parameters in extending the sorption capacity.

It is well known that production of powdered activated carbon (PAC) suffers from some major drawbacks of weight loss during preparation and handling steps. On the contrary, granular activated carbons (GAC) have attrition resistance i.e., least tendency of mass loss depending on the precursors. That's why in this study all the powdered activated adsorbent (KCAC, KFAC and AOPA) were prepared under optimum condition to ensure maximum output of the process.

However, all the powdered activated adsorbent prepared under optimum conditions need to be further characterized in order to study their physio-chemical features which influence the removal effeciency (Chapter 6). The effects of parameters affacting the adsorption performance of the prepared activated adsorbents such as adsorbate initial concentration, contact time, solution temperature, solution pH as well

as the adsorption isotherms, kinetics and thermodynamic behaviors are further evaluated and the results are discussed in the following Chapter 7. The regeneration effeciency of the spent adsorbents is also presented.

CHAPTER SIX
RESULTS AND DISCUSSION
Activated Adsorbent Characterization

6.1 Introduction

This chapter presents the experimental results and discussion on the characterization of the prepared activated adsorbent (KCAC, KFAC, AOPA and MFSAC). The physical and chemical properties of the prepared adsorbent are determined. This gives insight about the sorption mechanism of metallic cations (lead, copper and manganese) onto their surface. A summary is presented in the last part of this chapter.

6.2 Physical Characterization of Prepared Activated Adsorbent

The adsorption performance of the activated adsorbent is highly influenced by the physical properties. In this study, all the adsorbents prepared were characterized for their physical characteristics by determining the BET surface area, micropore-mesopore surface area, total pore volume and avarage pore diameter including bulk density and iodine number measurement. SEM analysis of the prepared sorbent was done to study their surface morphology. Table 6.l lists the operating canditions applied to prepare the powdered activated adsorbent (KCAC, KFAC and AOPA) from different starting materials which were optimized for the adsorption of divalent cations of lead, copper and manganese from synthetic water in Chapter Five (Section-5.4). The preparation variables used for granular activated sorbent (MFSAC) derived from mangostene fruit shell (MFS) are also provided in the same Table.

.

Table 6.1 Powdered and Granular Activated Adsorbent preparation under Optimum condition

Starting Material Carbonaceous	Activated Adsorbent	Activation Condition			Yield
	Powdered Activated Carbon (PAC)	Activation Temperature (°C)	Activation Time (Hour)	KOH: Char, Ratio -	-
Kenaf Core (KC)	KCAC (Pb)	651.53	1.00	1.00	22.59
	KCAC(Cu)	568.00	2.02	1.75	27.55
	KCAC(Mn)	584.27	1.68	1.74	23.51
Kenaf Fiber (KF)	KFAC (Pb)	700.00	1.00	1.35	22.22
	KFAC (Cu)	500.00	1.25	3.00	26.99
	KFAC(Mn)	573.96	1.31	3.00	20.06
Starting Material Carbonaceous	**Granular Activated Carbon (GAC)**	**Activation Temperature (°C)**	**Activation Time (Hour)**	**KOH: Char, Ratio -**	**Yield -**
Mangostene Fruit Shell(MFS)	MFSAC	750.00	2.00	1.00	32.57
Starting Material Mineral Based	**Powdered Adsorbent**	**Activation Temperature (°C)**	**Activation Time (Hour)**	**OPA: NaOH Ratio -**	**Yield -**
Natural Palm ash (OPA)	AOPA	160.00	8.00	5.00	N/A

N/A- Not applicable

6.2.1 Surface Area and Pore Characteristics

The surface area and pore characteristics of the prepared sorbent including the pore volume and pore size distribution were analyzed using Quantachrome Autosorb 6B, an automated gas sorption system through nitrogen adsorption isotherm at 77 °K and the results obtained for each sample were calculated by the software provided with the system. The surface area and pore characteristics determined by the software (Micropore version 2.26) are presented in Table 6.2(a).

Table 6.2(a) Surface area and pore characteristics of prepared activated adsorbents

Starting Material Carbonaceous	Type of Activated Carbon (PAC)	BET Surface area (m^2/g)	Cumulative Adsorption Surface area(BJH) (m^2/g)	Micropore Surface area (m^2/g)	Meso pore Volume (cc/g)	Micro pore Volume (cc/g)	Total Pore Volume (cc/g)	Average pore Diameter °A	Bulk Density (g/mL)	Iodine Number (mg/g)
Kenaf Core (KC)	KCAC (Pb)	1532.02	974.87	1043.00	0.2129	0.6194	0.8323	23.79	0.304	955.43
	KCAC(Cu)	1020.03	545.45	815.04	0.1612	0.4177	0.5789	22.70	0.312	802.00
	KCAC(Mn)	1062.04	657.82	1004.30	0.1687	0.4378	0.6065	23.02	0.349	789.00
Kenaf Fiber (KF)	KFAC (Pb)	525.50	504.10	610.23	0.1051	0.2169	0.3220	24.91	0.353	510.67
	KFAC (Cu)	330.40	178.33	361.30	0.0540	0.1350	0.1890	22.90	0.332	310.22
	KFAC(Mn)	386.03	219.80	278.60	0.0725	0.1605	0.2330	24.10	0.339	333.87
Starting Material Carbonaceous	**Activated Carbon (GAC)**	**BET Surface area (m^2/g)**	**Cumulative Adsorption Surface area(BJH) (m^2/g)**	**Micropore Surface area (m^2/g)**	**Meso pore Volume (cc/g)**	**Micro pore Volume (cc/g)**	**Total Pore Volume (cc/g)**	**Average pore Diameter °A**	**Bulk Density (g/mL)**	**Iodine Number (mg/g)**
Mangostene Fruit Shell(MFS)	MFSAC	312.03	178.03	261.32	0.1177	0.1280	0.2457	28.90	0.435	298.78
Starting Material Mineral Based	**Activated Ash**	**BET Surface area (m^2/g)**	**Cumulative Adsorption Surface area(BJH) (m^2/g)**	**Micropore Surface area (m^2/g)**	**Meso pore Volume (cc/g)**	**Micro pore Volume (cc/g)**	**Total Pore Volume (cc/g)**	**Average pore Diameter °A**	**Bulk Density (g/mL)**	**Iodine Number (mg/g)**
Natural Palm Ash (OPA)	AOPA	467.10	334.65	561.9	0.349	0.199	0.548	46.91	0.154	192.22

The high BET surface areas and favourable pore size distribution of the prepared activated adsorbents are due to the preparation conditions applied for the activation process. For preparing activated adsorbent, pore size distribution plays a vital role. It was reported that, small pore size would fail to capture larger adsorbates where as large pore size might take the smaller adsorbate instantly but are unable to retain them permanently resulting in overall lower removal effeciency (Ahmenda *et al.,* 2000). If larger proportion of lignin is present inside the precursors, it will produce macroporous activated carbon, while high content of cellulose will yield microporous activated carbon (Savova *et al.,* 2003). It is well documented in the literature that, micropores are characterized by large surface area but they constitute lower fraction of pore volume compared to mesopores (Grigis *et al.,* 2002). For preparing activated carbon, semi carbonization step is important to disrupt the cellulosic backbone. Neverthless, this can enhance the BET surface areas and pore volumes by increasing the diffusion of KOH and CO_2 molecules into the pores and thereby increasing the KOH-carbon and CO_2-carbon reactions.

KOH can react with carbonaceous precursors to form micropores which can provide effective activation path for steam or any types of activating gases. However, the micropores present inside the carbon matrix can recombine leading to macropres and mesopores after heat treatment. Macropores acts as tunnels which enables the adsorbate to enter inside the smaller pores at the interior side of the carbon matrix where they can be adsorbed and retained. Presence of macropores does not contribute to the overall sorption process since they have low surface area but they affect significantly the admission of the adsorbate into the meso and micro pores (Qureshi, 2008). Therefore, an optimal addition of KOH with the precursor is necessary to ensure the proper pore size distribution. Stavropouios and Zabaniotou (2005) described the

reaction mechanism of KOH with carbon. Their findings revealed that, at first stage of activation, KOH would dehydrate to produce K_2O. K_2O would react further with CO_2 by the water-shift reaction to yield K_2CO_3 during the second phase of activation. Thus, intercalation of metalic potassium is reported for the drastic expansion of the carbonaceous precursors. This would finally provide enlarged specific surface area with high pore volume (Salman *et al.*, 2010, Tseng and Tseng, 2005). Oh and Park (2002) observed a drastic increment of BET surface area between 700 and 800 °C, which was mainly due to the remarkable increment of mesopores inside the carbon matrix of rice straw. The results obtained in this study are in concurrence with the activation mechanism established in the literature where Tseng *et al.* (2006) stated that CO_2 gasification could enhance the formation of mesopores resulting an increase in the surface area of corncob-based activated carbon. Hayashi *et al.* (2002) also revealed that, the total pore volume of chickpea husk-based activated carbons increased with an increase in activation temperature and the micropore volume was slightly decreased between 800 and 900 °C, but mesopore volume was increased rapidly.

As can be seen from Table 6.2(a), the BET surface areas and total pore volumes of the activated carbons prepared for adsorption of lead, Pb(II) cations are slightly higher than that derived for the other two cations' adsorption for the same precursor used. This trend is expected as higher activation temperature and IR are applied for preparing these activated carbons due to the larger cationic size of lead which needed activated carbons with larger pore size to effectively adsorb it, as compared to the other two cations. Overall the activated adsorbent prepared in this study showed characteristics which are comparable with other adsorbent derived from agro residues. Table 6.2(b) summarizes the physical properties determined by previous researchers for preparing activated adsorbent from agricultural residues for comparison.

Table 6.2(b) Physical characteristics of activated carbons from various agricultural residues

Precursors	BET Surface area (m^2/g)	Micropore volume (cm^3/g)	Mesopore Volume (cm^3/g)	Average pore Diameter,	Yield (%)	Adsorbate Treated	Reference
Rice husk	168-480	0.597-1.365	-	1.90-4.40	-	-	Yalcin and Sevinc, 2000
Corncob	54-722	0.062-0.417	-	1.102-2.529	-	MB, phenol, Pb^{2+}	El-Hendawy, 2005
Coconut Shell	1017-2634	0.494-1.913	-	1.99-3.49	14.50-38.90	Phenol, MB, Erythrosine red	Hu and Srinivasan, 2001
Corncob	309-2595	0.20-1.43	0.14-1.12	2.10-2.90	15.00-22.30	MB, basic brown l, acid blue 74, 2,4-	Tseng and Tseng 2005
Rice straw	280-790	-	-	2.13-2.69	-	-	Yun *et al.*, 2001
Jute Fiber Coconut fiber	912-1303	0.605-0.726	0.381-0.536	0.56-0.68	-	Acid red 27, Cu^{2+}	Phan *et al.*, 2006
Apricot stone	225-1092	0.15-0.63	-	-	5.20-25.70	Iodine	Sentorun-Shalaby *et al.*,2006
Oil palm shell	400-1300	0.21-0.69	-	1.90-2.40	-	NH_3, NO^2	Guo and Lua, 2002
Coconut shell	524.50	0.226	0.21	-	-	-	Achaw and Afrane. 2007
Oil palm fiber and oil palm Shell	400-1100	-	-	-	-	SO^2	Guo and Lua, 2000
Rice straw	370-2410	0.25-1.39	0.12-0.56	-	-	MB, iodine	Oh and Park, 2002
Chickpea	500-1750	0.20-1.00	0.18-0.75	-	-	-	Hayashi *et al.*, 2002
Euphorbia rigida	741.2	0.301	0.273	1.06	-	MB	Gercel *et al*., 2007
Rice husk	345-439	0.335-0.387	0.111-0.118	3.53-3.94	37.69-40.66	Phenol	Kennedy *et al*., 2007

Table 6.2(b) Continued

Precursors	BET Surface area (m^2/g)	Micropore volume (cm^3/g)	Mesopore Volume (cm^3/g)	Average pore Diameter,	Yield (%)	Adsorbate Treated	Reference
Date pit	28-945	0.017-0.545	0.012-0.358	-	-	MB	Girgis and El-Hendawy, 2002
Pistachio-nut Shell	800-1946	-	-	-	12.35-21.14	SO_2	Lua and Yang, 2004
Peanut hull	80.8-1177	0.053-0.597	0.043-0.570	-	22.00-36.00	MB	Girgis *et at.*, 2002
Palm shell	248-1170	-	-	-	11.85-27.84	CO_2	Adinata *et al.*, 2007
Sago waste	625	0.67	-	-	78.00	Mercury (II)	Kadirvelu *et al.*, 2004
CaOH modified Palm Ash	134.20	-	-	-	-	SO_2	Zainuddin *et al.*, 2005
NaOH modified Coal fly ash (21 h, room temperature)	49.00	-	-	-	-	Cu and Cd	Pretorius *et al.*, 2006
NaOH modified Coal fly ash (72 h, room temperature)	62.00	-	-	-	-	Cu and Cd	Pretorius *et al.*, 2006
NaOH modified Coal fly ash (21 h, room temperature) and refluxed with 3 M HCl	210.00	-	-	-	-	Cu and Cd	Pretorius *et al.*, 2006

- Not Calculated

The results also reveal that, all the activated adsorbents prepared in this study are mesoporous as their average pore diameters are larger than 2.2 °A . Thus the activated adsorbents are in the mesopores region according to the IUPAC classification (IUPAC, 1972). The activated carbons prepared from KC have relatively high BET surface areas rather than KF, MFS and AOPA. Overall the BET surface area obtained here are comparable with the commercial activated carbons such as lignite, F100, BPL from Calgon, US and BDH from Merck, which were reported to have BET surface areas of 600-650, 957, 972 and 1118 m^2/g respectively (Martin *et al.,* 2003).

The granular activated carbon, MFSAC prepared in this work has less surface area than the powdered activated carbon. This might be due to its slightly hard texture than the other two soft precursors of KC and KF or its granular particle size which can not ensure sufficient contact time or effective surface area for CO_2 and KOH to penetrate inside the carbon matrix and participate in the reaction mechanisms. Mangostene fryit shell based activated carbon (MFSAC) is used for batch and fixed bed adsorption studies in this work.

A significant increase in surface area is observed for NaOH treated oil palm ash (OPA) at high temperature. This might be due to the pozzolanic reaction carried out between alkali and SiO_2 and Al_2O_3 to form reactive species of hydrated silicate or hydrated aluminate. Similar trend was followed by $Ca(OH)_2$ treated palm ash and coal ash for sorption studies of SO_2 (Zainuddin *et al.,* 2005; Davini *et al.,* 1996). Fly ash from amaga coal was treated with NaOH at various temperature, time and concentration to produce highly reactive zeolite having adsorptive properties equal to 70-80% of commercial zeolite (Iyer and Scott, 2001). This reaction was also defined as hydration

reaction in previous literature (Zainuddin *et al.,* 2005). The subsequent section of XRF analysis also supports this phenomenon.

6.2.2 Determination of Bulk Density

For producing activated adsorbent, determination of bulk density is important as it ensures sufficient mechanical strength, thereby reducing weight losses during treatment process. It depends not only on the characteristics of the starting materials but also the activation method (Zahangir *et al.*, 2008).

It is observed from Table 6.2 (a) that, the bulk density of MFSAC is higher than KCAC and KFAC. This is due to its hard texture as compared to soft precursors of KC and KF. Similar phenomena have been reported for producing activated carbon from almond nutshell and rice husk by H_3PO_4 acid treatment (Qureshi, 2008). The previous one due to its hard texture showed bulk density of 0.52 g/ml whereas the later one had bulk density 0.25 g/ml (Qureshi, 2008). In the case of KCAC and KFAC, the activated sample prepared for Pb (II) cations have iodine number slightly higher than the other two cations. This might be due to the application of relatively higher temperature for preparation of these types of activated carbon. It was depicted earlier in ANOVA analysis also that, temperature had showed greatest impact for producing activated adsorbent here rather than the other two factors of ratio and time.

6.2.3 Determination of Iodine Number

Iodine number is one of the most fundamental parameter to characterize the activated adsorbents chemically. It provides the idea about the surface area of the prepared sorbent. The iodine number obtained in this work is reported in Table 6.2 (a). It is observed that KC based activated carbon showed highest iodine number. The result

obtained here further supports the BET surface area of the prepared sample. The high values of iodine number reflect a high surface area with significant amount of pores in the micro porous region (Gergova *et al.*, 1993). It was reported that, steam activated bagasse based activated carbon had iodine number 533.4 mg/g whereas rice husk based activated carbon showed iodine number of 228.6 mg/g (Qureshi, 2008). Physical activation of *Acacia Arabica* produced activated carbon having iodine number 780 mg/g whereas coconut shell showed high iodine number of 1082 mg/g (Usmani, 2001).

6.2.4 Surface Morphology

The surface morphology of the KC, KF and MFS precursors together with their respective chars and activated carbons, natural oil palm ash (OPA) and activated oil palm ash (AOPA) were examined using scanning electron microscopy (SEM). From the SEM micrographs obtained, the change in surface texture and pore development are clearly visible.

Plates 6.1(a)-(e) respectively show the SEM micrographs of the KC precursor, semi carbonized char of KC, and the activated samples prepared for lead, copper and manganese. Plates 6.2(a)-(e) and Plates 6.3(a)-(e) correspondingly show the SEM of micrographs of those obtained for KF and MFS. The SEM pictures of OPA and AOPA are illustrated in Plates 6.4(a)-(b).

As can be observed from SEM micrographs of the precursors (Plates 6.1(a) and 6.2(a)), the surface textures of the lignocellulosic precursors of KC and KF are comparatively rough and uneven with some minor pores observed on their surface. After semi carbonization process, some pores are developed and found on the surfaces of the chars, as shown in Plates 6.1(b), and 6.2(b).

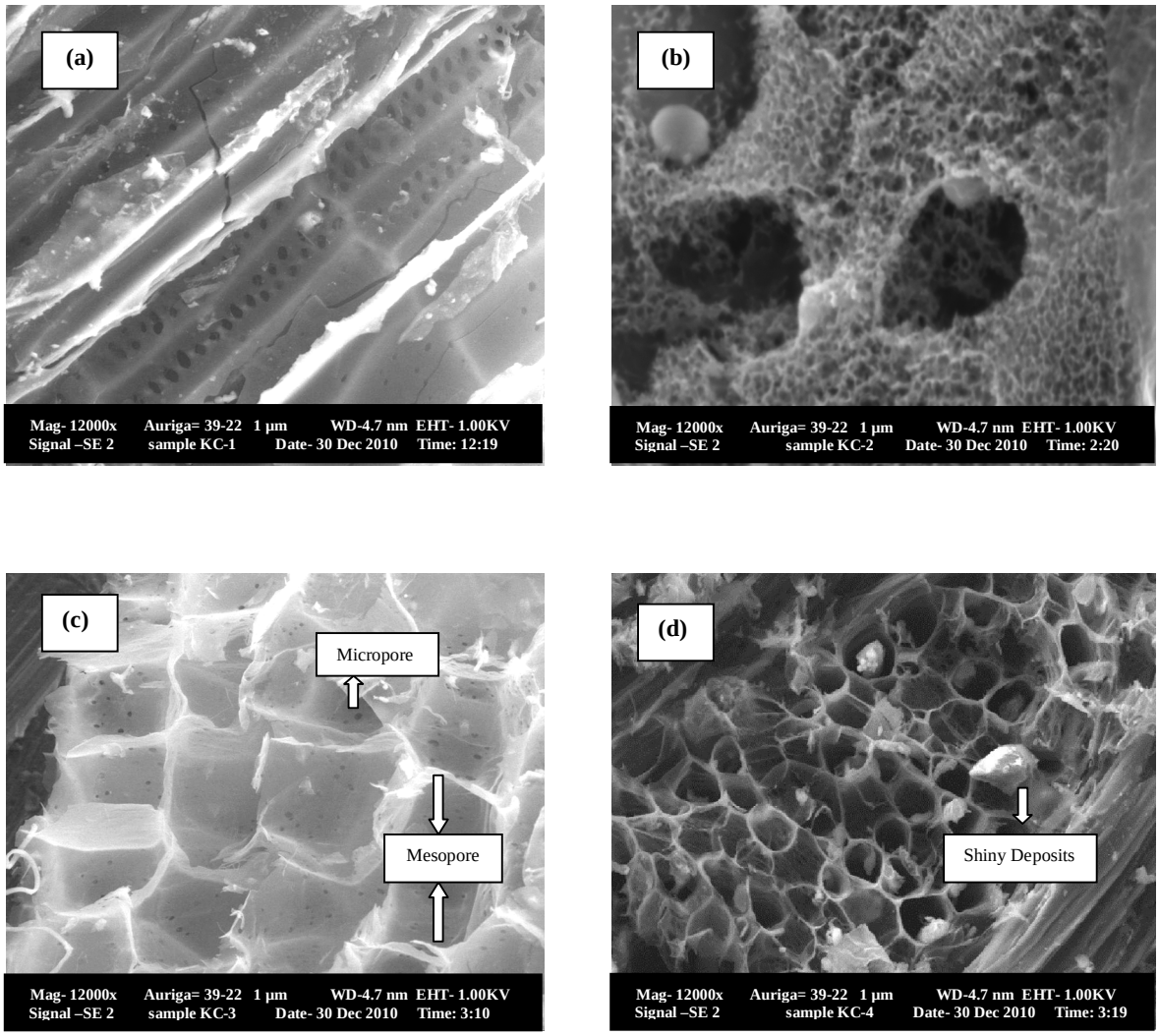

Plate 6.1 SEM Micrographs (x 12000) of (a) Raw Kenaf Core (b) Semi carbonized Kenaf Core (c) KCAC for Pb (d) KCAC for Cu (e) KCAC for Mn

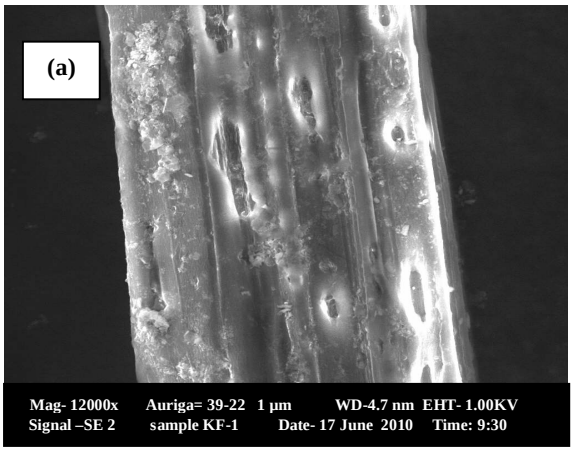

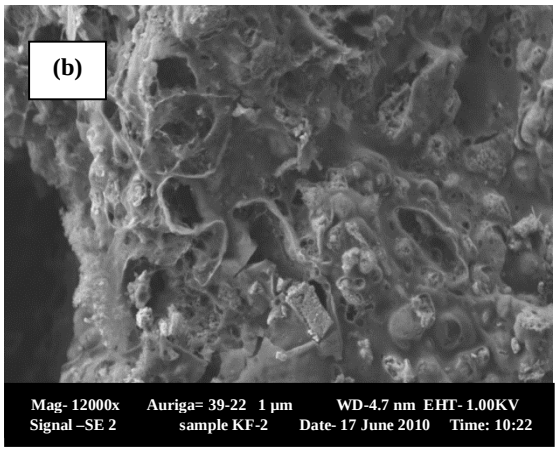

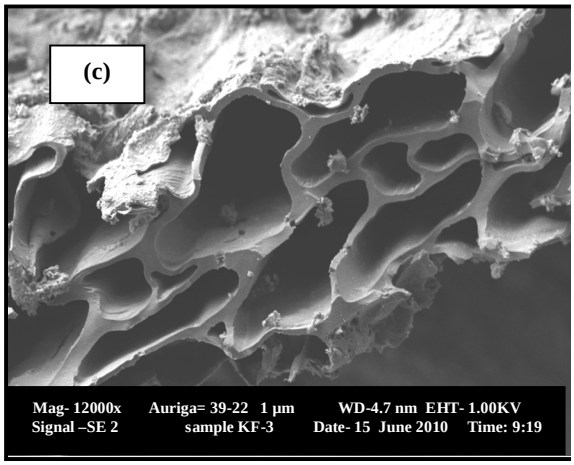

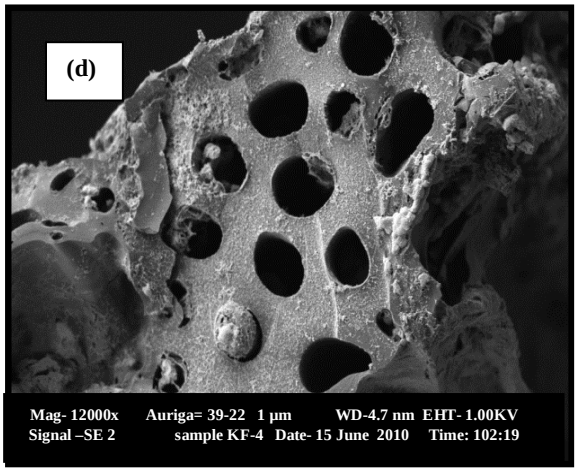

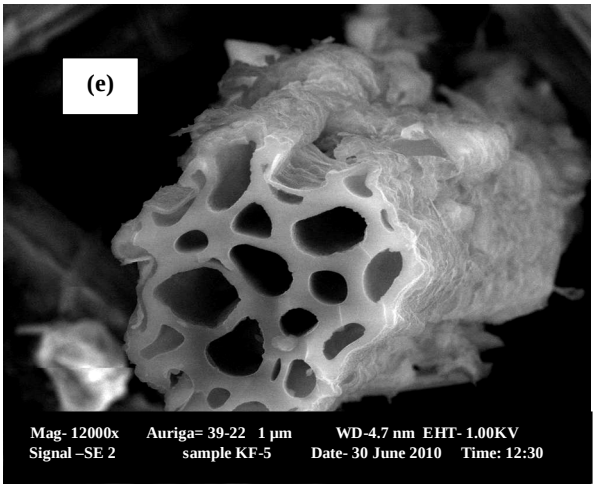

Plate 6.2 SEM Micrographs (x 12000) of (a) Raw Kenaf Fiber (b) Semi carbonized Kenaf Fiber (c) KFAC for Pb (d) KFAC for Cu (e) KFAC for Mn

The pores formed after semi carbonization stage are narrow, tapered and some of them are even blocked by tarry substances. The deposition of tarry substances occurred when the volatile materials were diffusing out of the carbon matrix into the gas main stream during the semi carbonization step. Some of the substances might have a collision with the pore walls, which leads to hydro cracking and eventually resulted in carbon deposition (Kamishita, 1977). For preparing guava seed based activated carbon, it was observed that semi carbonization alone did not create sufficient porosities due to the incomplete decomposition of organic constituents present in the carbonaceous precursors. In that case, the pores were significantly blocked by the residues of carbonization products (Rahman and Saad, 2003).

All the activated carbons produced from KC demonstrate homogeneous pore size distributions with uniform pore arrangements. As shown in Plates 6.1(c)-(e) and 6.2 (c)-(e), the pores available on the surfaces of the activated carbons prepared from KC are well pronounced with distinct pore walls. They are arranged in a group of honey-combed structures. In addition to that, the matters which are blocking the pores on the chars are gasified by the activation process. Thus they are carried away with the exhaust gas leaving most of the pores clear and easily absorbable by the cations. Inside the walls of the large pores, small amount of minute pores are visible for activated carbon prepared from KC for lead. Some shiny tarry deposition was observed on the right side of KCAC prepared for copper. However, at higher temperature some pore walls were broken leading to half circular pores on the surface of KCAC prepared for manganese. It was observed that after CO_2 activation at higher temperature, clear and well-developed pore structure was obtained on the pistachio-nut shell-based activated carbon (Yang and Lua, 2003).

Cylinder-like tubes are observed in the SEM micrographs of KFAC indicating that the activated carbons prepared from this precursor are made up of cylinder-like tubes. The pores are mainly developed by the side of the axis parallel to the cylindrical structure of the samples. Similar types of pore arrangement were observed in the activated carbon prepared from palm fiber, jute and coconut fibers (Tan, 2008, Phan *et al.,* 2006).The rough texture of KF changes due to the cross linking of the reactive points of the cylinders caused by the disruption of the original polymeric arrangement of the precursor material (i.e. the cellulose and lignin units of the precursor) (Phan *et al.*, 2006). Consequently, the reconstitution of the new matrix structure during the carbonization and the subsequent activation processes in the presence of different activating agent results in the formation of well developed pores (Achaw and Afrane, 2007) in KF based activated carbon.

Figure 6.3 (a) shows the surface morphology of raw mangostene fruit shell (MFS) with some occasional pores over its surface. After the semi-carbonization step, the surface becomes rough and uneven like KC and KF with some irregular shaped pores. Some anonymous fragments are observed on the surface of char which might be due to the residues of tarry substances formed during the semi-carbonization stage. The activated carbons produced from MFS demonstrate homogeneous pore size distributions with uniform pore arrangements having circular or elliptical shape. As shown by Figure 6.3(c), the pores available on the surfaces of the activated carbons are visible, well pronounced with distinct and smooth pore walls. The results showed that, KOH and CO_2 are effective in creating well developed pores on the surfaces of the precursors leading to the activated carbons with large surface areas and pore volume.

The pore size of the activated carbons prepared for adsorption of lead were comparatively larger with relatively thin pore walls for KC and KF based activated carbon as high temperature has been used to prepare the sample. These results are further supported by total pore volume and average pore diameter demonstrated by KC and KF activated carbon prepared for sorption of lead in section 6.2.

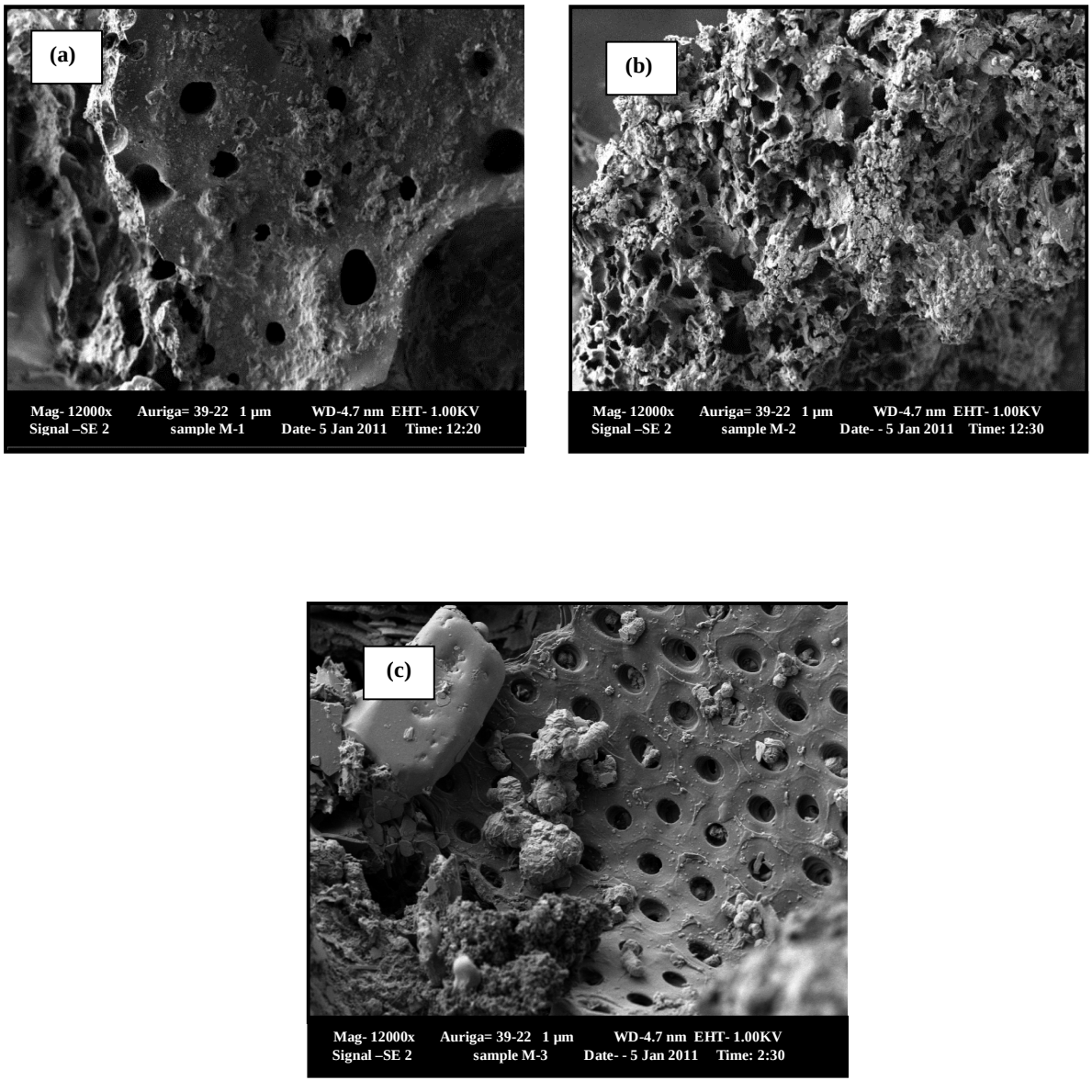

Plate 6.3 SEM Micrographs (x 10000) of (a) Raw Mangostene Fruit Shell (MFS) (b) Semi carbonized Mangostene Fruit Shell (MFS) (c) Granular Activated Carbon MFSAC

Figures 6.4 (a)-(b) show the surface texture of natural and activated oil palm ash. Compared to the ligno cellulosic precursors, the surface texture of natural oil palm ash is smooth, dense without any cracks and crevices due to grinding and several times washing with distilled water. However, substantial number of shallow pores with different structure is observed after activation of the sample. Due to this well developed porosities created by sodium hydroxide, activated oil palm ash has extended surface area and adsorption capacity than the natural oil palm ash. After activation, the structure looks like amorphous silica which is a highly reactive species and can form surface complexes with the cations under investigation.

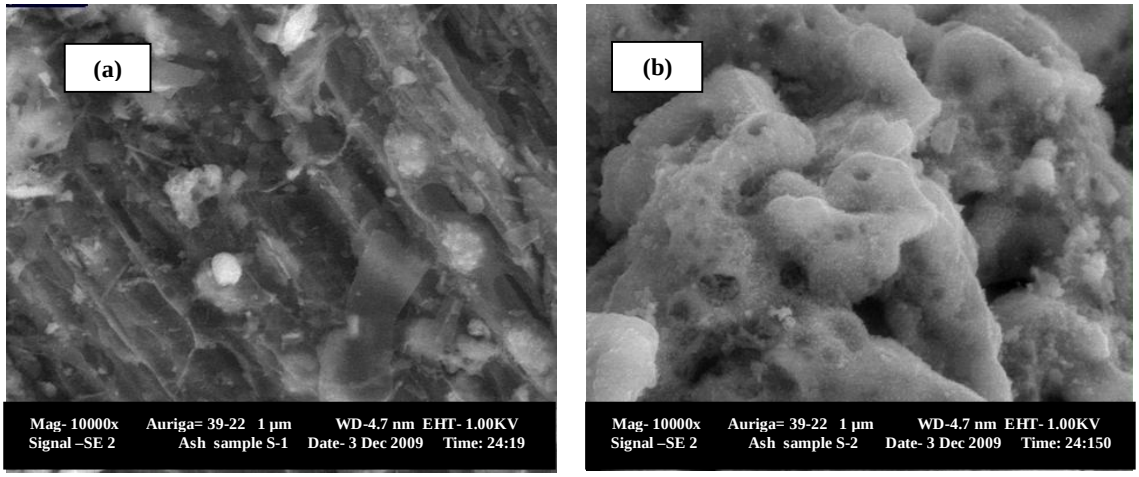

Plate 6.4 SEM Micrographs (x 10000) of (a) Natural Oil palm ash (NOPA) (b) Activated Oil palm ash (AOPA)

Similar morphological feature has been shown by base modified acid etched South African coal fly ash after Na-P1 zeolite synthesis by previous researchers (Pretorius and Woolard, 2003). The result obtained for activated ash is further supported by FTIR analysis in the subsequent section of 6.2.4.

6.3 Chemical Analysis of prepared Activated Adsorbent

The chemical properties of the prepared adsorbent were determined in terms of elemental composition analysis including proximate (TGA) and ultimate (C, H, N and others) analysis for activated carbons (KCAC, KFAC and MFSAC) and XRF analysis for natural and activated ash (OPA and AOPA) samples. FTIR analysis was carried out to determine surface chemistry of the prepared sorbent.

6.3.1 Elemental Composition Analysis of Activated Carbon

Proximate and ultimate analysis of the prepared powdered (PAC) and granular activated carbon (GAC) derived from lignocellulosic precursors of KC, KF and MFS were carried out.

6.3.1.1 Proximate Analysis of Activated Carbon

The proximate analysis of carbon samples gives moisture content, volatile content, the fixed carbon (i.e., bio-char) and the ash residues (mineral) content based on the complete combustion of the sample. For proximate analysis, the KC, KF and MFS precursors as well as their respective semi-carbonized and activated carbons prepared under different conditions were analyzed using thermogravimetric (TGA) analysis. It is observed that, the percentage of volatile matter of the precursors decreased significantly by carbonization and activation processes. The results obtained from thermogravimetric analysis for this work and previous researches based on lignocellulosic precursors are listed in Table 6.3 (a) and 6.3 (b).

Table 6.3 (a) Proximate Analysis of precursors and Powdered (PAC) and Granular (GAC) Activated carbon

Starting Material Carbonaceous	Activated Carbon (PAC)	Proximate Analysis (%)				References
		Moisture	Volatile Matter	Fixed Carbon	Ash	
Kenaf Core Activated Carbon KCAC	Raw Kenaf Core (KC)	5.90	76.87	12.33	4.90	This Work
	Semi-carbonized Kenaf Core	5.05	57.19	32.54	5.22	This Work
	KCAC (Pb)	3.55	16.35	71.22	8.88	This Work
	KCAC(Cu)	4.33	22.76	65.28	6.63	This Work
	KCAC(Mn)	3.09	19.51	69.96	7.04	This Work
Kenaf Fiber Activated Carbon KFAC	Raw Kenaf Fiber (KF)	9.87	69.14	11.45	9.54	This Work
	Semi-carbonized Kenaf Fiber	7.99	52.80	28.89	10.32	This Work
	KFAC (Pb)	5.43	13.03	69.66	11.88	This Work
	KFAC (Cu)	6.89	19.11	63.11	10.89	This Work
	KFAC(Mn)	6.33	19.47	62.77	11.43	This Work
Starting Material Carbonaceous	**Activated Carbon (GAC)**	**Proximate Analysis (%)**				**References**
		Moisture	**Volatile Matter**	**Fixed Carbon**	**Ash**	
Mangostene Fruit Shell(MFS)	Raw Fruit Shell (MFS)	4.78	72.88	18.80	3.54	This Work
	Semi-carbonized Fruit Shell	3.98	60.17	29.87	5.98	This Work
	MFSAC	3.33	32.66	54.02	9.92	This Work

Table 6.3 (b) Proximate Analysis of Powdered (PAC) and Granular (GAC) Activated carbon derived from other lignocellulosic precursors

Starting Material	Activated Carbon (PAC)	Proximate Analysis (%)				References
		Moisture	Volatile Matter	Fixed Carbon	Ash	
Ligno cellulosic Carbonaceous Precursors	Apricot Stone	2.10-2.40	4.30-6.40	86-89	2.20-7.00	Sentorum-Shalaby *et al.*, 2006
	Rice Husk	9.58	12.83	72.12	5.46	Mohd Din, 2005
	Coconut Shell	7.92	8.95	81.63	1.49	Mohd Din, 2005
	Rice Straw	5.52	17.93	52.14	24.40	Mohd Din, 2005
	Bagasse	16.30	46.15	26.00	11.54	Satyawali and Balakrishnan, 2007
	Coffee Residue	5.36-12.64	26.04-37.78	38.49-60.28	5.15-11.49	Boonamnuayvitaya et al., 2005
	Pistachio-nut shell	-	11.32-19.80	74.12-83.51	-	Yang and Lua 2003
	Coconut husk	9.50	27.53	35.13	27.84	Tan 2008
	Palm Fiber	6.01	14.26	58.75	20.98	Tan 2008
	Empty Fruit Bunch	10.30	21.65	54.15	18.90	Tan 2008
	Palm Shell	6.21	15.37	71.48	6.94	Tan 2008

Table 6.3 (a) and (b) show that the proximate content of each activated carbon is different based on the original structure, preparation condition and properties of the precursors. The fixed carbon content has shown opposite trend of increasing pattern in the activated carbons rather than the raw and semi carbonized samples. This is because at high temperature, the organic substances present inside the carbon matrix become unstable. Their bonding is broken. The volatile substances are discharged both as gas and liquid products. KCAC has exhibited the highest fixed carbon value of 71.22-69.96 %. These results are analogous with the commercial activated carbon, F200 from Calgon, US having 76.11% of fixed carbon. Nevertheless, the ash contents of the activated carbons prepared from KF are comparatively higher than KC and MFS. This is attributed to its soft texture. It is observed that all the precursors contain less amount of ash before activation. After semi-carbonization and activation, the ash content has increased significantly The high ash contents of the activated carbons prepared from KF is due to it's soft texture compared to MFS and KC. Bituminous coal based activated carbon was also reported to have high ash content of about 26.1% (El Qada *et al.*, 2006). H_2S0_4 acid activated sludge-based activated carbon and rice straw-based activated carbon prepared by CO_2 activation were found to contain 39.2% and 30.4-73.3% of ash content respectively (Martin *et al*., 2003; Yun *et. al*., 2001).

6.3.1.2 Ultimate Analysis of Activated Carbon

The ultimate analysis gives the composition of the biomass as well as the prepared activated carbon in wt% of carbon, hydrogen and nitrogen (the major components) and others (sulfur and oxygen). The results obtained for ultimate analysis in this study and from previous researches conducted on lignocellulosic precursors are listed in Table 6.4 (a) and 6.4 (b) respectively.

Table 6.4 (a) Ultimate Analysis of precursors and Powdered (PAC) and Granular (GAC) Activated carbon

Starting Material Carbonaceous	Activated Carbon (PAC)	Ultimate Analysis (%)				References
		Carbon	Hydrogen	Nitrogen	Others	
Kenaf Core Activated Carbon KCAC	Raw Kenaf Core (KC)	51.22	15.79	5.56	27.43	This Work
	Semi-carbonized Kenaf Core	57.05	13.49	5.04	24.42	This Work
	KCAC (Pb)	72.66	6.25	1.43	19.66	This Work
	KCAC(Cu)	66.32	7.79	1.56	24.33	This Work
	KCAC(Mn)	70.09	7.51	1.03	21.37	This Work
Kenaf Fiber Activated Carbon KFAC	Raw Kenaf Fiber (KF)	42.85	5.33	0.33	51.49	This Work
	Semi-carbonized Kenaf Fiber	47.26	7.34	0.34	44.98	This Work
	KFAC (Pb)	71.67	3.03	1.66	23.64	This Work
	KFAC (Cu)	68.87	5.17	1.10	24.86	This Work
	KFAC(Mn)	69.91	3.29	0.80	26.0	This Work
Starting Material Carbonaceous	**Activated Carbon (GAC)**	**Ultimate Analysis (%)**				**References**
		Carbon	**Hydrogen**	**Nitrogen**	**Others**	
Mangostene Fruit Shell(MFS)	Raw Fruit Shell (MFS)	48.98	7.34	6.32	37.36	This Work
	Semi-carbonized Fruit Shell	52.33	6.76	5.44	35.47	This Work
	MFSAC	62.66	6.43	3.22	27.69	This Work

Table 6.4 (b) Ultimate Analysis of Powdered (PAC) and Granular (GAC) Activated carbon

Starting Material	Activated Carbon (PAC)	Ultimate Analysis (%)				References
		Carbon	Hydrogen	Nitrogen	Others	
Ligno cellulosic &Carbonaceous Precursors	Elbistan Lignite	53.0	5.8	1.8	39.4	Cetinkaya *et al.*, 2003
	Activated Sewage Sludge	89.8	1.2	3.1	5.9	Wen *et al.*, 2011
	Commercial Activated carbon from wood	92.1	1.6	3.3	3.0	Wen *et al.*, 2011
	Activated carbon from coconut shell	90.7	1.3	3.7	4.3	Wen *et al.*, 2011
	Activated carbon from coconut shell	87.2	2.1	5.3	5.4	Wen *et al.*, 2011
	$ZnCl_2$ activated Bamboo	75.31	3.01	0.73	20.95	Alothman *et al.*, 2011

All the samples have moderate nitrogen content. It is observed that the carbon content increased significantly after activation of the raw precursors revealing that physiochemical activation method used here is suitable to develop activated carbon from the selected precursors which can subsequently enhance the uptake capacity for divalent cations from contaminated water. From ultimate analysis, it is observed that, elemental carbon content is slightly higher than fixed carbon determined by proximate analysis. With the increase of temperature and impregnation ratio, hydrogen content is decreasing. It was observed that, hydrogen content of $ZnCl_2$ activated bamboo based activated carbon was decreasing with increase of temperature and impregnation ratio (Alothman *et al.*, 2011).

6.3.2 Elemental Composition Analysis of Natural and Activated Palm Ash

The results obtained for chemical composition analysis of natural oil palm ash and activated oil palm ash is listed in Table 6.5. It is observed that after activation, there is less amount of SiO_2, Fe_2O_3 and Al_2O_3 present inside the sample. This might be due to dissolution and reaction of these oxide components with NaOH to form reactive species (Pretorius *et al.*, 2003). A similar phenomenon has been observed for NaOH activated coal fly ash where the base activation has selectively removed Si from ash producing an active sorbent with high cation exchange capacity (Pretorius *et al.*, 2003). However, it is reported earlier in the literature also silanolic groups in neutral, protonated or deprotonated forms are able to promote specific interactions with cations (Fiore and Zanetti, 2009). Table 6.5 (a) and (b) summarizes the percentage composition of natural and activated palm ash with other types of ash obtained from literature.

Table 6.5 (a) Elemental (Mineral oxide) composition of powdered adsorbent prepared from natural oil palm ash (OPA)

Starting Material Mineral Based	**Mineral Oxide (Weight %) composition**											
	SiO_2	**K_2O**	**Na_2O**	**CaO**	**MgO**	**P_2O_5**	**TiO_2**	**Fe_2O_3**	**Al_2O_3**	**SO_3**	**MnO**	**References**
Natural Oil Palm Ash (NOPA)	70.45	2.99	1.09	1.19	2.78	1.99	1.22	9.54	7.34	0.22	0.40	This Work
Activated Oil Palm Ash(AOPA)	51.70	5.69	2.00	10.90	11.20	5.95	0.41	5.77	5.50	0.10	0.44	This Work

Table 6.5 (b) Elemental (Mineral oxide) composition of powdered adsorbent prepared from different types of ash

Starting Material Mineral Based	**Mineral Oxide (Weight %) composition**									
	Na	**Mg**	**Al**	**Si**	**Ca**	**Cr**	**Fe**	**Ni**	**Si/Al**	**References**
Unmodified Coal Fly Ash	0.24	0.42	14.93	19.76	2.40	5.01	1.68	2.75	1.32	Pretorius *et al.*, 2003
1M NaOH activated Coal Fly Ash	6.39	0.55	15.89	17.95	2.08	5.02	1.93	1.41	1.14	Pretorius *et al.*, 2003
2 M NaOH activated Coal Fly Ash	7.14	0.73	16.91	16.63	2.67	0.03	1.85	0.01	0.98	Pretorius *et al.*, 2003
1M NaOH & 3M HCl activated Coal Fly Ash	6.37	0.00	13.68	26.82	0.03	5.89	0.27	0.11	1.96	Pretorius *et al.*, 2003

6.3.3 Surface Functional Groups Analysis

The adsorption characteristics of an adsorbent are predominantly influenced by the surface functional groups which were determined from the Fourier Transform spectroscopy analysis and presented by the FTIR spectrums (Figures 6.1-6.4). Analysis of FTIR spectrum provides information about the molecular structure of the functional groups present on the samples under investigation. Usually simple spectra are obtained from samples with few IR active covalent bonds whereas a complex spectrum gives more adsorption bands (Dinesh, 2011).

The functional groups present onto the surface of the powdered and granular activated carbons (KCAC, KFAC and MFSAC) are similar up to a certain extent. This is because the same activating agents are applied to get the activated carbons. Overall, noteworthy differences in the intensities of the peaks are observed due to the different nature of the original precursors and the activating conditions applied to prepare the carbons. However, the presence of carboxyls, hydroxyls, phenols, lactones and ketonic groups have been observed over the surface of lignocellulosic precursors as well as their semi-carbonized and activated sample.

The trend of the FTIR spectrum for all the lignocellulosic precursors contains some main peaks which are almost similar. Some major peaks around 2800-2900cm^{-1}, 1500-1650 cm^{-1} and 1000-1200 cm^{-1} are related to C-H stretching of alkane, C=C stretching of aromatics, C-O-C stretching vibration of esters, ether and phenol groups. The O-H stretching vibrations at bandwidth of 3400-3800 cm^{-1} are present in the raw precursors, semi carbonized sample and activated carbons prepared from all the three precursors. However, the peaks are shifted to a lower or higher frequency level compared to those observed in the FTIR spectrums of the original precursors. It was

reported by Gerçel *et al.,* (2007) that during activation stage, the chemical activating agent broke many bonds comprises of aliphatic and aromatic species in the lignocellulosic precursor. This results in volatilization and liberation of many light and volatile organic components causing incomplete aromatization over the carbon surface. O-H functional group has been found on the surface of most of the activated carbons, including the commercial grade activated carbons (Jung *et al*., 2001). The broad peaks at 2300-2400 cm^{-1} is found on the spectrums of the activated carbons prepared from KF which shows the presence of carboxylic acid, -COOH functional group. The peaks detected at 1000-1100 cm^{-1} in the spectrums of all the activated carbons prepared represents the presence of C-O-C stretching vibrations of esters, ether or phenol groups whereas the weak to medium peaks located at 450-900 cm^{-1} is assigned for C-H out-of plane bending of benzene derivatives, O-H stretching vibrations of C-O-H band. The results obtained agreed with the previous research where C-H out-of plane bending vibration for benzene derivatives were found on the surface of various activated carbons (Guo and Lua, 2003). The weak peak detected at 1400-1550 cm^{-1} on the spectrum of KCAC, KFAC and MFSAC are due to C=O stretching vibration of carboxylate anions. As can be observed from the spectrum obtained here, that some functional groups intensity becomes less, more or shifted to a higher or lower frequency level, even disappeared after carbonization and activation process. This is due to the thermal degradation which has destroyed some intra molecular bonding of the functional groups with the carbon matrix.

Yang and Lua (2003) reported that, different oxygen groups were present in the raw pistachio-nut shell, which were decreased after the heat treatment causing aromatization of the carbon structure. It was reported also, that after carbonization the

chemical structure of the raw date pit was changed significantly. Some aliphatic C-H groups were lost where as some aromatic C=C and oxygen groups were developed after activation process (El-Hendawy, 2005). When the activation temperature was increased, some poly aromatic structures were formed due to destruction of C=O and C-O groups. After KOH treatment of rice straw, the peak intensities of ester groups and phenolic ether groups were decreased significantly. The researchers described that, KOH had destroyed the lignin structure containing ester and ether linkage after activation of rice straw (Oh *et al.*, 2003).

The dissociation of surface functional groups to obtain specific surface electrical charge significantly affects the sorption or desorption properties of targeted contaminants from waste water. If adsorbate species and the adsorbent surface have similar charge, then repulsion occurs resulting less removal efficiency (Aygun *et al.*, 2003). Overall the surface functional groups observed onto the prepared samples have high affinity towards the positive cations chosen here as sorbate.

Following Figures 6.1, 6.2 and 6.3 demonstrated the FTIR spectrum of KC, KF and MFS precursors along with their respective semi-carbonized sample with activated carbon prepared under different optimum condition. The results obtained from the spectrum are summarized in Tables 6.6, 6.7 and 6.8. On the contrary, the FTIR spectrum of natural oil palm ash and activated oil palm ash are illustrated by Figure 6.4 and Table 6.9. Like activated carbon, it is quite clear from the spectra of natural and activated oil palm ash that some peaks have shifted by the activation and some peaks have disappeared after the treatment with sodium hydroxide.

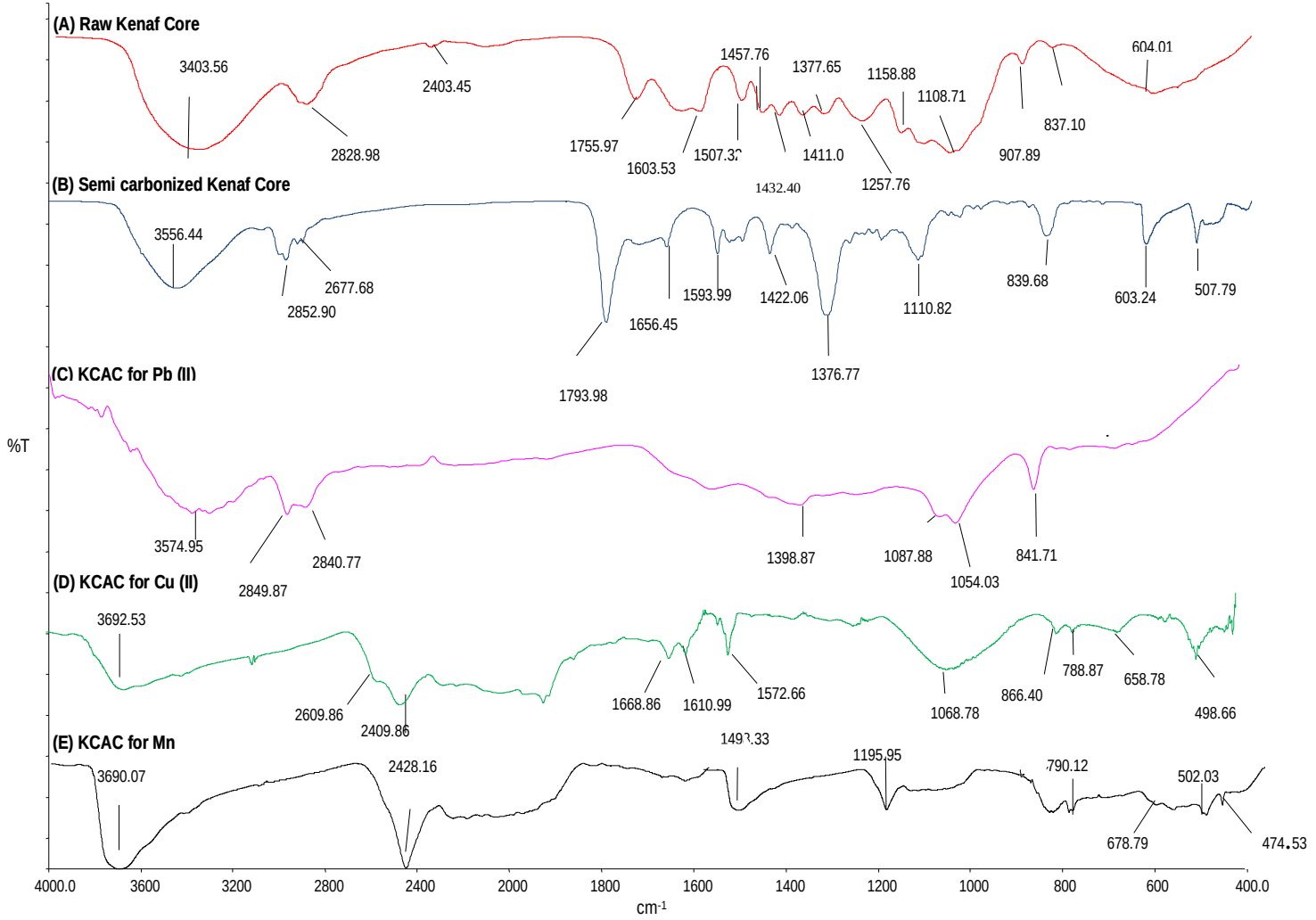

Figure 6.1 FTIR Spectrum of Kenaf Core (KC), semi-carbonized Kenaf Core (KC) and Activated Carbon (KCAC)

Table 6.6 FTIR Spectrum of Kenaf Core (KC), semi-carbonized Kenaf Core (KC) and Activated Carbon (KCAC)

IR Peak Number	Precursors	Frequency(cm^{-1})				Peak Assignment
	Raw Kenaf Core (KC)	Semi carbonized Kenaf Core	Activated Kenaf Core (Pb)	Activated Kenaf Core (Cu)	Activated Kenaf Core (Mn)	
1	-	-	-	498.66	474.53	C-H out-of-plane bending of benzene derivatives
2	-	-	-	507.79	502.03	C-H bending
3	604.01	603.24		658.78	678.79	C-O-H
4	-	-	-	788.87	790.12	C-H
5	837.10	839.68	841.71	866.40	-	C-H
6	907.89	-	-	-	-	O-H bending
7	-	-	1087.88,1054.03	1068.78	-	C-O-C stretching of esters, ethyl or phenyl group
9	1108.71,1158.88	1110.82	-	-	1195.95	-C-N stretching
10	1257.76	-	-	-	-	C-O stretching
11	1377.65	1376.77	1398.87	-	-	CH_3 deformation
13	1411.00,1432.45,1457.76	1422.06	-	-	1498.33	in-plane OH bending and C-O stretch of dimmers
14	1507.32	1593.99	-	1572.66	-	C=C ring stretching of benzene derivatives
15	1603.53	1656.45	-	1668.86,1610.99	-	C=O stretching

Table 6.6 Continued

IR Peak Number	Precursors		Frequency(cm^{-1})			Peak Assignment
	Raw Kenaf Core (KC)	Semi carbonized Kenaf Core (KC)	Activated Kenaf Core (Pb)	Activated Kenaf Core (Cu)	Activated Kenaf Core (Mn)	
16	1755.97	1793.98	-	-	-	C=O stretching
17	2403.45	-	-	2409.86	2428.16	C=C stretching vibration of ketones, aldehydes or carboxylic group
18	-	2677.68	-	2609.86	-	C=C stretching vibration of ketones, aldehydes or carboxylic group
19	2828.98	2852.90	2840.77,2849.87	-	-	C-H stretching
20	3403.56	3556.44	3574.95	3692.53	3690.07	O-H stretching vibration of hydroxyl functional groups

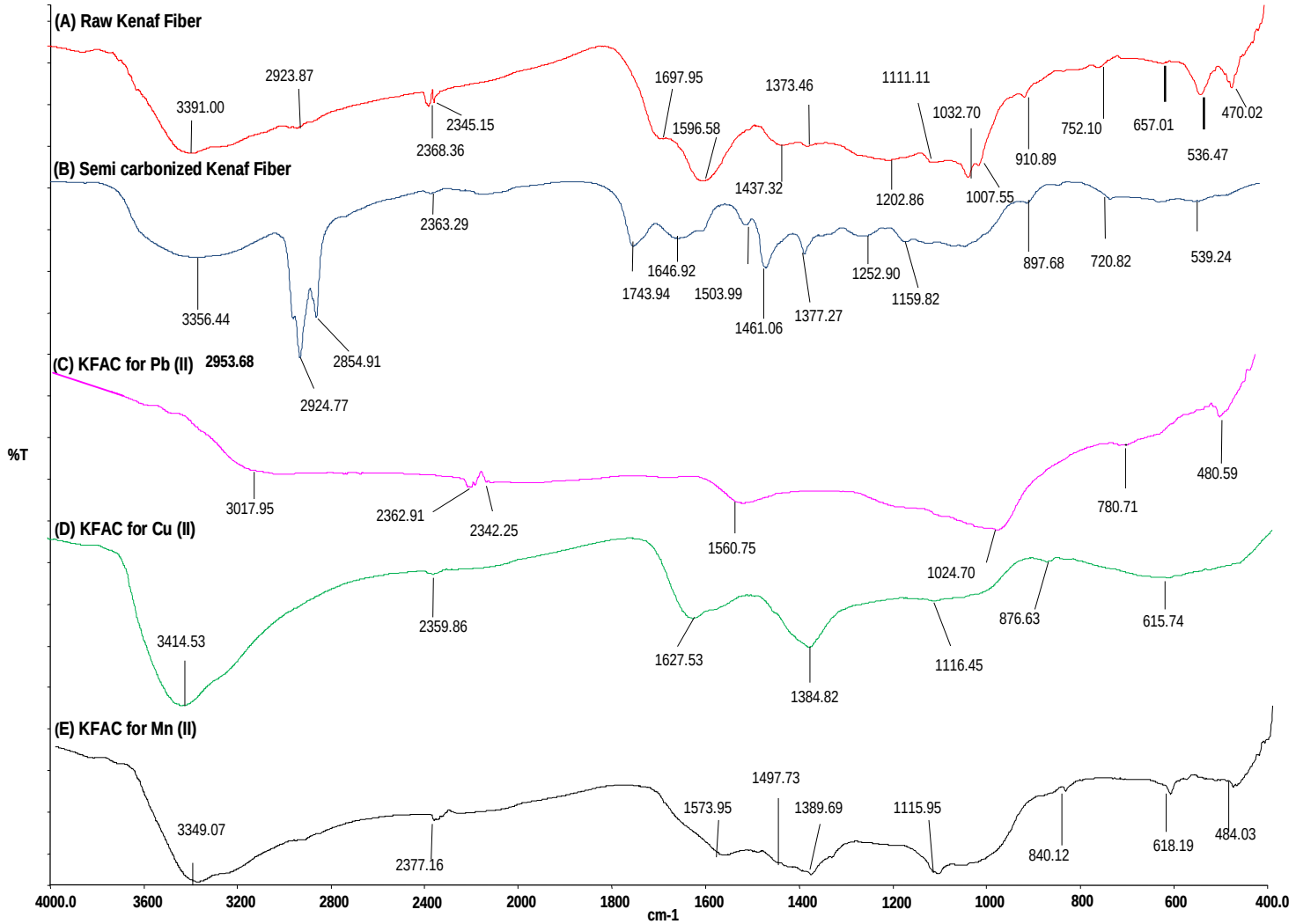

Figures 6.2 FTIR Spectrum of Kenaf Fiber (KF), semi-carbonized Kenaf Fiber (KF) and Activated Carbon (KFAC)

Table 6.7 FTIR Spectrum of Kenaf Fiber (KF), semi-carbonized Kenaf Fiber (KF) and Activated Carbon (KFAC)

IR Peak Number	Precursors	Frequency(cm^{-1})				Peak Assignment
	Raw Kenaf Fiber (KF)	Semi carbonized Kenaf Fiber(KF)	Activated Kenaf Fiber	Activated Kenaf Fiber	Activated Kenaf Fiber (Mn)	
1	470.02	-	480.59	-	484.03	C-H out-of-plane bending of benzene derivatives
2	536.47	539.24	-	-	-	C-H bending
3	657.01	-		615.74	618.19	C-O-H
4	752.10	720.82	780.71	-	-	C-H
5	-	897.68	-	876.63	840.12	C-H
6	910.89	-	-	-	-	O-H bending
7	1007.55	-	1024.71	-	-	C-O-C stretching of esters, ethyl or phenyl group
8	1032.70	-	-	-	-	C-O-C stretching of esters, ethyl or phenyl group
9	1111.11	1159.82	-	1116.45	1115.95	-C-N stretching
10	1202.86	1252.90	-	-	-	C-O stretching
11	1373.46	-	-	1384.82	1389.69	CH_3 deformation
12	-	1377.27	-	-	-	$-NO_2$ aromatic nitro compound
13	1425.24	1461.06	-	-	1497.73	in-plane OH bending and C-O stretch of dimmers
14	1596.58	1503.99	1560.75	-	1573.67	C=C ring stretching of benzene derivatives
15	1697.95	1646.92	-	1627.53	-	C=O stretching

Table 6.7 Continued

IR Peak Number	Precursors		Frequency(cm^{-1})			Peak Assignment
	Raw Kenaf Fiber (KF)	Semi carbonized Kenaf Fiber(KF)	Activated Kenaf Fiber (Pb)	Activated Kenaf Fiber (Cu)	Activated Kenaf Fiber (Mn)	
16	-	1743.94	-	-	-	C=O stretching
17	2345.15	-	2342.25	-	-	C=C stretching vibration of ketones, aldehydes or carboxylic group
18	2368.36	2363.29	2362.91	2359.86	2377.16	C=C stretching vibration of ketones, aldehydes or carboxylic group
19	-	2854.91	-	-	-	C-H stretching
20	2923.87	2924.77	-	-	-	C-H stretching
21	3391.00	3356.44	3017.95	3414.53	3349.07	O-H stretching vibration of hydroxyl functional groups

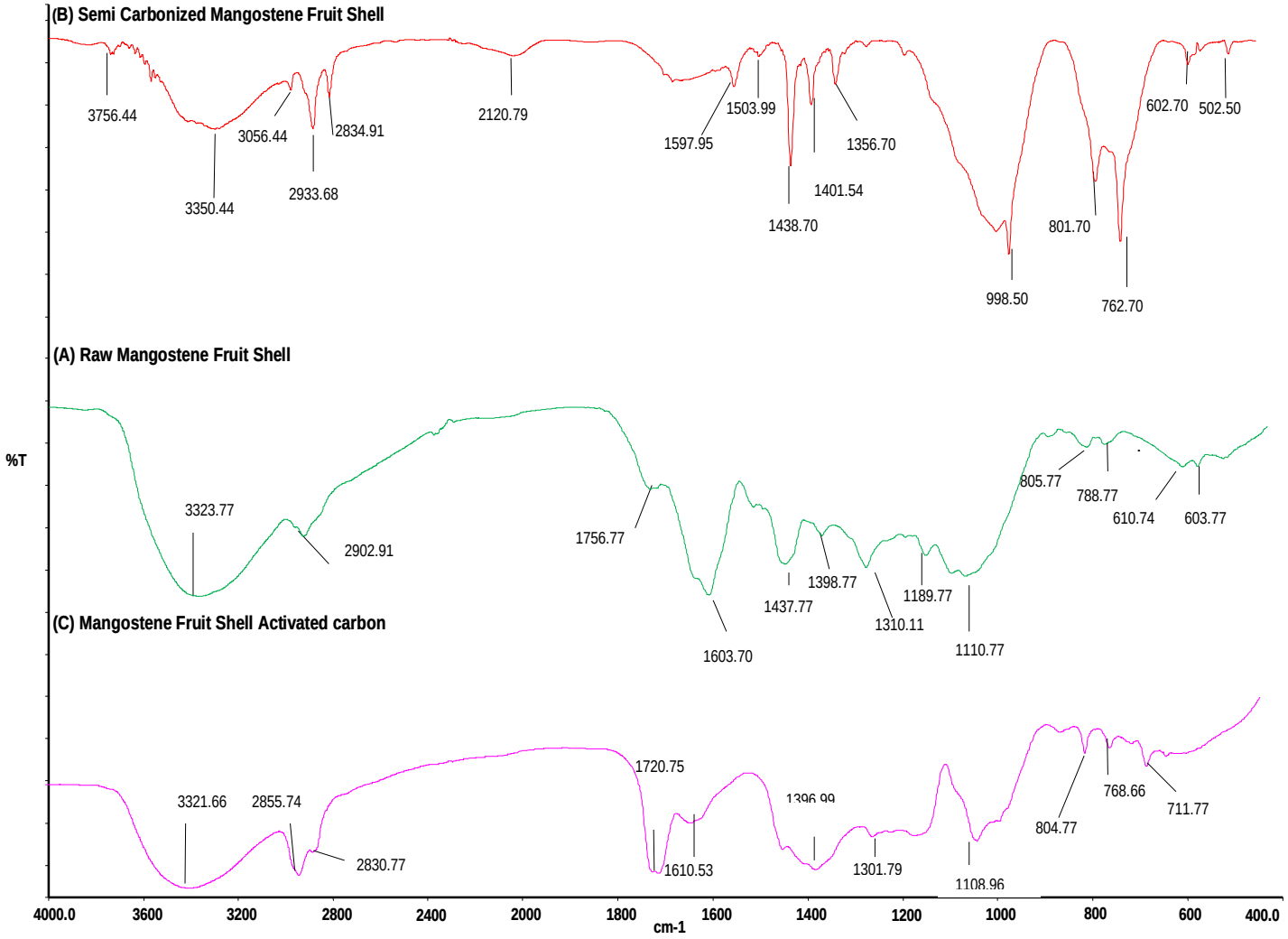

Figure 6.3 FTIR Spectrum of raw mangostene fruit shell, semicarbonized and activated carbon

Table6.8FTIR Spectrum of Mangostene Fruit shell (MFS), semi-carbonized Mangostene Fruit Shell (MFS) and Activated Carbon (MFSAC)

IR Peak Number	Precursors		Peak	Assignment
	Raw Mangostene Shell (MFS)	Semi carbonized Mangostene Shell (MFS)	Activated Mangostene Shell (MFS)	
1	-	502.50	-	C-H bending
2	603.77,610.74	602.70	-	C-O-H bending
3	788.77	762.70	711.77, 768.66	C-H
4	805.77	801.70	804.77	C-H
5	-	998.50	-	O-H bending
6	1110.77,1189.77	-	1108.96	-C-N stretching
7	1310.11,	-	1301.79	$-NO_2$ aromatic nitro compound
8.	1398.77	1356.70	1396.99	CH_3 deformation
8	1437.77	1401.50,1438.70	-	In plane O-H bending and C-O stretch of dimers
9	-	1503.99,1597.66	-	C=C ring stretching of benzene derivatives
10	1603.70	-	1610.53	C=C ring stretching

Table 6.8 Continued

IR Peak Number	Precursors			Peak Assignment
	Raw Mangostene	Semi Carbonized Mangostene Shell (MFS)	Activated Mangostene	
11	1756.77	-	1720.75	C=O stretching
12	-	2120.79	-	C-H bending
13	-	2834.91	2830.77,2855.74	C-H stretching
14	2902.91	2933.68	-	C-H stretching
15	-	3056.44	-	O-H stretching vibration of hydroxyl functional groups
16	3323.77	3350.70	3321.66	O-H stretching vibration of hydroxyl functional groups
17	-	3756.44	-	O-H stretching vibration of hydroxyl functional groups

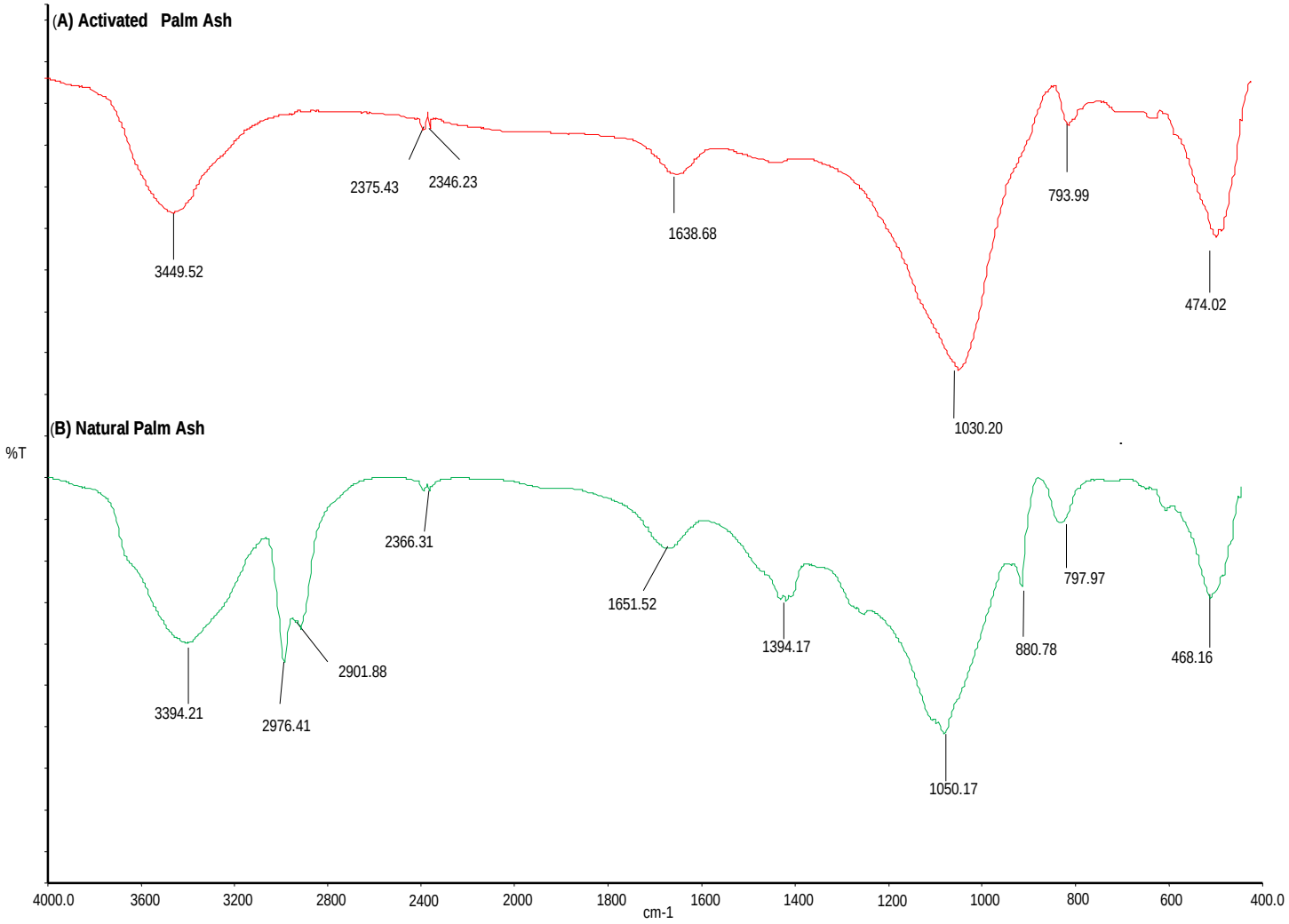

Figure 6.4 FTIR spectrum of Natural oil Palm Ash (OPA) and Activated Oil Palm Ash (AOPA)

Table 6.9 FTIR Spectrum of Natural (OPA) and Activated Oil Palm Ash (AOPA)

IR Peak Number	Natural Oil Palm Ash (NOPA)	Activated Oil Palm Ash (AOPA)	Peak Assignment
1	468.16	474.02	Bending Vibration of Si-O group
2	797.79	793.99	C-H out of plane deformation
3	880.78	-	Si-H Deformation
4	1050.17	1030.20	Si-O-Si Stretching Vibration
5	1394.17	-	Aliphatic CH_3 Deformation
6	1651.52	1638.68	C=C Stretching Vibration
7	2366.31	2346.23, 2375.43	CΞC Stretching Vibration of Alkyne
8	2901.88	-	Aliphatic CH_2 Vibration
9	2976.41	-	Aliphatic CH_2 Vibration
10	3394.21	3449.52	O-H Stretching Vibration of Hydroxyl group

The broad peak for natural and activated samples of palm ash between 3000-3600 cm^{-1} reflects the presence of –OH group which might be due to stretching vibration of Si-OH group. Both the spectra contains band around 1600 cm^{-1} showing the existence of CO groups of aldehydes and ketones. Similar types of peak assignment were observed for bagasse fly ash and rice husk ash adsorbent prepared for Ni (II), Cd (II) and Zn (II) sorption from waste water (Srivastava *et al.*, 2007).

6.4 Summary

The outcome of this study is the establishment of suitability of different indigenous raw materials to be converted as value added products of powdered and granular adsorbent. Apart from the processing steps mentioned earlier (Chapter 5), the prepared sorbent must undergo several steps of surface characterization (Chapter 6) to ensure the sorption performance prior to commercial production. The physio-chemical characteristics determined here reflects that the prepared sorbent has got sufficient potential to be used for waste water treatment. In this context the sorption performance of the prepared sorbent has been further evaluated by batch (Chapter 7) and fixed bed adsorption (Chapter 8) system.

CHAPTER SEVEN
RESULTS AND DISCUSSION
Batch Adsorption Studies

7.1 Introduction

Adsorption studies for divalent cations of lead Pb(II), copper Cu(II) and manganese Mn(II) are carried out to delineate the effect of contact time, temperature, pH and initial metal ion concentration on equilibrium adsorption capacity. Batch sorption process gives the experimental results for equilibrium isotherms, kinetics as well as the thermodynamics of sorption process onto the prepared sorbent. The mechanism of adsorbate adsorbent interaction is discussed through intra particle diffusion. The last section provides the regeneration of the prepared sorbent. A summary is presented in the last part of this chapter.

7.2 Effect of Contact Time and Initial Concentration of Adsorbate

Batch equilibrium experiments are performed by using 50 ml of the adsorbate (lead, Pb(II) copper, Cu(II) and manganese, Mn(II)) solutions of known initial concentrations ranging from 50 to 100 mg/l with equivalent mass of 0.2 g of the prepared adsorbent (KCAC, KFAC, MFSAC and AOPA). Figures 7.1(a)-(d), 7.2(a)-(d) and 7.3 (a)-(d) illustrate the adsorption uptake of Pb(II), Cu(II) and Mn (II) cations versus the contact time, t (minutes) at various initial concentrations (50-100 mg/l) onto KCAC, KFAC, MFSAC and AOPA respectively at 30 °C.

The extent of dispersion of the solute within equilibrium contact time in the case of batch sorption process is a crucial factor as it affects the process of overall mass transfer. Thus the residual equilibrium concentration, C_e (mg/l) with respective sorption

amount, q_t (mg/g) was measured at predetermined interval of time.

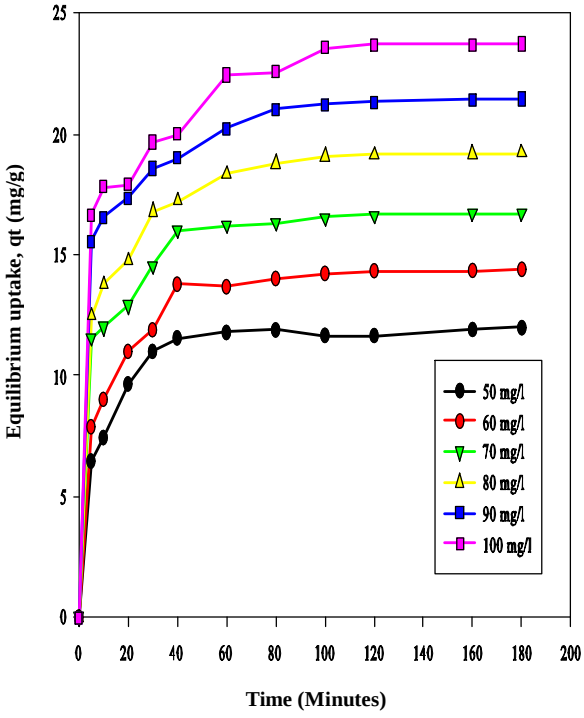

(a) KCAC

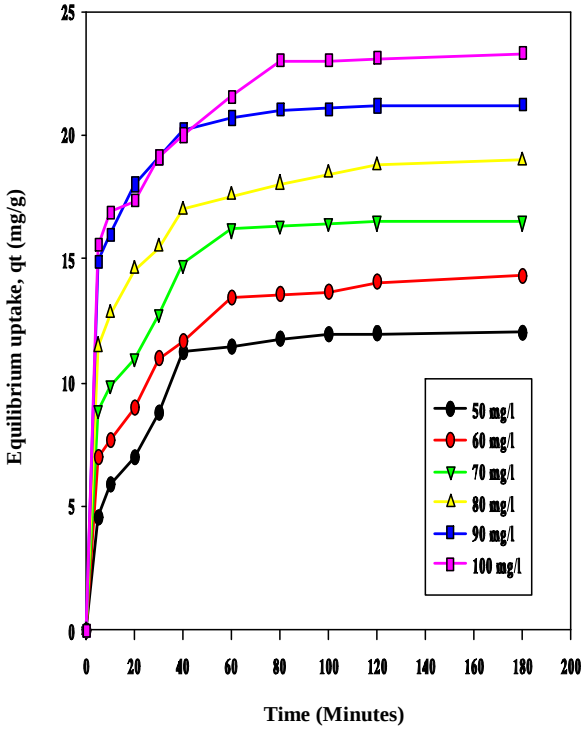

(b) KFAC

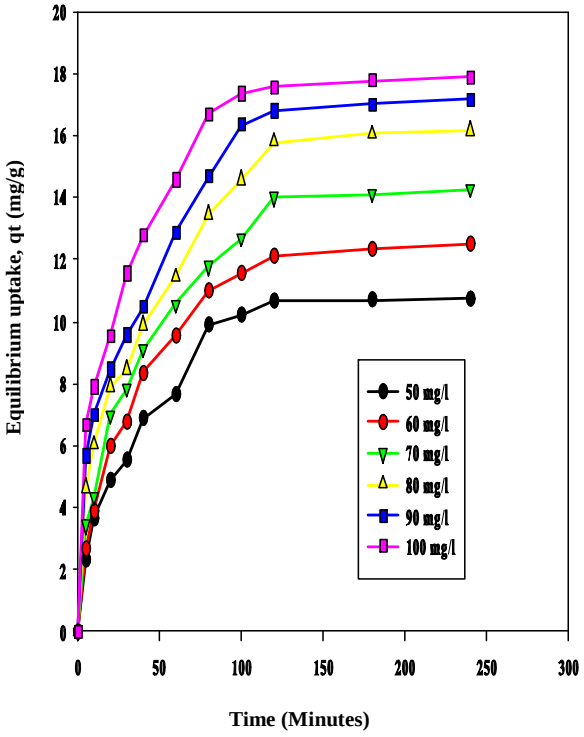

(c) MFSAC

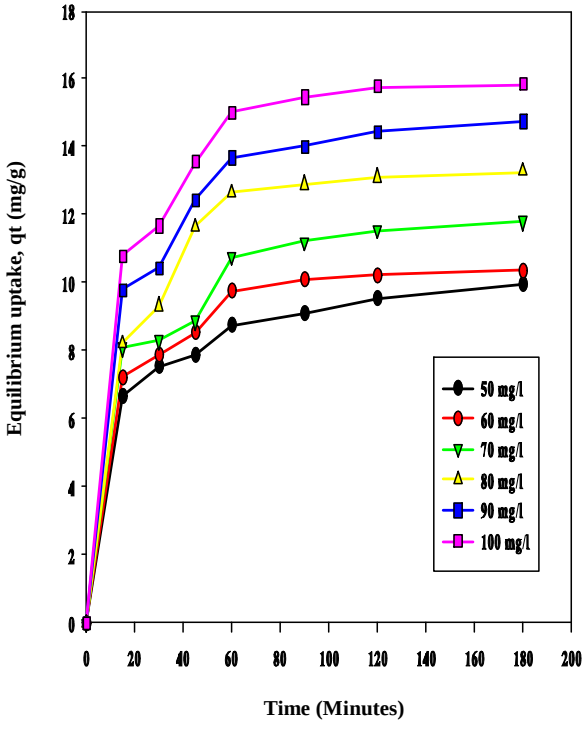

(d) AOPA

Figure 7.1 Effect of contact time at various initial concentrations of Pb (II) cations onto (a) KCAC (b) KFAC (c) MFSAC (d) AOPA at (30±1) °C

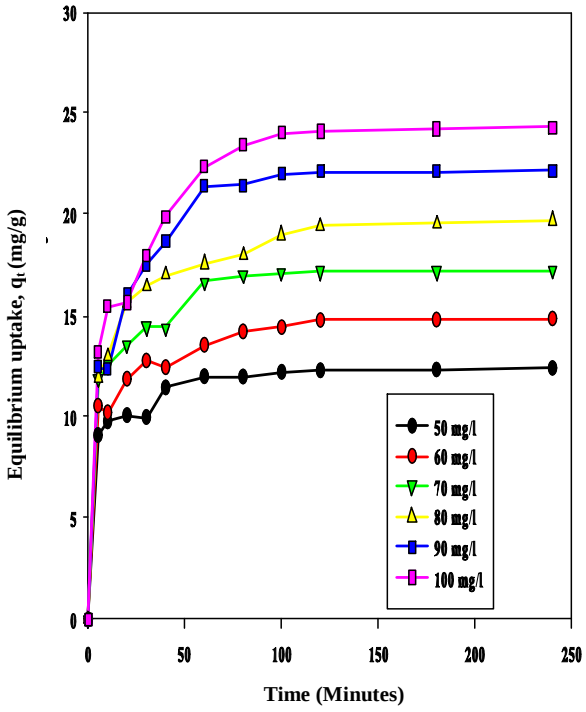

(a) KCAC

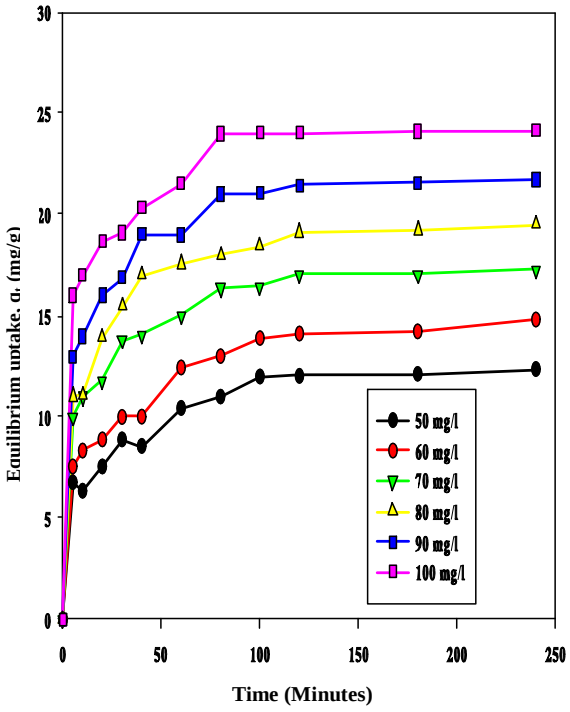

(b) KFAC

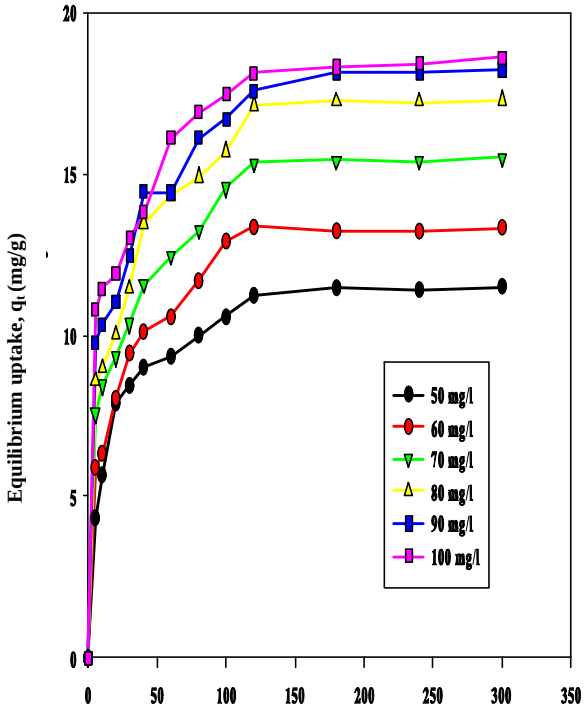

(c) MFSAC

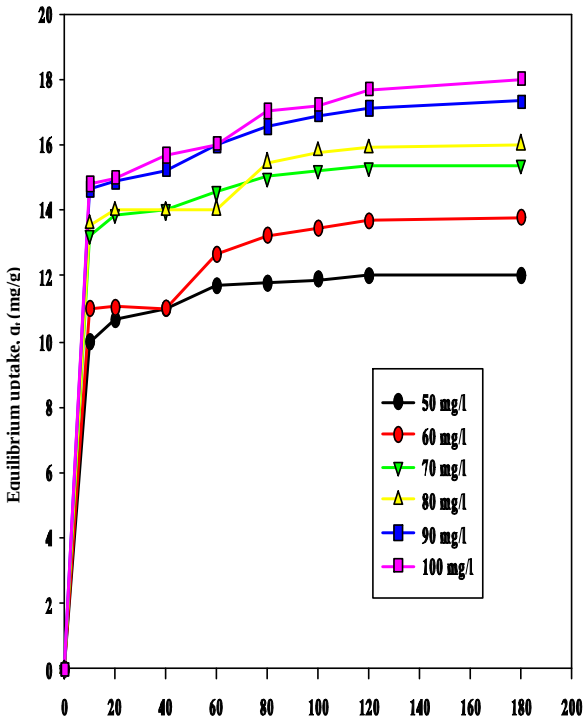

(d) AOPA

Figure 7.2 Effect of contact time at various initial concentrations of Cu (II) cations onto (a) KCAC (b) KFAC (c) MFSAC (d) AOPA at (30 ±1) °C

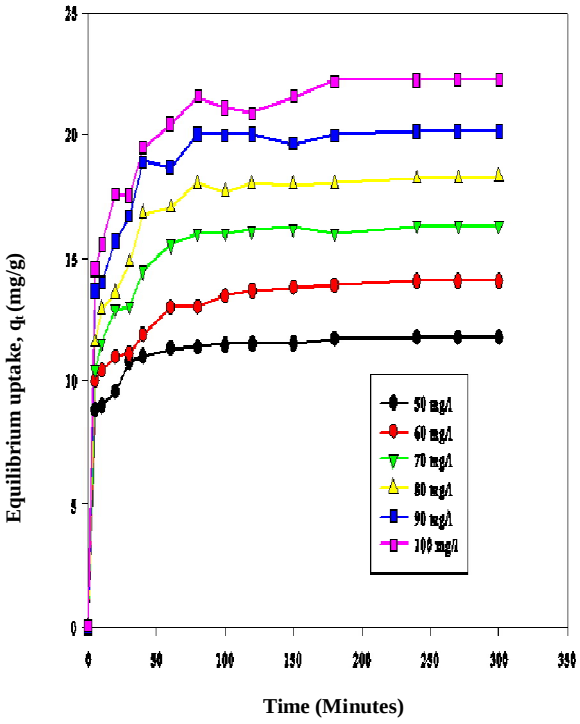

(a) KCAC

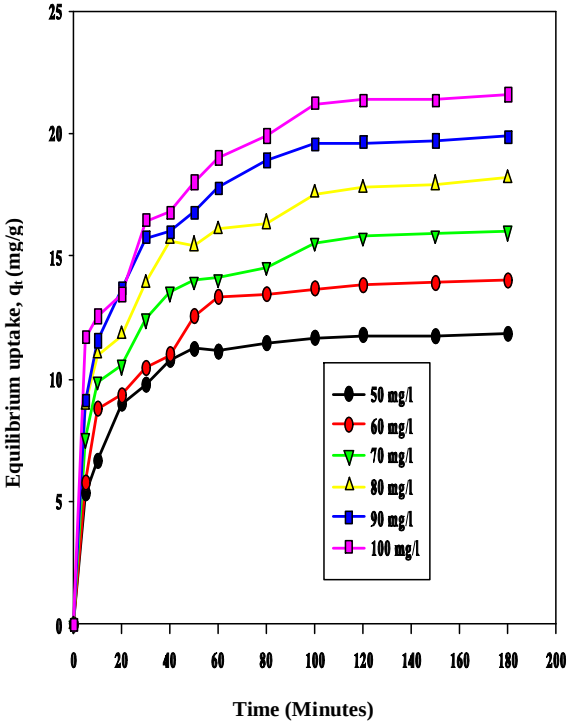

(b) KFAC

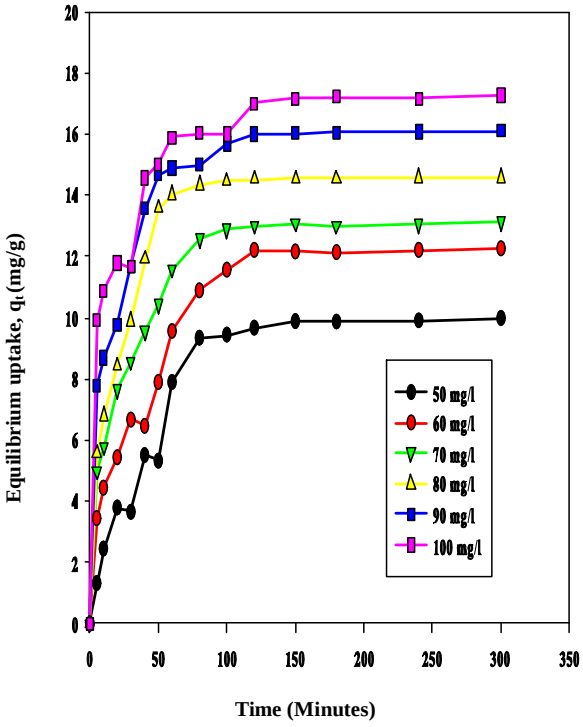

(c) MFSAC

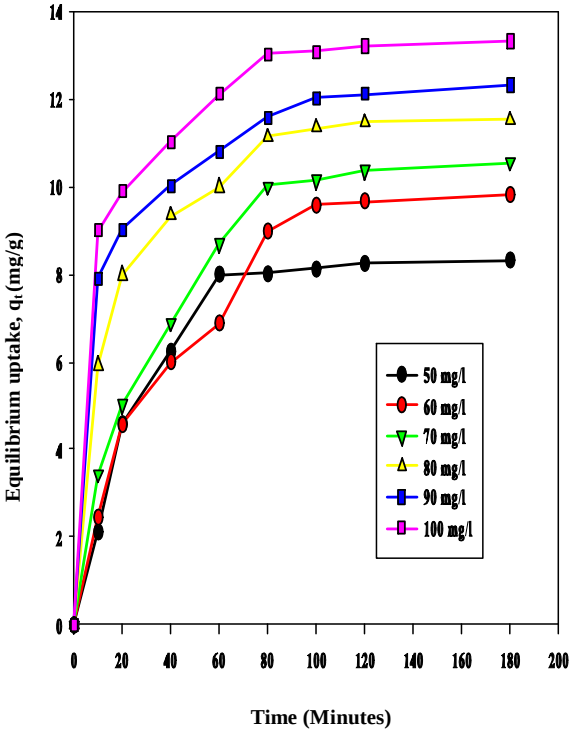

(d) AOPA

Figure 7.3 Effect of contact time at various initial concentrations of Mn (II) cations onto (a) KCAC (b) KFAC (c) MFSAC (d) AOPA at (30±1) °C

Agitation time influences the formation of the external film which creates a boundary layer over the surface of the sorbent. During preliminary investigation, it was observed that activated carbon is much more reactive as compared to the ash residues (Chapter 5). Thus, the experimental uptake, q_t (mg/g) with respect to time, t (minutes) was taken more frequently for powdered and granular activated carbon. It is clear from the plots (Figures 7.1(a-d), 7.2(a-d) and 7.3(a-d)) that for all the four activated adsorbents, the amount of equilibrium uptake, q_t (mg/g) increased with time. However, there is a maximum point after which the system has reached a constant value; beyond this no significant amount of solute is removed from the solutions. This particular point is known as the 'equilibrium point'. At this equilibrium point, the cations desorbing from the activated sorbents are in a state of dynamic equilibrium with the amount of the cations adsorbed onto the prepared sorbents. The amount of cations adsorbed at the equilibrium time reflects the maximum capacity of that sorbent under the applied working conditions.

The plots obtained here show two distinct regions of sorption. The initial region is quite fast and rapid. The steepness of this initial stage is larger in the case of powdered activated adsorbents (KCAC, KFAC and AOPA) compared to the granular adsorbent (MFSAC). The second stage is almost parallel to the x- axis and relatively slow near the equilibrium. Almost all the sorption curves are single and smooth with few exceptions reflecting that the saturation or exhaustion point of the sorbent has been reached by the preselected adsorbate. At initial stage, there are a large number of vacant surface sites which can readily absorb the cations. After a lapse of time, the active surface sites had been exhausted. Thus, it becomes difficult to be occupied by the remaining cations. This happens due to repulsive forces between the solute (cations attached onto the solid surface) and the free ions (cations dispersed in the liquid phases)

remaining in the solution. Similar observation was reported earlier for the sorption of divalent cations of Pb(II), Cd(II) and Ni(II) cations onto sawdust (Bulut and TEZ Zeki, 2006).

The adsorption uptake at equilibrium is found to increase with increasing initial cation concentrations. This is because at higher initial concentration, the driving force for mass transfer becomes larger. Consequently, there will be more equilibrium uptake. On the contrary, opposite trend is observed for removal percentage. It is observed that when initial concentrations are increased from 50 mg/l to 100 mg/l, the percentage removal of the cations is decreasing. This happens because at lower concentration, the ratio between the initial number of cations present inside the solution relative to the number of active sites is low. At higher initial concentrations, more cations are available in the solutions, yet the provided quantity of the sorbent is kept fixed. Thus, the ratio between sorbate-cations and the active vacant sites of the sorbent becomes larger leading to lower removal percentage. This trend is evident and agreed well with the previous literature depicting sorption of Methylene Blue cations onto fly ash (Basava Rao and Ram Mohan Rao, 2006).

About 94.89%, 93.23%, 71.44% and 63.32% of Pb(II) cations are removed by KCAC, KFAC, MFSAC and AOPA respectively from 100 mg/l of solution. Higher percentage of copper is removed by the prepared sorbent which might be due to its smaller cationic size and highest position in the reactivity chain based on Irving William series. It is observed that approximately 97.24%, 96.54%, 73.23% and 71.99% of Cu(II) cations are removed by KCAC, KFAC, MFSAC and AOPA respectively from 100 mg/l. Relatively less removal percentage is observed for sorption of manganese onto the prepared sorbent. This might be due to its less stable surface complex formation

tendency. Approximately 89.00%, 86.23%, 69.02% and 53.22% of Mn(II) cations are removed by KCAC, KFAC, MFSAC and AOPA respectively from 100 mg/l solution.

It can be seen from the graphs above that, longer contact times of 80 minutes are required by Pb(II) cations for higher initial concentrations of 80, 90 and 100 mg/l solution while 60 minutes is required for 50, 60 and 70 mg/l solution to reach equilibrium for KCAC. In the case of adsorption, initially the adsorbate species needs to overcome first the boundary layer. In the second phase, it has to diffuse through the boundary layer and adsorb onto the adsorbent surface. Eventually at the last stage, they need to diffuse into the porous structure of the adsorbent. This phenomenon takes a relatively extended contact time. Therefore, adsorbate solutions with higher initial concentrations might take relatively longer contact time to attain equilibrium due to the presence of a higher amount of adsorbate species. For KFAC, all the concentrations have reached equilibrium within 80 minutes and for MFSAC, it takes 80 to 100 minutes based on the concentration ranges. Approximately 60 to 90 minutes are required for sorption of Pb(II) onto AOPA. Adsorption of Pb(II) onto MFSAC overall takes relatively less time to reach equilibrium due to the different characteristics of the adsorbent. This may be due to the larger cationic size of Pb (II) cations for which the granular adsorbent surface of MFSAC becomes exhausted quickly. It had been described by previous researchers where approximately 5 hours were required for Pb(II) cations to reach equilibrium (Anirudhan *et al.*, 2001) using polyacrylamide grafted tin oxide gel whereas modified cellulosic materials and modified bark took only 20 minutes and 2 hours respectively (Okieimen *et al.*,1987 ; Gaballah *et al.*, 1998).

In the case of Cu(II) cations, approximately 100 minutes and 120 minutes are required by KCAC and MFSAC respectively. It takes 80 minutes for AOPA sample to

attain equilibrium for Cu(II) cations. Around 60 to 100 minutes contact time are required for the sorption of Cu (II) cations onto KFAC depending on the initial concentration ranges. However, sawdust needed 90 minutes to accomplish the equilibrium state for sorption of copper (Azmal *et al.*, 1998) whereas pine bark showed relative slower reaction kinetics and took 24 hours to reach equilibrium (Duvnjak and Al-Asheh, 1998).

For lower concentrations of 50, 60 and 70 mg/l, around 40 minutes are required and a higher concentration range of 80, 90 and 100 mg/l take 80 minutes to reach equilibrium for the sorption of Mn(II) cations onto KCAC. Within 50 to 100 minutes, the system attains equilibrium for Mn(II) sorption onto KFAC. However, it takes 150 minutes and 80 minutes respectively for sorption equilibrium of Mn(II) cations onto MFSAC and AOPA. It is reported earlier that sorption of Mn (II) cations onto raw and acid treated corncob biomass took around 80 minutes to reach equilibrium (Abideen *et al.*, 2011). It was reported that, sorption of Mn(II) cations onto electric arc furnace slag took 180 minutes when the initial concentration was 10 mg/l and it took 240 minutes for 100 mg/l solution to reach equilibrium (Beh *et al.*, 2010).

Relatively longer contact time is required for Cu(II) and Mn(II) ions to reach equilibrium upon the granular adsorbent of MFSAC. Similar trend is also observed for continuous flow sorption system by using fixed bed column in this study and this will be discussed afterwards in Chapter 8 (Fixed Bed Adsorption Study). This phenomenon is attributed to the smaller cationic size of Cu(II) and Mn(II) which can provide larger vacant sites for monolayer formation and unstable surface complexes leading to successive adsorption-desorption steps for Mn(II) cations. The results also revealed that, comparatively longer contact time is needed for adsorption of Cu(II) and Mn(II) cations

onto the granular adsorbent of MFSAC compared to the powdered form of activated adsorbent (KCAC, KFAC and AOPA). It is reported earlier also that, the rate of reaction varies reciprocally with the square of the particle size (Eckenfelder, 2000). Similar trend has been observed for the sorption process of Methylene blue cations onto coconut husk and palm shell based activated carbon (Tan, 2008).

In general, the sorption performance of an adsorption system varies with the category and physio-chemical properties of the sorbent and sorbate used. In this study, KCAC shows the highest equilibrium uptake and removal percentage, followed by KFAC, MFSAC and AOPA. The relatively high adsorption uptakes of KCAC and KFAC compared to MFSAC are due to their relatively high surface areas and pore volumes (Table 6.2-a). BET surface area and pore volume of an activated carbon is one of the most important characteristics needed for liquid phase applications. It is observed that AOPA showed less removal percentage compared to MFSAC despite its larger surface area.

It has been reported that, sometimes adsorbent with higher surface area takes the adsorbate very quickly from the solution but cannot retain them due to its lower affinity towards the adsorbate which is chiefly contributed by the intensity of various functional groups or pore size distribution (Ahmenda *et al.*, 2000; Qureshi, 2008; Patrick, 1995). Similar observation has been reported for adsorption uptake of Methylene Blue cations onto KOH activated coconut husk and oil palm empty fruit bunch activated carbon where the latter possesses a higher surface area than the former one. Despite its high surface area, oil palm empty fruit bunch based activated carbon failed to retain Methylene Blue cations permanently resulting in lower removal efficiency (Tan, 2008).

Besides physical characteristics, the adsorption performance of an activated adsorbent is also influenced by its surface chemistry. The functional groups on the surfaces of the activated adsorbent act as chemical binding agents. From the FTIR spectrums obtained (Figures 6.1-6.4), the high adsorption capacity of the activated adsorbent prepared in this study are due to the presence of functional groups such as hydroxyl, carbonyl and alkyl groups (Habib *et al.,* 2007). These groups can easily dissociate and create negatively charged sites over the solid surface of the sorbent. This causes electrostatic attraction between the surface of the activated sorbent and the positively charged cations under investigation (El Qada *et al.,* 2008).

7.3 Effect of Solution Temperature

The consequence of solution temperature on the removal percentage of Pb (II), Cu (II) and Mn (II) ions by the activated adsorbent prepared were studied by changing the solution temperature from 30 ℃, 50 ℃ and 70 ℃, while keeping the other process parameters such as adsorbate volume (50 ml), pH (5.5) and initial metal ion concentration constant (100 mg/l). To observe the removal efficiency, highest metal ion concentration (100 mg/l) was chosen for all types of sorbent to maintain consistency with the results depicted earlier in Chapter 5 (section 5.5).The effect of temperature on collective sorption performances for all the concentration ranges (50-100 mg/l) studied here will be discussed further in terms of thermodynamic characterization of each adsorbate-adsorbent system in the subsequent section of this study. Figures 7.4, 7.5 and 7.6 show the removal percentages versus the solution temperature for different adsorbent for lead, copper and manganese respectively.

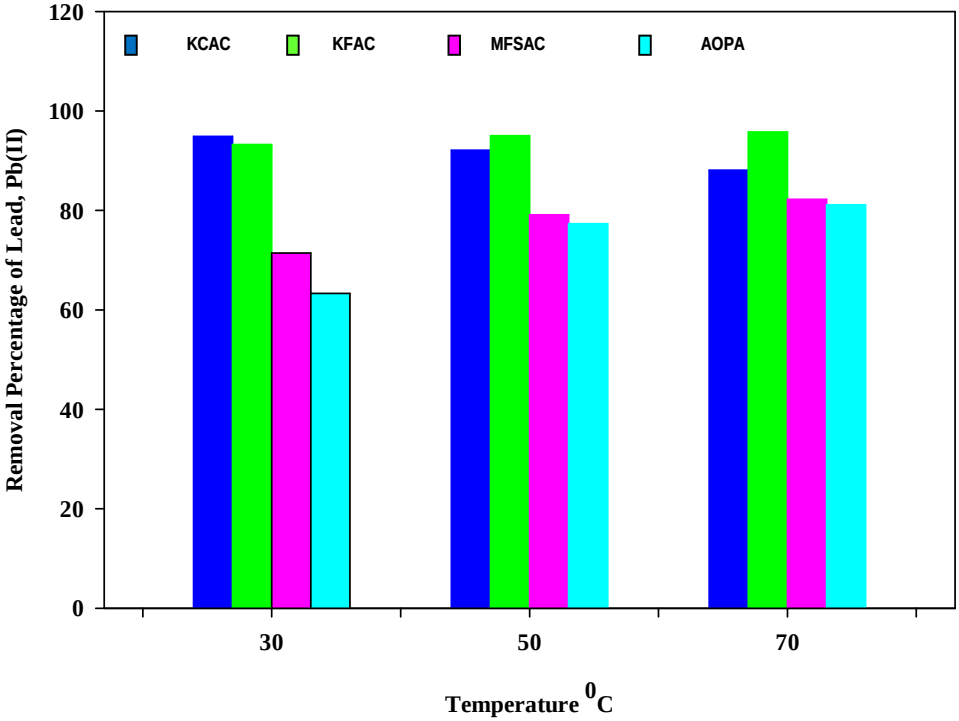

Figure 7.4 Effect of solution temperature on removal percentages of Pb (II) cations onto KCAC, KFAC, MFSAC and AOPA

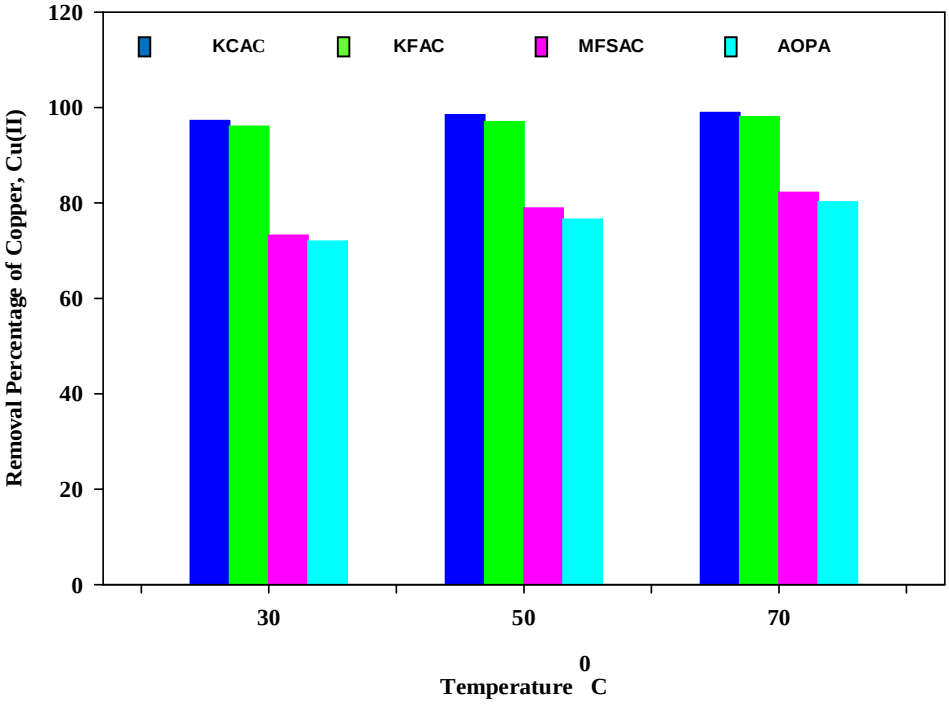

Figure 7.5 Effect of solution temperature on removal percentages of Cu (II) cations onto KCAC, KFAC, MFSAC and AOPA

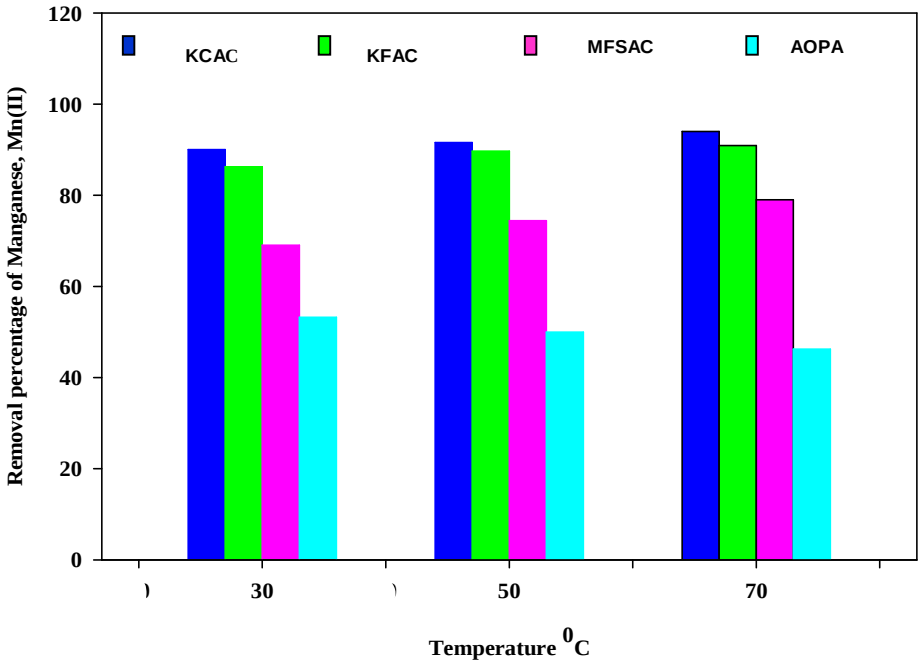

Figure 7.6 Effect of solution temperature on removal percentages of Mn (II) cations onto KCAC, KFAC, MFSAC and AOPA

It is evident from these three bar charts (7.4-7.6) that, the effects of solution temperature on the adsorption capacity of the activated adsorbents were found to depend on the type of adsorbent-adsorbate system. Adsorption capacity of lead has decreased for increasing temperature in the case of KCAC and this reflects the exothermic nature of sorption. For lead, the sorption capacity is found to increase with increase in solution temperature of 30 ℃, 50 °C and 70 °C, indicating the endothermic sorption reactions for other sorbents (KFAC, MFSAC and AOPA). It had been observed for adsorption of divalent cations of Pb(II) cations onto kaolinite, montmorillonite, poly (oxo-zirconium) kaolinite, poly(oxo-zirconium) montmorillonite, TBA–kaolinite and TBA–montmorillonite that increasing temperature has resulted in decreased removal

efficiency (Sen-Gupta *et al.,* 2005). Similar trend of exothermic nature of sorption was reported for adsorption of Pb(II) onto bagasse fly ash (Gupta and Ali, 2004) also. All the adsorbent prepared here has shown an endothermic nature of sorption for Cu(II), while for Mn(II) except palm ash, other adsorbent of KCAC, KFAC and MFSAC showed endothermic nature of sorption. These findings are consistent with previous literature where rubber wood activated adsorbent showed exothermic nature of sorption in case of Cu(II) cations (Kalavathy *et al.,* 2005). On the contrary, raw and acid treated corncob biomass showed an endothermic reaction pattern (Abideen *et al.*, 2011) and fly ash showed exothermic tendency towards divalent cations of Mn(II) (Sharma *et al.,* 2007).

Increasing the temperature increases the velocity of adsorbate species towards the interior of the adsorbent. This results in a greater diffusion of the adsorbate molecules across the exterior of the boundary layer as well as into the pores of the adsorbent. This takes place due to the decrease in surface tension and viscosity of the solution (Wang and Zhu, 2007) also. Karthikeyan *et al.,* (2005) stated that the improvement in the removal percentage might be due to the chemical interaction between adsorbents and adsorbate, construction of some new adsorption sites or the amplified rate of intraparticle diffusion of adsorbate species into the pores of the activated adsorbents at higher temperatures. Senthilkumaar *et al.,* (2006) also illustrated analogous explanation and they attributed the increase in adsorption with the increase in temperature to the possibility of an increase in the porosity and in the total pore volume of the adsorbent. On the contrary, decrease in adsorption affinity with the increase in temperature is due to the involvement of the desorption step in the sorption mechanism. It might also take place due to the weakening of Van der wall forces between the active sites of the activated sorbent and the cationic species.

7.4 Effect of initial pH of the solution

In order to study the effect of initial pH on the removal percentage of divalent cations of Pb(II), Cu(II) and Mn(II) onto the prepared activated adsorbent, the solution pH was adjusted from pH 2 to 12 while other parameters were kept constant. The initial concentrations of the investigated cations were fixed at 100 mg/L.

In general, initial pH value may enhance or depress the adsorbate uptake. This is attributed to the change of the charge of the adsorbent surface with the change in pH value. Besides, the solution pH also governs the degree of ionization of the adsorbate species (El Qada *et al*, 2006). Figures 7.7, 7.8 and 7.9 display the effect of initial pH on the removal percentage of Pb(II), Cu(II) and Mn(II) cations respectively.

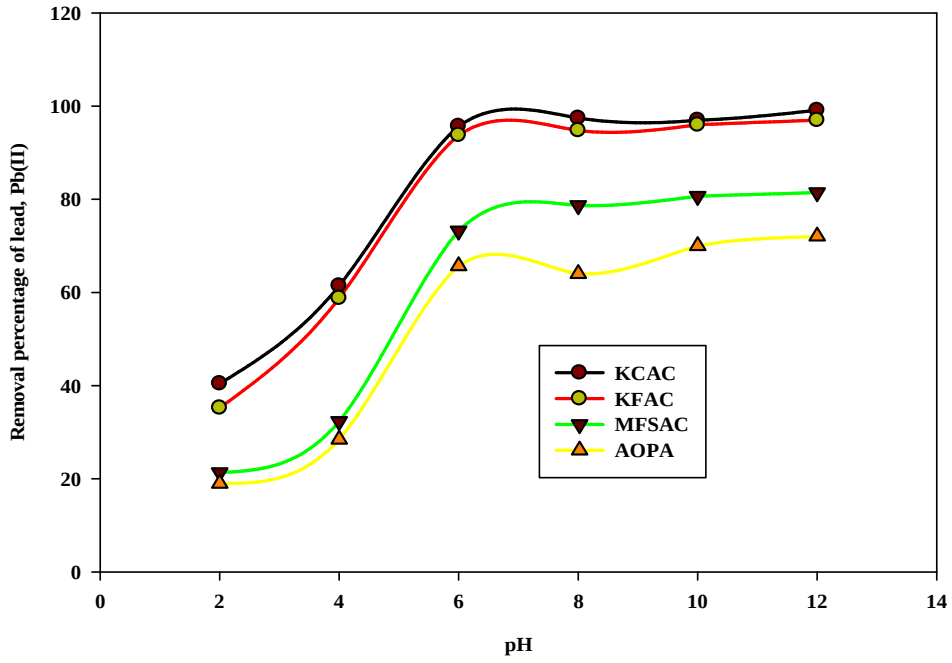

Figure 7.7 Effect of solution initial pH on the removal percentage of Pb (II) cations onto KCAC, KFAC, MFSAC and AOPA

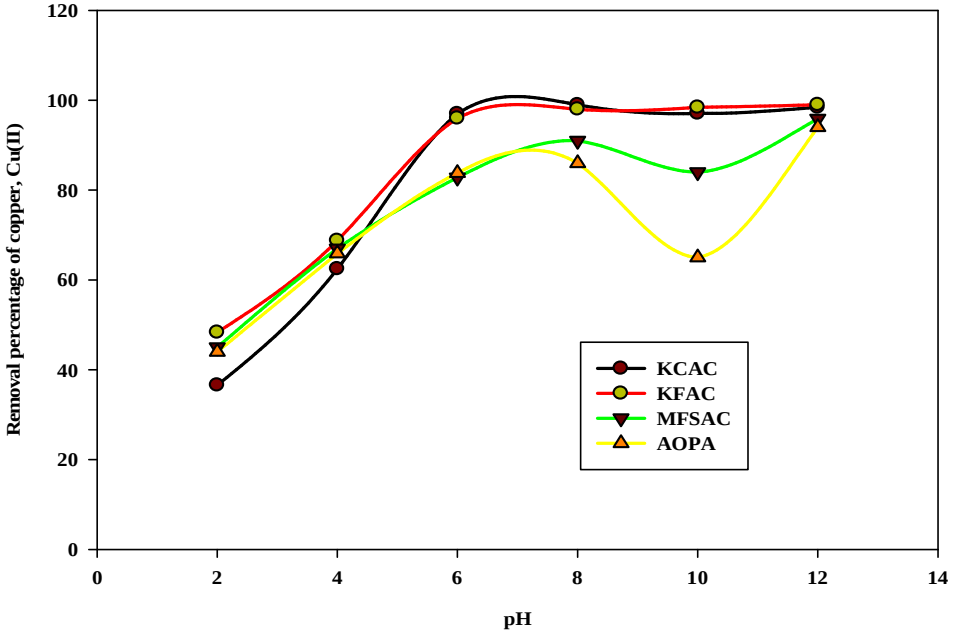

Figure 7.8 Effect of solution initial pH on the removal percentage of Cu (II) cations onto KCAC, KFAC, MFSAC and AOPA

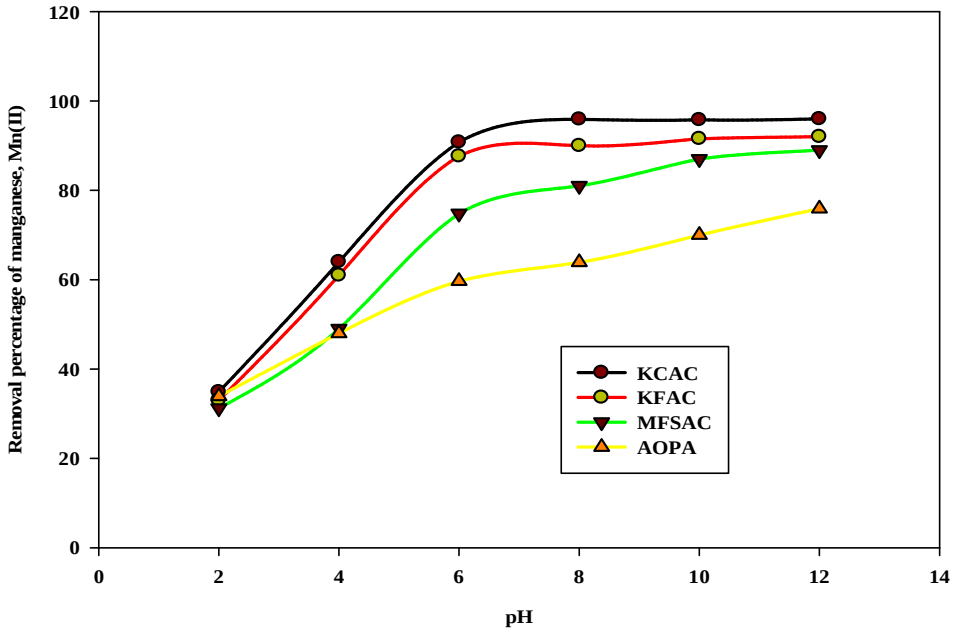

Figure 7.9 Effect of solution initial pH on the removal percentage of Mn (II) cations onto KCAC, KFAC, MFSAC and AOPA

At lower pH values, a higher concentration of H^+ and H_3O^+ ions in the solution compete with positive M^{2+} cations for the adsorption sites resulting in a smaller removal percentage. Thus adsorption is reasonably low below pH 4 for all the cations under investigations. At around pH 6, there are three main species of divalent cations present in their respective solution. These species can interact with the surface hydroxide (-OH) groups and gets adsorbed by the ion exchange and hydrogen bonding mechanisms resulting in greater removal efficiency. Similar observation has been reported for Cd(II) and Zn(II) adsorption on rice husk ash (Srivastava *et al.*, 2008).

(a) Ion Exchange:

$$(-RO^+H_2) + M^{2+} \longrightarrow (RO)\,M + 2H^+ \qquad (I)$$

$$(-RO^+H_2) + M(OH)^+ \longrightarrow (-RO)\,MOH + 2H^+ \qquad (II)$$

It is also reported in the literature that, divalent cations can attach themselves to two adjacent –OH groups by the following reaction scheme:

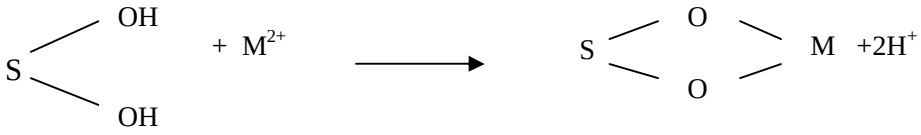

(III)

Two oxyl groups present in the structure can donate two pairs of electrons to form four coordination number compounds with the release of two hydrogen ions (Doris *et al.*, 2000).

(b) Hydrogen Bonding:

$$2(\text{--R-OH}) + M(OH)_2 \longrightarrow (\text{-R-OH})_2 \text{ ----- } M(OH)_2 \qquad (IV)$$

Similar observation has been reported for Cu(II) adsorption onto orange peel, saw dust and bagasse (Habib *et al.,* 2007) and Pb(II) onto activated periwinkle shell and commercial activated carbon (Badmus *et al.,* 2007). It is also observed that for sorption of Mn (II) ions, basic medium favors the removal percentage to a greater extent. However after pH 8, the removal percentage is almost the same except for AOPA and MFSAC. Similar trend was reported for sorption of Mn(II) ions onto *Bombax malabaricum* and *Peltophorum ferrugineum* (Emmanuel *et al.,* 2009).

In addition to that, carboxylic groups (-COOH) also take part in the adsorption process. It is well known that the carboxylic groups present on the surface of the activated carbon have pK_a values from 3 to 5. Therefore, at a higher pH of 6, the acidic groups of -COOH starts to dissociate. Thus more interaction between the negatively charged carboxylate ions and positively charged M^{2+} ions takes place which resulted in a higher removal efficiency. This process is illustrated by the equation below-

$$\text{(c)}\quad nR\text{-}COOH + M^{2+} \longrightarrow (R\text{-}COO)_n M + nH^{+} \qquad \text{(V)}$$

Where, R represents the carbon matrix. M^{2+} is a transition metal having empty d-orbital that can be occupied easily by the lone electron pair of oxygen in –COOH and –OH of the activated carbon surface to form stable complexes. Thus it can be postulated that the adsorption process of M^{2+} can occur by ion exchange, hydrogen bonding and surface complexation.

From the FTIR spectrum, methoxy ($-OCH_3$) group has also been identified. Divalent cations like Pb (II), Cu(II) and Mn(II) can readily form surface complexes by the following scheme:

(d) $M^{2+} + 2O\text{-}CH_3 \longrightarrow H_3C\text{-}O \cdots M \cdots O\text{-}CH_3$ (VI)

$M^{2+} + O\text{-}H + 2O\text{-}CH_3 \longrightarrow H\text{-}O \cdots M \cdots O\text{-}CH_3$ (VII)

Similar trend has been observed for the sorption of Cd(II) cations onto coir pith adsorbent (Bharathi *et al.,* 2011). However, it is well known that at basic pH heavy metals like Pb(II), Cu (II) and Mn(II) will start to precipitate. Therefore, to avoid cooperative effects of adsorption and precipitation, all the batch experiments were conducted in slightly acidic medium of pH 5.5.

The results from the experiments described in this study show that Pb (II), Cu(II) and Mn(II) ions can be absorbed efficiently onto activated oil palm ash. The ability of activated oil palm ash to remove the cations is the result of a number of mechanisms, including surface adsorption, chemisorptions, complexation, ion exchange, microprecipititation and metal hydroxide complexation. However, after pH 8, there is a sharp decrease in adsorption observed for Cu(II) ions onto MFSAC and AOPA. This decrease is probably due to formation of soluble hydroxyl complexes or hydrolysis of metallic cations (Badmus *et al.,* 2007). It is reported earlier that hydrolysis of metallic cations takes place by the substitution of metallic ligands in the inner coordination sphere with the –OH group (Badmus *et al.,* 2007). The overall phenomenon takes place after the removal of the outer hydration sphere of metallic cations. After pH 8, there is again an increase in the removal percentage which results in an S-like adsorption curve. This S-like curve reflects the cumulative effect of adsorption and precipitation (Inbaraj and Sulochana, 2002).

In order to understand the detailed mechanism by which the cations have been removed from the solution by adsorption, it is essential to identify the chemical constituent present on the adsorbent. The high percentage of SiO_2 may also be involved in the adsorption phenomena through SiO- bond with the cations, as presented by following scheme:

$$-SiO_2 + H_2O = -SiO^- + H_3O^+ \quad \text{(I)}$$

$$-SiO^- + M^{2+} = -SiO^-M^{2+} \quad \text{(II)}$$

$$-SiOH + M^{2+} = -SiO^-M^{2+} \quad \text{(III)}$$

Overall it can be concluded that, the removal of the studied metallic cations from waste water samples by adsorption involves complex mechanisms which are partly predominated by adsorption and surface complexation. It can also proceed via chemical precipitation and pore filling mechanisms which will be explained further by the intra-particle diffusion mechanism.

7.5 Batch Adsorption Studies

The adsorption isotherm gives a picture of the distribution of adsorbate species between aqueous and solid phase - over the adsorbent surface at an equilibrium state. To design a batch sorption process, the experimental data should be fitted to different types of isotherm models. This is important to establish the most appropriate correlation for the isotherm curves (El-Guendi, 1991). Adsorption isotherm basically gives an idea about the interaction between the solutes and the adsorbents. It is used for optimizing solvent solute ratio at specific operating condition. In this work, the adsorption isotherm study was carried out by using three isotherm models namely Langmuir, Freundlich and Temkin isotherm models.

For two parameter models of Langmuir, Freundlich and Temkin, the linearized forms of the mathematical equations were applied to fit the equilibrium data as they are simpler and more commonly used by previous researchers compared to the non-linearized form. Therefore, a comparison could be made for the parameters and constant values obtained from the present study with those reported earlier in the literature. The applicability of the isotherm models to fit the adsorption data was compared by observing the correlation coefficients, R^2 values. The closer the R^2 values are to unity, the better is the fit. However, the existing models may deviate from the experimental data depending on the specific properties of adsorbate-adsorbent system and the shape of the isotherm curve depicted earlier in Section 3.3.

7.5.1 Batch Adsorption Isotherms for sorption of Lead

Figures 7.10 (a)-(d), 7.11 (a)-(d) and 7.12 (a)-(d), show the plots of the linearized equations for Langmuir, Freundlich and Temkin isotherms respectively for the adsorption of divalent cations of lead, Pb(II) at 30, 50 and 70 °C onto KCAC, KFAC, MFSAC and AOPA.

Based on the hypothesis proposed by Langmuir, the sorption energy is invariable and self-governing and does not depend on surface loading. It depicts that, adsorption takes place on restricted sites with no interaction between sorbate species. Maximum adsorption occurs when the surface is covered by a monolayer of adsorbate (Langmuir, 1918). The Langmuir approach is expressed by Equation 3.1 whereas its linearized form is given earlier by Equation 3.2. When C_e/q_e is plotted against C_e, for the adsorption of Pb(II) onto the prepared sorbent, a straight line with a slope of $1/q_{max}$ and intercept of $1/ q_{max}K_L$ is obtained.

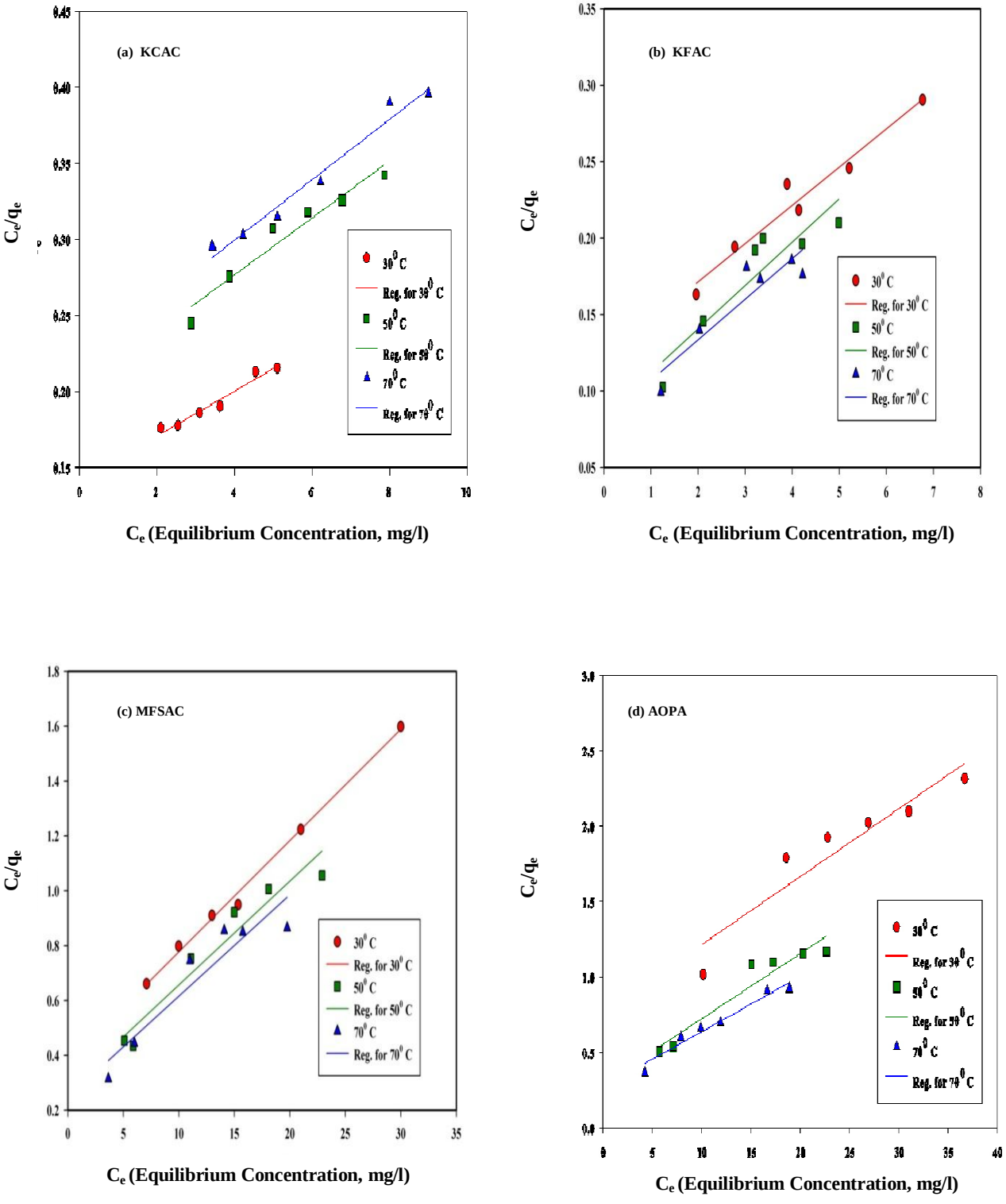

Figure 7.10 Linear Regression Analysis of Langmuir Isotherm of Lead, Pb (II) onto (a) KCAC (b) KFAC (C) MFSAC (d) AOPA at different Temperature

In this work KCAC, KFAC, MFSAC and AOPA show relatively better linearity for the Langmuir model at room temperature with correlation coefficients between 0.888 to 0.995. This confirms that each of Pb(II) cations has an equal adsorption activation energy. The results also demonstrate that the formation of monolayer surface loading of divalent cations of lead are at the outer surfaces of the prepared sorbent. This phenomenon has been further confirmed by observing the non linear isotherm curve between C_e and q_e afterwards in Section 7.5.4 for all the prepared activated adsorbent.

At higher temperatures, the experimental data deviate slightly from the Langmuir model, especially for KFAC and MFSAC (Appendix E). This might be due to the different shapes of isotherm curves depicted earlier in Section 3.3 or the involvement of successive adsorption-desorption step under predefined sorption condition or the disruption of surface functional groups at higher temperature.

The logarithmic form of Freundlich isotherm is given by Equation 3.5. The plots of log q_e versus log C_e gives a straight line with a slope of *1/n* and an intercept of log K_F . Freundlich constants, K_F and n are calculated where n gives an indication of how favorable the adsorption process is at different temperature and K_F (mg/g $(L/mg)^{1/n}$) depicts the adsorption or distribution coefficient of Pb(II) onto the adsorbent for a unit equilibrium concentration. Temkin isotherm presumes that the heat of sorption involved for all the adsorbate in the layer would decline linearly with the extent of surface exposure due to adsorbent-adsorbate interactions. Temkin model is expressed by Equation 3.6 .The linear plot of q_e versus ln C_e gives a straight line with B as the slope and ($In\ K_T$) as the intercept, where K_T (L/g) and B are Temkin constants. Figure 7.11 and 7.12 show the linear regression analysis for Freundlich and Temkin isotherm model at different temperature.

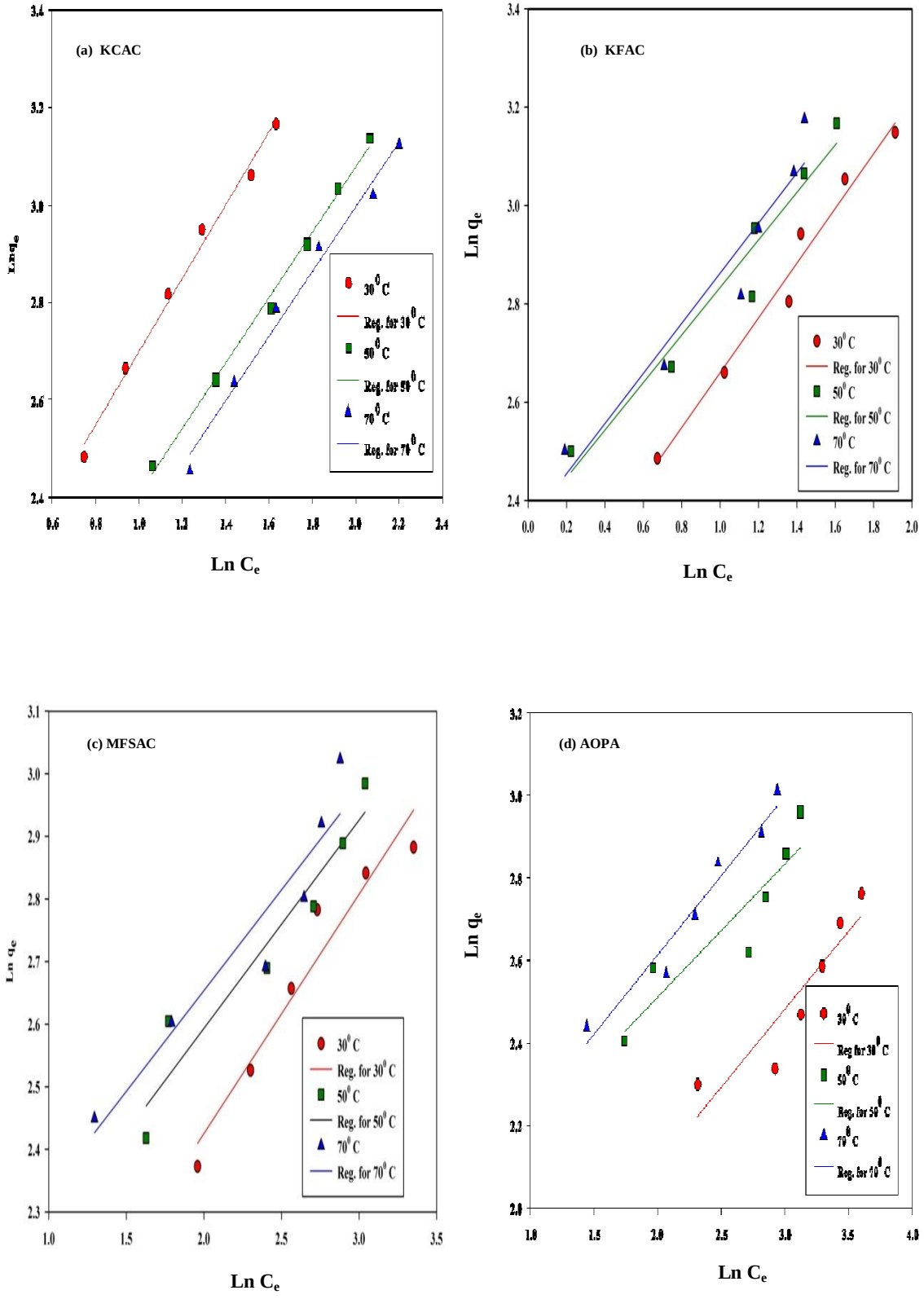

Figure 7.11 Linear Regression Analysis of Freundlich Isotherm of Lead, Pb (II) onto (a) KCAC (b) KFAC (C) MFSAC (d) AOPA at different Temperature

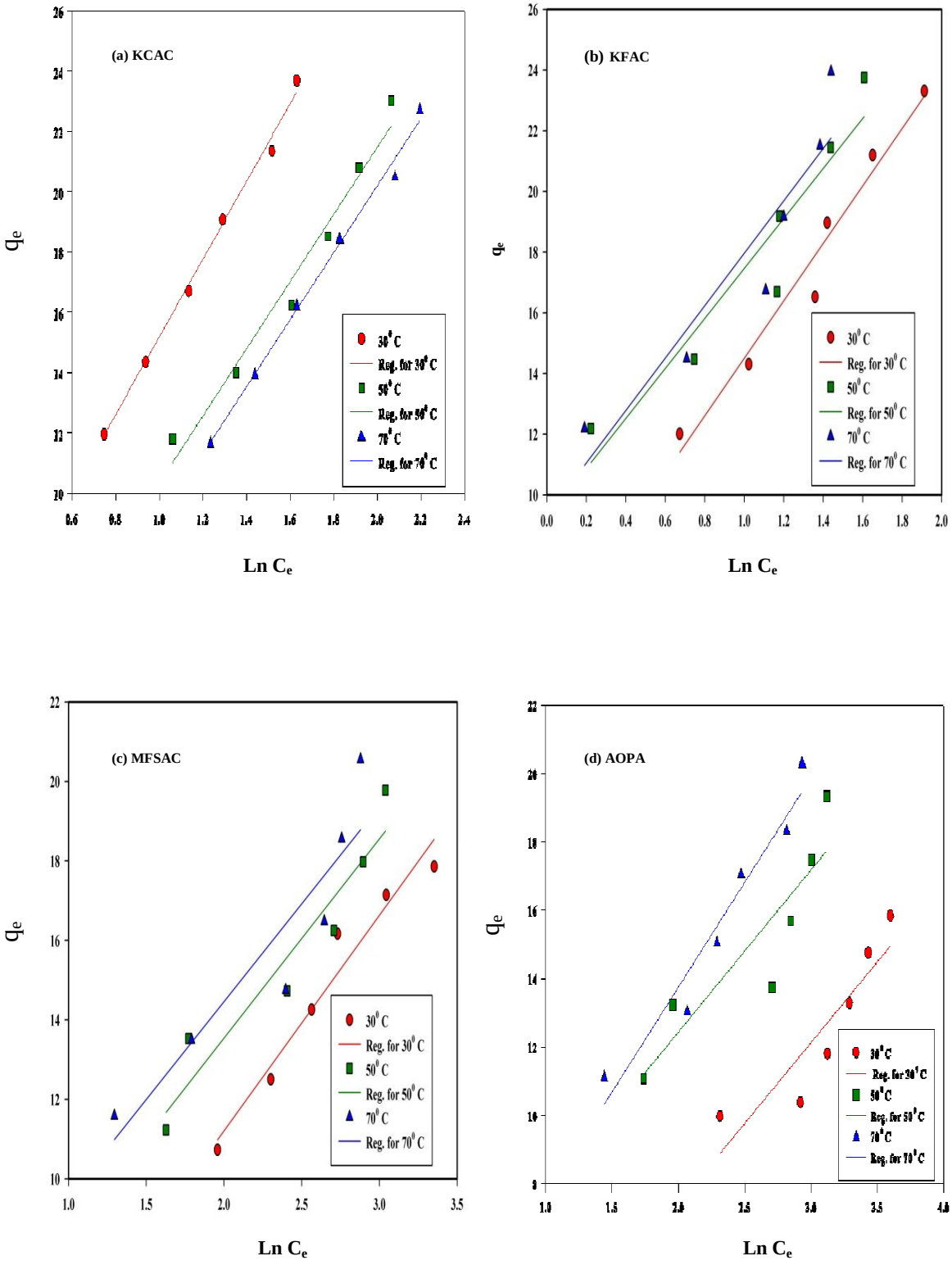

Figure 7.12 Linear Regression Analysis of Temkin Isotherm of Lead, Pb (II) onto (a) KCAC (b) KFAC (C) MFSAC (d) AOPA at different Temperature

It is observed that, the equilibrium data fits the Freundlich and Temkin model well compared to the Langmuir model at room temperature for KCAC and KFAC while sorption onto MFSAC and AOPA follow the Langmuir model rather than the Freundlich model. The results obtained for higher temperature of 50 °C and 70 °C is tabulated in Appendix E. If the experimental data follows Freundlich isotherm, it exhibits non cooperative, non specific sorption characteristics of the surface of the prepared sorbents (KCAC and KFAC).

Adsorption of divalent cations of Pb(II) on various adsorbents was found to follow the Langmuir and Freundlich isotherm models. The adsorption of Pb(II) ions onto bagasse fly ash (Gupta and Ali, 2004), coke (Lopez-Delgado *et al.*, 1996), illite (Farrah *et al.*,1980), olive mill by products (Gharaibeh *et al.*, 1998), ground nut husk (Okieimen *et al.*, 1991), river bed sediment (Jain and Ram, 1997), chemically treated rice husk and saw dust (Saravanane *et al.*, 2002) also followed Langmuir and Freundlich isotherm model.

Table 7.1 summarizes all the constants and R^2 values obtained for the adsorption of lead on KCAC, KFAC, MFSAC and AOPA at (30±1) °C temperature for the three isotherm models used. Model parameters obtained at higher temperature are tabulated in Appendix D.

Table 7.1 Langmuir, Freundlich and Temkin Isotherm models at (30±1) °C for the adsorption of Lead, Pb (II) onto KCAC, KFAC, MFSAC and AOPA

Activated sorbent	Linear Regression analysis of Isotherm									
	Langmuir Isotherm				Freundlich Isotherm			Temkin Isotherm		
	Maximum Monolayer adsorption capacity	Langmuir Constant	Separation Factor	Correlation Coefficient	Affinity Factor	Freundlich Exponent	Correlation Coefficient	Binding Constant	Temkin Constant	Correlation Coefficient
	q_{max}	K_L	R_L	R^2	K_F	1/n	R^2	K_T	B	R^2
	(mg/g)	(l/mg)	-	-	$(mg/g(l/mg)^{1/n})$	-	-	(l/g)	-	-
KCAC	71.42	0.985	0.092	0.957	7.015	0.750	0.991	1.19	12.95	0.995
KFAC	40.00	0.207	0.050	0.956	8.190	0.557	0.977	1.70	9.469	0.967
MFSAC	25.00	0.108	0.007	0.995	5.259	0.382	0.939	1.07	5.428	0.956
AOPA	22.22	0.059	0.145	0.888	3.855	0.377	0.845	0.663	4.686	0.820

The separation factor, R_L of the Langmuir isotherm defined by Weber and Chakkravorti (1974) is expressed in Chapter 3 (Equation 3.3). This parameter indicates the characteristics of the sorption process. However, the separation factor R_L obtained from Langmuir equation and *1/n* values obtained from the Freundlich model are all below the value one, confirming that lead is favorably adsorbed on all the activated sorbent prepared (Fytianos *et al.*, 2000).

Table 7.2 lists the comparison of maximum monolayer adsorption capacity, q_{max} (mg/g) of Pb(II) cations on various adsorbents. The adsorption capacity of Pb(II) cations onto the prepared sorbent in some cases is relatively high. However, accurate comparison of monolayer adsorption capacity sometimes becomes difficult as different workers used different concentration, temperature and pH range and it is well known that adsorption capacity increases significantly for increasing concentration and pH of the working solution.

Among all the adsorbents prepared, powdered adsorbent showed greater removal efficiency than the granular one. The highest removal percentage of 94.45% was obtained for KCAC due to its larger surface area followed by KFAC, MFSAC and AOPA. This observation is consistent with the results obtained earlier where the relatively high adsorption capacity of KCAC, KFAC was due to their relatively high surface areas, pore volumes and powdered form as compared to the granular form of MFSAC. Thus for Pb(II) cations, activated carbon adsorbent (KCAC, KFAC and MFSAC) is better than activated ash (AOPA) to obtain high removal efficiency.

Table 7.2 Comparison of maximum monolayer sorption capacity (mg/g) of divalent cations of lead, Pb(II) onto different adsorbents

Type of Adsorbent	Adsorbent	Maximum Monolayer Sorption capacity, q_m (mg/g)	References
Agricultural Residues	KCAC	71.42	This Work
	KFAC	40.00	This Work
	MFSAC	25.00	This Work
Ash residues	AOPA	22.22	This Work
Agricultural Residues	Barley Straw	15.2	Larsen and Schierup 1981
	Coir Fiber	18.9	Conard and Hansen 2007
	Coir	48.84	Quek *et al.,* 1998
	Hazel nut shell	1.78	Cimino *et al.,* 2000
	Sago Industry Waste	46.6	Quek *et al.,* 1998
Clay Materials	Bentonite	6	Cadena *et al.,* 1990
	China Clay	0.289	Yadava *et al.*, 1991
	Woolastonite	0.217	Yadava *et al.*, 1991
Peat	Rastunsuo peat	20.038	Tummavuori and Aho 1980
	Sphagnum moss peat	40	MeLelland and Rock 1988
Ash Residues	Activated Rice Husk	12.61	Feng *et al.,* 2004
	Fly Ash	18.0	Ricou *et al.,* 1999

7.5.2 Batch Adsorption Isotherms for sorption of Copper

The linear plots of Langmuir, Freundlich and Temkin isotherms for adsorption of Cu(II) cations at 30, 50 and 70 °C onto KCAC, KFAC, MFSAC and AOPA are illustrated by Figures 7.13 (a)-(d), 7.14 (a)-(d) and 7.15 (a)-(d) respectively. The sorption affinities of Cu (II) cations for different adsorbent are compared by using non linear plots of C_e versus q_e in the following section of 7.5.4. However, the experimental data has been deviated from the theoretical model depending on temperature.

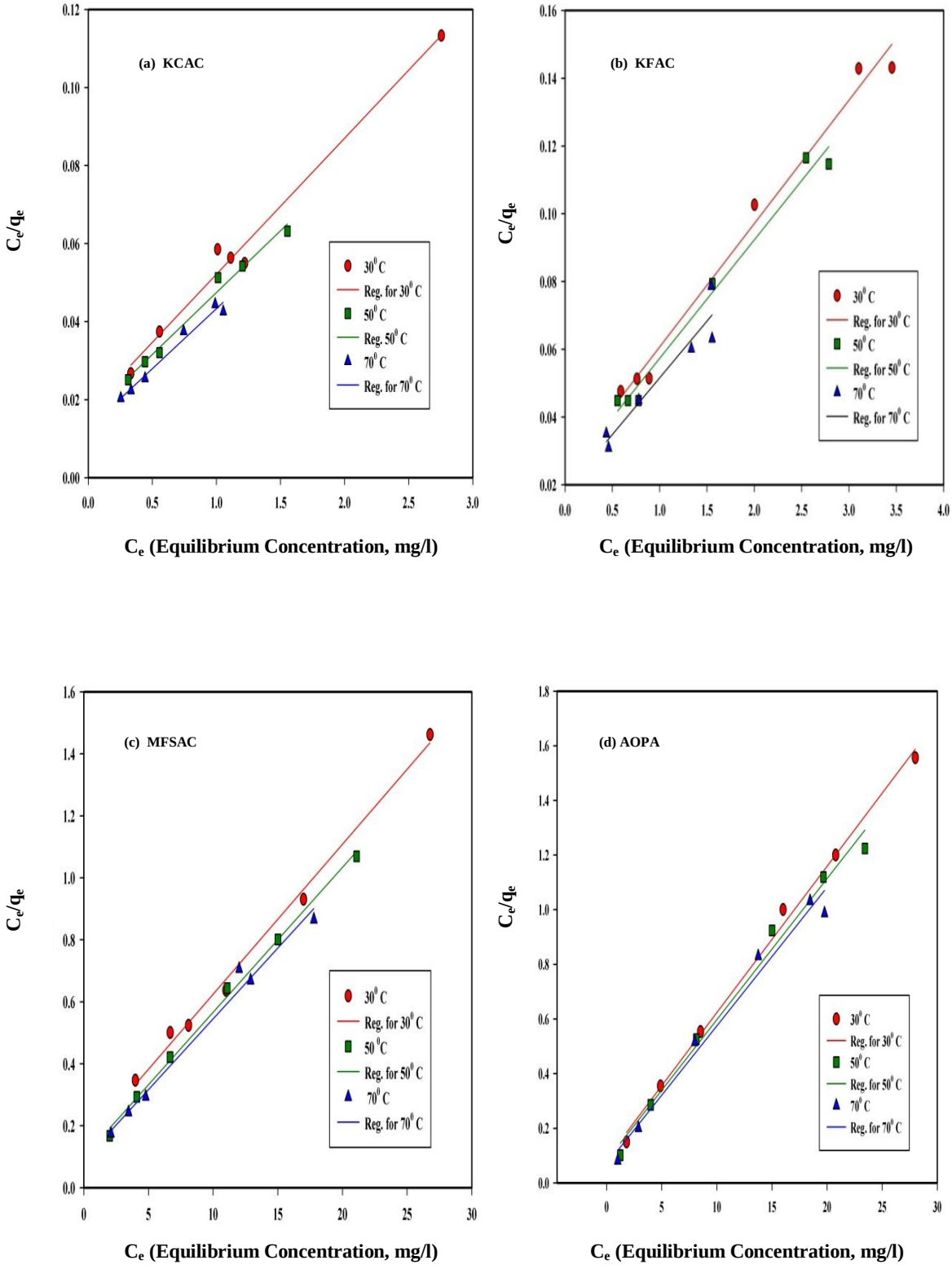

Figure 7.13 Linearized Langmuir Isotherm Model for sorption of copper, Cu (II) cations onto (a) KCAC (b) KFAC (c) MFSAC (d) AOPA at different temperatures

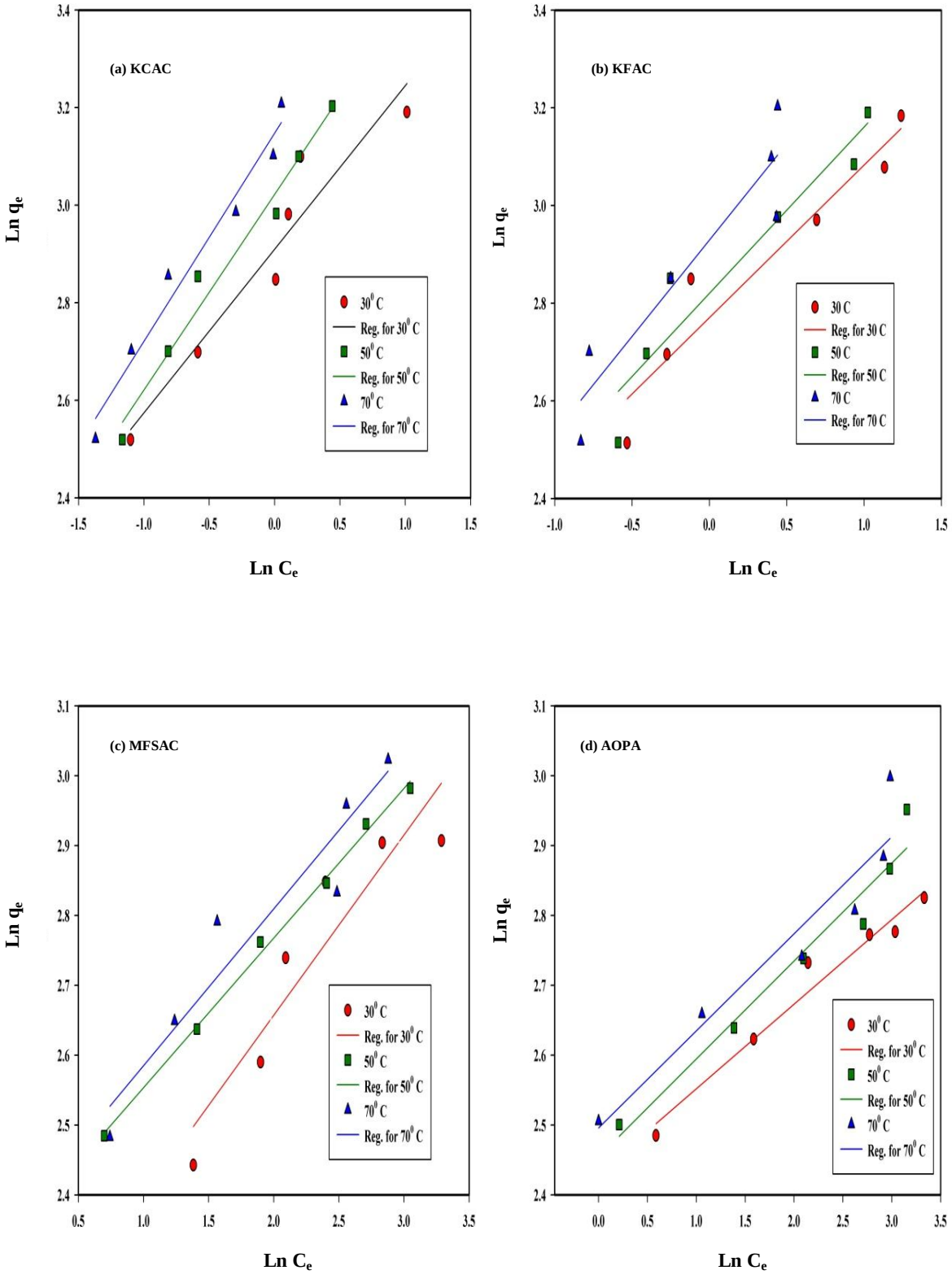

Figure 7.14 Linearized Freundlich Isotherm Model for sorption of copper, Cu(II) cations onto (a) KCAC (b) KFAC (c) MFSAC (d) AOPA at different temperatures

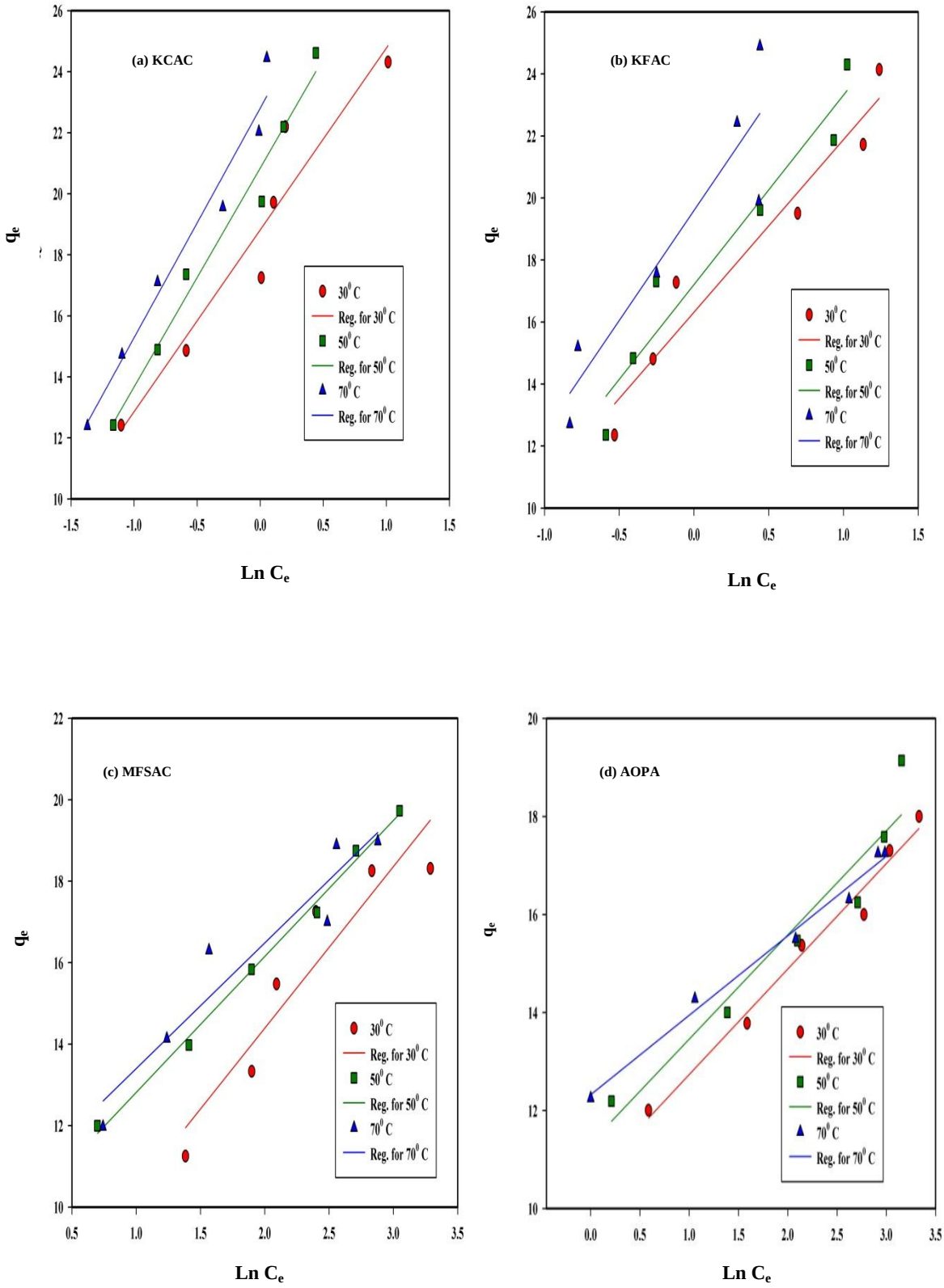

Figure 7.15 Linearized Temkin Isotherm Model for sorption of copper Cu(II) cations onto (a) KCAC (b) KFAC (c) MFSAC (d) AOPA at different

In contrast to Pb (II) cations, the equilibrium data for Cu (II) follows the Langmuir model with high correlation coefficients of 0.985-0.996 at room temperature for all the activated adsorbent under investigation. This phenomenon is consistent for higher temperature as well. However, the values obtained for constants and R^2 vary, depending on the overall nature of the adsorption systems for all the concentration range. The thermodynamic behavior of the adsorption processes will be further discussed in section 7.6.

Table 7.3 summarizes all the constants and R^2 values obtained from the three isotherm models for the adsorption of copper on KCAC, KFAC, MFSAC and AOPA at room temperature. Appendix E summarizes the results for higher temperatures of 50 and 70 °C. Referring to Table 7.3, it is observed that, the R^2 values obtained here are better for Langmuir and Temkin model compared to the Freundlich model for Cu(II) sorption onto KCAC, KFAC, MFSAC and AOPA. A similar trend is also observed at higher temperatures. Based on the fundamentals of the Langmuir theory, it can be concluded that the binding of Cu (II) cations are mainly chemisorptive in nature that means the binding of each Cu (II) cation took place by chemical forces (Sen Gupta *et al.*, 2005). The trend obtained from these plots is similar to that found for the adsorption of Pb (II) cations earlier where all the R_L values are between 0 and 1. This indicates that, the adsorption of Cu (II) cations onto the activated adsorbent tested is also favorable under the conditions being studied. However, the Freundlich exponent 1/n is below the value one representing a favorable process. This suggests that some heterogeneity of the surfaces or pores of the activated adsorbents play a vital role in the adsorption of Cu (II) cations.

Table 7.3 Langmuir, Freundlich and Temkin Isotherm models at (30±1) °C for the adsorption of Copper, Cu (II) onto KCAC, KFAC, MFSAC and AOPA

Activated sorbent	Linear Regression analysis of Isotherm									
	Langmuir Isotherm				Freundlich Isotherm			Temkin Isotherm		
	Maximum Monolayer adsorption capacity	Langmuir Constant	Separation Factor	Correlation Coefficient	Affinity Factor	Freundlich Exponent	Correlation Coefficient	Binding Constant	Temkin Constant	Correlation Coefficient
	q_{max}	K_L	R_L	R^2	K_F	1/n	R^2	K_T	B	R^2
	(mg/g)	(l/mg)	-	-	$(mg/g(l/mg)^{1/n})$	-	-	(l/g)	-	-
KCAC	29.412	2.00	0.005	0.985	18.356	0.335	0.922	23.57	5.952	0.920
KFAC	27.780	1.499	0.007	0.986	15.950	0.312	0.919	18.75	5.564	0.938
MFSAC	20.830	0.343	0.028	0.994	8.570	0.258	0.866	5.108	3.965	0.883
AOPA	18.867	0.602	0.016	0.996	11.370	0.121	0.966	137.13	2.150	0.979

Table 7.4 Comparison of maximum monolayer sorption capacity (mg/g) of divalent cations of copper onto different adsorbents

Type of Adsorbent	Adsorbent	Maximum Monolayer Sorption capacity, q_m (mg/g)	References
Agricultural Residues	KCAC	29.41	This Work
	KFAC	27.78	This Work
	MFSAC	20.83	This Work
Ash residues	AOPA	18.87	This Work
Agricultural Residues	Cellulose pulp waste	4.98	Ulmanu *et al*., 2003.
	Sugar beet pulp	20.96	Reddad *et al*., 2002
	Aquatic Plant	15.95	Keskinkan *et al.*2003
	Rice husk	29.00	Wong *et al.*, 2003
	Cotton Ball	11.40	Ozsoy and Kumbur, 2006
Activated Carbon	Commercial Activated Carbon	2.91-5.56	Adil, 2006
Clay Materials	Kaolinite	11.04	Yavuz *et al.*, 2003
Ash Residues	Fly Ash	1.39	Panday *et al.*, 1985
	Fly Ash +wollastonite	1.38	Apak *et al.*, 1998
	Coal Fly Ash	20.92	Papandreou *et al.*, 2007

The results agreed well with the studies carried out by previous researchers which reported that the Langmuir model gave a better fit to explain the experimental data for the adsorption of Cu(II) cations using different adsorbents such as banana pith carbon (Low *et al.*, 1995), activated coir (Baes *et al.*, 1996), peanut hull carbon (Periasamy and Namasivayam 1996) and sugar beet pulp (Pehlivan *et al.*, 2006). Some adsorbents such as banana and orange peel (Annandurai *et al.*, 2003), pecan shell carbon (Bansode *et al.*, 2003) and tea waste (Cay *et al.*, 2004) followed Freundlich model where as rubber wood saw dust (Kalavathi *et al.*, 2005) followed Temkin isotherm. Table 7.4 lists the comparison of the maximum monolayer adsorption capacity, q_m (mg/g) of Cu(II) cations for various types of adsorbents.

The activated adsorbent prepared in this work showed relatively large adsorption capacity for Cu(II) cations compared to the previous works found in the literature. Among the activated adsorbents prepared, KCAC shows the highest adsorption capacity for copper at 30 ^{o}C followed by KFAC, MFSAC and AOPA. The phenomenon of high uptake capacity of KCAC is also consistent for the sorption of Pb(II) cations onto this activated carbon. This might be attributed due to its high surface area and pore volume compared to the other two adsorbents.

On the other hand, opposing trend is observed for AOPA and MFSAC. Despite its high surface area and physical form, AOPA shows less removal efficiency compared to MFSAC. This is due to large pore size diameter of AOPA that could not retain smaller cations of Cu (II) resulting in smaller removal efficiency (Ahmenda *et al.*, 2000). Similar trend of adsorption capacity by the prepared adsorbent is also followed for the higher temperature ranges.

7.5.3 Batch Adsorption Isotherms for sorption of Manganese

Figures 7.16(a)-(d), 7.17(a)-(d) and 7.18(a)-(d) show the plots of the linearized equations for Langmuir, Freundlich and Temkin isotherms for adsorption of manganese, Mn(II) cations at 30, 50 and 70°C onto KCAC, KFAC, MFSAC and AOPA respectively.

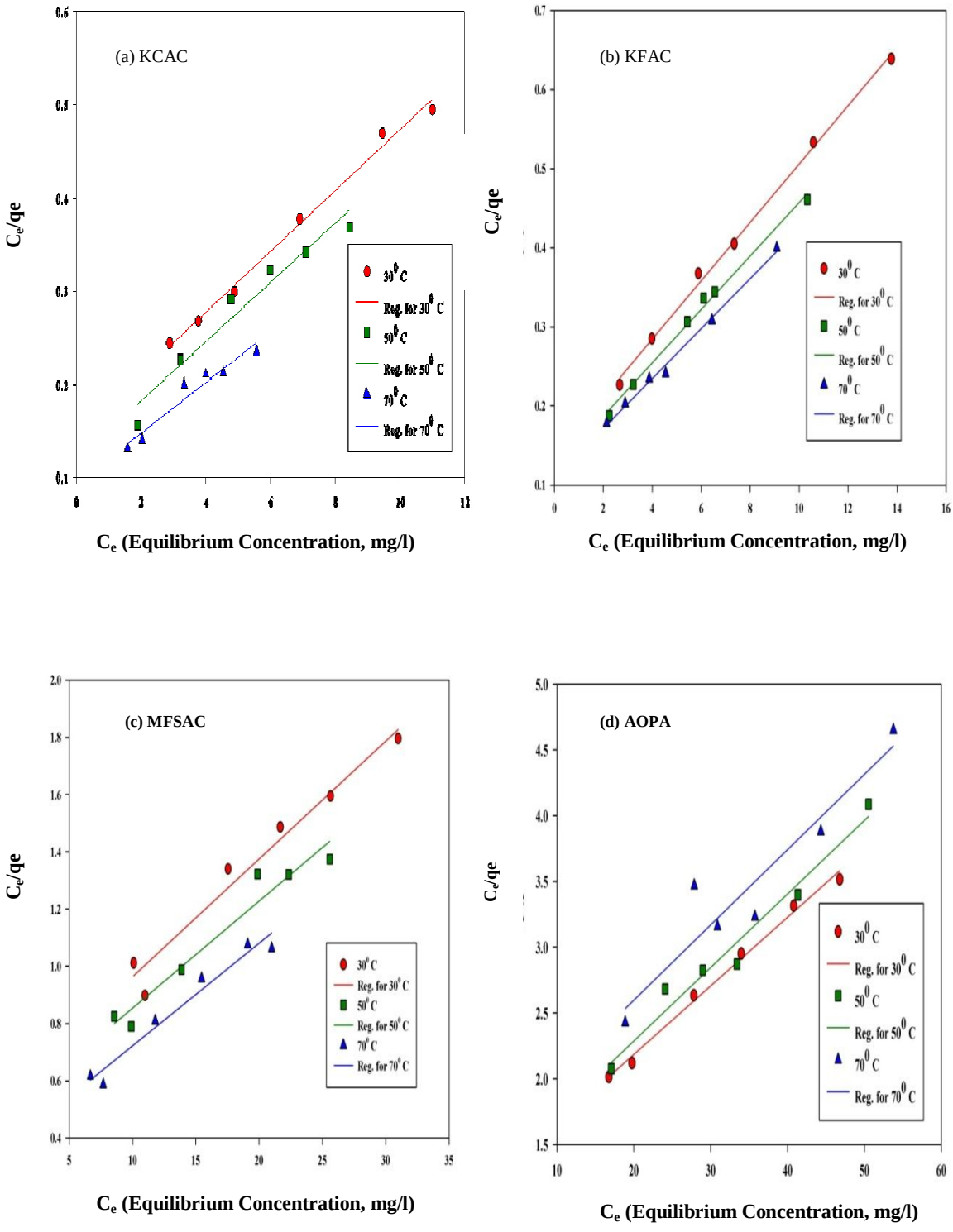

Figure 7.16 Linearized Langmuir Isotherm Model for sorption of manganese, Mn(II) cations onto (a) KCAC (b) KFAC (c) MFSAC (d) AOPA at different temperatures

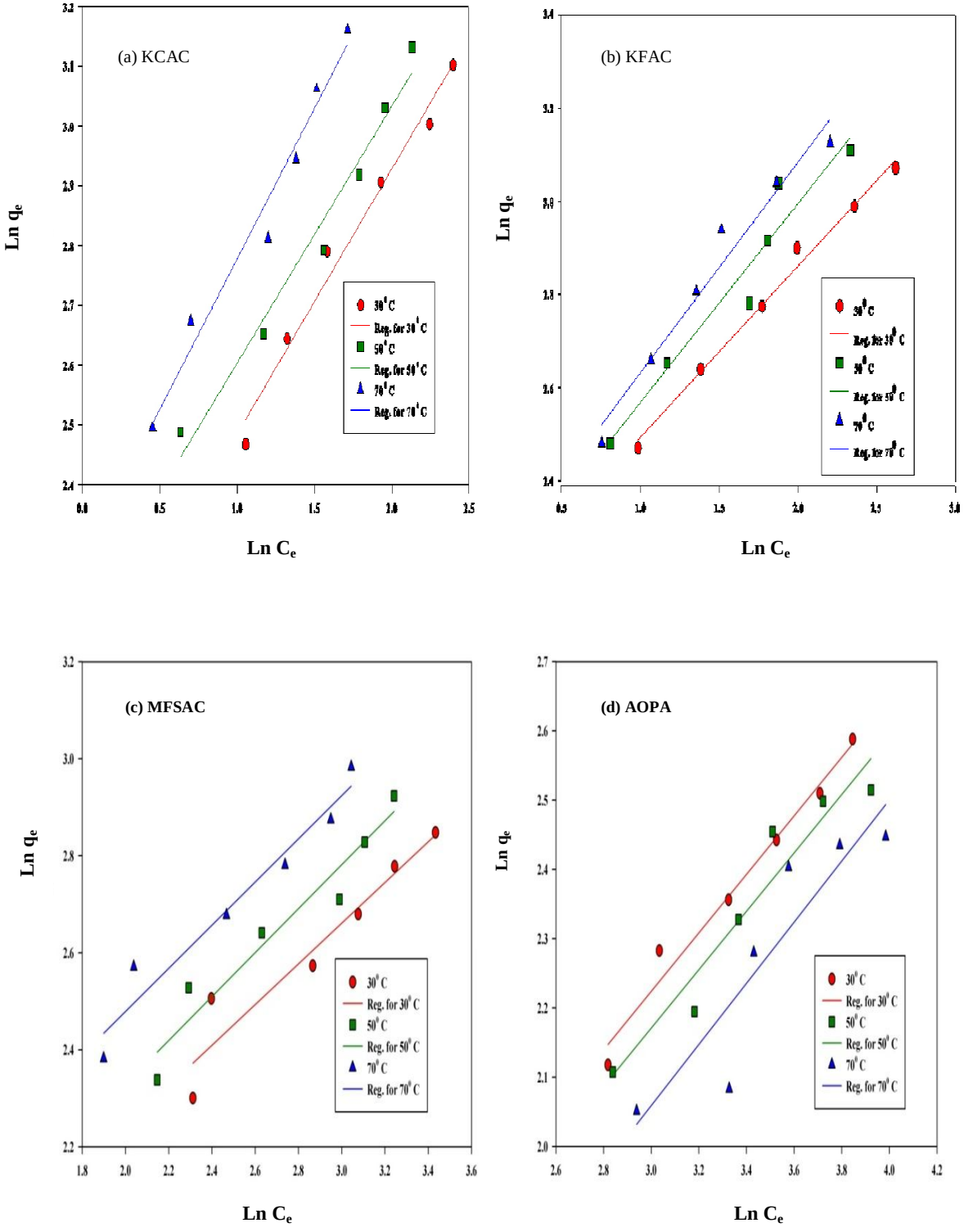

Figure 7.17 Linearized Freundlich Isotherm Model for sorption of manganese, Mn (II) cations onto (a) KCAC (b) KFAC (c) MFSAC (d) AOPA at different temperatures

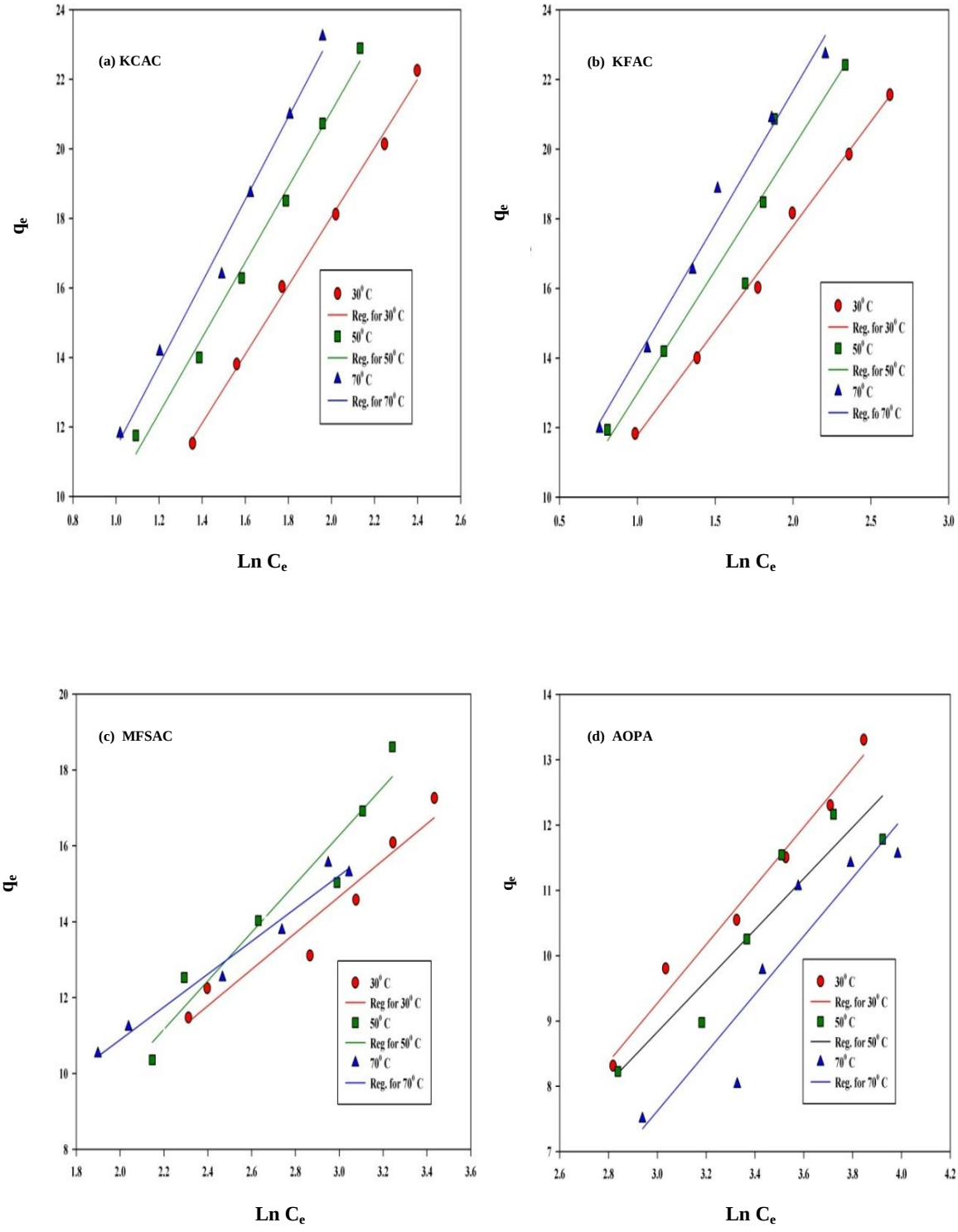

Figure 7.18 Linearized Temkin Isotherm Model for sorption of manganese, Mn (II) cations onto (a) KCAC (b) KFAC (c) MFSAC (d) AOPA at different temperature

Table 7.5 summarizes all the constants and R^2 values obtained from the three isotherm models for adsorption of manganese, Mn(II) onto KCAC, KFAC, MFSAC and AOPA at room temperature. Appendix E summarizes the results for higher temperatures of 50 and 70 °C. Referring to Table 7.5, very good linearity are observed for Langmuir, Freundlich and Temkin model onto KCAC, KFAC, MFSAC and AOPA at room temperature. However, at higher temperature of 70 ^{0}C the adsorbate-adsorbent system deviated for sorption of Mn(II) cations onto AOPA. This might be due to its least tendency to form stable surface complexes compared to Pb(II) and Cu(II) cations.

Based on the maximum monolayer adsorption capacity, it can be concluded that MFSAC although having a granular texture with less surface area shows a high sorption capacity than AOPA and is consistent for Pb(II) and Cu(II) cations as well. This might be attributed to the presence of a higher number of surface functional groups onto the surface of MFSAC and large pore diameter of AOPA which could not retain the small cations of manganese (Patrick, 1987).

The overall trend obtained for the Langmuir separation factor, R_L and Freundlich exponent 1/n being below the value of one (like Pb (II) and Cu (II) cations) for all the temperature ranges studied represent favorable adsorption processes. Similar trend was observed for Mn(II) sorption onto raw and acid treated corncob biomass. It showed good linearity for the Langmuir and Freundlich model where the exponent 1/n below the value of 1 represented normal Langmuir isotherm (Abideen *et al.*, 2011). Table 7.5 and 7.6 lists the Langmuir maximum monolayer adsorption capacity, q_m (mg/g) of Mn (II) ions obtained in this study with various types of adsorbents.

Table 7.5 Langmuir, Freundlich and Temkin Isotherm models at (30±1) °C for the adsorption of Manganese, Mn (II) onto KCAC, KFAC, MFSAC and AOPA

Activated sorbent	Linear Regression Analysis of Isotherm									
	Langmuir Isotherm				Freundlich Isotherm			Temkin Isotherm		
	Maximum Monolayer adsorption capacity	Langmuir Constant	Separation Factor	Correlation Coefficient	Affinity Factor	Freundlich Exponent	Correlation Coefficient	Binding Constant	Temkin Constant	Correlation Coefficient
	q_{max} (mg/g)	K_L (l/mg)	R_L -	R^2 -	K_F (mg/g(l/mg)$^{1/n}$)	1/n -	R^2 -	K_T (l/g)	B -	R^2 -
KCAC	31.25	0.2172	0.043	0.992	7.6983	0.445	0.980	1.788	7.328	0.989
KFAC	27.78	0.263	0.036	0.997	8.365	0.368	0.990	2.627	5.997	0.994
MFSAC	24.39	0.075	0.118	0.965	4.067	0.419	0.918	1.056	4.801	0.937
AOPA	19.23	0.046	0.180	0.993	2.604	0.422	0.978	0.392	4.492	0.981

Table 7.6 Comparison of maximum monolayer sorption capacity (mg/g) of divalent cations of Manganese onto different adsorbents

Type of Adsorbent	Adsorbent	Maximum Monolayer Sorption capacity, q_m (mg/g)	References
Agricultural Residues	KCAC	31.25	This Work
	KFAC	27.77	This Work
	MFSAC	24.39	This Work
Ash residues	AOPA	19.23	This Work
Agricultural Residues	Raw Corn Cob	6.54	Abideen *et al*., 2011.
	Treated Corn Cob	7.87	Abideen *et al*., 2002
Activated Carbon	Activated Carbon A(Furfural/Tar from Steam pyrolysis of apricot stone=70:30)	10.20	Savova *et al*., 2003
			Savova *et al*., 2003
	Activated Carbon B(Furfural/Tar from Steam pyrolysis of apricot	9.78	Savova *et al*., 2003
	Activated Carbon C(Furfural/Tar from Steam pyrolysis of apricot	7.96	Savova *et al*., 2003
	Carbon D (Tar)	3.89	Savova *et al*., 2003
Clay Materials	Bentonite	2.81	Datchaneekul 2006
Miscellaneous	Cow Bone charcoal	29.56	Moreno *et al*., 2010
	Electric Arc Furnace Slag	2.30	Beh *et al*., 2010

7.5.4 Selective Adsorption Capacities of the cations

Figures 7.19, 7.20 and 7.21 show the actual relationship between C_e (mg/l) and q_e (mg/g) at 30 °C for all the adsorbate under investigation. The experimental data has been fitted with the theoretical values obtained from the Langmuir model onto different activated adsorbents for all the cations under investigation.

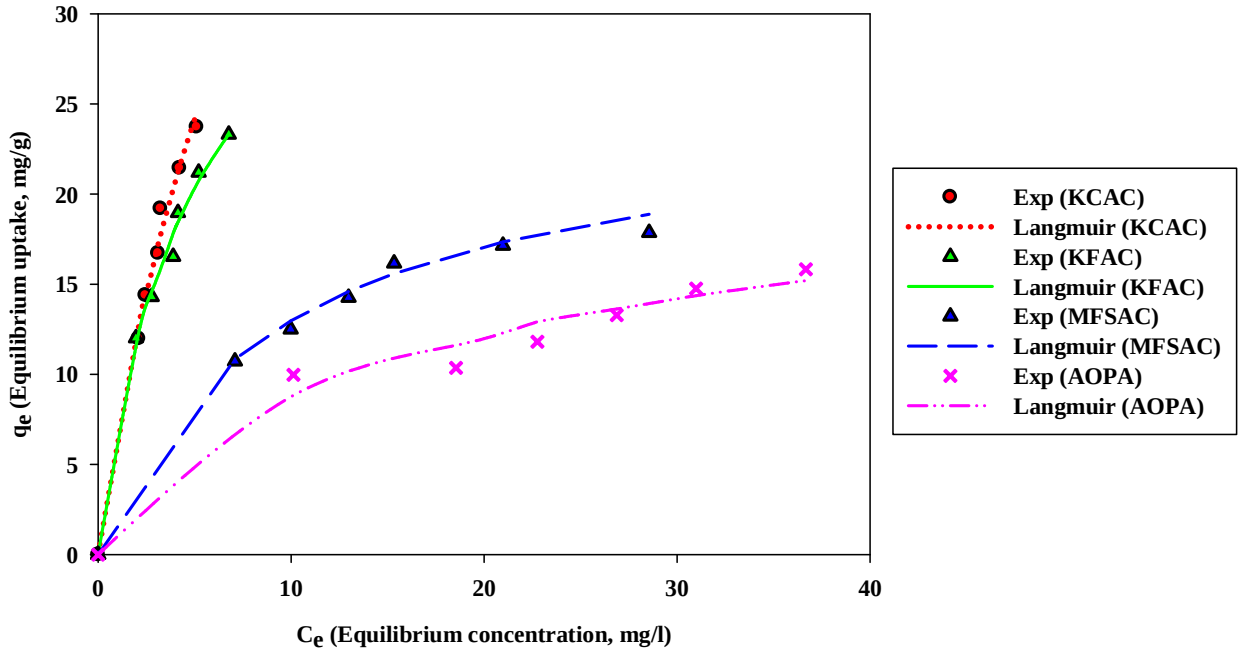

Figure 7.19 Relation between experimental C_e and q_e with model fitting by Langmuir Isotherm for Lead, Pb(II) cations

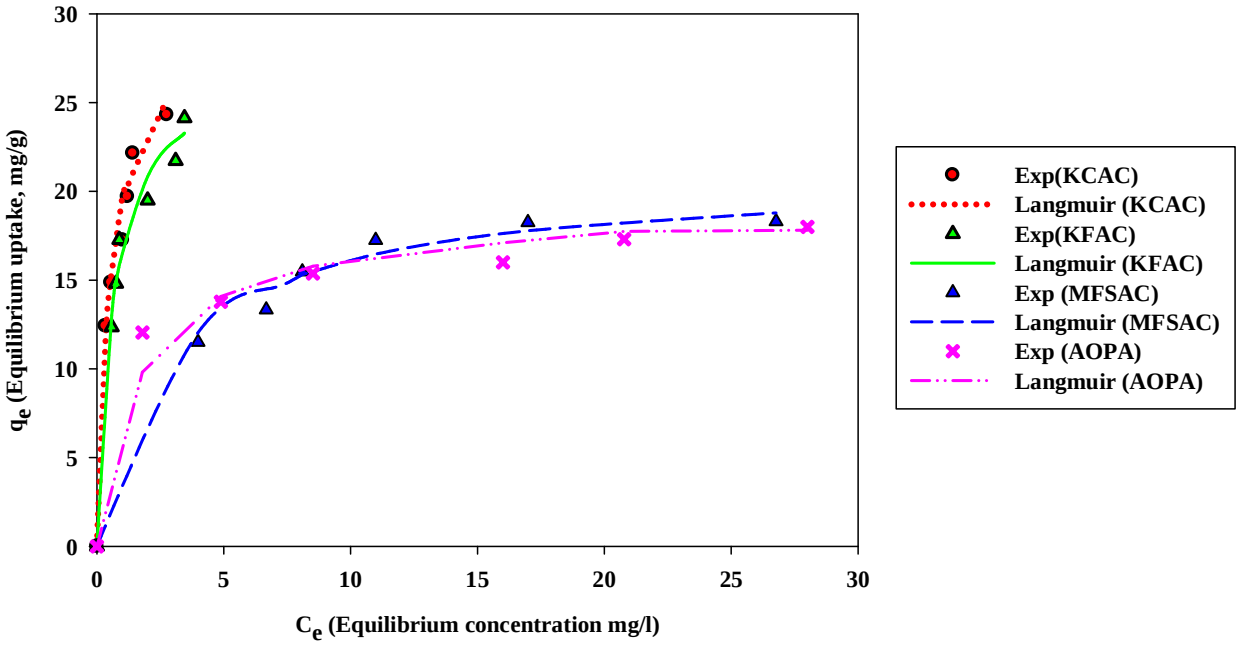

Figure 7.20 Relation between experimental C_e and q_e with model fitting by Langmuir Isotherm for Copper, Cu(II) cations

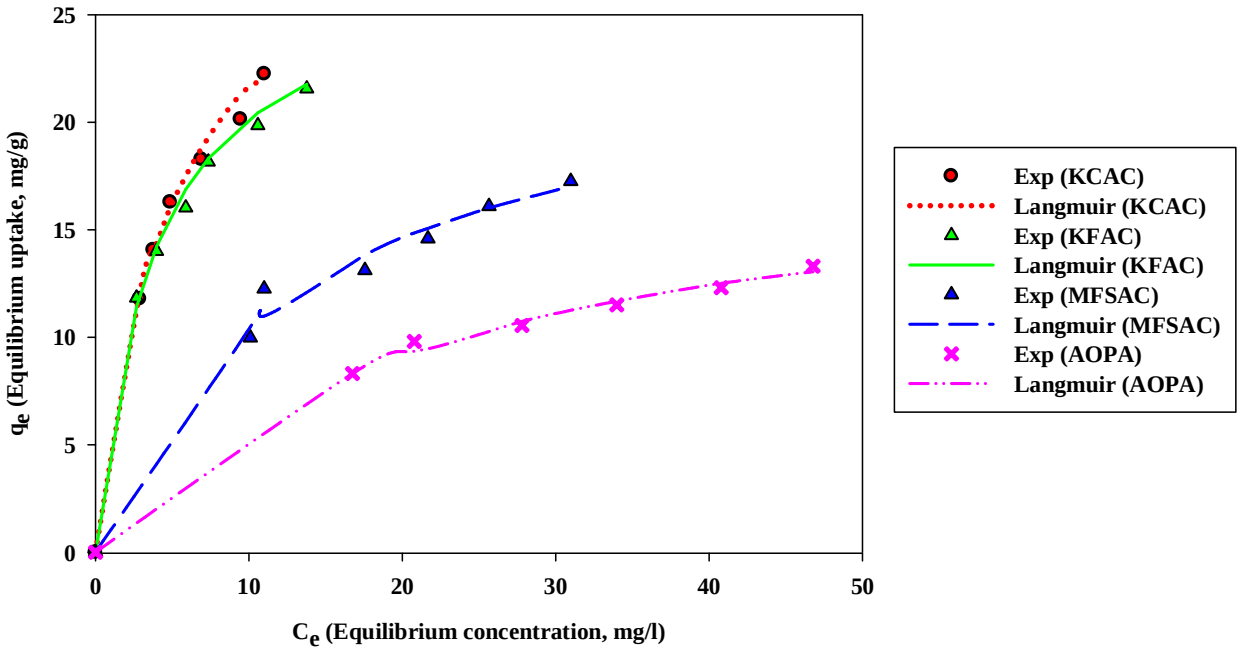

Figure 7.21 Relation between experimental C_e and q_e with model fitting by Langmuir Isotherm for Manganese, Mn(II) cations

From Figures 7.19-7.21, it can be observed that the cations under consideration are showing typical non linear trend of sorption which is characterized as L-type or Type I isotherm based on Brunner's classification. This indicates a favorable sorption process under fixed pH, contact time, temperature, adsorbent dosage and selected concentration range (50-100 mg/l). However, the slopes obtained for KCAC and KFAC are steeper than MFSAC and AOPA showing greater affinities towards the preselected cations. The curve obtained for KCAC and KFAC can be categorized as H-type isotherm compared to other two sorbent (MFSAC and AOPA) prepared here, which are depicted as extreme version of L-type isotherm by some literature (Datchaneekul, 2005). Thus, the K_F values obtained from Freundlich isotherm for these two activated adsorbents (KCAC and KFAC) are higher than MFSAC and AOPA for all the cations.

Overall, Langmuir monolayer sorption capacity observed here is higher for Pb(II) cations compared to the other two sorbates. This phenomenon can be explained in terms of the HSAB (Pearson, 1968) principle. Based on this, the basal structural unit of carbon can act as soft Lewis base which prefers to take soft Lewis acid such as Pb(II) cations. Whereas Cu(II) is regarded as a harder cation which prefers surface oxide groups (Adil, 2006). The sorption of Pb(II) can take place simultaneously on both harder and softer sites of the carbon leading to larger values of q_{max} (mg/g). Thus in some literature, Pb(II) is categorized as marginally soft ions (IUPAC 2002) or borderline cations (Adil, 2006; Ahrland *et al.*, 1958). However, the Freundlich constant, K_F determined here is highest for sorption studies of Cu(II) onto the prepared sorbent rather than the other two cations which is consistent with it's position based on the Irving William series.

7.6 Thermodynamic Characterization of Batch Adsorption Studies

The thermodynamic behaviors for the adsorption of lead, copper and manganese on the prepared activated adsorbent in this study were analyzed using the thermodynamic equations as expressed by Equations 3.22-3.23. Based on Equations 3.20 and 3.21 the values of $\Delta H°$ and $\Delta S°$ were calculated respectively from the slope and intercept of the plot of In K_L versus 1/T, where K_L (L/mg) was Langmuir isotherm constant obtained at three different solution temperatures of 30, 50 and 70 °C. $\Delta G°$ was further determined from Equation 3.21 as depicted earlier.

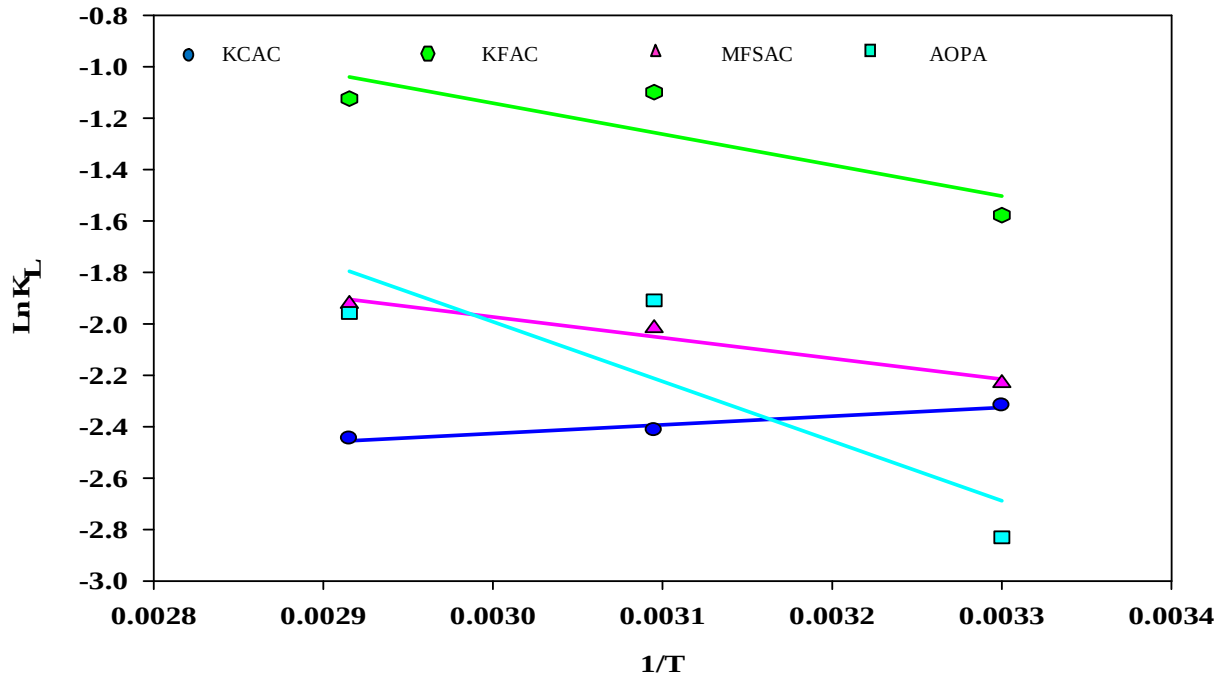

Figure 7.22 Plots of ln K_L versus 1/T for sorption studies of Lead, Pb(II) cations

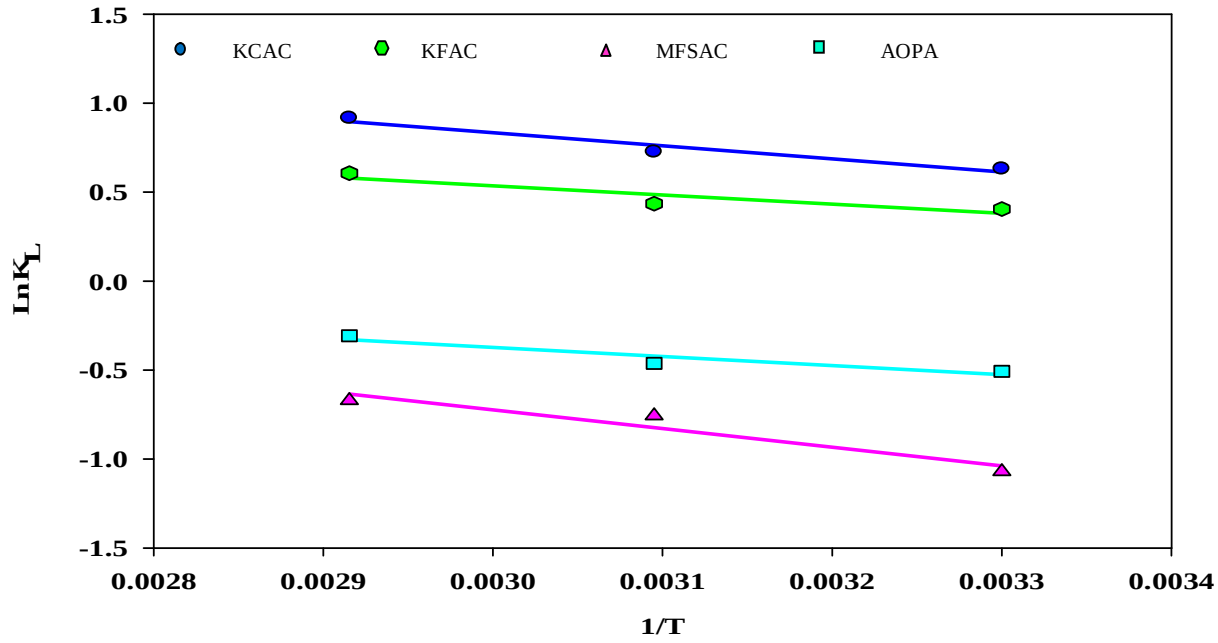

Figure 7.23 Plots of ln K_L versus 1/T for sorption studies of Copper, Cu(II) cations

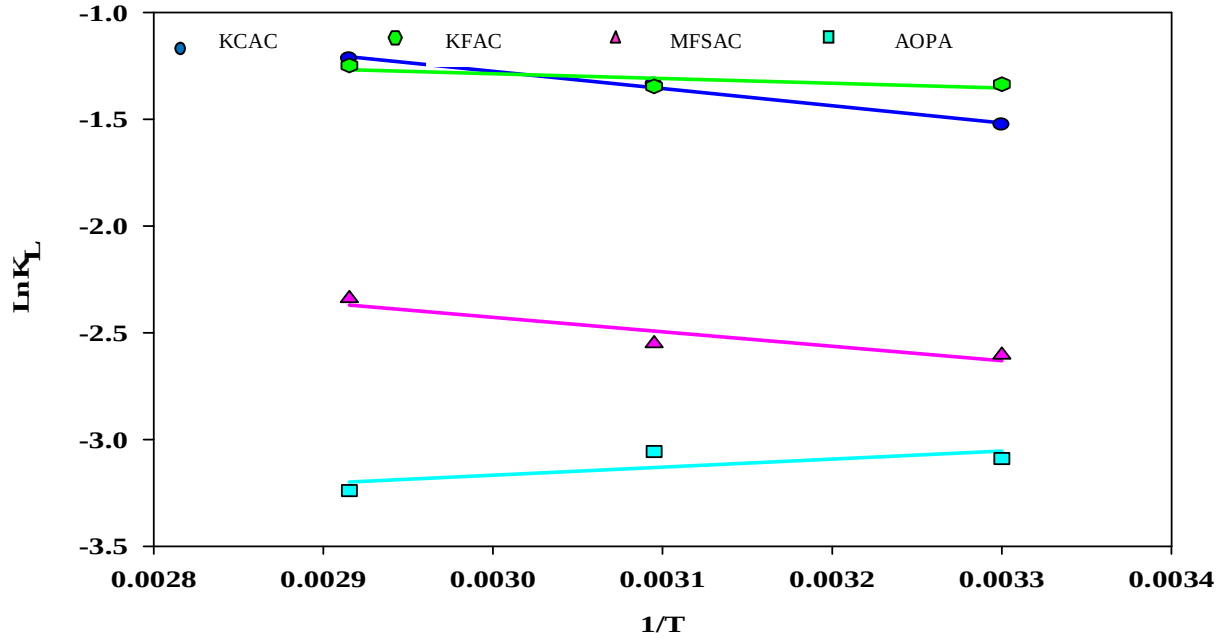

Figure 7.24 Plots of ln K_L versus 1/T for sorption studies of Manganese, Mn(II) cations

As can be observed from these three plots, the slopes of the linear lines are either positive or negative depending on the specific adsorbate-adsorbent system. This indicates that some of the adsorption process is endothermic in nature while some systems are exothermic. The calculated values of ΔH°, ΔS°, ΔG° and ΔE° for sorption of Pb(II) cations onto KCAC, KFAC, MFSAC and AOPA are listed in Table 7.7.

Table 7.7 Thermodynamics parameters for adsorption of Pb (II) from synthetic water onto activated adsorbents at different temperatures

Activated Adsorbent	**Enthalpy of Reaction ΔH° (kJ/mol)**	**Entropy of Reaction ΔS° (j/mol-K)**	**Gibbs Free Energy ΔG° (kJ/mol)**			**Correlation Coefficient R^2**
			303 °K	**323 °K**	**343 °K**	**-**
KCAC	-2.802	-0.0285	-5.836	-6.479	-6.972	0.942
KFAC	+10.02	+0.2056	-3.973	-2.951	-3.205	0.742
MFSAC	+6.709	+3.7165	-5.618	-5.416	-5.481	0.964
AOPA	+19.297	+0.0413	-7.129	-5.125	-5.582	0.742

The results reveal that the ΔH° values obtained for the adsorption of lead onto KCAC is negative where as other adsorption processes for lead onto KFAC, MFSAC and AOPA show positive values of ΔH°. Negative value of ΔH° indicates the exothermic nature of the adsorption interactions where as positive value reflects the endothermic nature. Tables 7.8 and 7.9 present the values of ΔH°, ΔS° and ΔG° for adsorption of Cu(II) and Mn(II) cations onto KCAC, KFAC, MFSAC and AOPA.

Table 7.8 Thermodynamics parameters for adsorption of Cu (II) from synthetic water onto activated adsorbents at different temperatures

Activated Adsorbent	Enthalpy of Reaction ΔH° (kJ/mol)	Entropy of Reaction ΔS° (j/mol-K)	Gibbs Free Energy ΔG° (kJ/mol)			Correlation Coefficient R^2 -
			303 °K	323 °K	343 °K	
KCAC	+6.108	+0.0253	+1.591	+1.949	+2.613	0.948
KFAC	+4.281	+0.0173	+1.019	+1.168	+1.728	0.832
MFSAC	+8.738	+0.0202	-2.695	-2.031	-1.911	0.923
AOPA	+4.250	+0.0097	-1.276	-1.241	-0.877	0.883

Table 7.9 Thermodynamics parameters for adsorption of Mn (II) from synthetic water onto activated adsorbents at different temperatures

Activated Adsorbent	Enthalpy of Reaction ΔH° (kJ/mol)	Entropy of Reaction ΔS° (j/mol-K)	Gibbs Free Energy ΔG° (kJ/mol)			Correlation Coefficient R^2 -
			303 °K	323 °K	343 °K	
KCAC	+6.704	+0.0095	-3.844	-3.585	-3.471	0.990
KFAC	+1.914	-0.0049	-3.373	-3.615	-3.559	0.652
MFSAC	+5.636	-0.0033	-6.558	-6.847	-6.670	0.870
AOPA	-3.135	-0.0357	-7.782	-8.207	-9.237	0.553

It is found that (Table 7.8 and 7.9), the adsorptions of copper ions on all the adsorbents are endothermic while adsorption of manganese on AOPA is exothermic in nature. Overall, these findings are consistent with the results obtained in the earlier section 7.3 describing the effects of solution temperature on the removal percentages of the above mentioned adsorbates from synthetic waste water.

In the case of exothermic sorption processes, the adsorption uptake decreases with increase in solution temperature. This might be due to the successive desorption of adsorbate species in the equilibrium mixture. This is due to the deterioration of weak

Van der Waals forces between the active sites on the activated sorbent and the adsorbate species. It has also been reported earlier that increase in temperature might decrease the uptake as the physical bonding between the adsorbate and the active sites of the adsorbent is destabilized (Chandra *et al.,* 2007).

Opposite phenomena is observed for the endothermic processes. In case of endothermic reactions, increase in temperature would increase the rate of diffusion of the adsorbate species across the external boundary layer as well as inside the pores of the adsorbent particle. This might be due to the decrease in the viscosity of the solution (Wang and Zhu, 2007). Furthermore, an increase in removal percentage of the sorbents at higher temperature might be due to the amplification of pore size distribution. It was depicted also that the active surface sites increased proportionally with the increase in temperature (Bulut and TEZ ZEKI, 2007).

However, it is essential not to go beyond the optimum temperature limit because the increase in temperature causes an agglomeration process and beyond the critical temperature, desorption takes place spontaneously leading to a reduced rate of sorption with contact time. It was suggested by previous researchers that the increase in removal percentage with the increase in temperature is due to the increase in kinetic forces i.e, the mobility of the sorbate species inside the sorbent matrix (Senthilkumaar *et al.,* 2006).

These results demonstrate that the thermodynamic behaviors of an adsorption system is dependent on the type of sorbent and sorbate being investigated. It is also influenced by the particle size or physical form of the adsorbent, its physical properties

and the surface functional groups of the sorbent as well as the characteristics and nature of the sorbate.

From the literature, the adsorption of Pb(II) cations onto Kaolinite, montmorillonite, poly hydroxyl zirconium tailored kaolinite, montmorillonite clays and bagasse fly ash were reported to exhibit exothermic sorption (Sen Gupta *et al.,* 2005; Gupta and Ali, 2004). On the other hand, the adsorption of Pb(II) onto lignin (Srivastava *et al.,* 1994) was found to be endothermic in nature. Sorption of Cu(II) cations onto rubber wood activated carbon was found to be exothermic where as Mn(II) cations exhibited endothermic nature of sorption onto raw and acid treated corn cob and exothermic reaction of sorption onto fly ash (Abideen *et al.,* 2011 and Sharma *et al.,* 2007).

The highest limit in the change of enthalpy for physisorption is usually 80 kJ/mol where as the chemisorption is between 80- 420 kJ/mol (Gercel *et al.,* 2007). Based on the results depicted by Tables 7.7, 7.8 and 7.9; all the ΔH° values obtained in this study are less than 80kJ/mol. This implies that all the sorption processes observed here follow a physisorption mechanism. These findings have also been reported for the adsorption of Pb(II) onto wollastonite and lignin (Yadova *et al.,* 1991, Srivastava *et al.,* 1994), Cu(II) onto activated sawdust (Azmal *et al.,* 1998) and Mn(II) onto raw and acid treated corncob agro-residues (Abideen *et al.,* 2011).

Pb(II) cations adsorption onto KCAC shows negative ΔS° values. Rest of the sorbent-sorbate system based on lead and copper showed positive ΔS° values. The positive values of ΔS° reflect the affinity of the activated adsorbent for the selected sorbates under investigation. This demonstrates increased randomness at the solid-solution interface with some structural changes on the adsorbents' surface during the

sorption processes. The negative values of ΔS° correspond to a decrease in the degree of freedom of the adsorbed species (Bulut and TEZ ZEKI, 2007). Most sorption systems obtained from the literature demonstrated positive values of ΔS°, nevertheless, negative values of ΔS° are also probable and shown by some adsorption systems. In this study, most of the adsorption systems are found to exhibit positive values of ΔS° except for adsorption of manganese onto KFAC, MFSAC and AOPA. Negative values of ΔS° values were also observed for the sorption of Pb(II) onto wollastonite and china clay (Yadava *et al.,* 1991), phenol onto montmorillonite clay (Maarof, 2004), sorption of divalent Cu(II) onto phosphoric acid activated rubber wood sawdust (Kalavathy *et al.,* 2005) and adsorption of uranium (VI) onto the surface of commercial activated carbon from Merck, Germany (Mellah *et. al.,* 2006).

Negative values of ΔG° obtained for adsorption of Pb(II) and Mn(II) cations onto the activated adsorbents indicate spontaneous adsorption. Similar observations were reported for adsorption studies of lead onto china clay and wollastonite (Yadava *et al.,* 1991), copper onto kaolinite and activated slag (Yavuz *et al.,* 2003, Gupta *et al.,* 1998) and manganese onto kaolinite (Yavuz *et al.,* 2003) and raw and acid treated corn cob biomass (Abideen *et al.,* 2011). The adsorption of Cu(II) cations onto KCAC and KFAC show positive ΔG° whereas negative values of ΔG° is exhibited for MFSAC and AOPA. The positive values of ΔG° indicate the non-spontaneous nature of adsorption processes within the range of temperature being studied. This phenomenon had also been observed for adsorption of copper onto sawdust adsorbent (Azmal *et al.,* 1998). In this present study, the values of ΔG° obtained are less than 20 kJ/mol. This shows that some physisorption steps were involved during the sorption process (Gercel *et al.,* 2007).

Overall, it could be concluded that the thermodynamic characteristics of a sorption system vary with the types of the sorbent and sorbate being used as they possessed different physical and chemical characteristics which influence the adsorption mechanism. There is no consistent trend which could be predicted on the thermodynamic behavior of the adsorption processes and the actual factor for this phenomenon.

7.7 Batch Kinetic Studies of Adsorbate

The methodology followed in determining kinetic parameters for sorption systems was mostly identical to that applied previously for the regression analysis of isotherms. The difference is that the water samples were withdrawn at predetermined interval of time and the residual concentrations of the adsorbate denoted as C_e (mg/l) were measured. The quantity C_t (mg/l) provides the necessary information about the quantity of adsorbate adsorbed C_{ad} (mg/l) or removed by the adsorbent at any time t (minute). Based on that, the solid phase concentration or uptake capacity, q_t (mg/g) at any time, uptake capacity at equilibrium time, q_e (mg/g) and removal percentages were calculated by using Equation 7.1 and 7.2 respectively.

$$q_t = \frac{X}{m} \tag{7.1}$$

$$\text{and, } X = (C_0 - C_t)V = C_{ad}V \tag{7.2}$$

where, C_0 (mg/l) is the initial concentration, V (ml) is the volume of liquid taken and m (g) is the mass of adsorbent.

The kinetics of adsorption provides the rate of sorbate uptake onto the activated sorbent within the equilibrium contact time. The pseudo-first-order, pseudo-second-

order kinetic models and Elovich equation were implemented to evaluate the rate constant of the adsorption process. The experimental data were fitted with the aforementioned models and linear regression analyses were carried out and the constants were calculated by using Sigma Plot, Version 2010.

7.7.1 Pseudo-First Order Kinetic Studies

The pseudo-first-order kinetic model proposed by Langergren and Svenska, (1898) has been extensively used by different literatures to envisage sorption kinetics and was expressed earlier by Equation 3.10. The linear plots of log ($q_e - q_t$) against t (minutes) gives the slope as the rate of reaction, k_1 and intercept of log q_e. Theoretical $q_{e(cal)}$ (mg/g) can be calculated from the mathematical model and compared with the experimental $q_{e(exp)}$(mg/g) values.

Figures 7.25 (a)–(d), 7.26(a) –(d) and 7.27(a) –(d) respectively show the linearized plots of the pseudo-first order kinetic model for sorption of Pb(II), Cu(II) and Mn(II) cations onto KCAC, KFAC, MFSAC and AOPA at 30 °C for various initial concentrations (50-100 mg/l). As can be observed from these graphs, the results obtained for all the adsorbate-adsorbent systems are approximately similar, with negative slopes and positive intercepts for all the initial concentrations.

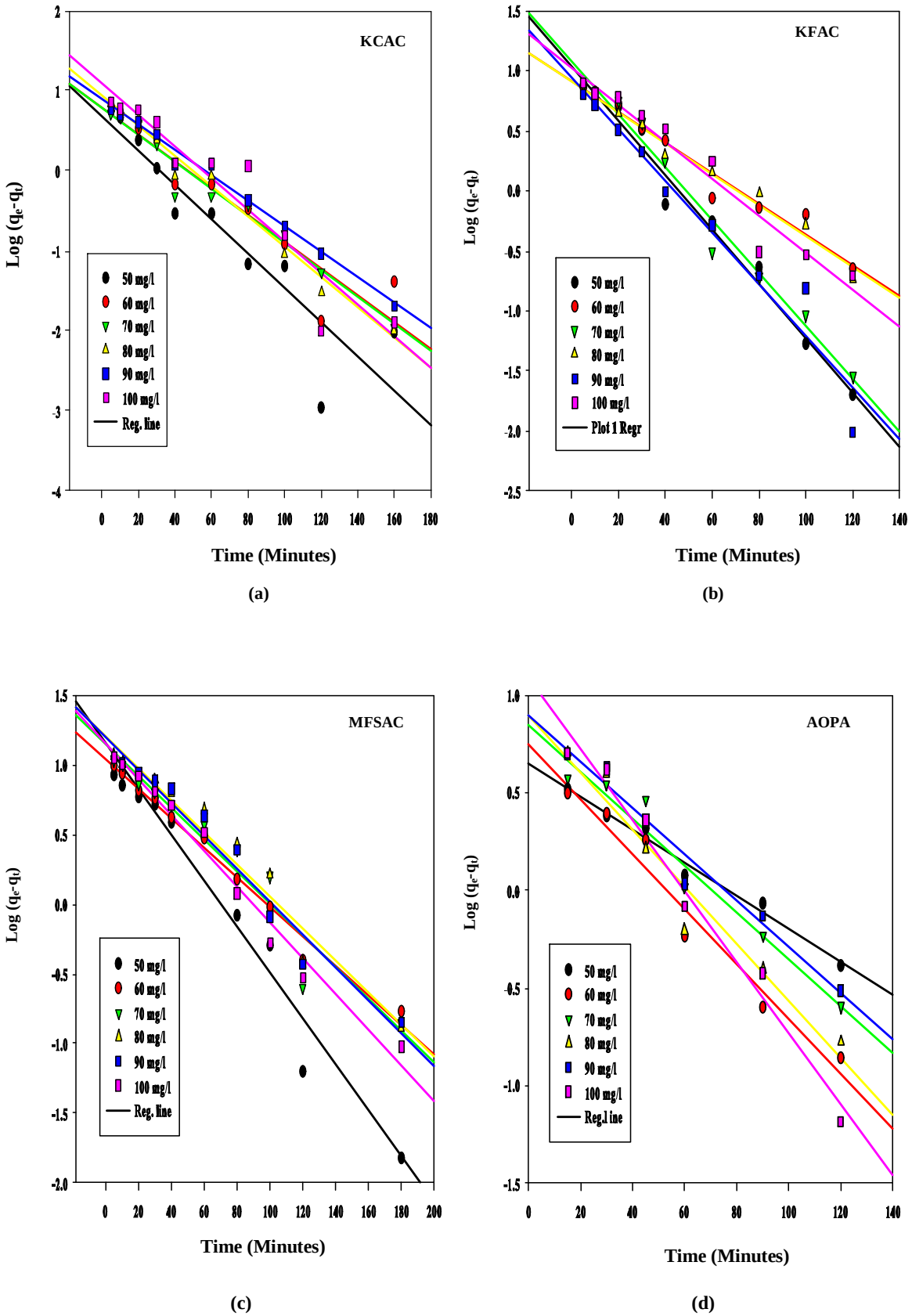

Figure 7.25 Linearized plots for Pseudo first order kinetics for sorption of Lead, Pb(II) cations onto (a) KCAC (b) KFAC (c) MFSAC (d) AOPA

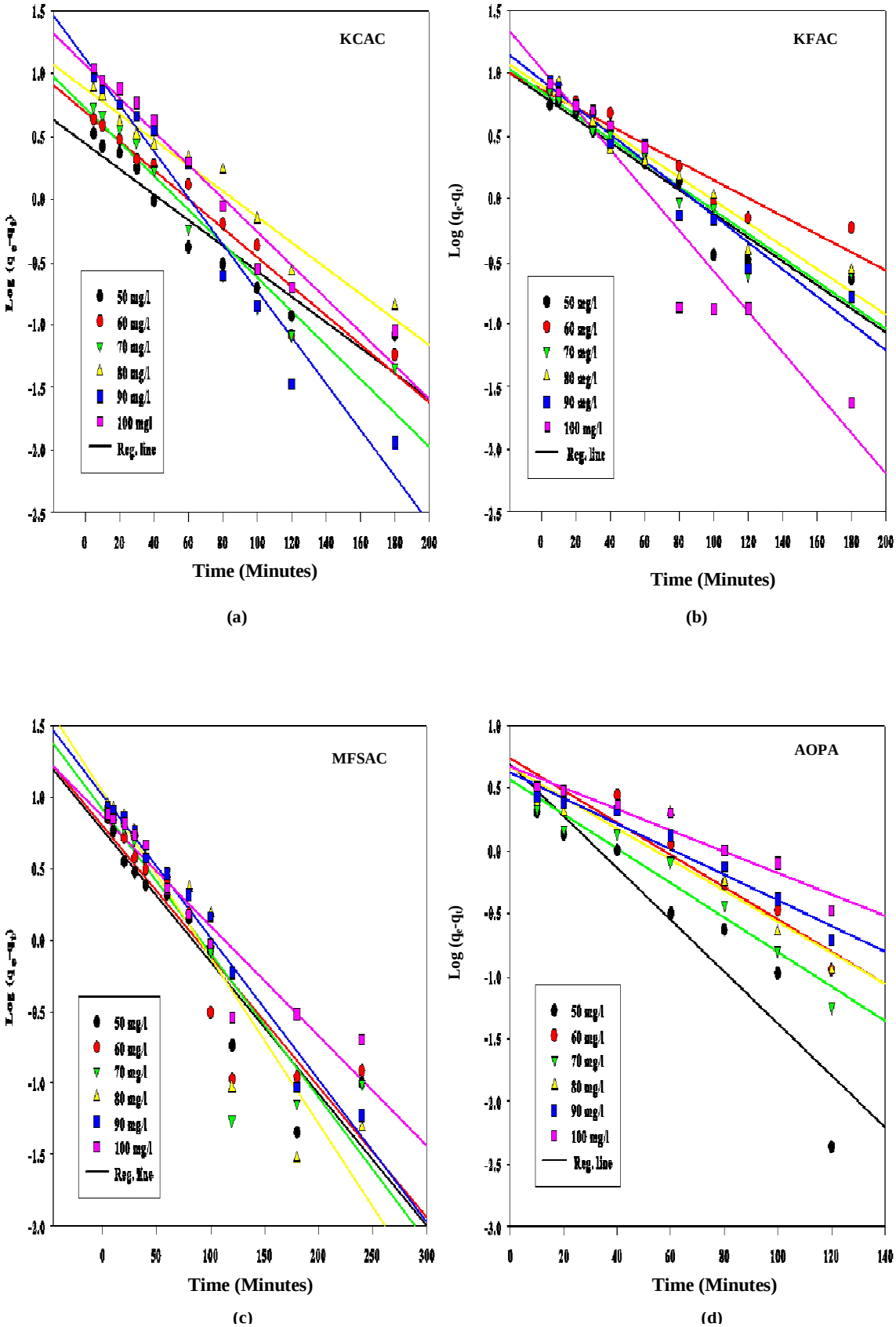

Figure 7.26 Linearized plots for Pseudo first order kinetics for sorption of copper, Cu(II) cations onto (a) KCAC (b) KFAC (c) MFSAC (d) AOPA

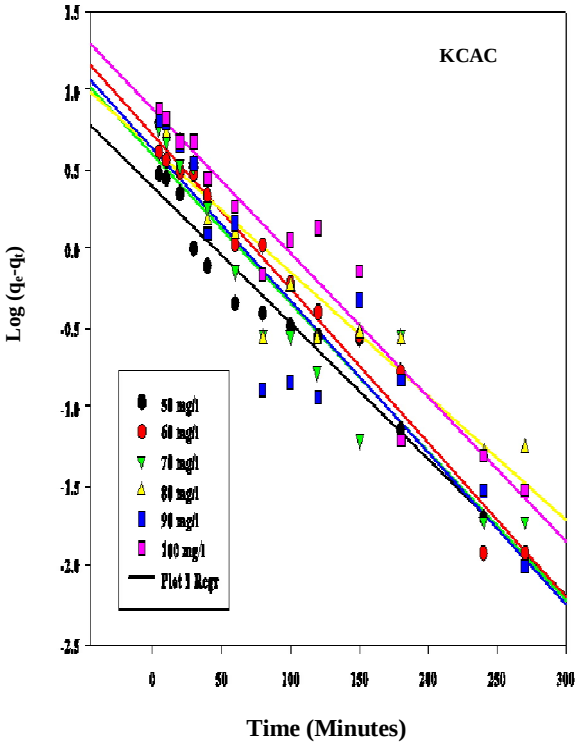

(a)

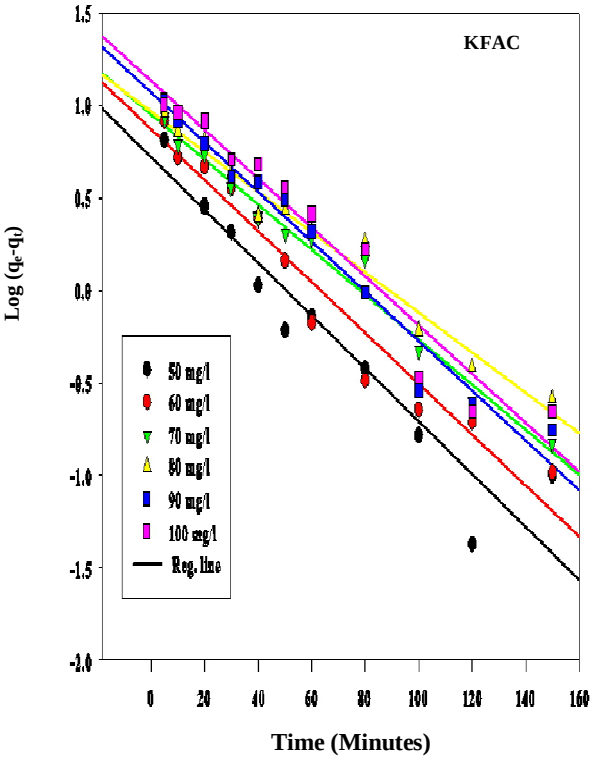

(b)

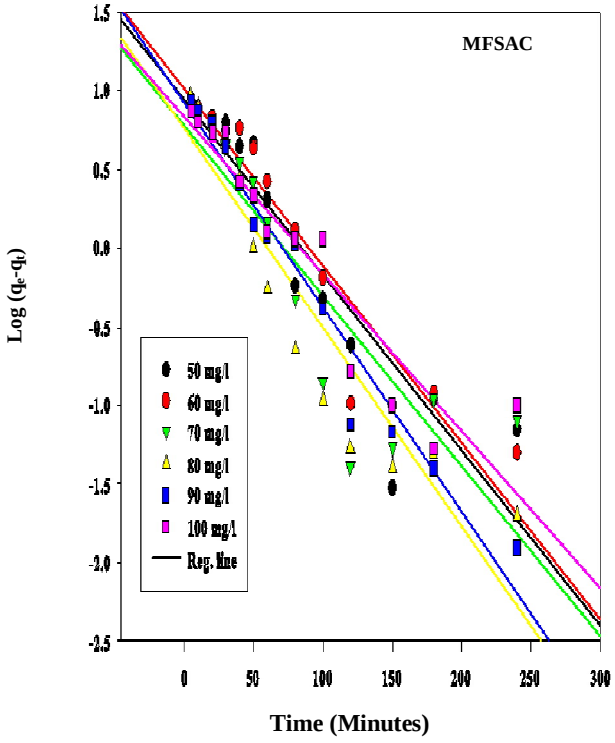

(c)

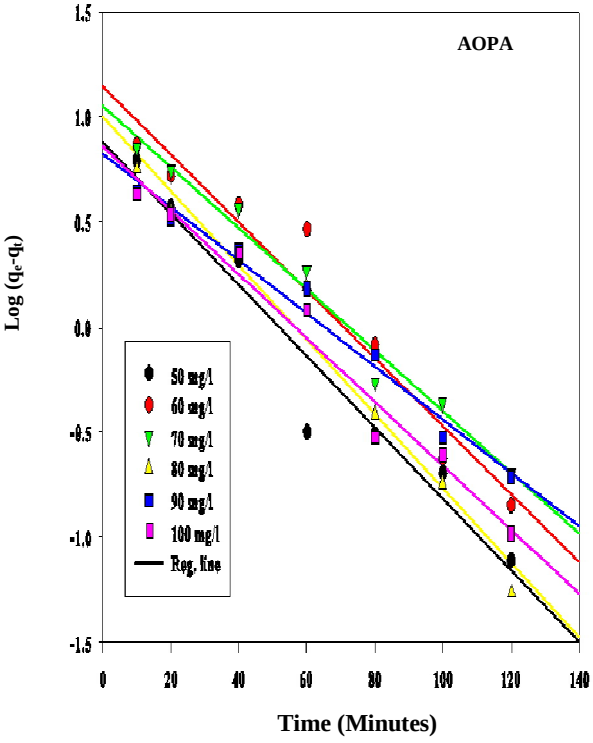

(d)

Figure 7.27 Linearized plots for Pseudo first order kinetics for sorption of Manganese, Mn(II) cations onto (a) KCAC (b) KFAC (c) MFSAC (d) AOPA

It is clear from these graphs (Figures 7.25-7.27) that pseudo first order model is followed by the system for the initial contact period of time. However, with the lapse of time, the experimental data deviates from the theoretical one resulting in scattered point near exhaustion. This shows that pseudo first order model fails to predict the sorption process for the entire region of contact time. This reveals that the system is following physisorption mechanism only partially. This finding supports the presence of active functional groups onto the prepared samples depicted earlier in Section 6.1.

The experimental and calculated q_e values together with the model constants, and correlation coefficient, R^2 determined from the pseudo-first-order kinetics for sorption of Pb(II), Cu(II) and Mn(II) cations onto KCAC, KFAC, MFSAC and AOPA at 30 °C are tabulated in Tables 7.10, 7.11 and 7.12 respectively. The applicability of this kinetic model to describe the sorption process is further validated by the normalized standard deviation Δq (%) values summarized in the same table.

As can be seen from Tables 7.10, 7.11 and 7.12, the rate constant, k_1 and initial rate of sorption h, obtained for the pseudo-first-order model do not show a consistent trend with increasing concentration range for all the cations studied here as some R^2 values are relatively small. The first order rate constant, k_1, is relatively small which agrees well with the sorption kinetics of Pb(II) cations onto biogas slurry (1.75×10^{-1}) and kaolinite clay (5.8×10^{-3}) (Namasivayan and Yamuna1995; Orumwense 1996). The sorption kinetics of Cu(II) cations onto coir pith (1.97×10^{-2}) (Namasivayam and Kadirvelu 1997) and Mn (II) cations onto electric arc furnace slag (2.1×10^{-2}) followed pseudo first order kinetics (Beh *et al.*, 2010).

Table 7.10 Pseudo First Order Kinetics Model parameters for adsorption of Pb (II) from synthetic water by using activated adsorbent at room temperature (30±1) °C, agitation speed 150 rpm and pH 5.5

Sorbent	Initial Concentration	Equilibrium Concentration	uptake capacity	Theoretical uptake capacity	1st order Rate Constant	Initial Rate of Sorption	Coefficient	SD (%)
	C_0	C_e	$q_{e,exp}$	$q_{e,cal}$	k_1	h	R^2	Δq
	(mg/l)	(mg/l)	(mg/g)	(mg/g)	$(min)^{-1}$		-	-
KCAC	50	2.10	11.975	4.819	0.048	0.231	0.847	19.9
	60	2.45	14.387	6.209	0.037	0.230	0.891	18.9
	70	3.10	16.722	6.023	0.036	0.216	0.965	21.3
	80	3.23	19.191	8.511	0.041	0.349	0.980	18.6
	90	4.22	21.445	7.603	0.035	0.266	0.990	21.5
	100	5.11	23.723	12.274	0.043	0.527	0.904	16.1
KFAC	50	1.96	12.010	11.092	0.051	0.566	0.982	2.70
	60	2.78	14.305	8.279	0.028	0.232	0.965	14.9
	70	3.89	16.528	11.830	0.048	0.573	0.980	10.0
	80	4.14	18.965	8.260	0.028	0.228	0.982	19.9
	90	5.21	21.198	8.872	0.048	0.429	0.952	20.6
	100	6.77	23.308	10.691	0.035	0.374	0.954	19.1
MFSAC	50	7.09	10.728	14.289	0.037	0.526	0.956	11.1
	60	9.98	12.505	10.965	0.023	0.252	0.985	4.10
	70	12.98	14.255	13.931	0.025	0.352	0.941	0.76
	80	15.34	16.165	16.107	0.028	0.442	0.960	0.12
	90	20.98	17.143	15.632	0.029	0.467	0.968	2.93
	100	28.56	17.860	14.093	0.032	0.454	0.980	7.03
AOPA	50	10.12	9.9693	4.425	0.018	0.796	0.983	24.9
	60	18.55	10.363	7.727	0.032	0.247	0.938	20.5
	70	22.77	11.809	8.434	0.025	0.211	0.946	12.8
	80	26.88	13.280	7.852	0.032	0.251	0.954	18.3
	90	30.99	14.753	7.780	0.025	0.195	0.968	21.1
	100	36.68	15.831	12.303	0.041	0.504	0.978	9.97

Table 7.11 Pseudo First Order Kinetics Model parameters for adsorption of Cu (II) from synthetic water by using activated adsorbent at room temperature (30±1) °C, agitation speed 150 rpm and pH 5.5

Sorbent	Initial Concentration	Equilibrium Concentration	uptake capacity	Theoretical uptake capacity	1st order Rate Constant	Initial Rate of Sorption	Coefficient	SD (%)
	C_0	C_e	$q_{e,exp}$	$q_{e,cal}$	k_1	h	R^2	Δq
	(mg/l)	(mg/l)	(mg/g)	(mg/g)	$(min)^{-1}$		-	-
KCAC	50	0.33	12.417	2.786	0.1382	0.385	0.919	24.5
	60	0.56	14.861	5.023	0.0253	0.127	0.950	20.9
	70	1.01	17.248	5.248	0.0322	0.169	0.935	22.0
	80	1.11	19.722	7.413	0.0207	0.153	0.960	24.9
	90	1.22	22.195	10.74	0.0345	0.371	0.941	16.3
	100	2.75	24.311	11.93	0.0299	0.357	0.957	16.1
KFAC	50	0.59	12.353	8.433	0.0253	0.214	0.981	10.0
	60	0.76	14.810	12.618	0.0300	0.378	0.950	4.68
	70	0.89	17.278	7.717	0.0138	0.106	0.937	17.5
	80	2.00	19.499	8.356	0.0276	0.230	0.962	18.1
	90	3.10	21.724	8.222	0.0207	0.170	0.929	19.7
	100	3.45	24.136	10.666	0.0276	0.295	0.979	17.7
MFSAC	50	3.99	11.503	5.929	0.0184	0.109	0.886	14.6
	60	6.68	13.331	6.353	0.0184	0.117	0.833	15.8
	70	8.10	15.475	8.185	0.0230	0.188	0.811	14.2
	80	10.99	17.253	11.066	0.0276	0.305	0.877	10.8
	90	16.99	18.253	10.544	0.0230	0.243	0.977	12.7
	100	26.77	18.308	7.278	0.0161	0.117	0.898	18.2
AOPA	50	1.80	12.003	5.395	0.048	0.259	0.894	20.8
	60	4.89	13.778	6.039	0.030	0.181	0.952	21.2
	70	8.52	15.371	3.741	0.029	0.108	0.964	28.6
	80	16.01	15.999	5.035	0.028	0.141	0.894	25.9
	90	20.78	17.305	4.046	0.023	0.093	0.970	28.9
	100	28.00	17.999	5.082	0.023	0.117	0.939	27.1

Table 7.12 Pseudo First Order Kinetics Model parameters for adsorption of Mn (II) from synthetic water by using activated adsorbent at room temperature (30±1) °C, agitation speed 150 rpm and pH 5.5

Sorbent	Initial Concentration	Equilibrium Concentration	uptake capacity	Theoretical uptake capacity	1st order Rate Constant	Initial Rate of Sorption	Coefficient	SD (%)
	C_0 (mg/l)	Ce	$q_{e,exp}$ (mg/g)	$q_{e,cal}$ (mg/g)	k_1 $(min)^{-1}$	h	R^2 -	Δq -
KCAC	50	2.88	11.781	2.506	0.0184	0.046	0.960	22.7
	60	3.76	14.061	5.296	0.0210	0.111	0.974	17.9
	70	4.87	16.287	3.917	0.0200	0.078	0.898	21.9
	80	6.90	18.273	4.276	0.0161	0.068	0.893	22.1
	90	9.45	20.375	4.325	0.0138	0.059	0.844	22.7
	100	11.00	22.250	7.638	0.0201	0.154	0.930	18.9
KFAC	50	2.68	11.831	5.199	0.0345	0.179	0.912	16.9
	60	3.99	14.003	7.379	0.0294	0.217	0.951	14.3
	70	5.89	16.028	8.913	0.0276	0.246	0.980	13.4
	80	7.35	18.162	9.311	0.0230	0.214	0.972	14.7
	90	10.58	19.854	11.59	0.0300	0.348	0.967	12.6
	100	13.77	21.756	13.43	0.0207	0.278	0.948	11.5
MFSAC	50	10.09	9.978	8.7498	0.0250	0.219	0.857	3.55
	60	10.99	12.252	10.20939	0.0253	0.258	0.909	4.81
	70	17.56	13.110	5.9979	0.0230	0.138	0.778	15.7
	80	21.67	14.583	5.8076	0.0276	0.161	0.869	17.4
	90	25.65	16.087	8.3598	0.0300	0.183	0.960	13.9
	100	30.98	17.255	6.8706	0.0230	0.158	0.880	17.4
AOPA	50	16.65	8.313	7.6559	0.0392	0.300	0.945	2.99
	60	20.78	9.805	13.964	0.0369	0.506	0.947	16.0
	70	27.80	10.550	11.246	0.0322	0.362	0.979	2.49
	80	33.98	11.510	10.069	0.0392	0.395	0.969	4.73
	90	40.79	12.301	6.6374	0.0276	0.183	0.980	17.4
	100	46.78	13.310	7.2778	0.0345	0.251	0.972	17.1

The experimental equilibrium uptakes, $q_{e,exp}$ (mg/g), do not concur with the calculated $q_{e,cal}$ (mg/g) values from the pseudo first order model. This gives a relatively large $\Delta q\%$ ranging from 0.12 to 24.87% for sorption of Pb(II), 3.552- 17.374% for Cu(II) and 2.493-22.74% for Mn(II) cations onto the prepared sorbent. This reflects that the experimental data obtained for sorption of the cations under investigation does not completely follow the pseudo-first-order equation.

7.7.2 Pseudo-Second Order Kinetic Studies

The equilibrium data was also fitted with the linear form of pseudo-second-order equation proposed by Ho and McKay (1998). It is found to be able to predict the behavior of the sorption process for all the range of concentrations studied here. It is represented by Equation 3.12. The linear plots of t/q_t against t (minutes) gives $1/q_{e(cal)}$ as the slope and $1/k_2q_e^2$ as the intercept, where k_2 (g/mg-minutes) is the rate constant of the second-order adsorption.

Figures 7.28 (a)-(d), 7.29 (a)-(d) and 7.30 (a)-(d) respectively show the linearized plots of the pseudo-second-order kinetic model for the sorption of Pb(II), Cu (II) and Mn(II) cations onto KCAC, KFAC, MFSAC and AOPA at 30 °C for various initial concentrations. Overall, the pseudo-second-order kinetic model fits the experimental data better than the pseudo-first-order kinetic model as it correlates the experimental data well for all initial concentrations of the selected cations under investigation. It is observed that the regression lines are almost superimposed by the experimental data.

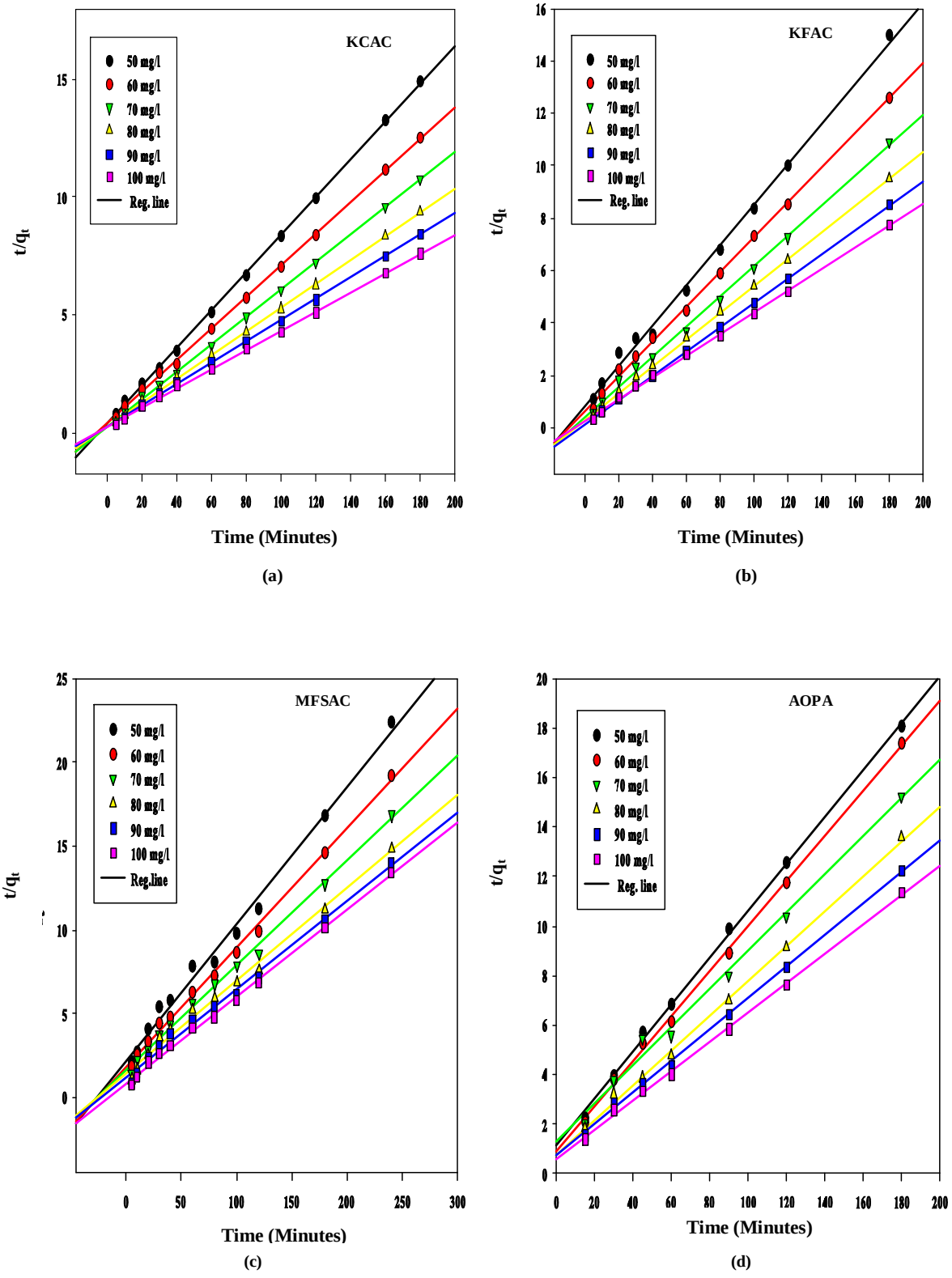

Figure 7.28 Linearized plots for Pseudo second order kinetics for sorption of Lead, Pb(II) cations onto (a) KCAC (b) KFAC (c) MFSAC (d) AOPA

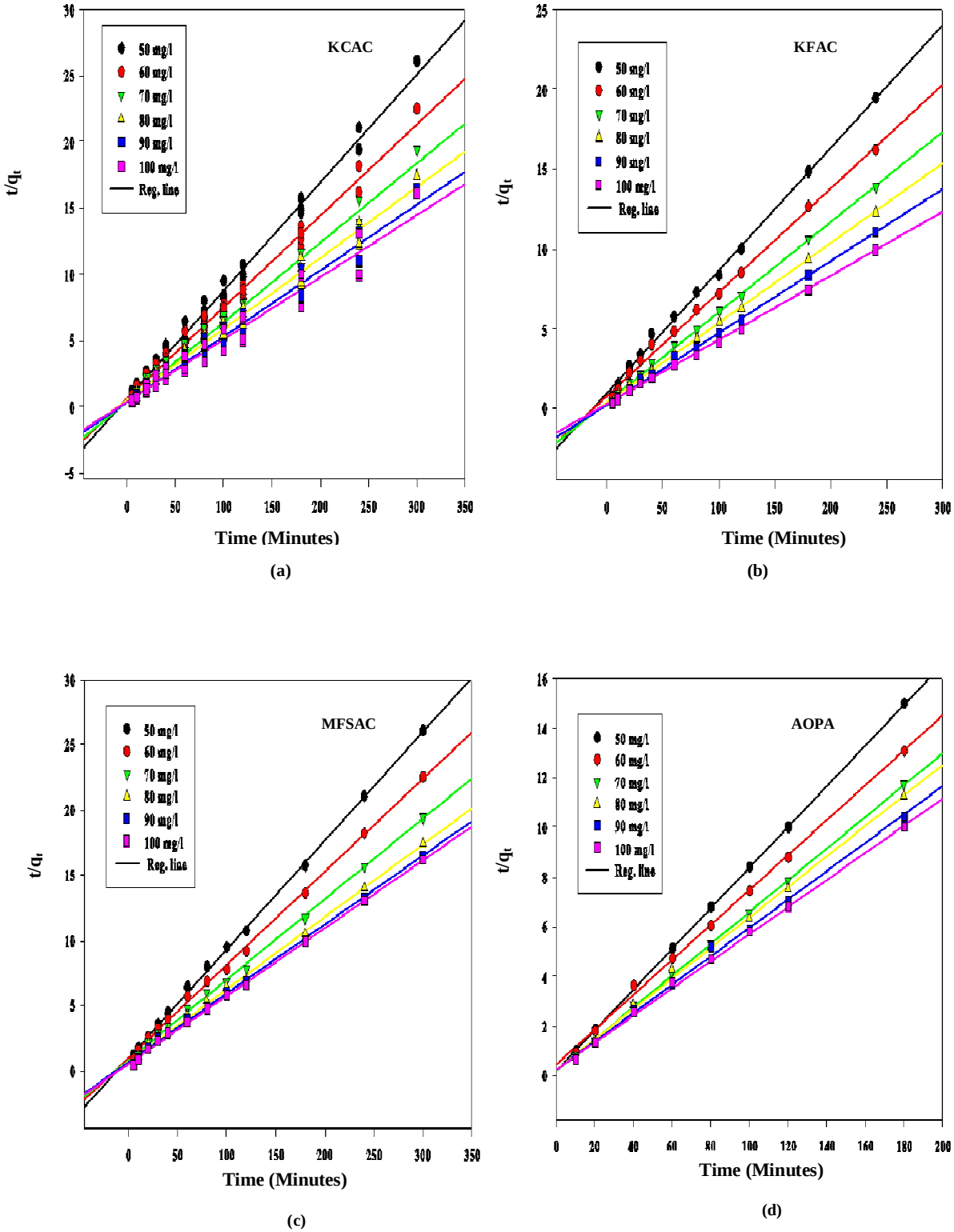

Figure 7.29 Linearized plots for Pseudo second order kinetics for sorption of Copper, Cu(II) cations onto (a) KCAC (b) KFAC (c) MFSAC (d) AOPA

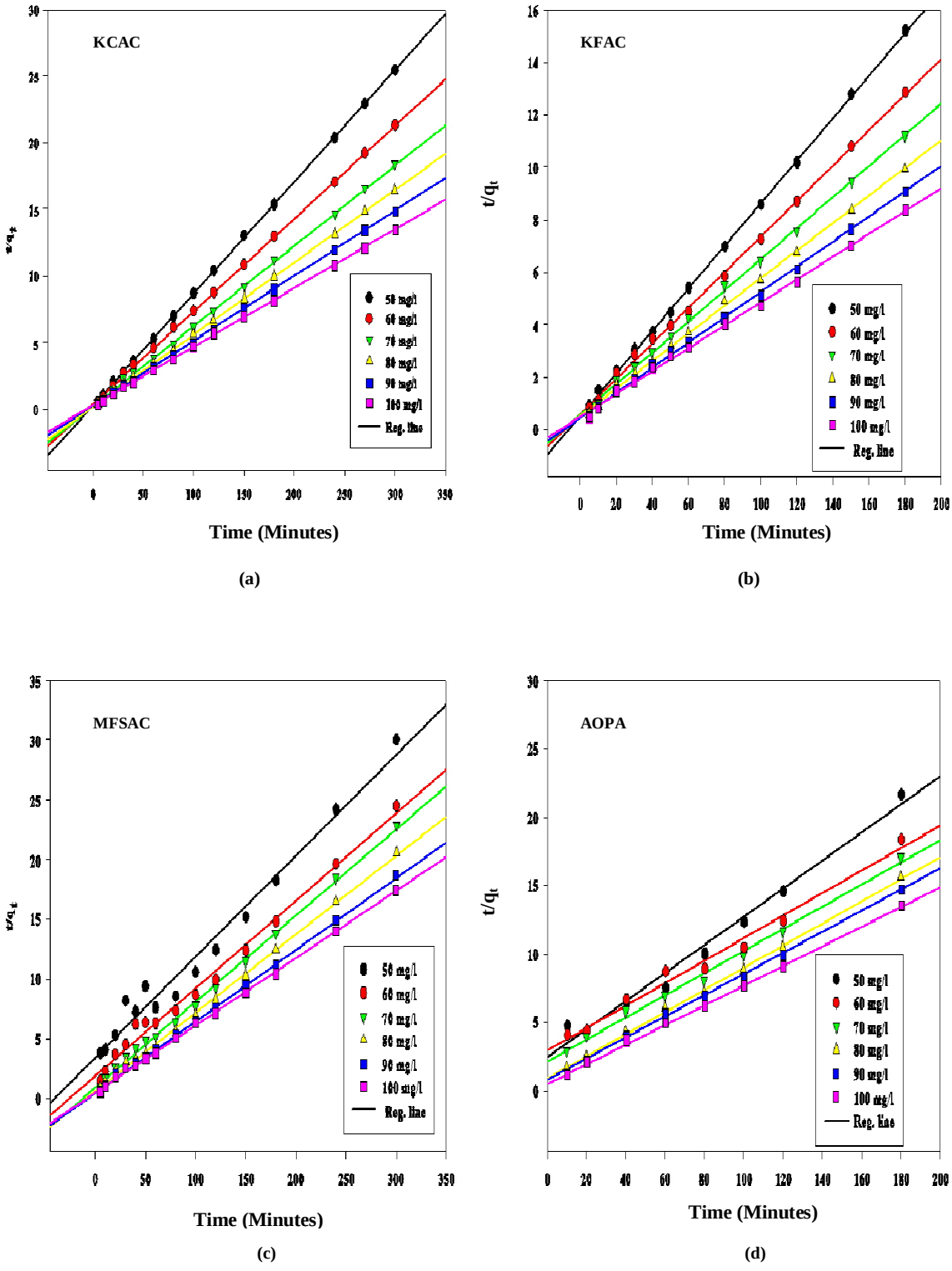

Figure 7.30 Linearized plots for Pseudo second order kinetics for sorption of Manganese, Mn(II) cations onto (a) KCAC (b) KFAC (c) MFSAC (d) AOPA

The experimental and calculated q_e values together with the model constants, and correlation coefficient, R^2 determined from the pseudo-second-order kinetic model for sorption of all the cations onto KCAC, KFAC, MFSAC and AOPA at 30 °C are tabulated in Tables 7.13, 7.14 and 7.15 respectively. The normalized standard deviation Δq (%) values are determined and summarized in the same tables.

From Tables 7.13, 7.14 and 7.15 it can be seen that all the R^2 values obtained from the pseudo-second-order model are closer to unity, indicating that the adsorption of the cations on all the four activated adsorbents studied fits the model well. Moreover, the experimental $q_{e,exp}$ (mg/g) values agreed satisfactorily with the calculated values $q_{e,cal}$ (mg/g) which resulted in Δq values raging from 0.807 to 6.65 % for Pb(II), 2.723 to 3.427% for Cu(II) and 0.092-6.534% for Mn(II) cations.

The pseudo-second-order kinetic model is based on the assumption that chemical adsorption is the rate controlling step. It can predict the behavior over the whole range of contact period (Tseng and Tseng, 2005). This suggests that the overall rate of the adsorption process studied here is controlled by chemisorption which proceeds by the exchange or sharing of valance electrons between the adsorbate and adsorbent.

Table 7.13 Pseudo Second Order Kinetics Model parameters for adsorption of Pb (II) from synthetic water by using activated adsorbent at room temperature (30±1) °C, agitation speed 150 rpm and pH 5.5

Sorbent	Initial Concentration	Equilibrium Concentration	uptake capacity	Theoretical uptake capacity	2nd order Rate Constant	Initial Rate of Sorption	Coefficient	SD (%)
	C_0	C_e	$q_{e,exp}$	$q_{e,cal}$	k_2	h	R^2	Δq
	(mg/l)	(mg/l)	(mg/g)	(mg/g)	$(min)^{-1}$		-	-
KCAC	50	2.10	11.975	12.340	0.0180	2.741	0.999	0.92
	60	2.45	14.387	14.925	0.0120	2.673	0.999	1.13
	70	3.10	16.722	17.241	0.0141	4.191	0.999	0.94
	80	3.23	19.191	20.000	0.0104	4.160	0.999	1.27
	90	4.22	21.445	22.222	0.0103	5.086	0.999	1.09
	100	5.11	23.723	25.000	0.0069	4.313	0.999	1.62
KFAC	50	1.96	12.010	12.987	0.007	1.181	0.996	2.77
	60	2.78	14.305	15.152	0.006	1.377	0.998	1.87
	70	3.89	16.528	17.544	0.007	2.155	0.997	1.94
	80	4.14	18.965	19.608	0.008	3.076	0.999	1.07
	90	5.21	21.198	21.739	0.005	2.362	0.999	0.81
	100	6.77	23.308	24.390	0.007	4.164	0.998	1.47
MFSAC	50	7.09	10.728	12.048	0.004	0.502	0.996	3.70
	60	9.98	12.505	14.085	0.003	0.545	0.997	3.80
	70	12.98	14.255	16.129	0.002	0.580	0.995	3.96
	80	15.34	16.165	18.519	0.001	0.593	0.980	4.39
	90	20.98	17.143	19.231	0.002	0.847	0.991	3.67
	100	28.56	17.860	19.608	0.002	0.888	0.989	2.95
AOPA	50	10.12	9.9693	10.989	0.005	0.652	0.994	3.87
	60	18.55	10.363	11.364	0.006	0.814	0.993	3.65
	70	22.77	11.809	13.889	0.002	0.521	0.987	6.65
	80	26.88	13.280	14.286	0.006	1.225	0.997	2.86
	90	30.99	14.753	15.873	0.005	1.259	0.998	2.87
	100	36.68	15.831	16.949	0.006	1.724	0.998	2.67

Table 7.14 Pseudo Second Order Kinetics Model parameters for adsorption of Cu (II) from synthetic water by using activated adsorbent at room temperature (30±1) °C, agitation speed 150 rpm and pH 5.5

Sorbent	Initial Concentration	Equilibrium Concentration	uptake capacity	Theoretical uptake capacity	2nd order Rate Constant	Initial Rate of Sorption	Coefficient	SD (%)
	C_0 (mg/l)	Ce (mg/l)	$q_{e,exp}$ (mg/g)	$q_{e,cal}$ (mg/g)	k_2 $(min)^{-1}$	h	R^2 -	Δq -
KCAC	50	0.33	12.417	12.658	0.0221	3.541	0.999	0.59
	60	0.56	14.861	15.385	0.0131	3.101	0.999	1.06
	70	1.01	17.248	17.857	0.0131	4.177	0.999	1.07
	80	1.11	19.722	20.408	0.0075	3.124	0.999	1.05
	90	1.22	22.195	23.256	0.0065	3.515	0.999	1.44
	100	2.75	24.311	25.641	0.0051	3.353	0.999	1.65
KFAC	50	0.59	12.353	13.158	0.0059	1.030	0.996	1.97
	60	0.76	14.810	15.625	0.0047	1.160	0.996	1.66
	70	0.89	17.278	18.519	0.0054	1.872	0.998	2.17
	80	2.00	19.499	20.000	0.0067	2.661	0.999	0.78
	90	3.10	21.724	22.727	0.0061	3.140	0.999	1.39
	100	3.45	24.136	26.316	0.0046	3.210	0.998	2.72
MFSAC	50	3.99	11.503	12.048	0.0068	0.987	0.999	1.37
	60	6.68	13.331	14.048	0.0056	1.105	0.998	1.55
	70	8.10	15.475	16.393	0.0047	1.263	0.998	1.71
	80	10.99	17.253	18.182	0.0042	1.388	0.998	1.55
	90	16.99	18.253	18.519	0.0039	1.337	0.996	0.42
	100	26.77	18.308	19.231	0.0050	1.849	0.998	1.46
AOPA	50	1.80	12.003	12.346	0.023	3.506	0.999	1.01
	60	4.89	13.778	14.286	0.011	2.245	0.998	1.30
	70	8.52	15.371	15.625	0.023	5.713	0.999	0.58
	80	16.01	15.999	16.393	0.013	3.494	0.997	0.87
	90	20.78	17.305	17.544	0.016	4.863	0.999	0.49
	100	28.00	17.999	18.519	0.012	4.115	0.998	1.02

Table 7.15 Pseudo Second Order Kinetics Model parameters for adsorption of Mn (II) from synthetic water by using activated adsorbent at room temperature (30±1) °C, agitation speed 150 rpm and pH 5.5

Sorbent	Initial Concentration	Equilibrium Concentration	uptake capacity	Theoretical uptake capacity	2nd order Rate Constant	Initial Rate of Sorption	Coefficient	SD (%)
	C_0 (mg/l)	Ce (mg/l)	$q_{e,exp}$ (mg/g)	$q_{e,cal}$ (mg/g)	k_2 $(min)^{-1}$	h	R^2 -	Δq -
KCAC	50	2.876	11.781	11.905	0.0242	3.430	0.999	0.29
	60	3.760	14.061	14.493	0.0113	2.374	0.999	0.85
	70	4.870	16.287	16.667	0.0130	3.611	0.999	0.65
	80	6.898	18.273	18.868	0.0105	3.738	0.999	0.90
	90	9.450	20.375	20.834	0.0112	4.861	0.999	0.63
	100	11.00	22.250	22.727	0.0072	3.719	0.999	0.60
KFAC	50	2.678	11.831	12.345	0.012	1.828	0.999	1.26
	60	3.987	14.003	14.925	0.007	1.559	0.998	1.90
	70	5.889	16.028	16.949	0.006	1.724	0.998	1.66
	80	7.352	18.162	19.231	0.005	1.849	0.998	1.70
	90	10.58	19.854	21.279	0.004	1.811	0.997	2.07
	100	13.77	21.756	23.256	0.003	1.622	0.997	1.99
MFSAC	50	10.09	9.978	11.904	0.0021	0.298	0.977	5.36
	60	10.99	12.252	13.698	0.0028	0.525	0.990	3.28
	70	17.56	13.110	13.888	0.0055	1.061	0.998	1.65
	80	21.67	14.583	15.384	0.0067	1.588	0.998	1.52
	90	25.65	16.087	16.949	0.0066	1.781	0.999	1.49
	100	30.98	17.255	17.857	0.0065	2.073	0.999	0.99
AOPA	50	16.65	8.313	9.804	0.0044	0.423	0.983	6.34
	60	20.78	9.805	12.346	00022	0.335	0.983	0.09
	70	27.80	10.550	12.500	0.0030	0.469	0.993	6.53
	80	33.98	11.510	12.500	0.0070	1.094	0.998	3.04
	90	40.79	12.301	12.987	0.0084	1.417	0.998	1.97
	100	46.78	13.310	14.085	0.0092	1.825	0.999	2.06

The results obtained in this study is in agreement with the previous works carried out on adsorption of Pb (II) cations on *pinus sylvestris* (Taty-costodes *et al.,* 2003), periwinkle shell activated carbon (Badmus *et al.,* 2007), peat (Ho and McKay 1998) and bottom ash (Kaur *et al.,* 1991), Cu(II) onto peat (Gosset *et al.,* 1986) and sago industry waste (Johnson *et al.,* 2008) and Mn(II) onto electric arc furnace slag (Beh *et al.,*2010) and raw and acid treated corn cob (Abideen *et al.,* 2011) where the adsorption processes were all best described by the pseudo-second-order kinetic model.

7.7.3 Elovich Equation

Elovich equation described by Ozacar and Sengil, 2005 is another most frequently used model for depicting chemisorption process and is expressed by Equation 3.16. The value of (1/b) is indicative of the number of sites available for sorption while (1/b) ln (ab) is the adsorption quantity when ln t is equal to zero; i.e., the adsorption quantity when t is 1 h.

Figures 7.31 (a) – (d), 7.32 (a) – (d) and 7.33 (a) – (d) show the linearized plots of the Elovich equation for sorption studies of Pb(II), Cu(II) and Mn(II) cations onto the prepared sorbent respectively for various initial concentrations at 30 °C. The parameters (1/b) and (1/b) ln (ab) are calculated from the slope and intercept of the linear plots of q_t versus ln t (hour) from the following graphs. The correlation coefficients and constant values determined from these plots are summarized in Tables 7.16, 7.17 and 7.18.

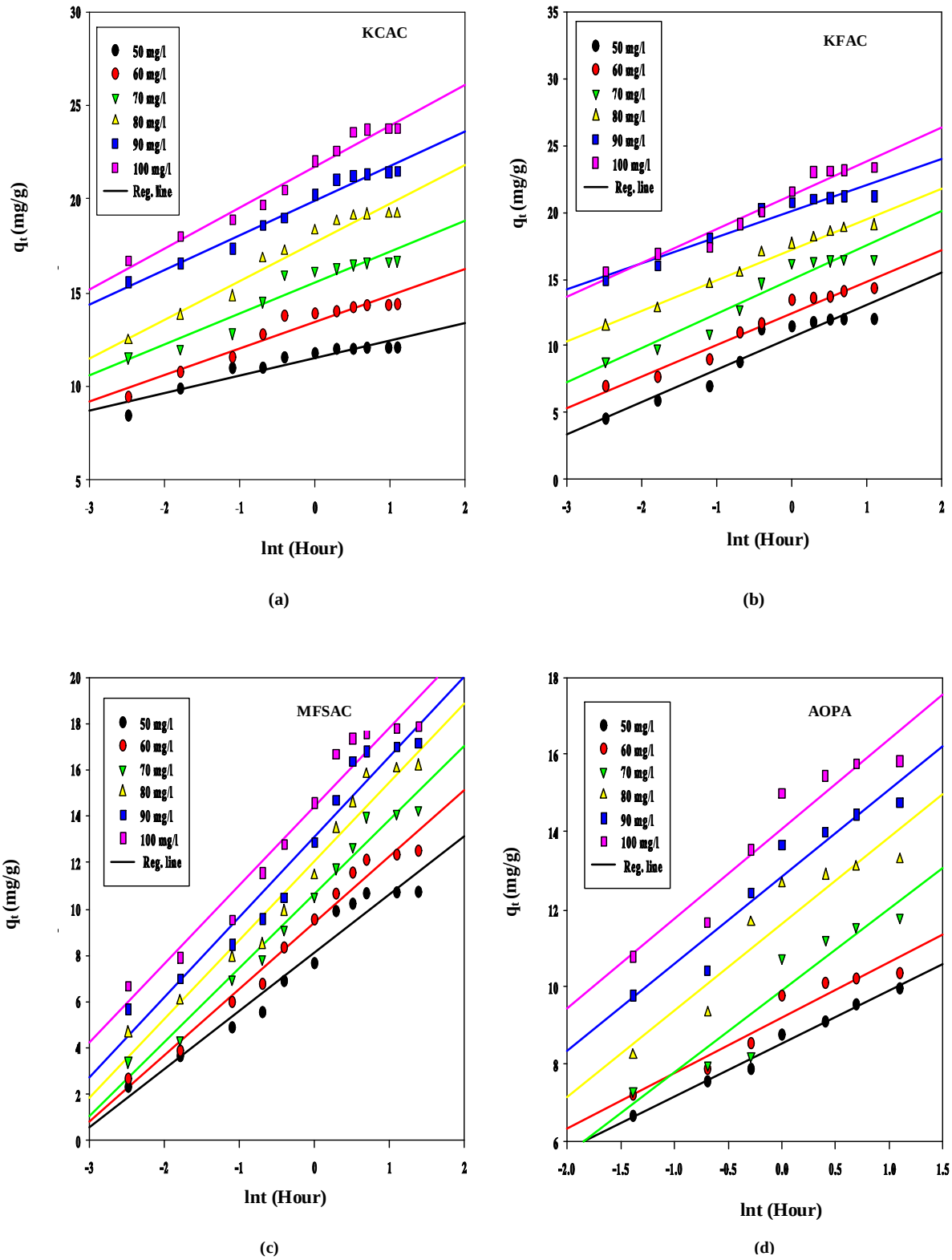

Figure 7.31 Linearized plots for Elovich Equation for sorption of Lead, Pb(II) cations onto (a) KCAC (b) KFAC (c) MFSAC (d) AOPA

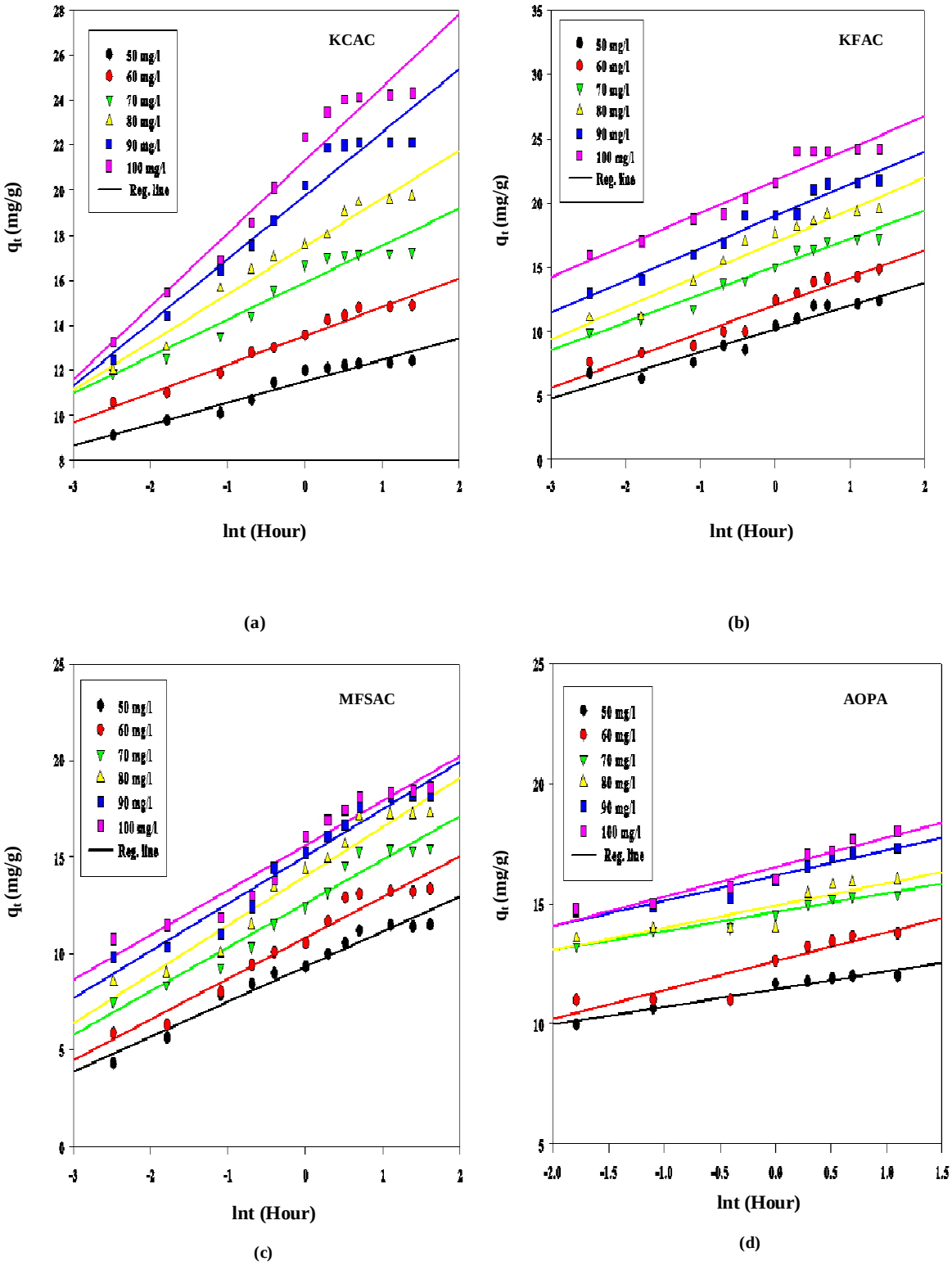

Figure 7.32 Linearized plots for Elovich Equation for sorption of Copper, Cu(II) cations onto (a) KCAC (b) KFAC (c) MFSAC (d) AOPA

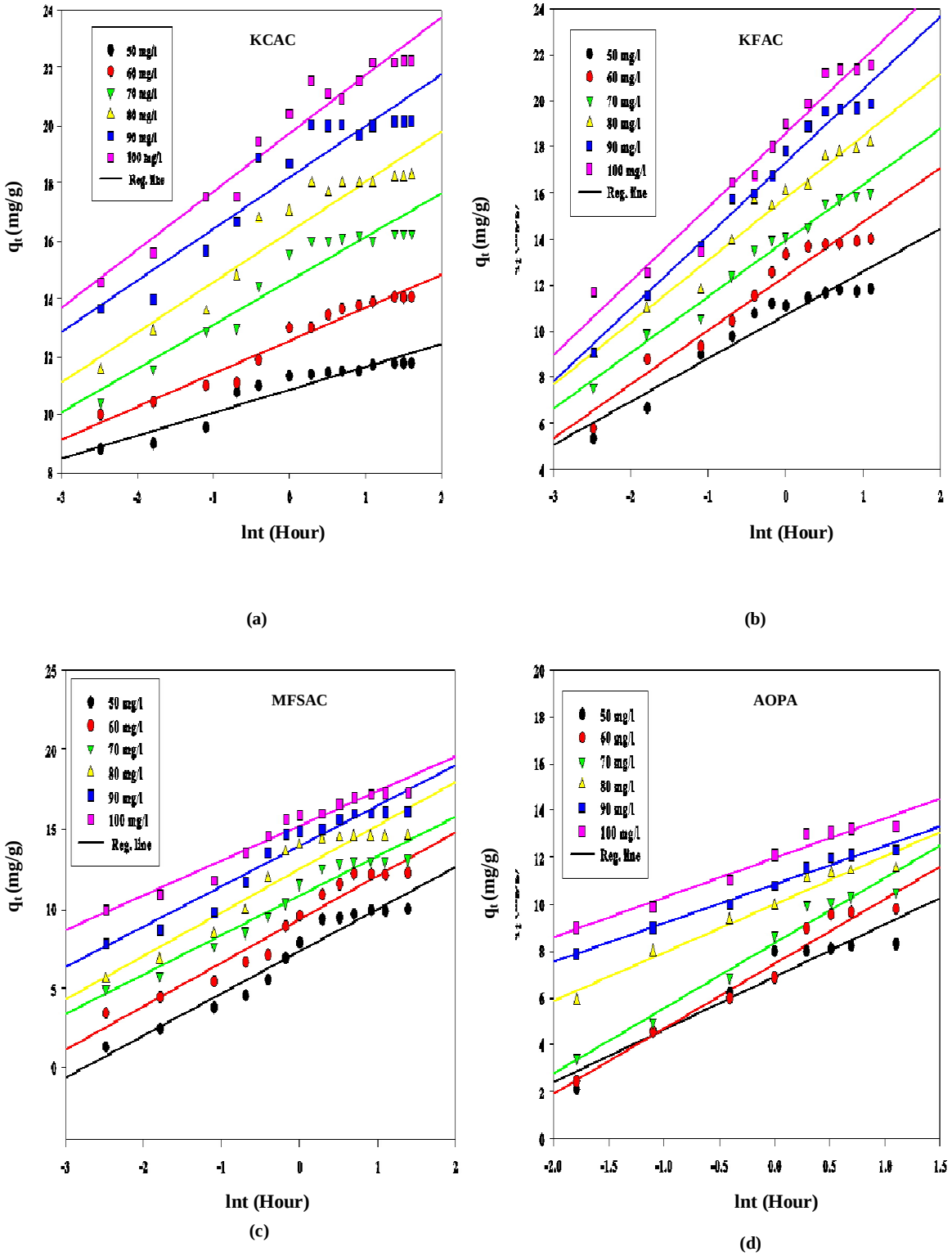

Figure 7.33 Linearized plots for Elovich Equation for sorption of Manganese, Mn(II) cations onto (a) KCAC (b) KFAC (c) MFSAC (d) AOPA

Table 7.16 Elovich Kinetics Model parameters for adsorption of Pb (II) from synthetic water by using activated adsorbent at room temperature (30±1) °C, agitation speed 150 rpm and pH 5.5

Sorbent	Initial Concentration	Equilibrium Concentration	uptake capacity	Theoretical uptake capacity	(1/b)lnab	1/b	Coefficient	SD (%)
	C_0	C_e	$q_{e,exp}$	$q_{e,cal}$	-	-	R^2	Δq
	(mg/l)	(mg/l)	(mg/g)	(mg/g)	(mg/g)	(mg/g)	-	-
KCAC	50	2.10	11.975	12.725	11-03	1.543	0.848	1.88
	60	2.45	14.387	15.475	13.92	1.416	0.926	2.28
	70	3.10	16.722	17.361	15.54	1.658	0.912	1.15
	80	3.23	19.191	19.967	17.71	2.054	0.957	1.22
	90	4.22	21.445	21.918	19.90	1.834	0.972	0.67
	100	5.11	23.723	24.148	21.75	2.183	0.972	2.99
KFAC	50	1.96	12.010	12.240	10.24	1.821	0.925	0.61
	60	2.78	14.305	14.540	12.13	2.195	0.935	0.52
	70	3.89	16.528	17.539	15.10	2.220	0.976	1.93
	80	4.14	18.965	19.705	16.95	2.508	0.946	1.23
	90	5.21	21.198	21.774	19.01	2.516	0.964	0.86
	100	6.77	23.308	24.068	21.12	2.683	0.966	0.33
MFSAC	50	7.09	10.728	11.848	8.420	2.473	0.958	3.15
	60	9.98	12.505	13.376	9.409	2.862	0.977	2.10
	70	12.98	14.255	15.043	10.56	3.234	0.969	1.67
	80	15.34	16.165	16.211	11.61	3.319	0.929	0.09
	90	20.98	17.143	18.085	13.21	3.517	0.944	1.66
	100	28.56	17.860	18.456	13.65	3.467	0.915	1.00
AOPA	50	10.12	9.9693	10.046	8.540	1.371	0.983	0.29
	60	18.55	10.363	10.765	9.197	1.427	0.919	1.47
	70	22.77	11.809	12.081	10.130	1.776	0.888	0.87
	80	26.88	13.280	14.088	11.640	2.229	0.879	2.29
	90	30.99	14.753	15.298	12.840	2.238	0.921	1.39
	100	36.68	15.831	16.602	14.061	2.313	0.908	1.84

Table 7.17 Elovich Kinetics Model parameters for adsorption of Cu (II) from synthetic water by using activated adsorbent at room temperature (30±1) °C, agitation speed 150 rpm and pH 5.5

Sorbent	Initial Concentration	Equilibrium Concentration	uptake capacity	Theoretical uptake capacity	(1/b)lnab	1/b	Coefficient	SD (%)
	C_0 (mg/l)	Ce (mg/l)	$q_{e, exp}$ (mg/g)	$q_{e, cal}$ (mg/g)	- (mg/g)	- (mg/g)	R^2 -	Δq -
KCAC	50	0.33	12.417	12.858	11.53	0.958	0.936	1.07
	60	0.56	14.861	14.944	13.55	1.269	0.971	0.17
	70	1.01	17.248	17.647	15.86	1.627	0.930	0.70
	80	1.11	19.722	19.851	17.51	2.131	0.970	0.20
	90	1.22	22.195	23.633	19.74	2.808	0.952	1.95
	100	2.75	24.311	25.836	21.34	3.243	0.953	1.89
KFAC	50	0.59	12.353	12.764	10.24	1.821	0.925	1.00
	60	0.76	14.810	15.173	12.13	2.195	0.935	0.74
	70	0.89	17.278	18.178	15.10	2.220	0.976	0.09
	80	2.00	19.499	20.427	16.95	2.508	0.946	1.44
	90	3.10	21.724	22.498	19.01	2.516	0.964	1.07
	100	3.45	24.136	25.639	21.92	2.683	0.966	1.88
MFSAC	50	3.99	11.503	12.279	9.366	1.810	0.962	1.95
	60	6.68	13.331	14.189	10.80	2.106	0.954	1.86
	70	8.10	15.475	16.217	12.58	2.260	0.955	1.38
	80	10.99	17.253	18.138	14.03	2.553	0.948	1.48
	90	16.99	18.253	18.956	15.01	2.452	0.951	1.11
	100	26.77	18.308	19.250	15.56	2.293	0.933	1.49
AOPA	50	1.80	12.003	12.267	11.44	0.753	0.953	0.78
	60	4.89	13.778	13.886	12.58	1.189	0.837	0.28
	70	8.52	15.371	15.519	14.64	0.801	0.954	0.34
	80	16.01	15.999	15.949	14.91	0.946	0.789	0.11
	90	20.78	17.305	17.313	16.17	1.040	0.930	0.02
	100	28.00	17.999	17.851	16.52	1.212	0.925	0.29

Table 7.18 Elovich Kinetics Model parameters for adsorption of Mn (II) from synthetic water by using activated adsorbent at room temperature (30±1) °C, agitation speed 150 rpm and pH 5.5

Sorbent	Initial Concentration	Equilibrium Concentration	uptake capacity	Theoretical uptake capacity	(1/b)lnab	1/b	Coefficient	SD (%)
	C_0 (mg/l)	Ce	$q_{e.exp}$ (mg/g)	$q_{e.cal}$ (mg/g)	- (mg/g)	- (mg/g)	R^2 -	Δq -
KCAC	50	2.876	11.781	12.123	10.86	0.785	0.898	0.81
	60	3.760	14.061	14.377	12.54	1.142	0.954	0.62
	70	4.870	16.287	17.048	14.62	1.509	0.913	1.30
	80	6.898	18.273	19.097	16.30	1.738	0.907	1.25
	90	9.450	20.375	21.057	18.21	1.769	0.887	0.93
	100	11.00	22.250	22.943	19.71	2.009	0.949	0.86
KFAC	50	2.678	11.831	12.743	10.68	1.878	0.917	2.23
	60	3.987	14.003	14.915	12.35	2.335	0.943	1.88
	70	5.889	16.028	16.631	13.96	2.432	0.975	1.05
	80	7.352	18.162	18.716	15.75	2.700	0.971	0.88
	90	10.58	19.854	20.823	17.35	3.161	0.979	1.41
	100	13.77	21.756	22.142	18.61	3.215	0.958	0.51
MFSAC	50	10.09	9.978	11.218	7.208	2.492	0.934	0.96
	60	10.99	12.252	13.406	9.233	2.593	0.936	2.61
	70	17.56	13.110	14.404	10.67	2.320	0.931	2.74
	80	21.67	14.583	16.335	12.28	2.520	0.876	3.33
	90	25.65	16.087	17.528	13.73	2.365	0.905	2.48
	100	30.98	17.255	18.335	15.05	2.041	0.934	1.74
AOPA	50	16.65	8.313	9.146	6.896	2.236	0.910	3.54
	60	20.78	9.805	11.955	7.484	2.778	0.961	7.75
	70	27.80	10.550	11.402	8.371	2.759	0.963	2.86
	80	33.98	11.510	12.237	10.00	2.037	0.958	2.23
	90	40.79	12.301	12.664	10.85	1.651	0.981	1.05
	100	46.78	13.310	13.817	11.96	1.691	0.960	1.34

From Tables 7.16, 7.17 and 7.18 it is observed that the R^2 values obtained for the Elovich equation are almost near to unity , yielding Δq% values raging from 0.29 to 2.88% for Pb(II), 0.016-1.947% for Cu(II) and 0.623-7.752% for Mn(II) cations The Elovich equation gave a better fit as compared to the pseudo-first-order model with small Δq% which further confirms the involvement of chemisorptions in the rate controlling step. It is observed that the values of 1/b ln (ab) increase with the increase of initial concentration range studied. This trend is expected because as the concentration range increases, a relatively large number of adsorbate ions will collide with the active sites of the adsorbents to form surface complexes. Eventually more uptakes by the prepared adsorbents will be observed.

7.8 Adsorption Mechanism Studies

The experimental data were further analyzed by using intraparticle diffusion model as the above three kinetic models were not sufficient to identify the diffusion mechanism. Intra particle diffusion model (Weber and Morris, 1962) was expressed earlier by Equation 3.19.

7.8.1 Intraparticle Diffusion

Figures 7.34 (a)-(d), 7.35 (a)-(d) and 7.36 (a)-(d) respectively show the intraparticle diffusion plots for the adsorption of Pb(II), Cu(II) and Mn(II) cations onto KCAC, KFAC, MFSAC and AOPA at 30 °C for various initial concentrations. The plots contain positive intercepts and slope with two distinct region of sorption.

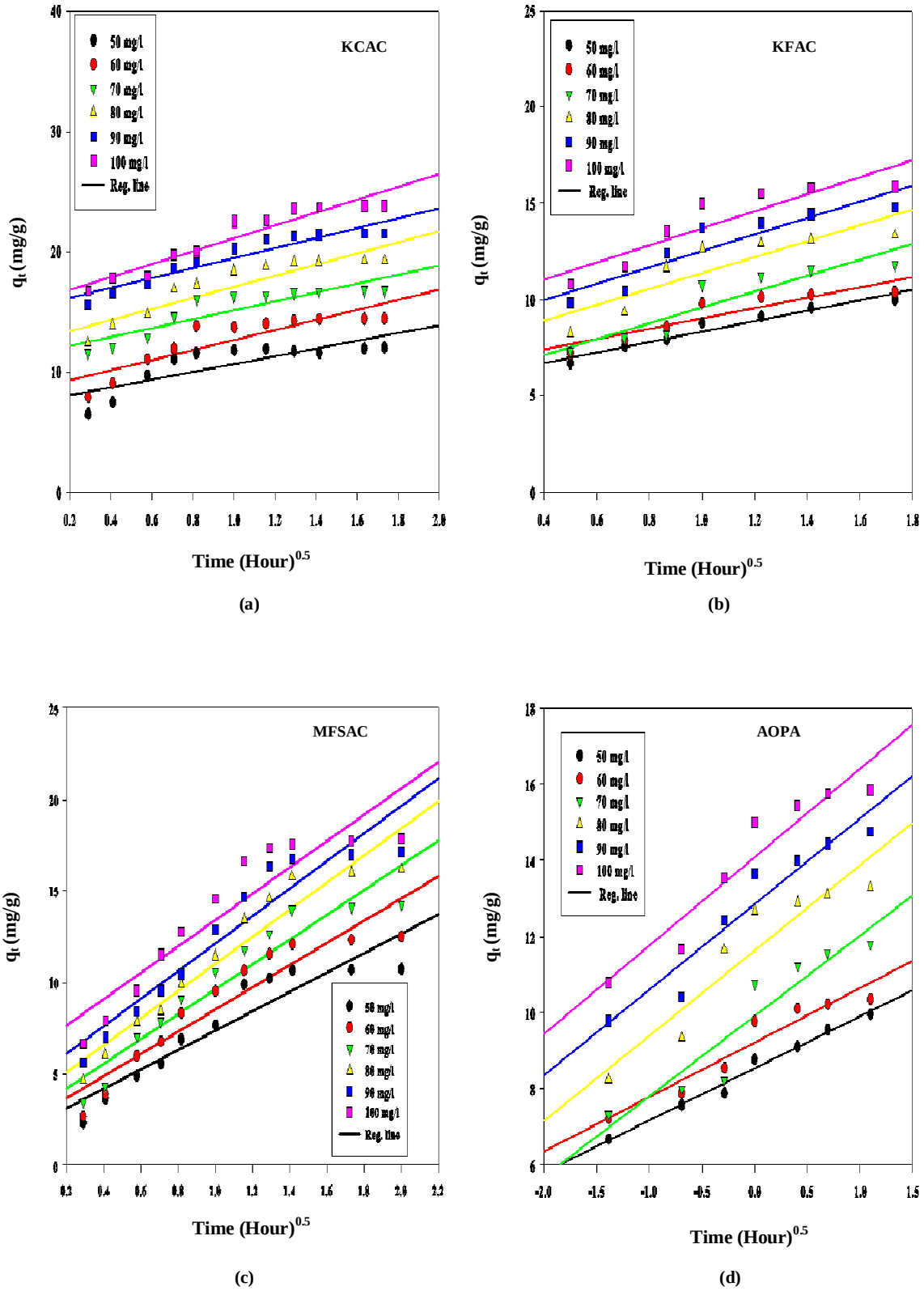

Figure 7.34 Linearized plots of intra particle diffusion studies for sorption of Lead, Pb(II) cations onto (a) KCAC (b) KFAC (c) MFSAC (d) AOPA

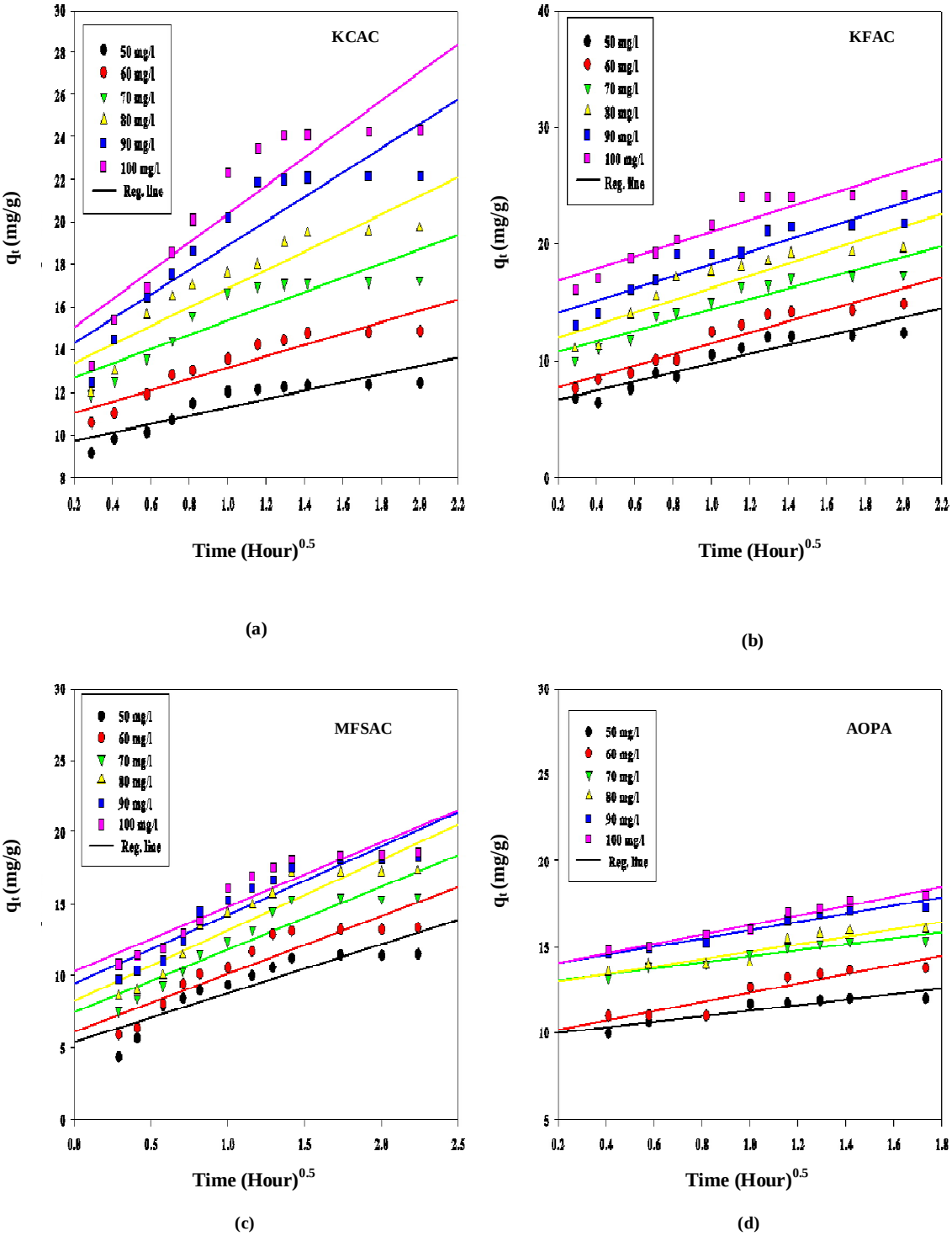

Figure 7.35 Linearized plots of intra particle diffusion studies for sorption of Copper, Cu(II) cations onto (a) KCAC (b) KFAC (c) MFSAC (d) AOPA

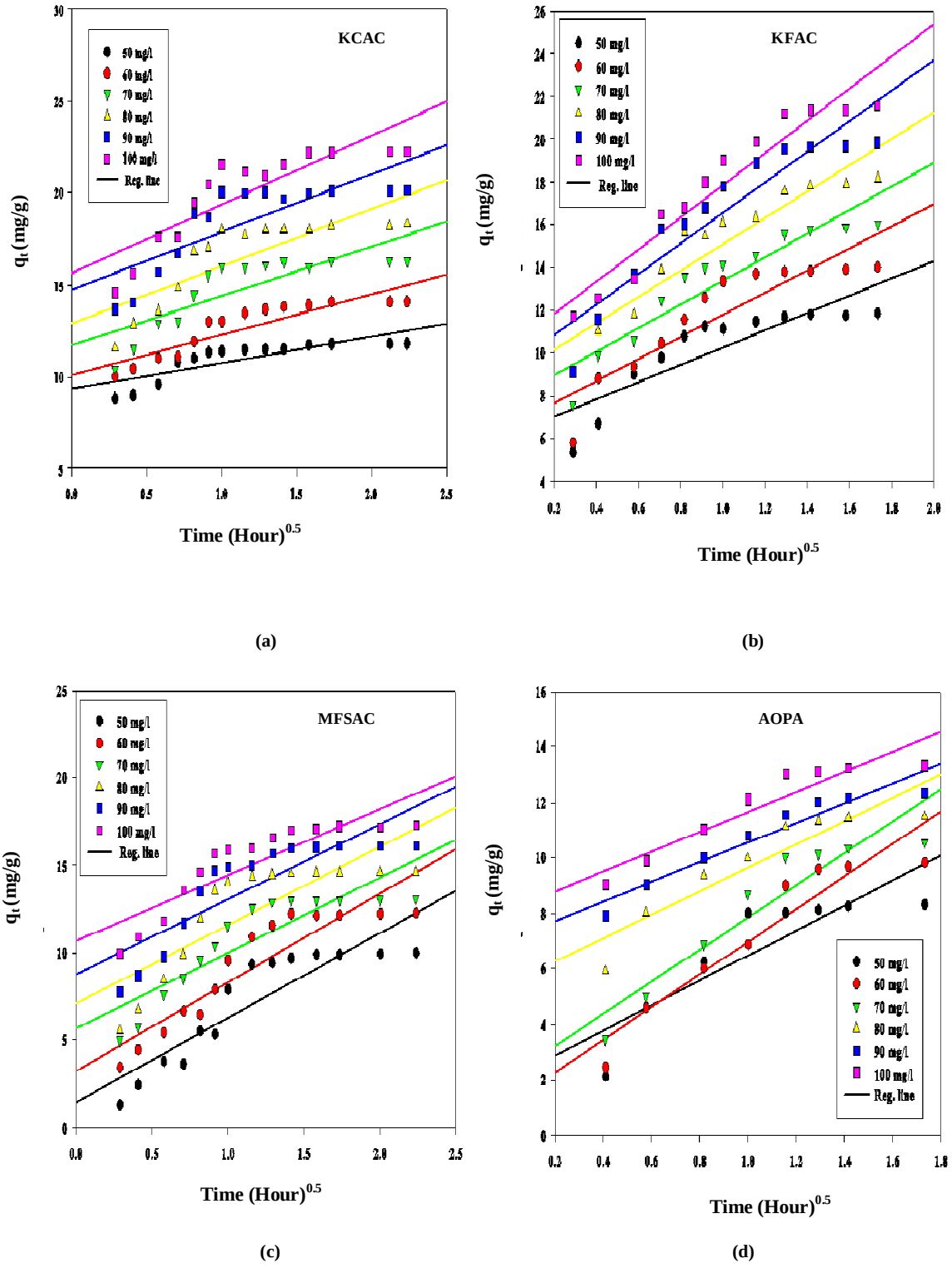

Figure 7.36 Linearized plots of intra particle diffusion studies for sorption of Manganese, Mn(II) cations onto (a) KCAC (b) KFAC (c) MFSAC (d) AOPA

As can be seen from all these plots, the first sharper region is completed within the initial 30-60 minutes time reflecting the immediate sorption or external surface sorption. This represents the mass transfer of the sorbate cations from the bulk solution to the sorbent surface. The second region, almost parallel to X-axis is the gradual sorption stage. The involvement of different stages in the entire sorption process indicates that the adsorption rate is initially faster and then it becomes slower near to the equilibrium time.

It is observed from all the intraparticle diffusion plots (Figures 7.34 (a)-(d)- 7.36 (a)-(d)) that, the linear lines do not pass through the origin. This divergence from the origin might be due to the difference in mass transfer rate in the preliminary and concluding stages of the sorption process (Mohanty *et al.*, 2005). This implies that intraparticle diffusion is not only the rate limiting mechanism in the sorption processes. Similar observation has been reported for the sorption of Cu (II) cations onto rubber wood sawdust (Kalavathy *et al.*, 2005).

The values of the intraparticle diffusion model constants (k_d and C) obtained for all the cations together with the R^2 values obtained are presented in Tables 7.19, 7.20 and 7.21. It is found that the values of the constant C for all the three cations generally increases with increasing initial concentrations of the solution. This trend is expected due to the greater driving force of sorbate cations (increase in effective numbers of collisions between cations and active sites) at higher concentration (Ozer and Dursun, 2007).

Table 7.19 Intra-particle Diffusion Model parameters for adsorption of Pb (II) from synthetic water by using activated adsorbent at room temperature (30±1) °C, agitation speed 150 rpm and pH 5.5

Sorbent	Initial Concentration	Equilibrium Concentration	uptake capacity	Theoretical uptake capacity	Reaction Rate Constant	Layer Effect	Coefficient	SD (%)
	C_0	C_e	$q_{e,exp}$	$q_{e,cal}$	K_{dif}	C	R^2	Δq
	(mg/l)	(mg/l)	(mg/g)	(mg/g)	($mg/h^{0.5}$)		-	-
KCAC	50	2.10	11.975	12.974	3.232	7.383	0.655	2.52
	60	2.45	14.387	15.663	4.207	8.376	0.796	2.67
	70	3.10	16.722	17.794	3.686	11.41	0.793	1.93
	80	3.23	19.191	20.493	4.580	12.56	0.838	2.05
	90	4.22	21.445	22.492	4.204	15.21	0.899	1.47
	100	5.11	23.723	24.963	5.348	15.70	0.909	1.58
KFAC	50	1.96	12.010	14.028	5.500	4.502	0.785	5.31
	60	2.78	14.305	15.944	5.553	6.326	0.868	3.62
	70	3.89	16.528	18.641	5.934	8.363	0.818	4.04
	80	4.14	18.965	20.507	5.310	11.31	0.870	2.57
	90	5.21	21.198	22.808	4.393	15.20	0.778	2.40
	100	6.77	23.308	22.238	4.393	14.63	0.899	1.45
MFSAC	50	7.09	10.728	12.785	5.147	2.491	0.838	5.78
	60	9.98	12.505	14.604	6.053	2.498	0.883	5.06
	70	12.98	14.255	16.530	6.943	2.644	0.903	4.81
	80	15.34	16.165	18.051	7.422	3.171	0.939	3.52
	90	20.98	17.143	19.792	7.648	4.496	0.902	4.64
	100	28.56	17.860	20.208	7.611	4.986	0.891	3.96
AOPA	50	10.12	9.9693	10.303	2.688	5.647	0.945	1.27
	60	18.55	10.363	10.986	2.727	6.263	0.839	2.27
	70	22.77	11.809	12.434	3.499	6.373	0.863	1.99
	80	26.88	13.280	14.366	4.151	7.177	0.762	3.09
	90	30.99	14.753	15.666	4.278	8.241	0.841	2.34
	100	36.68	15.831	16.934	4.376	9.355	0.812	2.63

Table 7.20 Intra-particle Diffusion Model parameters for adsorption of Cu (II) from synthetic water by using activated adsorbent at room temperature (30±1) °C, agitation speed 150 rpm and pH 5.5

Sorbent	Initial Concentration	Equilibrium Concentration	uptake capacity	Theoretical uptake capacity	Reaction Rate Constant	Layer Effect	Coefficient	SD (%)
	C_0 (mg/l)	Ce (mg/l)	$q_{e,exp}$ (mg/g)	$q_{e,cal}$ (mg/g)	K_{dif} ($mg/h^{0.5}g$)	C	R^2 -	Δq -
KCAC	50	0.33	12.417	13.209	1.963	9.283	0.794	1.92
	60	0.56	14.861	15.828	2.664	10.50	0.865	1.96
	70	1.01	17.248	18.686	3.323	12.04	0.784	2.51
	80	1.11	19.722	21.264	4.397	12.47	0.835	2.36
	90	1.22	22.195	24.644	5.747	13.15	0.807	3.33
	100	2.75	24.311	27.066	6.703	13.66	0.823	3.42
KFAC	50	0.59	12.353	13.656	3.970	5.716	0.889	3.18
	60	0.76	14.810	16.276	4.808	6.660	0.907	2.98
	70	0.89	17.278	19.188	4.753	9.682	0.904	3.33
	80	2.00	19.499	21.348	5.154	11.04	0.808	2.86
	90	3.10	21.724	23.554	5.307	12.94	0.864	2.54
	100	3.45	24.136	26.920	5.815	15.29	0.917	3.48
MFSAC	50	3.99	11.503	12.930	3.360	5.417	0.800	3.58
	60	6.68	13.331	13.717	3.399	6.117	0.828	0.84
	70	8.10	15.475	17.243	4.385	7.438	0.868	3.29
	80	10.99	17.253	19.278	4.938	8.237	0.856	3.39
	90	16.99	18.253	20.076	4.764	9.424	0.867	2.88
	100	26.77	18.308	20.321	4.477	10.31	0.086	3.17
AOPA	50	1.80	12.003	12.817	2.406	8.650	0.738	0.85
	60	4.89	13.778	14.692	3.538	8.564	0.814	2.35
	70	8.52	15.371	16.015	2.237	12.14	0.817	1.48
	80	16.01	15.999	16.477	2.637	11.91	0.844	1.06
	90	20.78	17.305	17.746	2.446	13.51	0.961	0.90
	100	28.00	17.999	18.656	3.266	13.00	0.898	1.29

Table 7.21 Intra-particle Diffusion Model parameters for adsorption of Mn (II) from synthetic water by using activated adsorbent at room temperature (30±1) °C, agitation speed 150 rpm and pH 5.5

Sorbent	Initial Concentration	Equilibrium Concentration	uptake capacity	Theoretical uptake capacity	Reaction Rate Constant	Layer Effect	Coefficient	SD (%)
	C_0 (mg/l)	C_e	$q_{e.\ exp}$ (mg/g)	$q_{e.\ cal}$ (mg/g)	K_{dif} (mg/h$^{0.5}$g)	C	R^2 -	Δq -
KCAC	50	2.876	11.781	12.483	1.418	9.307	0.671	1.65
	60	3.760	14.061	15.016	2.185	10.13	0.799	1.88
	70	4.870	16.287	17.505	2.614	11.66	0.666	2.07
	80	6.898	18.273	19.849	3.121	12.87	0.669	2.39
	90	9.450	20.375	21.798	3.161	14.73	0.648	1.94
	100	11.00	22.250	23.946	3.728	15.61	0.747	2.11
KFAC	50	2.678	11.831	13.190	4.041	6.191	0.738	3.32
	60	3.987	14.003	15.593	5.189	6.606	0.810	3.28
	70	5.889	16.028	17.417	5.515	7.865	0.872	2.50
	80	7.352	18.162	19.624	6.166	8.944	0.880	2.32
	90	10.58	19.854	21.815	7.139	9.451	0.868	2.85
	100	13.77	21.756	23.363	7.542	10.30	0.916	2.13
MFSAC	50	10.09	9.978	12.278	4.868	1.394	0.808	6.40
	60	10.99	12.252	14.579	5.063	3.258	0.838	5.27
	70	17.56	13.110	18.340	4.291	8.748	0.728	11.1
	80	21.67	14.583	17.132	4.494	7.083	0.675	4.85
	90	25.65	16.087	18.376	4.306	8.748	0.728	3.95
	100	30.98	17.255	19.106	3.759	10.701	0.768	2.98
AOPA	50	16.65	8.313	9.773	4.502	1.975	0.765	6.21
	60	20.78	9.805	11.266	5.899	1.049	0.898	5.27
	70	27.80	10.550	12.084	5.797	2.044	0.882	5.14
	80	33.98	11.510	12.698	4.214	5.400	0.850	3.65
	90	40.79	12.301	13.101	3.507	7.027	0.919	2.30
	100	46.78	13.310	14.249	3.562	8.080	0.884	2.49

7.9 Regeneration of spent adsorbent

The feasibility of the prepared adsorbent was further analyzed by using five types of regenerating agent. The procedure was explained earlier in Chapter 4 (Section 4.5). The percent desorption efficiency was calculated by using Equation 4.16 and the values obtained are summarized in the following Table 7.22.

Table 7.22 Percent Desorption of Metallic cations from spent activated adsorbents

Adsorbate	Adsorbent	Desorption Percentages				
		Distilled Water	CH_3COOH	HCl	HNO_3	H_2SO_4
Pb(II)	KCAC	6.776	11.332	74.778	81.878	62.545
	KFAC	3.667	9.898	77.676	78.887	67.789
	MFSAC	4.889	7.787	78.998	80.545	72.324
	AOPA	2.334	4.887	26.343	20.889	12.223
Cu(II)	KCAC	8.787	12.098	66.987	85.889	65.898
	KFAC	5.556	10.676	69.890	82.454	62.987
	MFSAC	6.887	8.889	80.787	85.879	75.435
	AOPA	3.667	6.565	28.768	22.789	14.004
Mn(II)	KCAC	9.878	13.987	57.987	92.343	67.778
	KFAC	7.009	11.565	60.234	88.567	65.787
	MFSAC	7.676	9.898	75.778	86.897	68.789
	AOPA	4.887	7.334	33.565	24.656	15.223

It is observed that the percent desorption is in general higher for Cu(II) and Mn(II) cations rather than Pb(II) cations. This might be due to the smaller cationic size of these two adsorbates for which they can be desorbed from the surface readily. However, satisfactory amount of desorption percentage is exhibited by powdered and granular activated carbon rather than the activated ash residues. Similar desorption efficiency had

also been observed for Cd (II) and Zn(II) cations from rice husk ash by using acid eluting agent (Srivastava *et al.,* 2008).

The sorption process takes place either by physical or chemical interactions, ion exchange or combination of all types of mechanisms. By using distilled water, small fractions of cations can be desorbed. Mineral acids are better than organic acids as desorbing agents. Basically, organic acids dissociate partially, releasing smaller amounts of exchangeable H^+ ions. On the contrary inorganic acids dissociate completely to produce sufficient number of H^+ cations. These take part in desorption mechanisms of metallic cations from adsorbent surface. Among the inorganic acids, HNO_3 acid acts as better eluting agent for activated carbon whereas HCl acid desorbs slightly higher fractions of metallic cations from activated ash. However, the desorption efficiency shown by activated ash is not significant. This shows that the sorption process onto activated ash residues is not completely reversible. Overall, HNO_3 desorption technique was shown to be a promising way to regenerate the cation loaded sorbent; especially in the case of powdered and granular activated carbon. Thus for column regeneration and recycling, HNO_3 acid solution has been used in the following Chapter 8.

7.10 Summary

In this study, the influences of process parameters for batch equilibrium processes were determined. The results revealed that the prepared sorbents are effective for the removal of divalent cations of Pb(II), Cu(II) and Mn(II) from waste water. The optimum sorption process takes place between pH 4-6 and the uptake increases with the increase of initial concentration. Linear regression analysis was carried out to evaluate kinetics and isotherm

parameters of the sorption processes. In terms of adsorption capacity and desorption efficiency, the prepared activated carbon (KCAC, KFAC and MFSAC) performed better than the activated ash sample (AOPA). Therefore, for column dynamics studies; granular activated carbon (MFSAC) has been selected for the preparation of fixed bed in subsequent section of Chapter 8.

CHAPTER EIGHT
RESULTS AND DISCUSSION
Fixed Bed Adsorption Studies

8.1 Introduction

This chapter discusses the fixed bed adsorption onto activated carbon prepared from mangostene fruit shell (MFSAC). Initial/influet concentrations of the adsorbate, fixed bed height and rate of influent on breakthrough curves were analyzed. The sorption dynamics were studied in terms of Thomas, Yoon- Nelson and Bohart-Adams Models. Regeneration and recycling efficiency of the column for each adsorbate are presented in the subsequent section. The chapter ends with a brief summary depicting the process parameters for fixed bed sorption.

8.2 Fixed-Bed Adsorption Studies

Fixed adsorption tests were carried out for adsorption of divalent cations of Pb (II), Cu (II) and Mn (II) onto MFSAC due to the suitability of this granular type activated adsorbent to be applied in continuous adsorption system. The time to reach breakthrough for different adsorbates were analyzed. The experimental results were plotted to obtain breakthrough curves which reflect the sorption behaviors of the adsorbate at definite time interval for continuous flow adsorption. It can be expressed in terms of the ratio of outlet adsorbate concentration to the inlet adsorbate concentration with respect to time (C_t/C_0 versus time, t). The equilibrium adsorbate uptake in the column or maximum capacity of the column (q_{eq}) at 50% breakthrough was calculated by using Equation 3.22 by Treybal approach. The

experiments were carried out at room temperature, (30 ±1) ℃ and the pH of the inlet solution was adjusted as 5.5.

8.2.1 Effect of Adsorbate Inlet Concentration

The effect of inlet concentration of the adsorbate on the column performance was studied by varying the inlet concentrations of 50, 70 and 100 mg/l for constant bed height of 4.5 cm and feed flow rate of 1 ml/min. The breakthrough curve is illustrated by Figures 8.1, 8.2 and 8.3 for lead Pb(II), copper Cu(II) and manganese Mn(II), respectively. Then the breakthrough time, t_b and complete exhaustion time, t_e for different concentrations were determined.

As can be observed from the following three plots (Figures 8.1, 8.2 and 8.3), the activated carbon beds were exhausted faster at higher adsorbate inlet concentrations. It is observed that, breakthrough point was reached quickly by higher concentration range of influent solution. This phenomenon is expected with increasing influent concentration because the binding sites were occupied rapidly and the adsorbent bed was saturated within a short period of time. When the inlet concentration was decreased, relatively longer contact time was required by the sorbent to be exhausted. This gave an extended breakthrough curve. The phenomenon exhibited that a higher volume of solution could be treated. This is evident due to slower transportation of adsorbate cations for lower concentrated solution. This results in overall decrease in diffusion or mass transfer coefficient (Tan *et al.*, 2008).

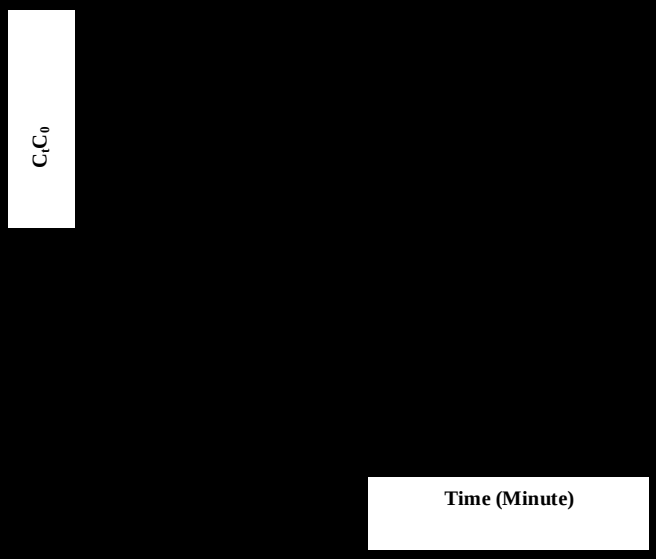
C_t/C_0
Time (Minute)


Time (Minute)

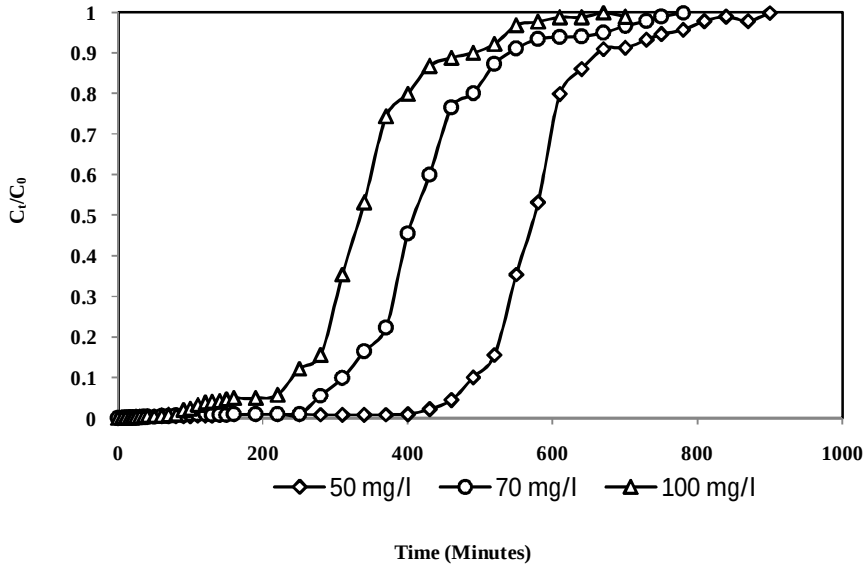

Figure 8.3 Breakthrough Curves for adsorption of manganese (II) onto MFSAC for different initial concentration (Flow rate 1 ml/min, pH 5.5, Temperature 30±1 °C)

As the concentration range was increased from 50 mg/l to 100 mg/l, the curve changed its shape from flatter concave to steep concave; the larger the influent concentration is, the steeper is the shape of the initial portion of the curve. The shape and gradient of the breakthrough curves showed different trends from one another for different metals. Nevertheless, it showed an S-shape curve for all the metals with a nearly flat line for the preliminary stage of the breakthrough curve. Similar trend was observed for the biosorption of Cr (VI) by thermally activated weed *Salvinia cucullata* (Baral *et al*., 2009), biosorption of Acid Blue 15 using fresh water *Azolla filiculodies* (Padmesh *et al.*, 2006), for removal of lead (II) ions using activated tea waste (Mondal, 2009) and immobilized *Pinus sylvestris* sawdust (Taty-Costodes *et al*., 2005) .

8.2.2. Effect of Activated Carbon Bed Height

Figures 8.4, 8.5 and 8.6 show the breakthrough curve obtained for the adsorption of Pb (II), Cu (II) and Mn (II) on MFSAC for two different bed heights of 3 and 4.5 cm (3.56 and 4.86g of MFSAC) at constant adsorbate feed flow rate of 1 ml/min and adsorbate inlet concentration of 100 mg/l.

It was observed from the figures that, a constant pattern of breakthrough curves was obtained for all the three metals over the range of bed depth studied. However, at higher bed height, the curves tended to be less steep. Tables 8.1, 8.2 and 8.3 show the comparison of column parameters for the three metals. Maximum equilibrium capacity of the column was increasing with increasing bed height.

As can be seen from the plots (Figures 8.4, 8.5 and 8.6), both break through and exhaustion time were found to increase with increasing bed height. The plots show that the shape and gradient of the breakthrough curves were slightly different with the variation of bed depth. This is expected because for higher bed height, there was more activated carbon present in the column. Thus there were more active sites for capturing metallic cations resulting greater uptake capacity. The increase in bed height will increase the mass transfer zone. The mass transfer zone travels from the entrance side of the fixed bed and proceed towards the outlet side. Therefore for same inlet concentration, an increase in bed height would cause a larger distance for the mass transfer zone to arrive at the exit of the column. Consequently it would result with an extended breakthrough time. For higher bed depth, the increase of adsorbent mass would provide a larger service area leading to an increase in the volume of waste water to be treated (Ahmad and Hameed, 2010 b; Tan *et al.*, 2008).

Pb>Mn>Cu. Cu(II) cations loaded column was exhausted earlier than Mn(II) cations having ionic radius 0.79 °A. This is expected due to its high reactivity based on Irving William series and smallest cationic size (0.71° A). Thus it can penetrate easily inside the pores of the adsorbent. Similar observation has been reported for phosphate treated rice husk adsorbent column (Mohan and Sreelakshmi, 2008). This can be explained in terms of the affinity factor of different cations toward the prepared adsorbent. Among the three cations, lead has the largest ionic radius with the highest electronegativity. It is probably due to this reason; lead occupied the adsorbent surface quickly. Copper is more reactive than manganese as it can readily form stable complexes. This is why although copper (0.73 °A) and manganese (0.79 °A) have almost similar ionic radius, copper adsorbed quickly resulting in an earlier saturation of the column compared to manganese. However, lead and copper showed almost similar uptake capacity as both of them are the highest two members of Irving-Williams series having similar electronegativities of 2.3 and 1.9 respectively depending on bed height and flow rate. Following Tables 8.1, 8.2 and 8.3 listed the exhaustion time and bed capacity for Pb (II), Cu (II) and Mn (II) respectively at different condition.

Tables 8.1 Column Adsorption data for Pb (II) onto MFSAC

Inlet Concentration (mg/l)	**Bed Height (cm)**	**Solution Flow Rate (ml/min)**	**Breakthrough Time, t_b (min)**	**Complete Exhaustion Time, t_e (min)**	**Empty Bed Contact Time, EBCT (min)**	**Bed Capacity, $t_{0.5}$ q_{eq} (mg/g)**
50	4.5	1	360	870	71.54	5.5230
70	4.5	1	240	810	71.54	5.5486
100	4.5	1	180	630	71.54	6.7028
100	3.0	1	100	540	47.69	4.7217
100	4.5	3	70	420	23.86	2.1285

Tables 8.2 Column Adsorption data for Cu (II) onto MFSAC

Inlet Concentration (mg/l)	Bed Height (cm)	Solution Flow Rate (ml/min)	Breakthrough Time, t_b (min)	Complete Exhaustion Time, t_e (min)	Empty Bed Contact Time, EBCT (min)	Bed Capacity, $t_{0.5}$ q_{eq} (mg/g)
50	4.5	1	280	870	71.54	4.7241
70	4.5	1	220	750	71.54	5.7350
100	4.5	1	200	660	71.54	6.0219
100	3.0	1	120	570	47.69	5.0261
100	4.5	3	60	630	23.86	5.6316

Tables 8.3 Column Adsorption data for Mn (II) onto MFSAC

Inlet Concentration (mg/l)	Bed Height (cm)	Solution Flow Rate (ml/min)	Breakthrough Time, t_b (min)	Complete Exhaustion Time, t_e (min)	Empty Bed Contact Time, EBCT (min)	Bed Capacity, $t_{0.5}$ q_{eq} (mg/g)
50	4.5	1	490	900	71.54	6.0757
70	4.5	1	340	780	71.54	6.1162
100	4.5	1	250	700	71.54	7.2573
100	3.0	1	130	550	47.69	4.1111
100	4.5	3	70	670	23.86	6.8562

At higher inlet concentration, higher equilibrium uptake was observed for column sorption system. This phenomenon is analogous with the batch sorption process depicted earlier in Chapter 7. However, the experimental results obtained for adsorption of Pb (II), Cu (II) and Mn (II) cations on MFSAC showed that the highest adsorption capacity was obtained using a solution of 100mg/l as the inlet concentration using 1 ml/l flow rate. It is depicted by previous literature that, the reduction of bed height would cause axial

dispersion to affect the overall mass transfer process. This causes reduction in diffusion of the adsorbate (Taty-Costodes *et al.,* 2005). This indicates that, the solute did not get enough time to diffuse into the whole of the adsorbent mass by using lower bed height and higher flow rate of adsorbate solution. In this study the empty bed contact time (EBCT) or standard contact time is calculated by using Equation 8.1 (Bharathi *et al.,* 2011).

EBCT= Bed Volume/Flow rate (8.1)

However, at higher flow rate and lower bed height; lower empty bed contact time (EBCT) was obtained. It was observed that, the lower the EBCT values, the lower is the diffusion process resulting in a lower adsorption capacity. Similar trend was followed for the sorption of cadmium onto coir pith (Bharathi *et al.,* 2011).

It can be concluded that, the developed column packed with MFSAC would demonstrate better performance by using lower flow rate (1ml/min) of the inlet solution. From Tables 8.1, 8.2 and 8.3 it is observed that, relatively longer breakthrough time, t_b (minutes) and exhaustion time, t_e (minutes) was required for lower flow rate of inlet solution. By using higher flow rate of inlet solution (3 ml/min), the equilibrium sorption capacity of MFSAC was lower for the same bed height (4.5 cm). This was due to inadequate contact time between the solute and the sorbent in the column and less diffusion of the solute into the pores of the adsorbent. At the end, the solute had to leave the column before equilibrium was reached. This phenomenon is expected and previously observed for various fixed bed sorption systems (Malkoc *et al.,* 2006, Al-Qodah and Lafi, 2003; Taty-Costodes *el al.,* 2005; Padmesh *et al.,* 2006,).

Overall, the adsorption capacity of MFSAC for the cations under investigation for fixed-bed experiments were found to be lesser than the values evaluated earlier from the batch experiments (Chapter Seven) for the same initial concentration. The difference between the adsorption capacity obtained from batch and fixed-bed system could also be attributed to the static mode of sorption in the adsorption column. Moreover, the effective surface areas of the activated sorbent (MFSAC) was lesser compared to those available in the stirred batch vessels (Al-Qodah and Lafi, 2003). This reflects that the performance of the prepared activated sorbent could be improved by applying higher bed height and lower flow rate of adsorbate solution for a fixed adsorbate inlet concentration.

8.3 Column Dynamics Study

As the adsorbate solution loaded with cations enters and moves through the column, the adsorption zone starts moving towards the end of the column and the effluent concentration starts rising with time. This point is referred as break point and the time taken for the inlet concentration to reach a specific breakthrough concentration is called the breakthrough time. However, the point at which the outlet concentration reaches 99% of its inlet concentration is termed as column exhaustion time, t_e (minutes).

The sorption performance of the cations through the column was analyzed by Thomas, Yoon Nelson and Bohart- Adams models at concentration ratio, C_t/C_0 >0.1 until 10% breakthrough i.e C_t/C_0 >0.90 for manganese and for concentration ratio, C_t/C_0 >0.05 until 10% breakthrough C_t/C_0 >0.90 for lead and copper by considering the drinking water standards and operating limit of the mass transfer zone (Naja and Volesky, 2006, Mohan

and Sreelakshmi, 2008). The column capacity q_{eq} (mg/g) was calculated at 50 % breakthrough capacity of the column as depicted earlier by Equation 3.22.

8.3.1. Application of Thomas model

The experimental data obtained from column studies were fitted with the Thomas model. The rate constant (k_{th}) and maximum sorption capacity, q_0 (mg/g) were evaluated from the linear plots of $\ln(C_0/C_t-1)$ against time, t(min). The figures are shown in Appendix F. The estimated values of k_{th} and q_0 (mg/g) are listed in Tables 8.4, 8.5 and 8.6 for lead, copper and manganese respectively.

Table 8.4 Thomas model parameters for lead (II) at different conditions using linear regression analysis

Initial Concentration (mg/l)	Bed Height (cm)	Flow Rate (ml/min)	k_{th}(ml/min-mg) x 10^{-4}	q_o (mg/g)	R^2
50	4.5	1	3.80	5523.06	0.986
70	4.5	1	3.00	5617.28	0.980
100	4.5	1	2.60	6702.88	0.976
100	3.0	1	3.10	4721.82	0.922
100	4.5	3	4.70	6435.51	0.864

Table 8.5 Thomas model parameters for copper (II) at different conditions using linear regression analysis

Initial Concentration (mg/l)	Bed Height (cm)	Flow Rate (ml/min)	k_{th}(ml/min-mg) x 10^{-4}	q_o (mg/g)	R^2
50	4.5	1	3.20	4725.43	0.980
70	4.5	1	2.43	5735.05	0.970
100	4.5	1	2.40	6021.94	0.926
100	3.0	1	2.70	5219.31	0.914
100	4.5	3	4.30	5634.51	0.911

Table 8.6 Thomas model parameters for manganese (II) at different conditions using linear regression analysis

Initial Concentration (mg/l)	Bed Height (cm)	Flow Rate (ml/min)	k_{th}(ml/min-mg) x 10^{-4}	q_o (mg/g)	R^2
50	4.5	1	5.20	6085.78	0.983
70	4.5	1	2.71	6162.33	0.975
100	4.5	1	1.70	7257.32	0.931
100	3.0	1	1.50	5574.90	0.890
100	4.5	3	2.80	6856.26	0.956

Referring to Tables 8.4-8.6, it can be observed that the column dynamics studied here followed Thomas model with high correlation coefficient, R^2. However, the data deviated slightly from linear regression analysis in the case of Pb(II) cations' sorption by using the highest process parameters (Concentration 100 mg/l, bed height 4.5 cm and flow rate 3 ml/min). Similar trend was followed for Mn(II) sorption by using concentration of 100 mg/l and bed height 3 cm and flow rate 1 ml/min.

From the Tables (8.4-8.6) it was noticed that the values of sorption capacity, q_0 (mg/g) increased with increase in initial concentration. This trend is consistent with batch sorption studies depicted earlier in this study (Chapter Seven) also. The values of q_0 (mg/g) decreased with the increase in inlet flow rate. On the contrary, q_0 (mg/g) values increased with increase in bed height. This phenomenon is expected and the reason behind this is explained in Section 8.2.4. Overall the regression coefficient, R^2 determined from Thomas model implied absence of axial dispersion where the rate limiting step was not predominated by external and internal diffusion (Ahmad *et al.,* 2010b). Similar trend had also been observed by Baral *et al.,* (2009) for sorption studies of Cr(VI) onto *Salvinia cucullata.*

8.3.2. Application of the Yoon-Nelson model

The experimental data were fitted with Yoon-Nelson model to investigate the breakthrough Characteristics of Pb (II), Cu (II) and Mn (II) ions onto MFSAC. The values of k_{YN} and τ were calculated from the linear plots of ln $C_t/(C_o - C_t)$ versus t (min) at different flow rates, bed heights and initial cation concentration. The figures are shown in Appendix F. The values of k_{YN} and τ for 50 % breakthrough time, $t_{0.5}$ (min) are listed in Tables 8.7, 8.8 and 8.9 for lead, copper and manganese respectively.

Table 8.7 Yoon- Nelson model parameters for lead (II) at different conditions using linear regression analysis

Initial Concentration (mg/l)	Bed Height (cm)	Flow Rate (ml/min)	k_{YN} (l/min)	ζ (min)	R^2
50	4.5	1	0.020	536.84	0.986
70	4.5	1	0.021	382.38	0.980
100	4.5	1	0.029	280.82	0.976
100	3.0	1	0.031	168.09	0.922
100	4.5	3	0.026	103.44	0.815

Table 8.8 Yoon- Nelson model parameters for copper (II) at different conditions using linear regression analysis

Initial Concentration (mg/l)	Bed Height (cm)	Flow Rate (ml/min)	k_{YN} (l/min)	ζ (min)	R^2
50	4.5	1	0.016	459.18	0.980
70	4.5	1	0.017	398.17	0.970
100	4.5	1	0.024	292.66	0.926
100	3.0	1	0.023	268.83	0.970
100	4.5	3	0.043	91.233	0.864

Table 8.9 Yoon- Nelson model parameters for manganese (II) at different conditions using linear regression analysis

Initial Concentration (mg/l)	Bed Height (cm)	Flow Rate (ml/min)	k_{YN} (l/min)	ζ (min)	R^2
50	4.5	1	0.026	591.53	0.983
70	4.5	1	0.019	427.84	0.975
100	4.5	1	0.017	352.71	0.931
100	3.0	1	0.015	199.80	0.890
100	4.5	3	0.028	111.07	0.956

Overall the experimental data fitted well with Yoon Nelson model with few exceptions including Pb(II) and Cu(II) sorption when the process variables were in maximum range (Concentration 100 mg/l, bed height 4.5 cm and flow rate 3 ml/min). Analogous tendency was observed for Mn(II) sorption by using concentration of 100 mg/l and bed height 3 cm and flow rate 1 ml/min.

The rate constant, k_{YN} increased with increase in initial concentration for column dynamics of Pb(II) and Cu(II) cations whereas the values decreased for Mn(II) cations with increase in initial concentration. With increase in flow rate and bed height, the values of k_{YN} decreased for Pb(II) cations but increased for Cu(II) and Mn(II) cations. In this study the time required for 50% exhaustion of column, ζ (min) decreased with increase in initial concentration and flow rate. It also decreased with decrease in bed height. This trend of 50 % column exhaustion time, ζ (min) is evident and explained earlier describing the experimental results in Section 8.3.4 (Tables 8.1-8.3). From the Tables (8.7-8.9) it can be seen that the experimental breakthrough times for 50 % breakthrough capacity of the column were very close to those predicted by the Yoon-Nelson model.

8.3.3 Application of the Bohart-Adoms model

The breakthrough characeteristics were further analyzed by using Bohart-Adams model. ln (C_t/C_0) values were plotted against time, t(min) at different flow rates, bed heights and initial cation concentrations and model constants such as maximum adsorption capacity (N_o) and the mass transfer coefficient (k_{AB}) were determined. The linear plots are given in Appendix F. The mass transfer coefficient (k_{AB}) and saturation concentration (N_o) values were calculated from the slope and intercept of the curve respectively and are shown in Tables 8.10, 8.11 and 8.12 for lead, copper and manganese respectively.

Table 8.10 Adams- Bohart parameters for lead (II) at different conditions using linear regression analysis

Initial Concentration (mg/l)	**Bed Height (cm)**	**Flow Rate (ml/min)**	**k_{AB} (L/mg-min) x 10^{-4}**	**N_0 (mg/l)**	**R^2**
50	4.5	1	2.20	434.899	0.949
70	4.5	1	1.71	473.567	0.914
100	4.5	1	1.60	478.041	0.891
100	3.0	1	1.50	426.182	0.709
100	4.5	3	2.10	629.265	0.622

Table 8.11 Adams- Bohart parameters for copper (II) at different conditions using linear regression analysis

Initial Concentration (mg/l)	**Bed Height (cm)**	**Flow Rate (ml/min)**	**k_{AB} (L/mg-min) x 10^{-4}**	**N_0 (mg/l)**	**R^2**
50	4.5	1	1.80	396.503	0.902
70	4.5	1	1.29	501.725	0.925
100	4.5	1	1.20	559.461	0.737
100	3.0	1	1.10	575.240	0.656
100	4.5	3	1.70	616.339	0.644

Table 8.12 Adams- Bohart parameters for manganese (II) at different conditions using linear regression analysis

Initial Concentration (mg/l)	Bed Height (cm)	Flow Rate (ml/min)	k_{AB} (L/mg-min) x 10^{-4}	N_0 (mg/l)	R^2
50	4.5	1	2.40	488.814	0.903
70	4.5	1	1.14	529.338	0.855
100	4.5	1	0.70	700.086	0.782
100	3.0	1	0.60	698.190	0.789
100	4.5	3	1.10	762.401	0.862

Adams-Bohart model is a comprehensive model for evaluating continuous flow sorption system in a column. However, its validity is restricted up to a certain extent. The poor correlation coefficient, R^2 reflects the lack of applicability of this model. Referring to the Tables 8.10-8.12, it can be observed that mass transfer coefficient increased with increase in bed height and flow rate but decreased with increase in initial concentration. This implies that the reaction kinetics was strongly influenced by external mass transfer (Ahmad *et al.,* 2010b). However, the sorption capacity N_0 increased with increasing initial concentration, flow rate and bed height for lead and manganese (Ahmad *et al.,* 2010b, Pakshiranjan and Swaminathan, 2006) but for copper increasing bed height reduced the sorption capacity slightly. Similar trend was observed for sorption of Cr (VI) onto thermally activated weed where by increasing the bed height from 2 to 4 cm, N_0 decreased significantly.

8.4. Regeneration of the Activated carbon

It is essential to reuse the cation loaded sorbent for economical feasibility of the process. The sorbent can be reused by carrying out consecutive adsorption-desorption cycles. The

regeneration efficiency of MFSAC was observed for four cycles. 1M HNO_3 acid solution was used as an eluting agent as it showed greater removal efficiency described earlier in Chaper Seven (Section 7.9). The eluting agent was passed inside the column at a flow rate of 3 ml/min for 16 hours. It was observed that, after 570 minutes, 600 minutes and 690 minutes, the elution capacity of lead, copper and manganese decreased significantly. Desorption efficiency (%) was calculated using Equation 4.14. The experimental data obtained for breakthrough time, exhaustion time and breakthrough uptake capacities (mg/g) for all the four cycles are tabulated in Table 8.13.

Referring to Table 8.13, it was observed that exhaustion time and column capacity at 50% breakthrough is decreased with each cycle. This is attributed to the undesirable effect of acid eluting agent on the surface functional groups or binding sites. At the same time, inadequate time for desorption allows the metal to be attached onto the surface of activated carbon. The sorption performance of the column was reduced. The column capacity has been found to decrease drastically after the fifth cycle for all the cations This reflects that the properties of the prepared activated carbon was detoriated due to acid treatment. Similar trend of desorption was observed in the regeneration of lead (II) by using coconut shell based granular activated carbon (Goel *et al.*, 2005). It was observed that regeneration effeciency (%) was found to be 40% after fifth cycle (Goel *et al.*, 2005).

Table 8.13 Regeneration of Column

Metal	Cycle No	Breakthrough Time (Minute)	Breakthrough Uptake (mg/g)	Bed Exhaustion time	Regeneration Efficiency (%)
Lead (II)	1	180	6.7028	630	original
	2	130	5.3243	450	79.43
	3	100	3.5658	180	53.19
	4	70	2.2987	120	34.29
Copper (II)	1	200	6.0219	660	original
	2	160	4.5434	480	75.44
	3	120	3.8767	260	64.38
	4	90	2.0988	160	34.85
Manganese (II)	1	250	7.2573	700	original
	2	200	6.2076	630	85.53
	3	160	5.4543	450	75.15
	4	180	4.8765	280	67.19

8.5 Summary

Physio-chemically activated mangostene fruit shell based activated carbon (MFSAC) was found to be a very effective sorbent for the purification of Pb (II), Cu (II) and Mn (II) contaminated synthetic aqueous solutions. The effects of different sorption parameters such as flow rate, influent concentration and quantity of sorbent on breakthrough curve characteristics of Pb (II), Cu (II) and Mn (II) cations were studied. The removal efficiency of all three cations was found to increase with an increase in sorbent amount (bed height) but decreases with an increase in both inlet concentration and flow rate of the adsorbate. The experimental data obtained here was fitted with Adams-Bohart, Thomas and Yoon-Nelson models. The shape and characteristics of the breakthrough curves were determined. Significant features of the different models such as rate constant (Adams-Bohart model), adsorption capacity (Thomas model) and time for 50% breakthrough (Yoon-Nelson model) were determined by linear regression analysis. Yoon Nelson and Thomas models were best to describe the experimental data.

Desorption and regeneration of the cation loaded adsorbent was carried out to observe the suitability of the adsorbent. Based on desorption and regeneration studies, it was concluded that the prepared adsorbent can be repeatedly use up to three cycles, after which the adsorption performance declined significantly for lead and copper. It revealed that ion exchange mechanism i.e., chemisorption dominated the sorption process in case of column mode studies. Therefore, eluting agent of 1M HNO_3 acid was chosen for regeneration purposes. The column exhaustion time for Mn(II) cations were greater than the other two cations under investigation.

CHAPTER NINE
CONCLUSIONS AND RECOMMENDATIONS

9.1 Conclusion

Based on the overall experimental observation discussed in Chapter 5, 6 7 and 8, the conclusions of the present research can be listed below:

1. The selected agricultural residues (Kenaf Core (KC), Kenaf Fiber (KF), Mangostene fruit peel (MFS) and oil palm ash (OPA)) are promising starting materials for the preparation of activated adsorbents by using Group I alkali metal hydroxide (KOH/NaOH) as a chemical activating agent.

2. The experimental design based on central composite design (CCD) clearly revealed that CO_2 activation temperature – x_1, time- x_2 and KOH impregnation ratio (IR) – x_3 were important factors influencing the adsorption performance of the powdered activated carbons (PAC) prepared from kenaf core (KC) and kenaf fiber (KF) for the adsorption of soft and border line divalent cations of Pb(II), Cu(II) and Mn(II). The effects of CO_2 activation temperature played the most significant role for producing activated carbon. However, temperature, time and impregnation ratio also showed noteworthy effects on the yields of all the powdered activated carbons prepared. Regression models were effectively developed to describe the correlation between the activated carbon preparation variables to the responses of removal percentage and yield. These models are appropriate and adequate in predicting the responses.

3. Activated ash samples were prepared from natural oil palm ash (OPA) by refluxing the sample with NaOH at different temperatures - x_1, ratios - x_2 and hydration time – x_3

based on the experimental design matrix. Regression models were also developed for activated ash (AOPA) in order to correlate the preparation variables with removal percentage of metallic cations under investigation.

4. The characterization results showed that all the powdered activated adsorbent prepared in this study had a relatively high BET surface area compared to granular activated carbon (MFSAC). The average pore diameters obtained for all the adsorbents are larger than 2.2 °A and this reflects their mesoporous nature. The SEM analyses of KCAC and KFAC proved that significant number of pores was developed during the activation process. However, a smaller number of pores was visible onto the surface of granular activated carbon (MFSAC) and activated palm ash (AOPA). Chemical composition analysis of the prepared activated carbons derived from different precursors was found to have different ultimate and proximate contents. On the contrary, significant amount of metallic oxide content was found over the surface of AOPA. FTIR analyses revealed the presence of different functional groups such as hydroxyl, carboxylate, carbonyl, alkyl and silicon oxide groups on the surfaces of the activated carbon and activated ash samples. The removal and regeneration efficiency of the prepared activated carbons were better than activated palm ash. The performances of the prepared activated adsorbents are better compared to commercial activated carbons.

5. An increase in initial cations concentrations (Pb(II), Cu(II) and Mn(II)) and contact time increased the adsorption uptakes of the activated adsorbent. However, the percent removal decreased with increasing initial concentrations. The removal efficiency of the cations onto the activated adsorbents is less below pH 4. Between pH 4-6, maximum adsorption is observed. This is attributed to the lessening of H^+ ions concentration in

solution, degree of ionization of the adsorbate species and change of the charge on the adsorbent surfaces with the change in solution pH.

6. Adsorption of all the cations onto the prepared activated adsorbent followed Type I isotherm for all the temperatures. The trend of adsorption capacity of the activated carbon followed the order of KCAC>KFAC>MFSAC for the selected cations. The order thus obtained is due to the extended surface area of the powdered activated carbon compared to the granular one. Although AOPA has a greater surface area compared to MFSAC, it still showed a slightly smaller removal percentages for all the cations. Overall, the adsorption performance of the activated carbons prepared is better than AOPA in terms of removal and regeneration efficiency.

7. Adsorption of metallic cations onto the surface of KCAC, KFAC, MFSAC and AOPA is best represented by the pseudo-second-order and Elovich kinetic models. All the adsorption processes studied were mainly governed by external mass transport where particle diffusion is the rate limiting step.

8. Different adsorbent-adsorbate systems were found to show different thermodynamic behaviors. Most of the systems under investigation show endothermic nature of sorption except for Pb (II) cations onto KCAC and Mn(II) cations onto the surface of AOPA.

9. Adsorption of Pb (II), Cu (II) and Mn (II) cations onto MFSAC is found to perform better with lower adsorbate inlet concentration, lower feed flow rate and higher activated carbon bed height for fixed-bed column. Overall, the adsorption capacity of MFSAC for Pb (II), Cu(II) and Mn(II) obtained from the fixed-bed experiments are found to be lower than the values obtained from the batch experiments for the same initial concentration used.

10. The breakthrough curve was analyzed by different models. The experimental data are well represented by Yoon- Nelson and Thomas model.

11. Desorption by using HNO_3 acid is shown to be the best possible technique for regenerating the spent activated carbon (KCAC, KFAC and MFSAC). HCl performs better as eluting agent in the case of activated ash samples (AOPA) loaded with metallic cations.

9.2 Recommendations

Some recommendations for future research are summarized below:

1. It is suggested to further evaluate the adsorption performance of the adsorbents prepared in this study for removing Pb (II), Cu (II) and Mn (II) cations from waste effluents emanating from different industrial process. This will provide insight concerning the adsorption mechanism and performance of the adsorbent which may be interfered by other components present in the effluents.

2. Competitive sorption of Pb (II), Cu (II) and Mn (II) cations in binary and ternary system should be observed for both batch and fixed bed studies. The effect of dissolved organic compounds onto the removal percentages of the selected cations should also be monitored.

3. The alkali and alkali-earth metals' cations of Na^{+}, Ca^{++} and Mg^{++} are commonly present in water. The effect of these hard cations on the removal efficiency of the

targeted metallic contaminants of Pb (II), Cu (II) and Mn (II) cations should be evaluated.

4. Palm ash should be used for fixed bed study to analyze the breakthrough curve for single and multi solute system.

5. It is recommended to modify the activated adsorbent prepared in this study with appropriate surfactants or oxidizing agents to enhance their adsorption performance since the adsorption ability of the activated carbons are found to be influenced by their surface charges and active functional groups.

6. Prepared activated carbon can be utilized to prepare ferric hydroxide loaded activated carbon composite to remove As (III) and As (IV) anions from waste water.

7. In this research, packed-bed reactor was used to prepare the activated carbons. It is recommended that fluidized-bed reactor could be used to carry out the carbonization and activation processes to ensure a more consistent temperature gradient, decrease in the pressure drop and increase in the reaction efficiency between the activating agents and the samples in order to produce activated carbons with higher yield and porosity.

8. Activated carbons with different physical and chemical characteristics are needed for different applications. It is suggested to further develop the activation methods for preparing activated carbons for the adsorption of other pollutants such as pesticides, dyes and phenolic compounds. The activation methods could be developed by changing the activating agents, activation path and operating conditions.

REFERENCES

Abdullah, K., Hussin, M.W., Zakaria, F., Muhammad, R. and Hamid Z. A. (2006). POFA: a potential cement replacement material in aerated concrete. *In Proceedings of the 6Th Asia pacific Conference on Structural Engineering and Construction*, September 5-6, 2006, B132-140, Kuala Lumpur, Malaysia.

Aber, S, Khataee, A. and Sheydaei M. (2009). Optimization of activated carbon fiber preparation from Kenaf K_2HPO_4 as chemical activator for adsorption of phenolic compounds. *Bioresource Technology*, 100, 6586-6591.

Abia, A. A., Horsfall, M. and Didi, O. (2003). The use of chemically modified and unmodified cassava waste for removal of Cd, Cu, and Zn ions from Aqueous solution. *Bioresource Technology*, 90, 345-348

Abideen, I. A., Ofudje, A.E., Mopelola, A.I. and Sarafadeen, O.K. (2011). Equilibrium kinetics and thermodynamics studies of the biosorption of Mn(II) ions from aqueous solution by Raw and acid treated corn cob Biomass. *American Journal of Applied Sciences*, 6(5), 302-309.

Achaw, O.W. and Aftane, G. (2007). The evolution of the pore structure of coconut shells during the preparation of coconut shell-based activated carbons. *Microporous and Mesoporous Materials*, 112(1-3), 284-290.

Adil, M. (2006). Preparation, modification and characterization of activated carbons for batch adsorption studies on the removal of selected metal ions. *M.Sc Thesis, University Technology, Malaysia*

Adinata, D., Wan Daud, W.M.A. and Aroua, M.K. (2007). Preparation and characterization of activated carbon from palm shell by chemical activation with K_2CO_3. *Bioresource Technology*, 98, 145-149.

Ahmad, A.A. (2006). Isotherm, Kinetics and Thermodynamic studies of Dyes adsorption from aqueous solution onto activated palm ash and Bentonite. *M.Sc Thesis, University Science Malaysia.*

Ahmad, A. A., Hameed, B.H. and Ahmad, A.L. (2009). Removal of disperse dye from aqueous solution using waste-derived activated carbon: Optimization study. *Journal of Hazardous Materials*, 170, 612–619.

Ahmad, A.A. and Hameed, B. H. (2010a). Effect of preparation conditions of activated carbon from Bamboo Waste for Real Textile wastewater. *Journal of Hazardous Materials*, 173, 487–493.

Ahmad, A. A. and Hameed, B.H. (2010b). Fixed bed adsorption of reactive azo dye onto granular activated carbon prepared from waste. *Journal of Hazardous Materials*, 175, 298–303.

Ahmedna, M., Marshall, W.E. and Rao, R.M. (2000). Production of granular activated carbons from select agricultural by-products and evaluation of their physical, chemical and adsorption properties. *Bioresource Technology*, 71, 113-123.

Ahrland, S., Chatt, J., and Davies, N. R. (1958). The Relative Affinities of Ligand Atoms for Acceptor Molecules and Ions. *Quarterly Reviews of the Chemical Society* XII (3), 265-276.

Ahmaruzzaman, M. (2010). A review on the utilization of fly ash. *Progress in Energy and Combustion Science*, 36, 327-363.

Aksu, Z. and Gonen, F. (2004). Biosorption of phenol by immobilized activated sludge in a continuous packed bed prediction of breakthrough curves. *Process Biochemistry*, 39, 599-613.

Alam, M.Z., Muyibi, S.A., Mansor, M.F. and Wahid, R. (2007a). Activated carbons derived from oil plam empty-fruit bunches: Application to environmental problems. *Journal of Environmental Science*, 19, 103-108.

Alam, Z., Muyibi, S.A. and Toramae, J. (2007b). Statistical optimization of adsorption processes for removal of 2,4-dichlorophenol by activated carbon derived from oil palm empty fruit bunches. *Journal of Environmental Sciences*, 19, 674-677.

Alfarra, A., Frackowiak, E., and Béguin, F. (2004). The HSAB Concept as a Means to Interpret the Adsorption of Metal Ions Onto Activated Carbons. *Applied Surface Science,* 228, 84-92.

Ali, M. F., Heng, L. Y., Ratnam, W., Nais, J. and Ripin, R. (2004). Metal distribution and contamination of the Mamut River Malaysia caused by Copper Mine Discharge. *Bulletin of Environmental Contamination and Toxicology*, 73, 535-542.

Allen, S.J. and Koumanova, B. (2005). Decolourisation of water/wastewater using adsorption (review). *Journal of the University of Chemical Technology Metallurgy*, 40, 175-192.

Althoman, Z. A., Habila, M.A. and Ali, R. (2011). Preparation of activated carbon using the copyrolysis of agricultural municipal solid wastes at a low carbonization temperature. *International conference on Biology, Environment and Chemistry, IPCBEE*, vol 24 (2011) IACSIT Press, Singapore.

Al-Qodah, Z. and Lafi., W. (2003). Adsorption of reactive dyes using shale oil ash in fixed beds. *Journal of Water Supply: Research and Technology*, 52, 189-198.

Anirudhan, T. S., Shukla, K. P. and Raji, C. (2001). Immobilization of heavy metals from aqueous solutions using polyacrylamide grafted hydrous tin (IV) oxide gel having carboxylate functional groups. *Water Research*, 35(1), 300–310.

Annadurai, A., Juang, R. S., and Lee D. J. (2003). Adsorption of heavy metals from water using banana and orange peels, *Water Science Technology*, 47, 185-190.

Apak, R., Tutem, E., Hugul, M. and Hijal J., (1998). Heavy metal cation retention by unconventional sorbents (Red mud and fly ases), *Water Research*, 32, 430-440.

Arami, M., Limaee, N:Y., Mahmoodi, N.M. and Tabrizi, N.S. (2005). Removal of dyes from colored textile wastewater by orange peel adsorbent: Equilibrium and kinetic Studies. *Journal of Colloid and interface Science*, 288, 371-376.

Ashraf, M. A., Jamil Maah, M. and Yusoff, I.B. (2010). Study of water quality and heavy metals in soils & water of Ex-mining area Bestari Jaya, Peninsular, Malaysia. *International journal of Basic & Applied Sciences*, 10(3), 7-17.

Attia, A.A., Girgis, B.S. and Fathy, N.A. (2008). Removal of methyiene blue by carbons derived from peach stones by H_3PO_4 activation: Batch and column studies. *Dyes and Pigments*, 76, 282-289.

Aygun, A., Yenisoy-Karakas, S. and Duman, I. (2003). Production of granular activated carbon from fruit stones and nutshells and evaluation of their physical, chemical and adsorption properties. *Microporous and Mesoporous Materials*, 66, 189-195.

Ayyappan, R., Carmalin-Sophia, A., Swaminathan, K. and Sandhya, S. (2005). Removal of Pb (II) from aqueous solution using carbon derived from agricultural wastes, *Process Biochemistry*, 40, 1293-1299

Azargohar, R. and Dalai, A.K. (2005). Production of activated carbon from Luscar char: Experimental and modeling studies. *Microporous and Mesoporous Materials*, 85, 219-225.

Azargohar, R. (2009). Production of Activated Carbon and its Catalytic application for oxidation of hydrogen sulphide. *PhD Thesis. University of Saskatchewan, Saskatoon, Canada.*

Azevedo, D.C.S., Araujo, J.C.S., Bastos-Neto, M., Torres, A.E.B., Jaguaribe, EF and Cavalcante, C.L. (2007). Microporous activated carbon prepared from coconut shells using chemical activation with zinc chloride. *Microporous and Mesoporous Materials*, 100, 361-364

Azmal, M., Khan, A. H., Ahmad, S. and Ahmad, A. (1998). Role of sawdust in the removal of Cu(II) from Industrial wastes. *Water Research*, 32, 3085-3091.

Babel, S. and Kurniawan, T. A (2003). Low-cost adsorbents for heavy metals uptake from contaminated water: A review. *Journal of Hazardous Materials*. B97, 219-243.

Bacaoui, A., Yaacoubi, A., Dahbi, A., Bennouna, C., Phan Tan Luu, R., Maldonado-Hodar, F.J., Rivera-Utrilla, J. and Moreno-Castilla, C. (2001). Optimization of conditions for the preparation of activated carbons from olive-waste cakes. *Carbon*, 39, 425-432.

Badmus, M.A.O, Audu, T.O.K. and Anyata, B.U. (2007). Removal of lead ion from industrial waste waters by activated carbon prepared from Periwinkle shells (*Typanotonus fuscatus*). *Turkish Journal of Engineering Environmental Science*, 31, 251-263.

Baes, A. U., Umali, S. J. P. and Mercado, R. L. (1996). Ion exchange and adsorption of some heavy metals in a modified coconut coir cation exchanger. *Water Science Technology*, 34, 193-200.

Balachandran M. (2004). Studies on Magnetic Iron Oxide loaded activated carbon. PhD Thesis, *Cochin University of Science and Technology, Cochin.*

Banerje, S. and Dastidar, M. G. (2005). Use of jute processing wastes for treatment of wastewater contaminated with dye and other organics. *Bioresource Technology*, 96, 1919-1928.

Bansode, P. R., Losso, J. N., Marshall, W. E., Rapo, R. M. and Portier, R. J. (2003). Adsorption of metal ions by pecans shell-based granular activated carbons. *Bioresource Technology*, 89, 115-119

Baral, S. S., Das, N., Ramulu, T. S., Sahoo, S. K., Das, S. N., and Chaudhury, G. R. (2009). Removal of Cr(VI) by thermally activated weed *Salvinia cucullata* in a fixed bed column. *Journal of Hazardous Materials*, 161, 1427-1435.

Basavo Rao, V.V. and Ram Mohon Rao, S. (2006). Adsorption studies on treatment of textile dyeing industrial effluent by fly ash. *Chemical Engineering Journal*, 116, 77-84.

Beh, C. I., Chuah, L., and Choong, T.S.Y. (2010). Adsorpption study of electric arc furnace slag for the removal of manganese from solution. *American Journal of Applied Sciences*, 7(4), 442-446.

Birbas, D. (2011). Preparation of activated carbon:Forest Residues activated with Phosphoric acid and Zinc Sulfate. *MSc. Thesis, Royale Institute of Technology 9KTH), Stockholm, Sweden.*

Bhattacharyya, K. G. and Sharma, A. (2003). Adsorption Characteristics of the dye, Brilliant Green on neem leaf powder. *Dyes and Pigments*, 57, 211-222.

Bharrathi, K. S., Badabhagni N., Nidheesh, P. V., Gandhimathi, R. and Ramesh, S.T. (2011). Breakthrough data analysis of adsorption of Cd(II) on coir pith column. *Electronic Journal of Environmental, Agriculture and Food Chemistry*. 10(8), 2638-2658.

Biofuels and Bio energy Information-Energy Saving Trust (2007) [Online]. [Accessed 1st December;2007].http://www.energysavingtrust.org.uk/generate_your_own_energy/types_of_renewables/biomass

Bohart G.C. and Adams, E. Q. (1920). Some aspect of the behavior of charcoal with respect to chlorine. *Journal of American Chemical Society*, 42, 523-529.

Boonamnuayvitaya, V., Sae-Ung, S. and Tanthapanichakoon, W. (2005). Preparation of activated carbons from coffee residue for the adsorption of formaldehyde. *Separation and Purification Technology*, 42, 159-168.

Bouchelta, C., Medjram, M.S., Bertrand, O. and Bellat, J.P. (2008). Preparation and characterization of activated carbon from date stones by physical activation with steam. *Journal of analytical and applied Pyrolysis*, 82, 70-77.

Brunauer, S., Emmet, P. H. and Teller, E. (1938). Adsorption of gases in multimolecular layers. *Journal of American Chemical Society*, 60, 309-319.

Burkert, J.F.M., Maugeri, F. and Rodrigues, M.I. (2004). Optimization of extracellular lipase production by Geotrichum sp. using factorial design. *Bioresource Technology*, 91, 77-84.

Bulut, Y. and Tez Zeki (2007). Removal of heavy metals from aqueous solution by sawdust adsorption. *Journal of Environmental Science*, 19, 160-166.

Cadena, F., Rizvi, R. and Peters R.W.(1990). Feasibility studies for the removal of heavy metals from solution usingtailored Bentonite. *In Hazardous and Industrial Wastes Proceedings of the Twenty Second Mid-Atlantic Industrial Waste Conference*. Drexel University, pp 77-94.

Cao, Q., Xie, K.C., Lv, Y.K. and Bao, W.R. (2006). Process effects on activated carbon with large specific surface area from corn cob. *Bioresearch Technology*, 97, 110-115.

Cay, S., Uyanik, A. and Ozai, K. A. (2004). Single and binary component adsorption of Cu (II) and Cd(II) from aqueous solutions using tea-industry waste. *Separation Purification Technology*, 38, 273-280

Cetinkaya, S., Sakintuna, B.V. and Yurtim, Y. (2003). Formation of crystal structures during activated carbon production from Turkish elbistan lignite. Fuel Chemistry Division Preprints, 48 (1), 67-69.

Chan, N. W., Anisah, L. A., Ab Latif I. and Suriati, G., (2003). River Pollution and Restoration towards sustainable water resources management in Malaysia. River Pollution and Restoration towards Sustainable Water Resources Management, 208-219. http:// eprints.utm.my/2533/1/ River-2003-Chan.pdf.

Chandra, T.C., Mirna, M.M., Sudaryanto, Y. and Ismadji, S. (2007). Adsorption of basic dye onto activated carbon prepared from durian shell: Studies of adsorption equilibrium and kinetics. *Chemical Engineering Journal*, 127, 121-129.

Chen, J. P., and Wang, X. (2000). Removing Copper, Zinc, and Lead Ion by Granular Activated Carbon in Pretreated Fixed-Bed Columns. *Separation Purification Technology,* 19, 157-167.

Cimino, G., Passerini, A. and Toscano, G. (2000). Removal of toxic cations and Cr (VI) from aqueous shell by hazelnut shell. *Water Research*, 34, 2955-2962.

Conrad, K. and Hansen, H. C. B. (2007). Sorption of Pb(II) and zinc on coir. *Bioresource Technology*, 98, 89-97.

Corapcioglu, M. O. and Huang, C. P. (1987). The Adsorption of Heavy Metals onto Hydrous Activated Carbon. *Water Research,* 21, 1031-1044.

Cooney and David, O. (1999). *Adsorption Design for Waste Water Treatment*, 2nd edition, 1999, Lewis Publisher CRC Press, Boca Raton, Florida.

Crini, G. (2006). Non-Conventional Low-cost adsorbents for dye removal: A review. *Bioresearch Technology* 97, 1061-1085.

Dabrowski, A. (2001). Adsorption from theory to practice. *Advance in Colloid Interface Science*. 93, 135-224.

Dahlan, I., Lee, K. T., Kamaruddin, A.H. and Mohamed, A. R. (2009). Evaluation of various additives on the preparation of rice husk ash (RHA)/CaO-based sorbent for flue gas desulfurization (FGD) at low temperature. *Journal of Hazardous Materials*, 161, 570-574.

Dahlan, I. Ahmad, Z. Fadly, M., Lee, K. T., Kamaruddin, A. H. and Mohammed, A. R. (2010). Parameters optimization of rice husk ash (RHA)/CaO/CeO2 sorbent for predicting SO2/NO sorption capacity using response surface and neural network models. *Journal of Hazardous Materials*, 178(1-3), 249-257.

Dastgheib, S. A. and Rockstraw, D. A. (2001). Pecan Shell Activated Carbon: Synthesis, Characterization, and Application for the Removal of Copper from Aqueous Solution. *Carbon.* 39: 1849-1855.

Datchaneekul, K. (2005). Removal of heavy metals in synthetic waste water by adsorption on Bentonite. *MSc. Thesis, Mahidol University, Thailand.*

Daud, W.M.A. and Ali, W.S.W. (2004). Comparison on pore development of activated carbon produced from palm shell and coconut shell. *Bioresource Technology*, 93, 63-69.

Davini, P. (1996). Investigation of the SO_2 adsorption properties of $Ca(OH)_2$- fly ash system. *Fuel*, 75(6), 713-716.

Dias, J.M., Alvim-Ferraz, M.C.M., Almeida, M.F., Rivera-Utrilla, J. and Sanchez-Polo, M. (2007). Waste materials for activated carbon preparation and its use in aqueous-phase treatment: A review. *Journal of Environmental Management*, 85, 833-846.

Didem, O. and Mericboyu, A. E. (2009). Removal of copper from aqueous solutions by adsorption onto chestnut shell and grapeseed activated carbons. *Journal of Hazardous Materials*, 168, 1118–1125.

Dinesh, S. (2011). Development and characterization of pellet activated carbon from new precursor. *BSc. Thesis, National Institute of Technology, Rourkela, India.*

Do, D.D. (1996). A Model for Surface Diffusion of Ethane and Propane in Activated Carbon. *Chemical Engineering Science,* 51(17), 4145-4158.

Dorris, K. L., Zhang, Y. and Shukla A. *et al*., (2000). The removal of heavy metal from aqueous solutions by sawdust adsorption removal of copper. *Journal of Hazardous Materials*, B80, 33–42.

Duvnjak, Z, Al-Asheh, S. (1998). Binary metal sorption by pine bark: Study of equilibria and mechanisms. *Separation Science and Technology*, 33(9), 1303–1329.

Eckenfelder, W.W. (2000). Industrial Water Pollution Control. *MacGraw Hill Companies, USA.*

Egila, J.N., Dauda, B.E.N., Iyaka, Y.A. and Jimoh T. (2011). Agricultural waste as low cost adsorbent for metal removal from waste water. *International Journal of Physical Sciences*, 6(8), 2152-2157.

El-Hendawy, A.N.A. (2005). Surface and adsorptive properties of carbons prepared from biomass. *Applied Surface Science,* 252, 287-295.

Elizalde-Gonzalez, M.P. and Hetnandez-Montoya, V. (2007). Characterization of manage pit as raw material in the preparation of activated carbon for wastewater treatment. *Biochemical Engineering Journal*, 36, 230-238.

El Qada, E. N., Allen, S.J. and Walker, G.M. (2006). Adsorption of Methylene Blue onto activated carbon produced from steam activated bituminous coal: A Study of equilibrium adsorption isotherm. *Chemical Engineering Journal,* 124, 103-110,

El Qada, E. N. Allen, S.J. and Walker, G.M. (2008). Adsorption of basic dyes from aqueous solution onto activated carbons. *Chemical Engineering Journal*, 135, 174-184.

El-Guendi, M. (1991). Homogeneous surface diffusion model of basic dyestuffs onto - natural clay in batch adsorbers. *Adsorption Science and Technology*, 8, 217-225.

Emmanuel, K. A. and Rao, A. V. (2009). Comparison study on adsorption of Mn(II) from aqeous solution on various activated carbon. *E Journal of Chemistry*, 6(3), 693-704.

Farrah, H., Halton, D. and Pickering, W.F., (1980). The affinity of metal ions for clay surfaces. *Chemical Geology,* 28, 55–68.

Farkas, A., Claudio, E. and Luigi, V. (2007). Assessment of the environmental significance of heavy metal pollution in superficial sediments of the River Po. *Chemosphere*, 68, 761-768.

Feng, Q., Lin, Q., Gong, F., Sugita, S., and Shoya, M. (2004). Adsorption of lead and mercury by rice husk ash. *Journal Colloid Interface Science*, 278, 1-8.

Fiol, N., Villaescusa, I., Martinez, M., Miralles, N., Poch, J. and Serarols, J. (2006). Sorption of Pb(II), Ni(II), Cu(II) and Cd (II) from aqueous solution by olive stone waste. *Separation Purification Technology*, 50, 132-140.

Fiore, S., and Zanetti, M. C. (2009). Sorption of Phenols: Influence of Groundwater pH and Soil Organic Carbon Content. *American Journal of Environmental Science*, 5(4), 546-554.

Freundlich, H.M.F. (1906). Over the adsorption in solution. *Journal of Physical Chemistry*, 57, 385-470.

Foo, K.Y. and Hameed, B.H. (2009). Value-added utilization of oil palm ash: A superior recycling of the industrial agricultural waste. *Journal of Hazardous Materials*, 172 , 523–531.

Fytianos, K., Voudrias, E. and Kokkalis, E. (2000). Sorption-desorption behaviour of 2, 4-dichlorophenol by marine sediments. *Chemosphere*, 40, 3-6.

Gaballah, I. and Kilbertus, G. (1998). Recovery of heavy metal ions through decontamination of synthetic solutionss and industrial effluents using modified barks. *Journal of Geochemical Exploration*, 62, 241–286.

Gercel, O., Ozcan, A., Ozcan, A.S. and Gercel, H.F. (2007). Preparation of activated carbon from a renewable bio-plant of Euphorbia rigida by H_2SO_4 activation and its adsorption behavior in aqueous solutions. *Applied Surface Science*, 253, 4843-4852.

Gergova, K. A., Galushko N. and Minkova, V. (1993). Investigation of the porous structure of activated carbons prepared by pyrolysis of agricultural by-products in a stream of water vapor. *Carbon*, 30(5), 721-727.

Gharaibeh, S.H., Abu-El-Sha'r, W.Y. and Al-Kofahi, M.M. (1998). Removal of selected heavy metals from aqueous solutions using processed solid residue of olive mill products. *Water Research*, 32 (2), 498–502.

Girgis, B.S., Yunis, S.S. and Soliman, A.M. (2002). Characteristics of activated carbon from peanut hulls in relation to conditions of preparation. *Materials Letters*, 57, 164-172.

Girgis, B.S. and El-Hendawy, A. N. A. (2002). Porosity development in activated carbons obtained from date pits under chemical activation with phosphoric. Acid *Microporous and Mesoporous Materials*, 52, 105-117.

Goel, J., Kadirvelu, K., Rajagopal, C., and Carg, V. K. (2005). "Removal of Pb(II) by adsorption using treated granular activated carbon: batch and column studies," *Journal of Hazardous Materials*, B 125, 2l1-210.

Gosset, T., Trancart, J. L. and Thevenot D. R. (1986). Batch metal removal by peat kinetics and thermodynamics. *Water Research*, 20, 21–26.

Guo, J. and Lua, A.C. (2000). Preparation of activated carbons from oil-palm-stone chars by microwave-induced carbon dioxide activation. *Carbon*, 38, 1985-1993.

Guo, J. and Lua, A.C. (2002). Characterization of adsorbent prepared from oil-palm shell by CO_2 activation for removal of gaseous pollutants. *Materials Letter*, 55, 334-339.

Guo, J. and Lua, A.C. (2003). Textural and chemical properties; of adsorbent prepared from palm shell by phosphoric acid activation. *Materials Chemistry and Physics*, 80, 114-119.

Guo, Y., Zhao, J., Zhang, H., Yang, S., Qi, J., Wang, Z. and Xu, H. (2005). Use of rice husk-based porous carbon for adsorption of Rhodamine B from aqueous solutions. *Dyes and Pigments*, 66, 123-128.

Guo, Y. and Rockstraw, D.A. (2007). Physicochemical properties of carbons prepared from pecan shell by phosphoric acid activation. *Bioresearch Technology*, 98, 1513-1521.

Gupta, V. K. and Ali, I. (2004). Removal of lead and chromium from wastewater using bagasse fly ash—a sugar industry waste, *Journal of Colloid and Interface Science*, 271, 321-328.

Habib, A., Islam, N., Islam, A. and Shafiqul Alam, A. M. (2007). Removal of Copper from Aqueous Solution Using Orange Peel, Sawdust and Bagasse. *Pakistan Journal Analytical Environmental Chemistry*, 8(1 & 2), 21 -25.

Haghseresht, F. and Lu, G. (1998). Adsorption characteristic of phenolic compounds onto coal-reject-derived adsorbents. *Energy Fuels*, 12, 1100-1107.

Hamdaoui, O. Naffrechoux, E., Suptil, J. and Fachinger, C. (2005). Ultrasonic desorption of p-chlorophenol from granular activated carbon. *Chemical Engineering Journal*, 106, 153-161.

Hameed B.H., Tan, A. W. and Ahmad, A. A. (2008). Optimization of basic dye removal by oil palm fiber based activated carbon using response surface methodology. *Journal of Hazardous Materials*, 158, 324-332.

Hassler, J.W. (1974). Purification with activated carbon: Industrial commercial Environmental, New York: Chemical Publishing Co., Inc.

Hayashi, J.I., Horikawa, T., Muroyama, K. and Gomes, V.G. (2002). Activated carbon from chickpea husk by chemical activation with K_2CO_3: preparation and characterization. *Microporous and Mesoporous Material*, 55, 63-68.

Henning, K.D. and Degel, J. (1990). Purification of air, water and off gas. [Online], (Accessed 15th August 2011]. Available from world wide web: http://www.activated-carbon.com/solrec3.html

Ho, Y.S., Wase, D.A.J. and Forster, C.F. (1994).The adsorption of divalent copper ions from aqueous solution by sphagnum moss peat. *Trans IChemE Part B*, 17,185–194.

Ho, Y.S. and Mckay, G. (1998). Sorption of dye from aqueous solution by peat. *Chemical Engineering Journal*, 70, 115-124,

Ho, Y.S. and McKay, G. (1999). The sorption of Lead (II) on peat. *Water Research*, 33, 578-584.

Hollman G. G., Steenbruggen, G. and Janssen, M. J. (1999). A two step process for synthesis of zeolite from coal fly ash. *Fuel*, 78, 1225-1230.

Hsu, T. C., Yu, C. C. and Yeh, C. M. (2008). Adsorption of Cu(II) from water using raw and modified coal fly ashes. *Fuel*, 87, 1355-1359.

Hu, Z. and Srinivasan, M.P. (2001). Mesoporous high-surface-area activated carbon. *Micraporous and Mesoporous Materials*, 43, 267-275.

Inbaraj, B.S. and Sulochana, N. (2002). Basic Dye adsorption on a low cost carbonaceous sorbent. *Indian journal of Chemical Technology*, 9, 201-210.

loannidou, O. and Zabaniotou, A. (2007). Agricultural residues as precursors for activated carbon production-A review. *Renewable and Sustainable Energy reviews,* 11, 1966-2005.

Ismadji, S. and Bhatia, S. K. (2001). Characterization of activated carbons using liquid phase adsorption. *Carbon*, 39, 1237-1250.

IUPAC (1972). IUPAC Manual of Symbols and Terminology. *Pure and Applied Chemistry*, 31, 587.

IUPAC Technical Report. (2002). “Heavy Metals”-A Meaningless Term- *Pure Applied Chemistry*, 74 (5), 793-807.

Iyer R. S. and Scott J. A. (2001). Power station fly ash-a review of value added utilization outside of the construction industry. *Resourse Conservation Recycling*, 31, 217-228.

Johns, M. M., Marshall, W. E., and Toles, C. A. (1998). Agricultural by-Products as Granular Activated Carbons for Adsorbing Dissolved Metals and Organics. *Journal of Chemical Technology & Biotechnology,* 71, 131-141.

Johnson, P. D., Watson, M. A., Brown, J. and Jefcoat, I. A. (2002). Peanut hull pellets as a single use sorbent for the capture of Cu (II) from wastewater. *Waste Management*, 22, 471-480

Johnson, T. A., Jain, N., Joshi, H. C. and Prasad, S. (2008). Agricultural and agro-processing wastes as low cost adsorbent for heavy metal removal from waste water: A Review. *Journal of Scientific and Industrial Research*, 67, 647-658.

Jung, M.W., Ahn, K.H, Lee, Y., Kim, K.P., Rhee, J.S., Tae Park, J. and Paeng, K.J. (2001). Adsorption characteristic of phenol and chlorophenols on granular activated carbons (GAC). *Microchemical Journal*, 70, 123-131.

Kadirvelu, K., Kavipriya, M., Karthika, C., Vennilamani, N. and Pattabhi, S. (2004). Mercury (II) adsorption by activated carbon made from sago waste. *Carbon,* 42. 745-752

Kalavathy, M, H., Karthikeyan, T, Rajgopal, S. and Miranda, L.R. (2005). Kinetic and isotherm studies of Cu(II) adsorption onto H_3PO_4 activated rubber wood sawdust. *Journal of Colloid and Interface Science*, 292, 354-362.

Kamishita, M., Mahajan, O.P. and Walker, P.L. (1977). Effect of carbon deposition on porosity and reactivity of lignite char. *Fuel*, 56, 444-450.

Karagoz, S., Tay, T., Ucar, S. and Erdem, M. (2008). Activated carbons from waste biomass by sulfuric acid activation, and their use on methylene blue adsorption. *Bioresource Technology*, 99(14),6214-6222.

Karagozoglu, B., Tasdemir, M., Demirbas, E. and Kobya, M. (2007). The adsorption of basic dye (Astrazon Blue FGRL) from aqueous solutions onto sepiolite, fly ash and apricot shell activated carbon: Kinetic and equilibrium studies. *Journal of Hazardous Materials*, 147,297-306.

Karacan, F., Ozden, U. and Karacan, S. (2007). Optimization of manufacturing conditions for activated carbon from Turkish lignite by chemical activation using response surface methodology. *Applied Thermal Engineering*, 27, 1212-1218

Karthikeyan, T., Rajgopal, S. and Miranda, L.R. (2005). Chromium(VI) adsorption, from aqueous solution by *Hevea Brasilinesis* sawdust activated carbon. *Journal of Hazardous Materials*, 124, 192-199.

Kaur, A., Malik, A.K., Verma, N. and Rao, A.L.J. (1991). Removal of copper and lead from wastewater by adsorption on bottom ash. *Indian Journal of Environmental Protection*, 11, 433–435.

Kavitha, D. and Namasivayam, C. (2007). Experimental and kinetic studies or, methylene blue adsorption by coir pith carbon. *Bioresource Technology*, 98, 14-21.

Kennedy, L.J., Vijaya, J.J., Kayalvizhi, K. and Sekaran, G. (2007). Adsorption of phenol from aqueous solutions using mesoporous carbon prepared by two stage process. *Chemical Engineering Journal* 132. 279-287.

Keskinkan, O., Goksu, M.Z.L., Yuceer, A., Basibuyuk, M. and Foster, C. F. (2003). Heavy metal adsorption characteristics of a submerged aquatic plant (*Myriophylamspirntum*). *Process Biochemistry*, 39, 179-183.

Khalili, N.R., Campbell, M., Sandi, G. and Golas, J. (2000). Production of microand mesoporous activated carbon from paper mill Effect of zinc chloride activation. *Carbon.* 39, 1905-1915

Khalid, N., Ahmad, S., Kiani, S. N. and Ahmed, J. (1998). Removal of lead from aqueous solution using rice husk. *Separation Science Technology*, 33, 2349-2362.

Kiran, B. and Kaushik, A. (2008). Cyanobacterial biosorption of Cr (VI): Application of two parameter and Bohart Adams models for batch and column studies. *Chemical Engineering Journal*, 144, 391-399.

Krishnan, K. A., and Anirudhan, T. S. (2002). Uptake of Heavy Metals in Batch Systems by Sulfurized Steam Activated Carbon Prepared from Sugarcane Bagasse Pith. *Industrial &. Engineering Chemistry Research,* 41, 5085-5093.

Kudesia V. P., (2000). Environmental Chemistry, *Pragati Prakasan, Merrut, pp 114-150*.

Kula, I., Ugurlu, M., Karaoglu, H, and Celik, A. (2008): Adsorption of Cd(II) ions from aqueous solutions using activated carbon prepared from olive stone by $ZnCl_2$ activation. *Bioresource Technology*, 99, 492-501.

Kumar, K.V. and Kumaran, A. (2005). Removal of methylene blue by mango seed kernel powder. *Biochemical Engineering Journal*, 27, 83-93.

Lafi, W. K. (2001). Production Of activated carbon from acorns and seeds. *Biomass and Bioenergy*, 20, 57-62.

Langergren, S. and Svenska, B. K. (1898); Zur theorie der sogenannten adsorption geloester stoffe. Veternskapsakad Nandlingar, 24, 1-39.

Langmuir, I. (1918), The adsorption of gases on plan surfaces of glass, mica and platinum. *Journal of the American Chemistry Society*, 40, 1361.

Larsen, V. J. and Schhierup, H. H. (1981). The use of straw for removal of heavy metals from waste water. *Journal of Environmental Quality,* 10, 188-193.

Lee, J., Ye, L., Landen, W.O. and Eitenmiller, R. R. (2009). Optimization of an extraction, procedure for the quantification of vitamin E in tomato broccoli using response surface methodology. *Journal of Food Composition Analysis*, 13 45-57.

Leimkuehler, E. P. (2010). Production, characterization and applications of activated carbon. *MSc. Thesis, University of Missouri, Missouri.*

Lim, J. L. and Okada, M. (2005). Regeneration of granular activated carbon using ultrasound. *Ultrasonic Sonochemistry,* 12, 277-282.

Lin, C. J. and Chang, J. E. (2001). Effects of Fly ash characteristics on the removal of Cu(II) from aqueous solution. *Chemosphere*, 44, 1185-1192.

Lin, S.H. and Juang, R. S. (2002). Heavy metal removal from waste water by surfactant modified montmorrilonite. *Journal of Hazardous Materials*, B92, 315-326.

Lizaman, C., Freer, J., Baeza, J. and Mansilla, H. D.(2002).Optimized photodegradation of Reactive Blue 19 on TiO_2 and ZnO suspensions. *Catalysis Today*, 76, 235-246.

Lopez-Delgado, A., Perez, C. and Lopez, F.A., (1996). The influence of carbon content of blast furnaces sludges and coke on the adsorption of lead ions from aqueous solution. *Carbon*, 34, 423– 426.

Low, K. S., Lee, C. K. and Lee, A. C. (1995). Removal of metals from electroplating waste using banana pith, *Bioresource Technology*, 51, 227-231.

Low, K. S., Lee, C. K. and Wong, S. L. (1995). Effect of dye modification on the sorption of Cu (II) by coconut husk. *Environmental Technology*, 16, 877-883.

Lu, Q. and Sorial, G.A. (2004). Adsorption of phenolics on activated carbon-impact of pore size and molecular oxygen. *Chemosphere*, 55, 671-679.

Lua, A.C. and Yang, T. (2004). Effect of activation temperature on the textural and chemical properties of potassium hydroxide activated carbon prepared from pistachio-nut shell. *Journal of Colloid and Interface Science*, 274, 594-601.

Lua, A.C., Lau, F.Y. and Guo, J. (2006). Influence of pyrolysis conditions on pore development of oil palm shell activated carbons. *Journal of Analytical and applied Pyrolysis*, 76, 96-102.

Lua, D., Caob, Q., Caoa, X. and Luoa, F. (2009). Removal of Pb(II) using the modified lawny grass: Mechanism, kinetics, equilibrium and thermodynamic studies. *Journal of Hazardous Materials*, 166, 239-247.

Malkoc, E., Nuhoglu, Y. and Abali, Y. (2006). Cr (VI) adsorption by waste acorn Quercus ithaburensis in fixed beds: Prediction of breakthrough curves. *Chemical Engineering Journal*, 119, 61-68.

Maarof, H. I. (2004). Removal of phenolic compounds from aqueous solution by adsorption on modified montmorillonite. *MSc Thesis, University Sains Malaysia.*

Marshall, W. E., Wartelle, L. H., Boler, D. E., Johns, M. M. and Toles, C. A. (1999). Enhanced metal adsorption by soybean hulls modified with citric acid. *Bioresouce Technology*, 69, 263-268

Martirena, F., Middendrof, B., Day, R. L., Gehrke, M., Roque, P. and Martinez, L. (2006). Rudimentary-low tech incinerators as a means to produce reactive pozzolan out of sugar cane straw. *Cement and Concrete Research*, 36, 1056-1061.

Martin, M.J., Artola, A., Balaguer, M.D. and Rigola, M. (2003). Activated carbons developed from surplus sewage sludge for the removal of dyes from dilute aqueous solutions. *Chemical Engineering Journal*, 94, 231-239.

Martinez, M.L., Torres, M.M., Guzman, C.A. and Maestri, D.M. (2006). Preparation and characteristics of activated carbon from olive stones and walnut shells. *Industrial Crops and Products*, 23, 23-28.

Mattson, J.S. and Mark H.B. (1971). *Activated Carbon Surface Chemistry and Adsorption from Solution*, Marcell Dekker, New York.

McLelland, J.K. and Rock, C.A. (1988). Pretreating landfill leachate with peat to remove metals. *Water, Air and Soil Pollution*, 37, 203-215.

Mehta, P. K. (1989). Pozzolanic and cementitous by products in concrete-a look at silica fume, slag and natural pozzolans in concrete. *In: Proceedings of the 3rd International Conference of American Concrete Research Institute*, Detroit, pp. 1-43.

Merrill, D. T., Maltby C.V., KahmarkK., Gerhardt m., and Melecer H. (2001). Evaluating treatment process to reduce metals concentration in in pulp and paper mill waste waters to extremely low values. *Tappi Journal*, 84, 52-58.

Mellah, A., Chegrouche, S. and Barkat, M. (2006). The removal of uranium (VI) from aqueous solutions onto activated carbon: kinetic and thermodynamic investigations. *Journal of Colloid and Interface Science*, 296, 434-441.

Meunier, N., Jerome, L., Jean-Francois, B. and Tyagi, R. D. (2003). Lead removal from acidic solution by sorption on cocoa shells, effect of some parameters. *Journal of Environmental Engineering*, 129, 693-698.

Mittal, A., Gajbe, V. and Mittal, J. (2008). Removal and recovery of hazardous triphenylmethane dye, Methyl. Violet through adsorption over granulated waste materials. *Journal of Hazardous Material*, 150, 364-375.

Mohanty, K., Das. D. and Biswas, M.N. (2005). Adsorption of phenol from aqueous solution using activated carbon from *Tectona grandis* sawdust by $ZnCl_2$ activation. *Chemical Engineering Journal*, 115, 121-131.

Mohan S. and Sreelakshmi G. (2008). Fixed Bed column study for heavy metal removal using phosphate treated rice husk. *Journal of Hazardous Materials*, 153, 75-82.

Mohd Din A. T. (2005) preparation, characteristic and adsorption performance of mesoporous activated carbons prepared from biomass. *MSc thesis, University Science Malaysia.*

Mondal, M.K. (2009). Removal of Pb(II) ions from aqueous solution using activated tea waste: Adsorption on a fixed-bed column. *Journal of Environmental Management*, 90, 3266-3271.

Montgomery, D.C. (2001). Design and Analysis of Experiments. *John Wiley and Sons, New York.*

Moreno J.C., Gómez R. and Giraldo L., (2010). Removal of Mn, Fe, Ni and Cu Ions from Wastewater Using Cow Bone Charcoal. *Materials*, 3, 452-466

Moreno-Castilla, C. (2004). Adsorption of organic molecules from aqueous solutions on carbon material. *Carbon*, 42. 83-94.

Mourao, P.A.M., Carrott, P.J.M. and Ribeiro Carrott, M.M.L. (2006) Application of different equations to adsorption isotherms of phenolic compounds on activated carbons prepared from cork. *Carbon*, 44, 2422-2429.

Myers, R.H. and Montgomery, D.C. (1995). Response Surface Methodologn: Process and Product Optimization Using Designed Experiments. *John Wiley and Sons, New York.*

Namane, A., Mekarzia, A., Benrachedi, K., Belhaneche-Bensemra, N. and Hellal, A. (2005). Determination of the adsorption capacity of activated carbon made from coffee grounds by chemical activation with $ZnCl_2$ and H_3PO_4. *Journal of Hazardous Materials*, 119, 189-194.

Namasivayam, C. and Yumuna R.T. (1995). Waste biogas residual slurry as an adsorbent for the removal of Pb(II) from aqueous solution and radiator manufacturing waste water. *Bioresource Technology*, 52, 125-131.

Namasivayam, C. and Kadirvelu, K. (1997). Agricultural solid waste for removal of heavy metals: adsorption of Cu(II) by coir pith carbon, *Chemosphere*, 34, 377-399.

Namasivayam, C. and Sangeetha, D. (2008). Application of coconut coir pith for the removal of sulfate and other anions from water. *Desalination*, 219, 1-13.

Naja, G. and Volesky, B. (2006). Behavior of the Mass Transfer Zone in a Biosorption Column. *Environmental Science Technology,* 40, 3996-4003.

Ng, C., Marshall, W.E., Rao, R.M., Bansode, R.R. and Losso, J.N. (2003). Activated carbon from pecan shell: process description and economic analysis. *Industrial Crops and products*, 17, 209-217.

Oh, G.H. and Park, C.R. (2002). Preparation and characteristics of rice-straw-based porous carbons with high adsorption capacity. *Fuel*, 81, 327-336.

Oh, G.H., Yun, C.H. and Park, C.R. (2003). Role of KOH in the one-stage KOH activation of cellulosic biomass. *Carbon Science*, 4, 180-184.

Okieimen, F. E., Maya, A. O. and Oriakhi, C. O., (1987). Sorption of cadmium, lead and zinc ions on sulphur containing chemically modified cellulosic materials. *International Journal of Environmental Analytical Chemistry*, 32, 23–27.

Okieimen, F.E., Okundia, E.U. and Ogheifun, D.E., (1991). Sorption of cadmium and lead ions on modified groundnut (*Arachis hypogea*) husk. *Journal of Chemical Technology & Biotechnology,* 51, 97–103.

Olivares-Marin, M., Fernandez-Gonzalez, C., Macias-Garcia, A. and Gomez-Setrano, V. (2006). Preparation of activated carbons from cherry stones by activation with potassium hydroxide. *Applied Surface Science*, 252, 5980-5983.

Ong, M. C. and Kamruzzaman, B. Y. (2009). An Assessment of Metals (Pb and Cu) contamination in Bottom Sediments from South China Sea Costal Waters, Malaysia. *American Journal of Applied Sciences*, 6(7), 1418-1423.

Orumwense, F.F.O. (1996). Removal of lead from water by adsorption on a kaolinite clay. *Journal of Chemical Technology & Biotechnology*, 65, 363–369.

Ozacar, M. and Sengil, I.A. (2005). A kinetic study of metal complex dye sorption onto pine sawdust. *Process Biochemistry*, 40, 565-572.

Ozer, A. and Dursun, G. (2007). Removal of methylene blue from aqueous solution by dehydrated wheat bran carbon. *Journal of Hazardous Materials*, 146, 262-269.

Ozer, A., Gurbuz, G., Calimli, A., and Korbathi, B. K. (2009). Biosorption of copper (II) ions on *Enteromorpha prolifera:* Application of response surface methodology (RSM). *Chemical Engineering Journal,* 146, 377-387.

Ozzay, H.D. and Kambur, H. (2006). Adsorption of Cu (II) ions on cotton ball. *Journal of Hazardous Materials, B 136, 911-916*

Padmesh, T.V.N., Vijayaraghavan, K., Sekaran, G. and Velan, M. (2006). Biosorption of Acid Blue 15 using fresh water macroalga Azolla filiculoides Batch and column studies. *Dyes and Pigments*, 71, 77-82.

Pakshirajan, K. and Swaminathan, T. (2006). Continuous Biosorption of Pb, cu and Cd by *Phanerochaete chrysosporium* in a packed column reactor. *Soil and Sediment Contamination*, 15, 187-197.

Pandey, K. K, Prasad, G. and Sing, V. N. (1985). Cu(II) removal from aqueous solutions by fly ash. *Water Research*, 19, 869-873.

Pan, S. C., Lin, C. C. and Tseng, D. H. (2003). Reusing sewage sludge ash as adsorbent for copper removal from waste water. *Resource Conservation Recycling*, 39, 79-90.

Papandreeou, A., Stournaras, C. J. and Panius, D. (2007). Copper and cadmium adsorption on pellets made from fired coal fly ash. *Journal of Hazardous Materials*, 148, 538-547.

Park, M., Choi, C. L., Lim, W. T., Kim, M. C., Choi, J. and Heo, N. H. (2000). Molten-salt method for the synthesis of zeolite materials: I. Zeolite formation in alkaline molten-salt system. *Microporous Mesoporous Materials*. 37, 81-89.

Patrick, J.W. (1985). Porosity in carbon characterization and applications. 1st Edition, *Halsted Press, New York, pp 195-208.*

Paul, N.M. (1995). Handbook of Water and Wastewater Treatment Technology. *Marcel Dekker, New York.*

Pearson, R. G. (1968). Hard and Soft Acids and Bases, HSAB, Part I. *Journal Chemical Education, 45, 581-587.*

Pehlivan, E., Cetin, S. and Yanik, B. H. (2006). Equilibrium studies for the adsoption of Zn (II) and Cu (II) from aqueous solutions using sugar beet pulp and fly ash. *Journal of Hazardous Materials*, 135, 193-199.

Peng, X., Luan, Z., Di, Z., Zhang, Z., and Zhu, C. (2005). Carbon Nanotubes-Iron Oxides Magnetic Composites as Adsorbent for Removal of Pb(II) and Cu(II) from Water. *Carbon,* 43, 855-894.

Periasamy, K. and Namasivayam, C. (1995). Adsorption of Pb(II) by peanut hull carbon from aqueous solution. *Separation Science Technology*, 30, 2223–2237.

Periasamy, K. and Namasivayam, C. (1996). Removal of copper(II) by adsorption onto peanut hull carbon from water and copper plating industry wastewater. *Chemosphere*, 32, 769–789.

Perry, R. and Green, D. W. (1997). Perry's Chemical Engineers Handbook, 7th Ed. *McMrow-Hill International Edition, Singapore, pp 16-18.*

Phan, N.H., Rio, S., Faur C., Le Coq, L., Le Cloirec, P. and Nguyen, T.H. (2006). Production of fibrous activated carbon from natural cellulose (jute, coconut) fibers for water treatment applications. *Carbon*. 44, 2569-2577.

Pretorius, P.J. and Wooland, C. D. (2003). The surface chemical properties of novel high surface area solids synthesized from coal fly ash. *South African Journal of Chemistry*, 56, 34-39.

Quek, S. Y., Wase D. A. J. and Forster, C. F. (1998). The use of sago waste for sorption of lead and Cu(II). *Water SA*, 24, 251-256.

Qurishi, K. (2008). Production of Granular activated carbon from agricultural waste for sugar decolorization and water treatment. *PhD Thesis. Mehran University of Engineering and Technology, Jamshoro, Pakistan.*

Radhika, M. and Palanivelu, K. (2006). Adsorptive removal of chlorophenols from aqueous solution by low cost adsorbent-Kinetics and isotherm analysis. *Journal of Hazardous Materials*, 138, 116-124.

Rahman, I.A. and Saad, B. (2003). Utilization of guava seeds as a source of activated carbon for removal of methylene blue from aqueous solution. *Malaysian Journal of Chemistry*, 5, 8-14.

Ramelow, U.S., Guidry, C.N., Fisk, S.D. (1996). A kinetic study of metal ion binding by biomass immobilized in polymers. *Journal of Hazardous Materials*, 46, 37–55.

Reddad, Z., Gerente, C., Andres, Y., Ralet, M. C., Thibault, J. F. and Cloirec, P. L. (2002). Ni(II) and Cu(II) binding properties of native and modified sugar beet pulp, *Carbohydrate Polymer*, 49, 23-21.

Ricou, P., Lecuyer, I., Le Cloirec, P. (1999). Removal of Cu^{2+}, Zn^{2+} and Pb^{2+} by adsorption onto fly ash and fly ash/lime mixing. *Water Science Technology*, 39, 239-247.

Roskill, (2007). [Online], [Accessed 1st December 2007]. Available from World Wide Web: http://www.roskill.com/reports/activated.

Saeed, A., Iqbal, M. and Akhtar, M. W., (2005) Removal and recovery of Pb(II) from single and multi metal (Cd, Cu, Ni, Zn) solutions by crop milling waste (black gram husk). *Journal of Hazardous Material*, 117, 65-73.

Salman, J.M. and Hameed, B. H. (2010). Effect of preparation conditions of oil palm fronds Activated Carbon on adsorption of bentazon from aqueous solutions. *Journal of Hazardous Material*, 175, 133-137.

Santhy, K. and Selvapathy, P. (2006). Removal of reactive dyes from wastewater by adsorption on coir pith activated carbon. *Bioresource Technology*, 97, 1329-1336.

Saifuddin, M., Salam, M.A. and Jumaat, Z. M. (2011). Utilization of Palm oil Fuel ash in concrete: A review, *Journal of Civil Engineering and Management*, 17(2), 234-247.

Saravanane, R., Sundararajan, T. and Reddy, S.S., (2002). Efficiency of chemically modified low cost adsorbents for the removal of heavy metals from waste water: a comparative study. *Indian Journal of Environmental Health*, 44 (2), 78– 87.

Sata, V., Jaturapitakkul, C. and Kiattikomol, K. (2004)., Utilization of palm oil fuel ash in high strength concrete. *Journals in Materials in Civil Engineering ASCE*, 16(6), 623-628.

Sata, V., Jaturapitakkul, C. and Kiattikomol, K (2007). Influence of pozzolan from various by products materials on mechanical properties of high strength concrete. *Construction and Building Materials*, 21(7), 1589-1598.

Satyawali, Y. and Balakrishnan, M. (2007). Removal of color from biomethanated distillery spentwash by treatment with activated carbons. *Bioresource Technology*, 98, 2629-2635.

Savovaa, D., Petrova, N., Yardimb, M. F., Ekincib, E., Budinovaa, T., Razvigorova, M., and Minkova, V. (2003). The influence of the texture and surface properties of carbon adsorbents obtained from biomass products on the adsorption of manganese ions from aqueous solution. *Carbon*, 41, 1897–1903

Seader, J.D. and Ernest, J.H. (1998). Separation process principles. *John Wiley and Sons, New York.*

Seco, A., Gabaldón, C., Marzal, P., and Aucejo, A. (1999). Effect of pH, Cation Concentration and Sorbent Concentration on Cadmium and Copper Removal by a Granular Activated Carbon. *Journal of Chemical Technology & Biotechnology*, 74, 911-918.

Seki, H. and Suzuki, A. (1996), Adsorption of lead ions on composite biopolymer adsorbent. *Industrial & Engineering Chemistry Research*, 35, 1378–1382.

Sengupta, S., and SenGupta, A. K. (2002). Trace Heavy Metal Separation by Chelating Ion Exchangers. In: SenGupta, A. K., ed. *Environmental Separation of Heavy Metals: Engineering Processes. New York: Lewis Publishers. 45-96.*

Sen Gupta, S., Krishna, G. and Bhattacharyya (2005). Interaction of metal ions with clays: I. A case study with Pb(II). *Applied Clay Science*, 30, 199– 208.

Senthilkumaar, S., Varadarajan, P.R., Porkodi, K. and Subbhuraam, C.V. (2005). Adsorption of methylene blue onto jute fiber carbon: kinetics and equilibrium studies. *Journal of Colloid and Interface Science*, 284, 78-82.

Senthilkumaar, S., Kalaamani, P., Porkodi, K., Varadarajan, P.R. and Subburaam, C.V. (2006). Adsorption of dissolved Reactive red dye from aqueous phase onto activated carbon prepared from agricultural waste. *Bioresource Technology*, 97, 1618-1625.

Sentorun-Shalaby, C., Ucak-Astarlioglu, M.G., Artok, L. and Sarici, C. (2006). Preparation and characterization of activated carbons by one-step steam pyrolysis/activation from apricot stones. *Microporous and Mesoporous Materials*, 88, 126-134.

Shriver, D. F., Atkins, P. W., and Langford, C. H. (1991). Inorganic Chemistry. *University Press, Oxford.*

Shigemoto, N., Shirakami, S., Hirano, S. and Hayashi, H. (1995). Characterization of Na-X , Na-A and coal fly as Zeolites from coal fly ash and their amorphous precursors by IR, MAS, NMR and XPS. *Journal of Material Science*, 30, 5777-5783.

Sharma, Y. C., Uma, Singh S. N. and Paras Gode, F. (2007).Fly ash for the removal of Mn(II) from aqueous solutions and waste water. *Chemical Engineering Journal*, 132, 319-323.

Shuit, S.H., Tan, K.T., Lee, K.T. and Kamaruddin, A.H. (2009). Oil palm biomass as a sustainable energy source: A Malaysian case study. *Energy*, 34, 1225-1235

Sing, K. K., Talat, M. and Hasan, S. H. (2006). Removal of lead from aqueous solutions by agricultural waste maize bran, *Bioresourse Technology*, 2124-2130.

Spahis, N., Addoun., A., Mahmoudi, H. and Ghaffour, N. (2008). Purification of water by activated carbon prepared from olive stones. *Desalination*, 222. 519-527.

Srinivasakannan, C. and Bakar, M.Z.A. (2004). Production of actiated carbon from rubber wood sawdust. *Biomass and Bioenergy*, 27. 89-96.

Srivastava, S. K., Sing, A.K. and Sharma, A. (1994). Studies on the uptake of lead and zinc by lignin obtained from black liquor-a paper industry waste material. *Environmental Technology*, 15, 353-361.

Srivastava, V. C., Mall, I. D. and Mishra, I. M. (2007). Absorption thermodynamics and isosteric heat of adsorption of toxic metal ions on to bagasse fly ash (BFA) and rice husk ash (RHA). *Chemical Engineering Journal*, 132, 267-278.

Srivastava, V. C., Mall, I. D. and Mishra, I. M. (2008). Removal of cadmium and zinc metal ions from binary aqueous solution by rice husk ash. *Colloids and Surfaces A: Physicochemical and Engineering Aspects*, 312, 172-184.

Stavropoulos, G.G. and Zabaniotou, A.A. (2005). Production and characterization of activated carbons from olive-seed, waste residue. *Microporous and Mesoporous Materials*, 82, 79-85.

Suzuki, R.M., Andrade, A.D., Sousa, J.C. and Rollemberg, M.C. (2007). Preparation and characterization of activated carbon from rice bran. *Bioresource Technology*, 98, 1985-1991.

Sudaryanto, Y., Hartono, S.B., Irawaty, W., Hindarso, H. and Ismadji, S. (2006). High surface area activated carbon prepared from cassava peel by chemical activation. *Bioresource Technology*, 97, 734-739.

Tanthapanichakoon, W., Ariyadejwanich, P., Japthong, P., Nakagawa, K., Mukai, S.R. and Tamon, H. (2005). Adsorption-desoption characteristics of phenol and reactive dyes from aqueous solution on mesoporous activated carbon prepared from waste tires. *Water Research*, 39, 1347-1353.

Tangchirapat, W., Jaturapitakkul, C. and Chindaprasirt, P. (2009). Use of palm oil fuel ash as supplementary cementitious materials for producing high strength concrete. *Construction and Building Materials*, 23(7), 2641-2646.

Tan, I. A. W. (2008). Preparation, characterization and evaluation of activated carbons derived from agricultural by-products for adsorption of Methylene blue and 2, 4, 6 – trichlorophenol. *PhD Thesis, University Science Malaysia, Malaysia.*

Tan, I. A. W., Ahmed A.L. and Hameed, B. H. (2008). Adsorption of basic dye using activated carbon prepared from oil palm shell: batch and fixed bed studies. *Desalination*, 225, 13-28.

Tan, T. C., and Teo, W. K. (1987). Combined Effect of Carbon Dosage and Initial Adsorbate Concentration on the Adsorption Isotherm of Heavy Metals on Activated Carbon. *Water Research*, 21, 1183-1188.

Taty-Costodes, V.C., Fauduet, H., Porte, C. and Ho, Y.S. (2005). Removal of lead (II) ions from synthetic and real effluents using immobilized Pinus sylvestris sawdust Adsorption on a fixed-bed column. *Journal of Hazardous Material*, 123, 135-144.

Temkin, M.I. and Pyzhev, V. (1940). Kinetics of ammonia synthesis on promoted iron catalyst. *Acta Physiochemical USSR*, 12. 327-356.

Thomas, H. C. (1944). Heterogeneous Ion exchange in a flowing system. *Journal of American Chemical Society*, 66, 1466-1664.

Toles, C. A., Marshall, W. E., and Johns, M. M. (1997). Granular Activated Carbons from Nutshells for the Uptake of Metals and Organic Compounds. *Carbon.* 35, 1407-1414.

Toles, C. A., Marshall, W. E., and Johns, M. M. (1998). Phosphoric Acid Activation of Nutshells for Metals and Organic Remediation: Process optimization. *Journal of Chemical Technology Biotechnology*, 72, 255-263.

Toles, C. A., Marshall, W. E., and Johns, M. M. (1999). Surface Functional Groups on Acid Activated Nutshell Carbons. *Carbon*, 37, 1207-1214.

Treybal, R.E. (1980). Mass Transfer Operations. 3rd ed. *McGraw Hill Publisher. New York, USA, pp. 447-522.*

Tsai, W.T., Chang, C.Y., Lin, M.C., Chien, S.F., Sun, H.F. and Hsieh, M.F. (2001). Adsorption of acid dye onto activated carbons prepared from agricultural waste bagasse by $ZnC1_2$ activation. *Chemosphere*, 45, 51-58.

Tseng, R.L. (2006). Mesopore control of high surface area NaOH-activated carbon. *Journal of Colloid and Interface Science*, 303, 494-502.

Tseng, R.L. and Tseng, S.K. (2005). Pore structure and adsorption performance of the KOH-activated carbons prepared from corncob. *Journal of Colloid and Interface Science*, 287, 428-437.

Tseng, R.L., Tseng, S.K. and Wu, F.C. (2006). Preparation of high surface area carbons from Corncob with KOH etching Plus CO_2 gasification for the adsorption of dyes and phenols from water. *Colloids and surfaces A: Physicochemical and Engineering Aspects*, 279, 69-78.

Tummavuori, J. and Aho, M. (1980). On the ion-exchange properties of peat. I: On the adsorption of some divalent metal ions (Mn^{2+}, Co^{2+}, Ni^{2+}, Cu^{2+}, Zn^{2+}, Cd^{2+} and Pb^{2+}) on peat. *Suo*, 31(4),79-83.

Turmuzi, M., Daud, W.R.W. Tasirin, S.M. Takriff, M.S. ans Iyuke. S.E. (2004). Production of activated carbon from candlenut shell by CO_2 activation. *Carbon*, 42, 453-455.

Ullmann (2002). Ullmann's Encyclopedia of Industrial Chemistry, 6th Edition, *Siley-VCH Publisher.*

Ulmanu, M., Maranon, E., Fernandez, Y., Castrillon, L., Anger L. and Dumitriu D. (2003). Removal of copper and cadmium ions from diluted aqueous solution by low cost and waste material adsorbents. *Water Air Soil Pollution*, 142, 357-373

Usmani, T. H. (2001). Preparation and characterization of activated carbon from rice husk, Acacia Arabica and low rank coals. *PhD. Thesis, University of Karachi, Pakistan.*

Vadivelan, V. and Kumar, K.N. (2005). Equilibrium, Kinetics, mechanism and process design for the sorption of methylene blue onto rice husk. *Journal Colloid and Interface Science*, 286, 90-100.

Vicente, G., Coteron, A., Martinez, M. and Aracil, J. (1993). Application of the factorial design of experiments and response surface methodology to optimize biodiesel production. *Industrial Crops and Products*, 8, 29-35.

Vinodhini, V. and Das, N. (2010). Packed bed column studies on Cr(VI) removal from tannery waste water by neem sawdust. *Desalination*, 264, 9-14.

Wang, S., Zhu, Z.H., Coomes, A. Haghseresht, F. and Lu, G.Q. (2005). The physical and surface chemical characteristics of activated carbons and the adsorption of Methylene blue from waste water. *Journal of Colloid and Interface Science*, 284, 440-446.

Wang, S. and Zhu, Z.H. (2007): Effects of acidic treatment of activated carbons on dye adsorption. *Dyes and Pigments*, 75, 306-314.

Weber, T.W. and Chakkravorti, R.K. (1974). Pore and solid diffusion model for fixed-bed adsorbents. *AIChE Journal*, 20, 228-238.

Weber, W.J. and Morris, J.C. (1962). *International Conference on Water Symposium*. Oxford: Pergamon.

Wen, Q., Li, C., Cai, Z., Zhang, W., Gao, H., Chen, L., Zeng, G., Shu, X. and Zhao, Y. (2011). Study on activated carbon derived from sewage sludge for adsorption of gaseous formaldehyde. *Bioresource Technology*, 102, 942-947.

WEPA, (Water Environment partnership in Asia) (2010) [online], [Accessed 15th October 2010]. Available from World Wide Web: http://www.wepadb.net/policies/state/malaysia/overview.htm.

WEPA, (Water Environment partnership in Asia) (2011) [online], [Accessed 25th July 2012]. Available from World Wide Web: http://www.wepadb.net/policies/state/malaysia/river.htm.

Wereko-Brobby, C.Y. and Hagen, E.B. (1996). Biomass Conversion and Technology, *John Wiley and Sons, New York, USA.*

Wong, K.K., Lee, C. K. and Haron, M. J. (2003). Removal of Cu and Pb by tartatric acid modified rice husk from aqueous solutions. *Chemosphere*, 50(1), 23-28.

World activated carbon forecasts to 2010 & 2015 (2009). [Online], [Accessed 20th November 2010]. Available from World Wide Web: http://www.bharatbook.com/bookdetail.asp?bookid=15136&publisher

Wu, F.C., Tseng, R.L. and Hu (2005) Comparisons of pore properties and adsorption performance of KOH-activated and steam-activated carbons. *Microporous and Mesoporous Materials*, 80, 95-106.

Wu, F.C. and Tseng, R.L. (2006). Preparation of highly porous carbon from fir wood by KOH etching and CO_2 gasification for adsorption of dyes and phenols from water. *Journal of Colloid and Interface Science*, 294, 21-30.

Wu, C.H. (2007). Adsorption of reactive dye onto carbon nanotube: Equilibrium kinetics and thermodynamics. *Journal of Hazardous Materials*, 144, 93-100.

Yadava, K.P., Tyagi, B.S. and Singh, V.N. (1991). Effect of temperatureon the removal of lead (II) by adsorption on china clay and wallastonite. *Journal of Chemical Technology & Biotechnology*, 51, 47– 60.

Yalcin, N. and Sevinc, V. (2000). Studies of the surface area and porosity of activated carbons prepared from rice husk. *Carbon*, 38, 1943-1945.

Yang, T. and Lua, A.C. (2003), Characteristics of activated carbons prepared from pistachio-nut shells by physical activation. *Journal of Colloid and Interface Science*, 267, 408-417.

Yavuz O., Altunkaynak Y., Guzel F. (2003). Removal of copper, nickel, cobalt and manganese from aqueous solution by Kaolinite, *Water Research*, 37, 948-952.

Yehaskel, A. (1978). Activated Carbon: Manufacture and regeneration, USA: Noyes Data Corporation.

Yoon, Y. N. and Nelson, J. H. (1984). "Application of gas adsorption kinetics. Part I. A theoretical model of respirator cartridge service time," *American Industrial Hygiene Association Journal*, 45, 509-516.

Yu, Q., Sawayama, S, Sugita, S., Shoya, M. and Isojima, Y. (1999). The reaction between rice husk ash and $Ca(OH)_2$ solution and the nature of its product. *Cement and Concrete Research*, 29, 37-43.

Yun, C.H., Park, Y.H. and Park, C.R. (2001). Effects of pre-carbonization on porosity development of activated carbons from rice straw. *Carbon*, 39, 559567.

Yupeng, G., Qi, J., Yang, S., Yu, K.,Wang, Z. and Xu, H. (2003). Adsorption of Cr(VI)on micro and mesoporous rice husk based activated carbon. *Materials Chemistry and Physics*, 78, 70-80.

Zabaniotou, A., Stavtopoulos, G. and Skoulou, V. (2008). Activated carbon from olive kernels in a two-stage process: Industrial improvement. *Bioresource Technology*, 99, 320-326.

Zahangir, M.A., Suleyman, A.M., Noraini, K. (2008). Production of activated carbon from oil Palm empty fruit bunches for removal of zinc. *Twelfth International Water Technology Conference, (IWTC12)*, Alexandria, Egypt. pp. 373-383.

Zainudin, N. F., Lee, K. T., Kamaruddin, K. T., Bhatia, S., and Mohamed, A. R. (2005). Study of adsorbent prepared from oil palm ash (OPA) for flue gas desulfurization. *Separation Purification Technology*, 45, 50-60.

APPENDIX A

Calibration Curve for Lead Pb(II), Copper Cu(II) and Manganese Mn(II)

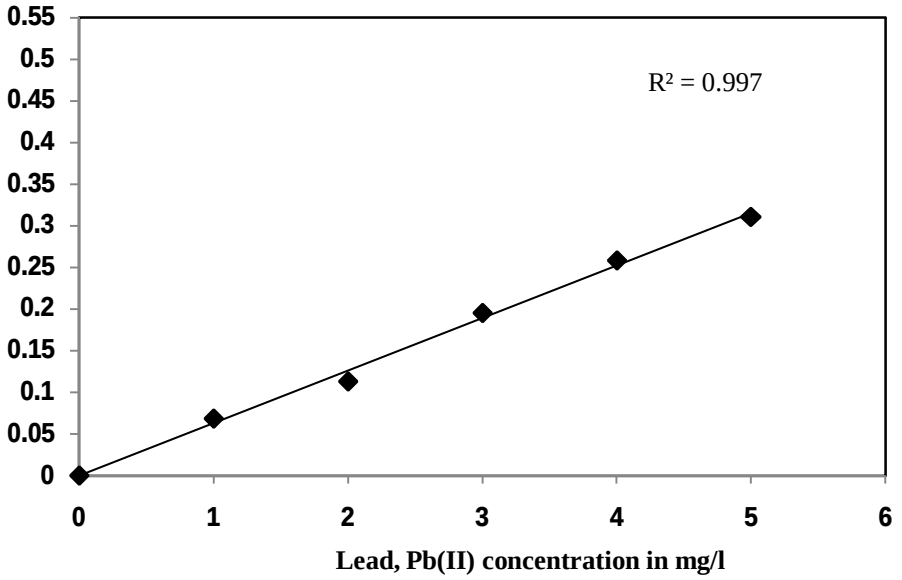

Figure A-1 Calibration Curve for sorption of Lead, Pb(II)

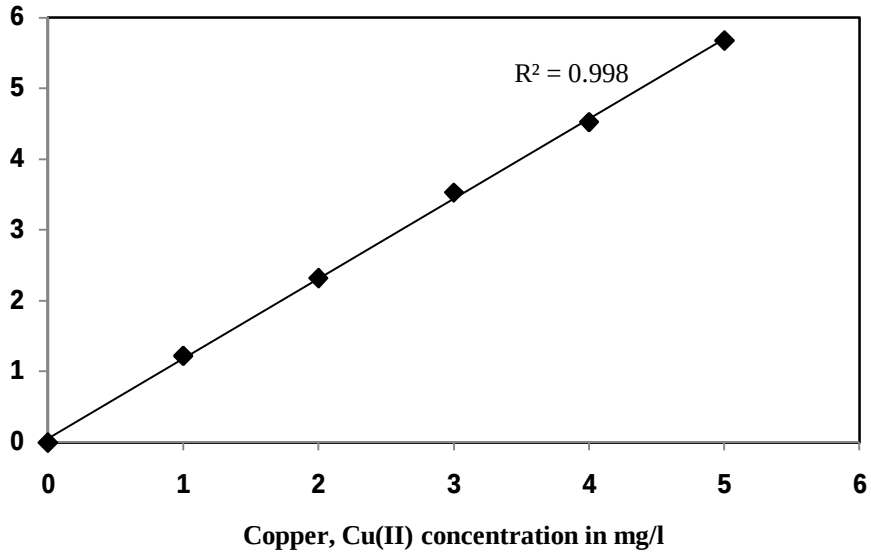

Figure A-2 Calibration Curve for sorption of Copper, Cu(II)

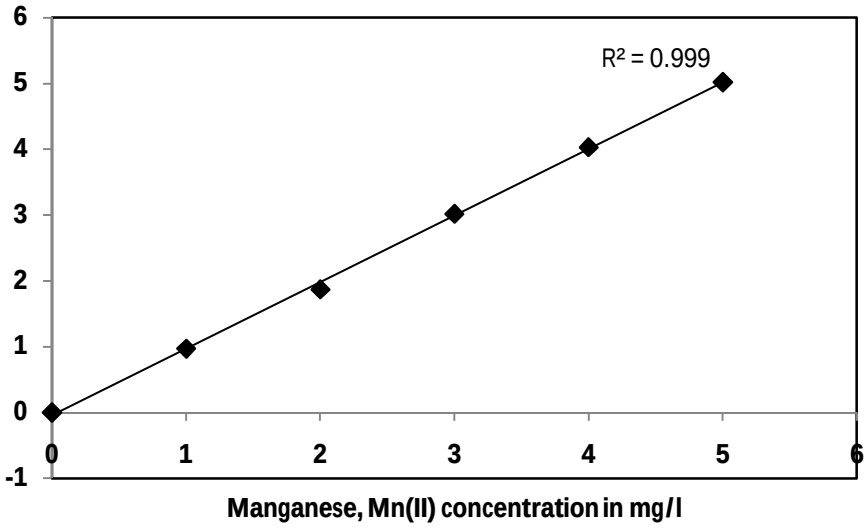

Figure A-3 Calibration Curve for sorption of Manganese, Mn(II)

APPENDIX B

Major Equipments used to prepare activated adsorbents, analyze aqueous sample and surface characterization system

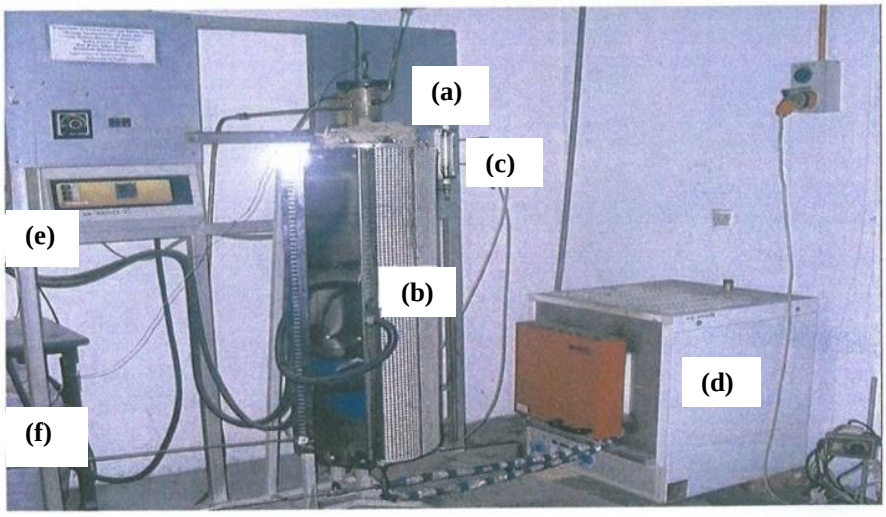

(a) Vertical Reactor closed with Thermocouple (b) Vertical Furnace (c) Gas Flow indicator (d) Oven (e) Temperature and time controlling unit (f) Exhaust pipe

Plate B-1 Experimental set up for Activated carbon (PAC and GAC) preparation

Plate B-2 Experimental set up for Activated ash (AOPA) preparation

Appendix C

Diagnostic Tests for preparation of activated adsorbents

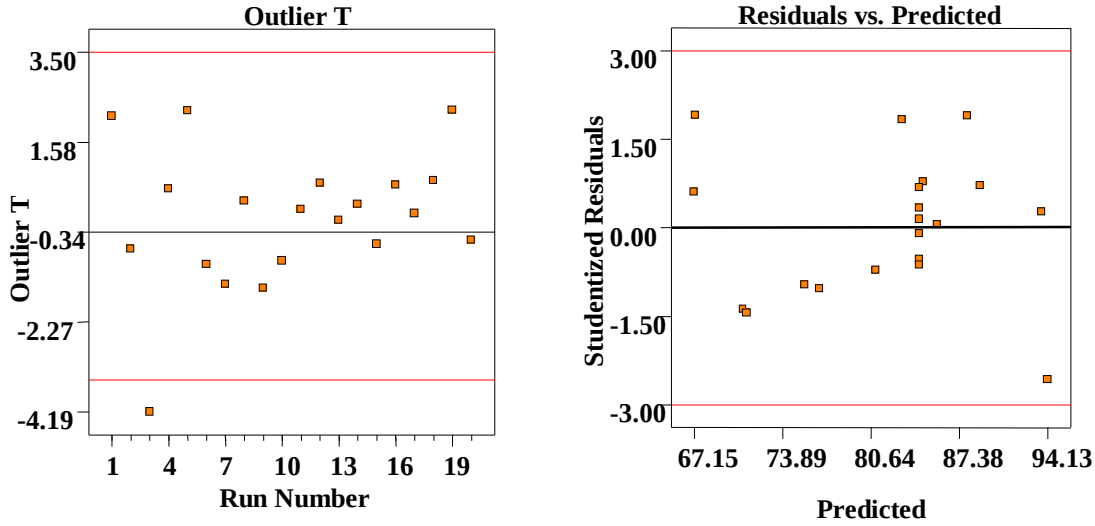

Figure C-1 (a) Outlier *t* plots (b) The studentized residuals and predicted response plots for removal % of Pb (II) onto Kenaf Core based Activated Carbon (KCAC)

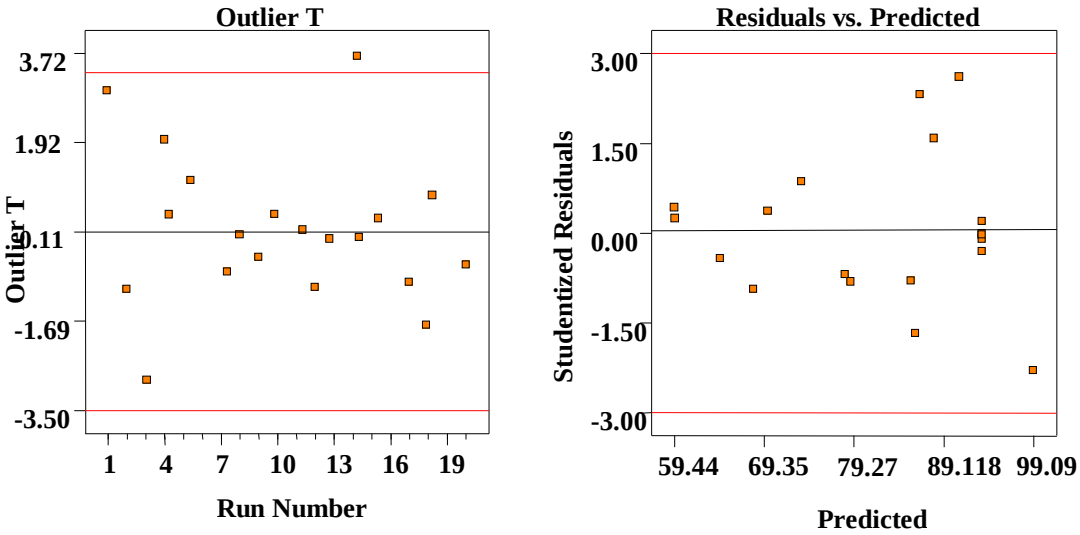

Figure C-2 (a) Outlier *t* plots (b) The studentized residuals and predicted response plots for removal % of Cu (II) onto Kenaf Core based Activated Carbon (KCAC)

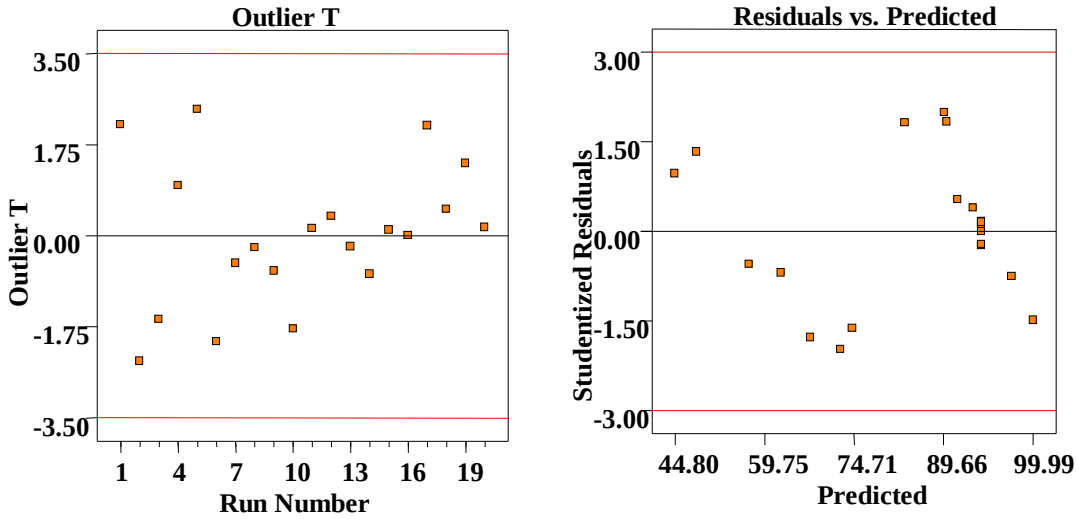

Figure C-3 (a) Outlier *t* plots (b) The studentized residuals and predicted response plots for removal % of Mn(II) onto Kenaf Core based Activated Carbon (KCAC)

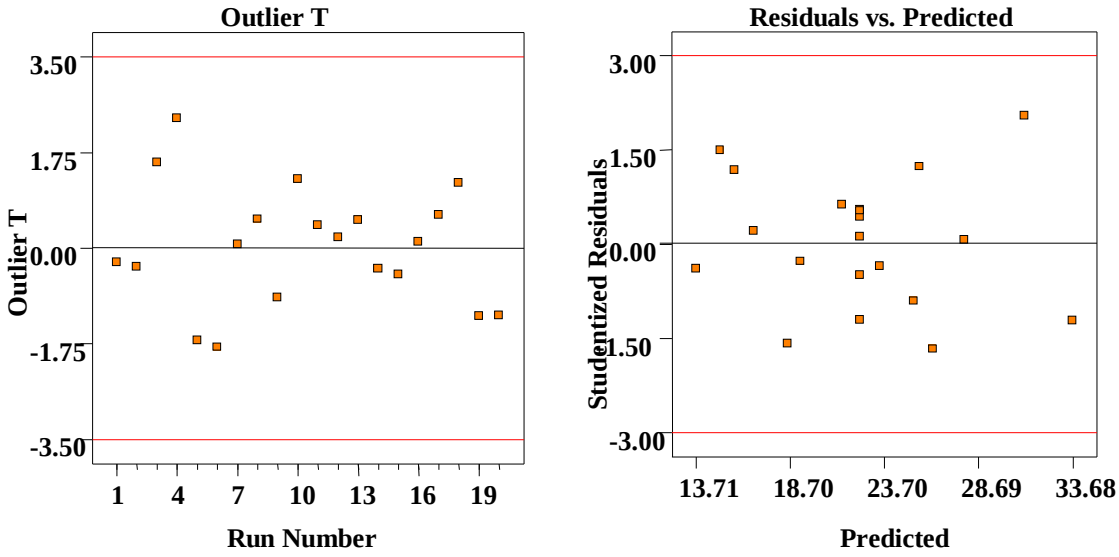

Figure C-4 (a) Outlier *t* plots (b) The studentized residuals and predicted response plots for production yield % of Kenaf Core Based Activated Carbon (KCAC)

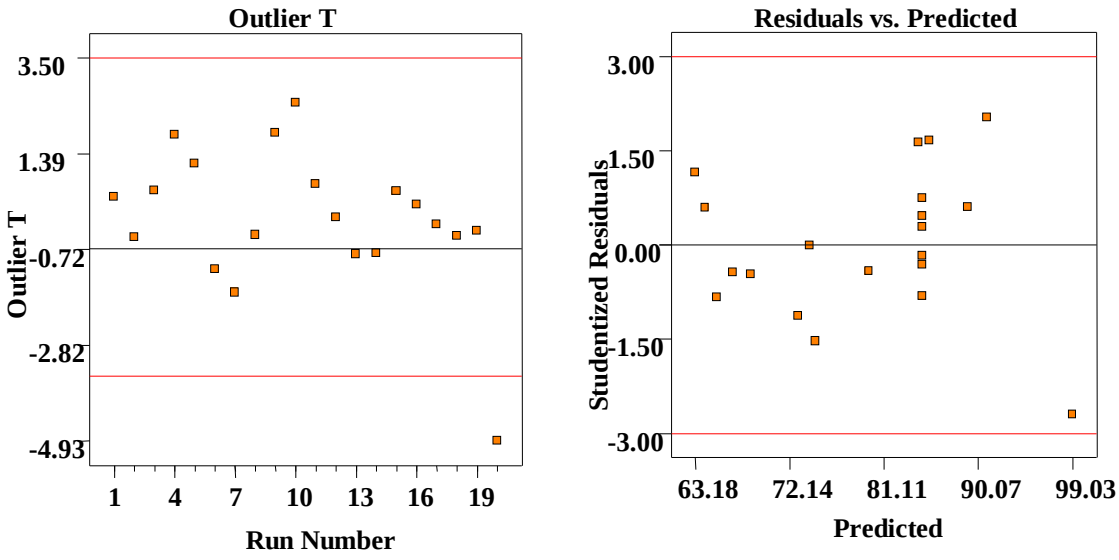

Figure C-5 (a) Outlier *t* plots (b) The studentized residuals and predicted response plots for removal % of Pb (II) onto Kenaf Fiber based Activated Carbon (KFAC)

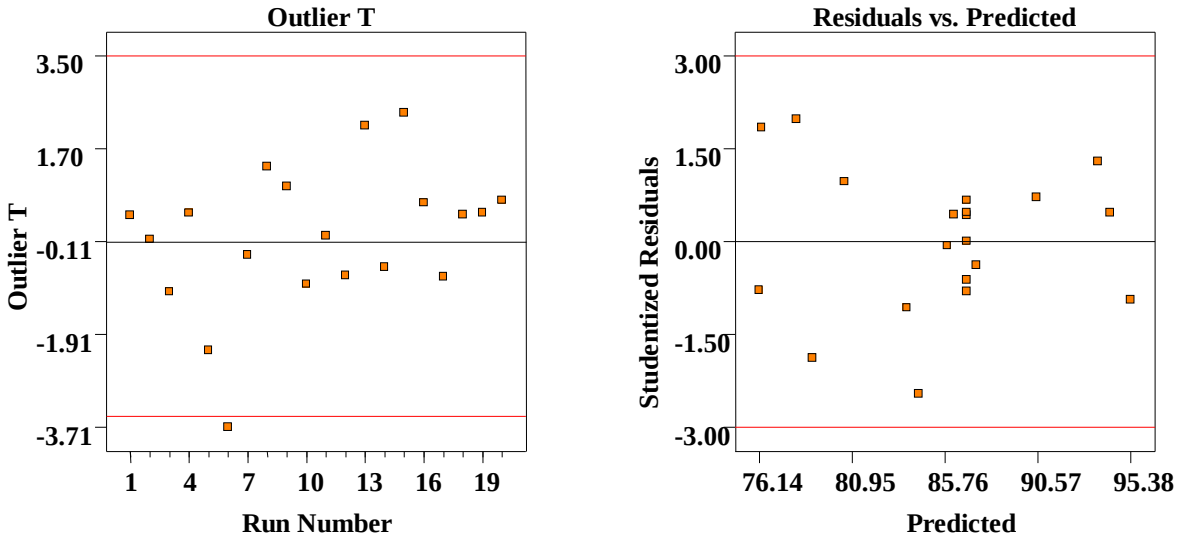

Figure C-6 (a) Outlier *t* plots (b) The studentized residuals and predicted response plots for removal % of Cu (II) onto Kenaf Fiber based Activated Carbon (KFAC)

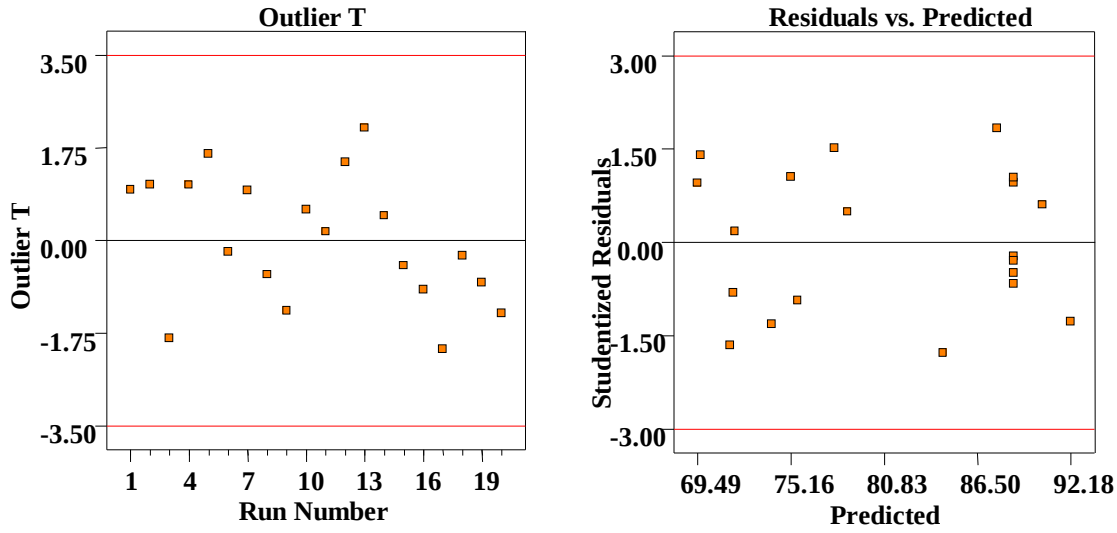

Figure C-7 (a) Outlier *t* plots (b) The studentized residuals and predicted response plots for removal % of Mn(II) onto Kenaf Fiber based Activated Carbon (KFAC)

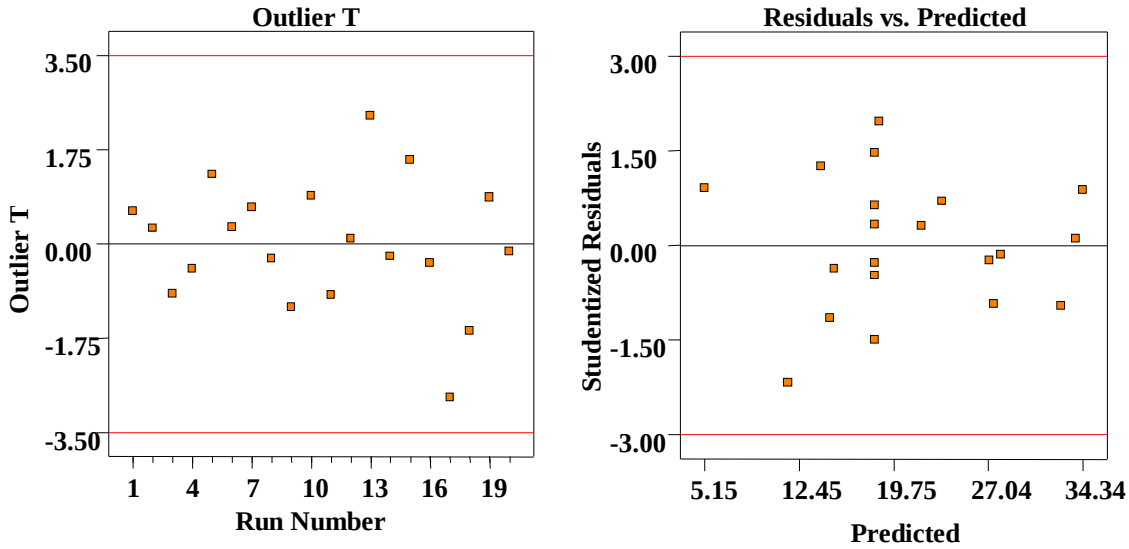

Figure C-8 (a) Outlier *t* plots (b) The studentized residuals and predicted response plots for production yield % of Kenaf Fiber Based Activated Carbon (KFAC)

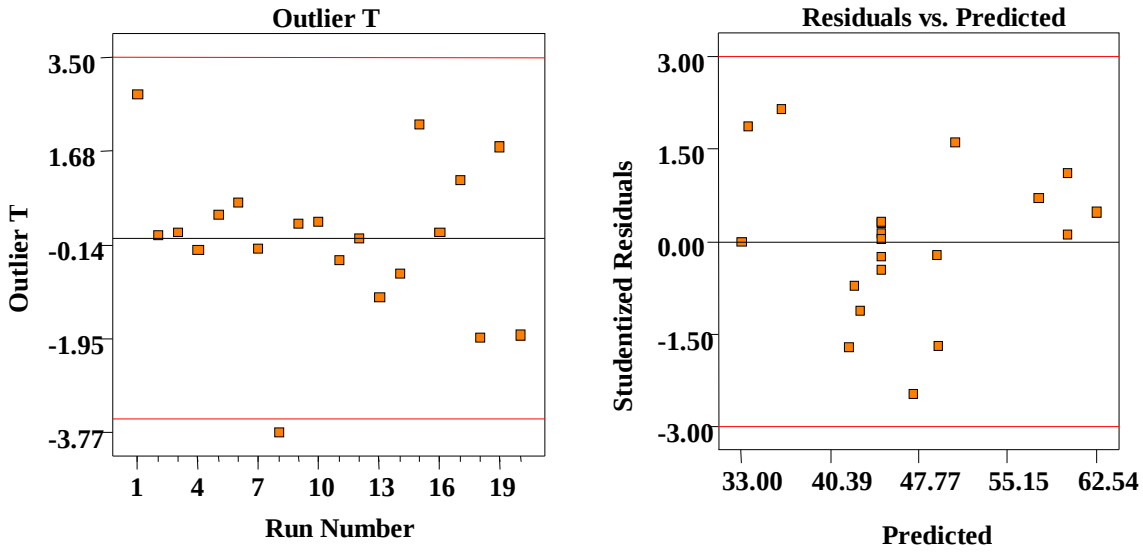

Figure C-9 (a) Outlier *t* plots (b) The studentized residuals and predicted response plots for removal % of Pb (II) onto activated oil palm ash (AOPA)

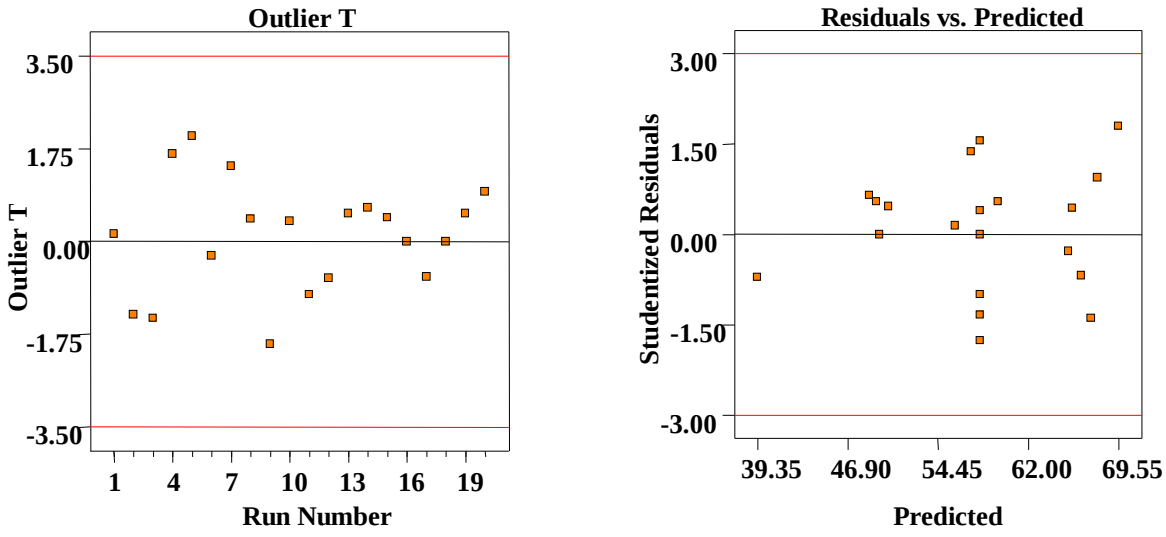

Figure C-10 (a) Outlier *t* plots (b) The studentized residuals and predicted response plots for removal % of Cu(II) onto Activated oil palm ash (AOPA)

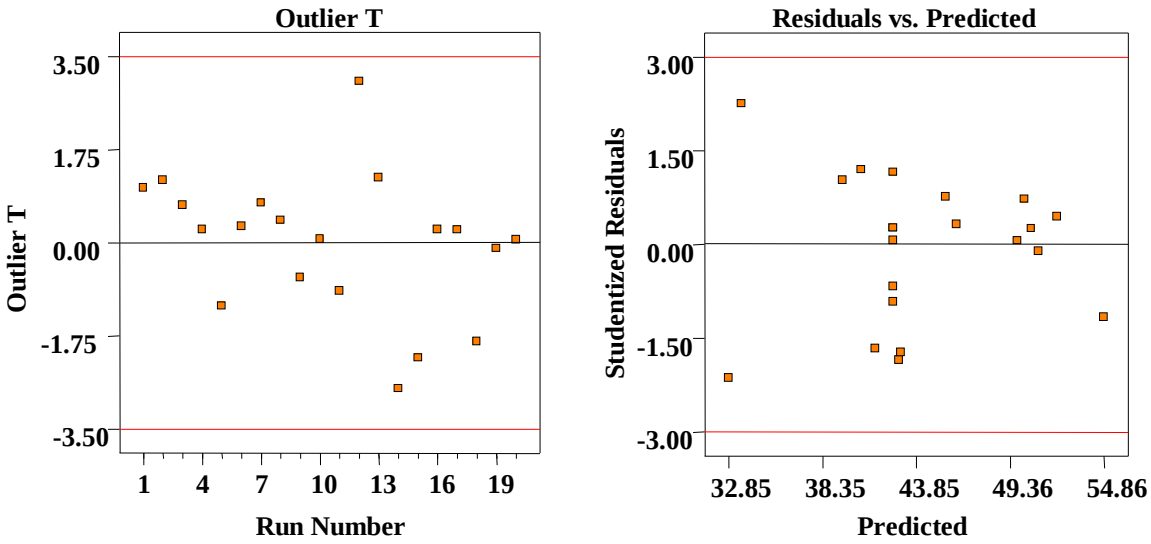

Figure C-11 (a) Outlier *t* plots (b) The studentized residuals and predicted response plots for removal % of Mn(II) onto activated oil palm ash (AOPA)

APPENDIX D

Optimization Ramp for preparation of powdered activated carbon from lignocellulosic precursors of Kenaf core and Kenaf fiber (KCAC and KFAC)

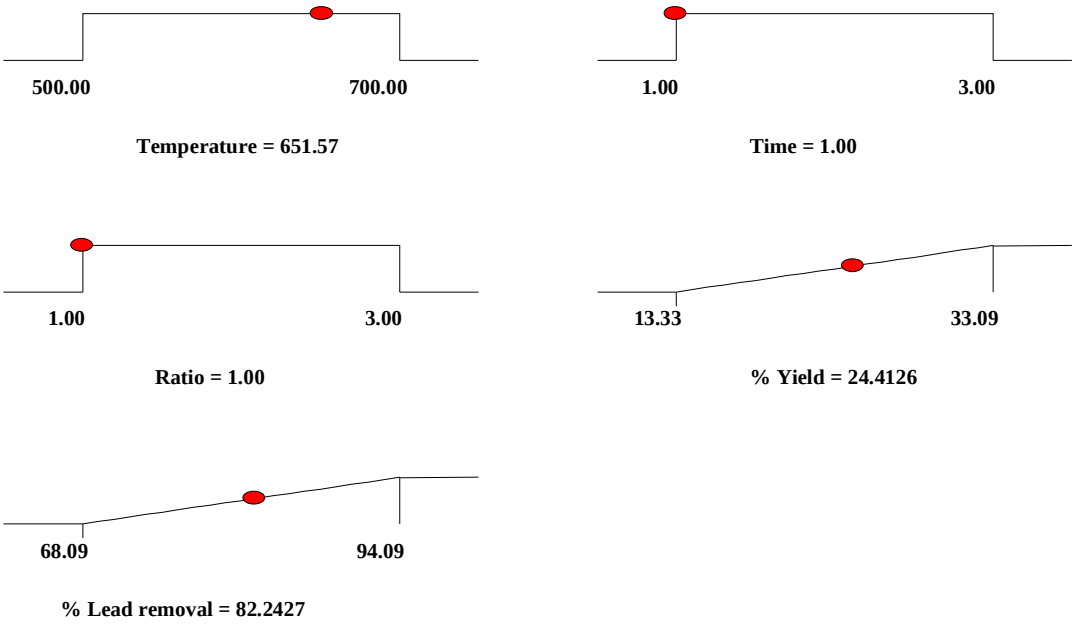

Figure D-1 Optimization Ramp for preparation of Kenaf core based activated carbon (KCAC) for lead, Pb (II)

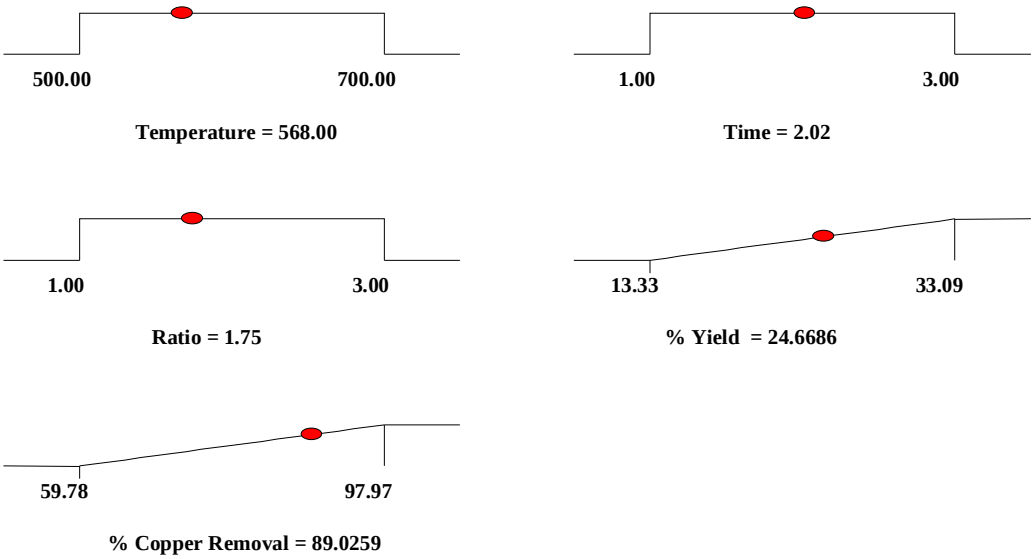

Figure D-2 Optimization Ramp for preparation of Kenaf core based activated carbon (KCAC) for copper, Cu (II)

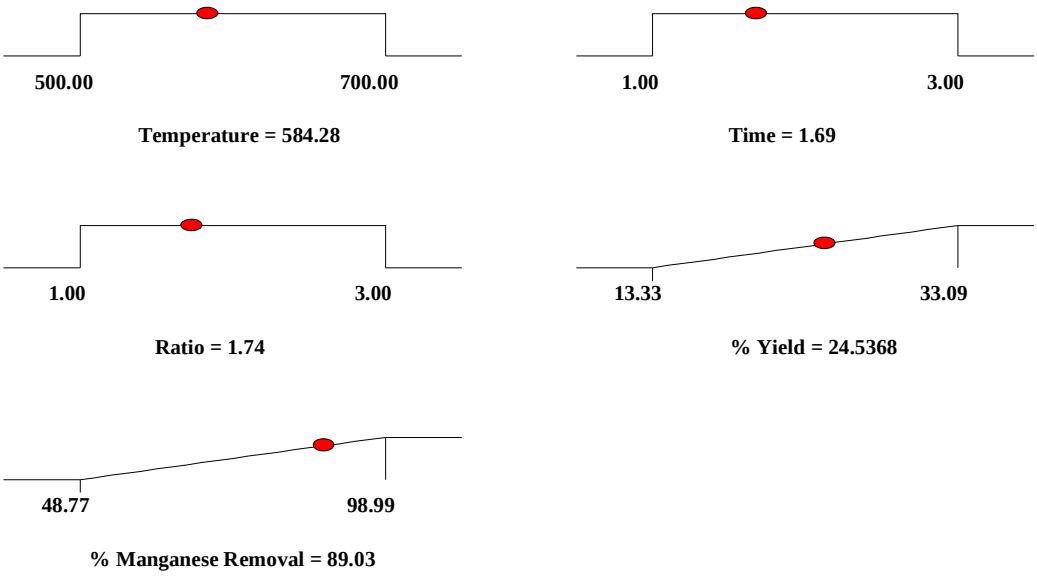

Figure D-3 Optimization Ramp for preparation of Kenaf core based activated carbon (KCAC) for manganese, Mn (II)

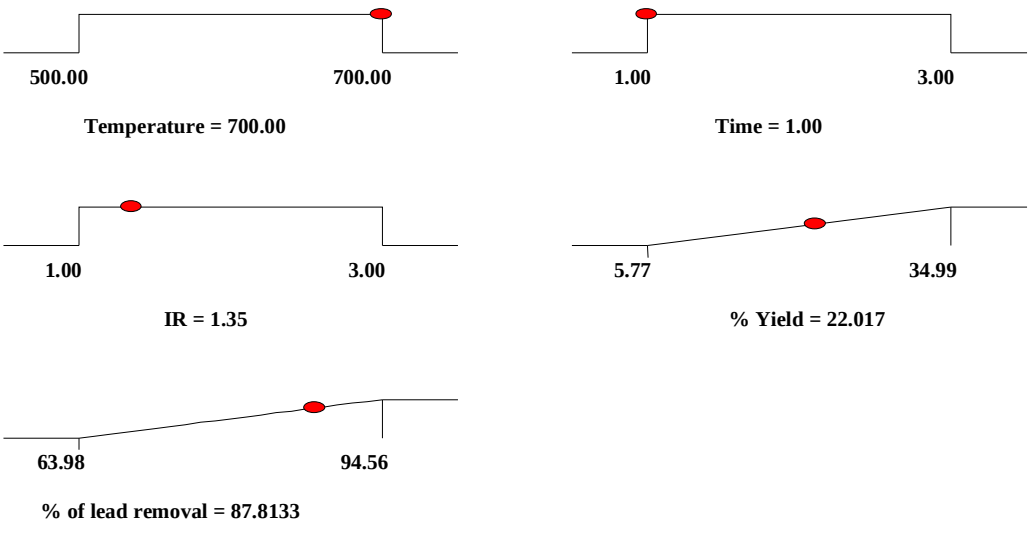

Figure D-4 Optimization Ramp for preparation of Kenaf Fiber based activated carbon (KFAC) for lead, Pb (II)

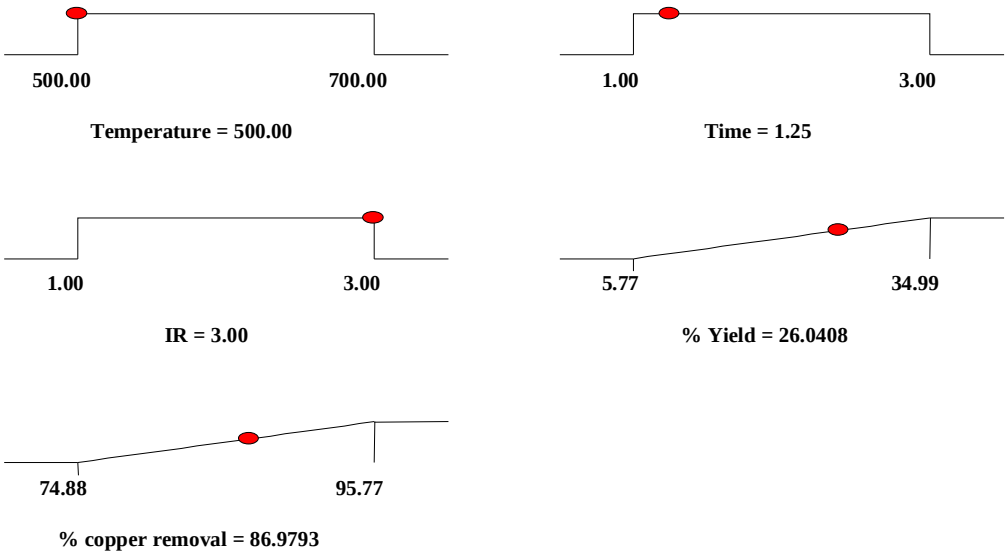

Figure D-5 Optimization Ramp for preparation of Kenaf Fiber based activated carbon (KFAC) for copper, Cu (II)

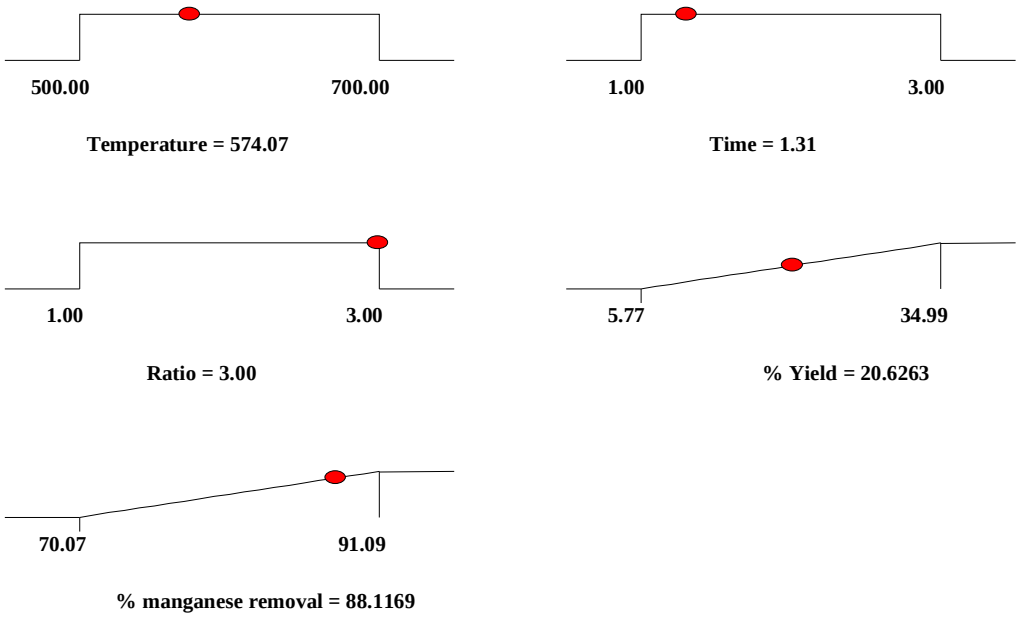

Figure D-6 Optimization Ramp for preparation of Kenaf Fiber based activated carbon (KFAC) for manganese, Mn (II)

APPENDIX E

Equilibrium Isotherm Modeling (Langmuir, Freundlich and Temkin Isotherm) at 50 °C and 70 °C temperature

Table E-1 Langmuir, Freundlich and Temkin Isotherm at 50 °C Temperature for adsorption of Lead, Pb (II) onto KCAC, KFAC, MFSAC and AOPA

Activated sorbent	Linear Regression analysis of Isotherm									
	Langmuir Isotherm				Freundlich Isotherm			Temkin Isotherm		
	Maximum Monolayer adsorption capacity	Langmuir Constant	Separation Factor	Correlation Coefficient	Affinity Factor	Freundlich Exponent	Correlation Coefficient	Binding Constant	Temkin Constant	Correlation Coefficient
	q_{max}	K_L	R_L	R^2	K_F	1/n	R^2	K_T	B	R^2
	(mg/g)	(l/mg)	-	-	$(mg/g(l/mg)^{1/n})$	-	-	(l/g)	-	-
KCAC	55.55	0.089	0.101	0.942	5.668	0.672	0.995	0.929	11.180	0.973
KFAC	37.04	0.333	0.030	0.899	10.49	0.483	0.947	3.070	8.232	0.909
MFSAC	27.03	0.133	0.006	0.937	6.876	0.332	0.925	2.014	5.014	0.916
AOPA	23.25	0.148	0.063	0.917	3.854	0.377	0.845	0.663	4.686	0.820

Table E-2 Langmuir, Freundlich and Temkin Isotherm at 70 °C Temperature for adsorption of Lead, Pb (II) onto KCAC, KFAC, MFSAC and AOPA

Activated sorbent	Linear Regression analysis of Isotherm									
	Langmuir Isotherm				Freundlich Isotherm			Temkin Isotherm		
	Maximum Monolayer adsorption capacity	Langmuir Constant	Separation Factor	Correlation Coefficient	Affinity Factor	Freundlich Exponent	Correlation Coefficient	Binding Constant	Temkin Constant	Correlation Coefficient
	q_{max}	K_L	R_L	R^2	K_F	1/n	R^2	K_T	B	R^2
	(mg/g)	(l/mg)	-	-	$(mg/g(l/mg)^{1/n})$	-	-	(l/g)	-	-
KCAC	52.63	0.086	0.193	0.972	5.285	0.666	0.986	0.986	11.110	0.994
KFAC	38.46	0.325	0.030	0.839	10.51	0.509	0.929	2.950	8.631	0.874
MFSAC	27.78	0.146	0.005	0.883	7.456	0.321	0.907	2.555	4.921	0.858
AOPA	27.02	0.141	0.066	0.964	6.290	0.387	0.957	1.287	6.098	0.947

Table E-3 Langmuir, Freundlich and Temkin Isotherm at 50 °C Temperature for adsorption of Copper, Cu (II) onto KCAC, KFAC, MFSAC and AOPA

Activated sorbent	Linear Regression analysis of Isotherm									
	Langmuir Isotherm				Freundlich Isotherm			Temkin Isotherm		
	Maximum Monolayer adsorption capacity	Langmuir Constant	Separation Factor	Correlation Coefficient	Affinity Factor	Freundlich Exponent	Correlation Coefficient	Binding Constant	Temkin Constant	Correlation Coefficient
	q_{max}	K_L	R_L	R^2	K_F	1/n	R^2	K_T	B	R^2
	(mg/g)	(l/mg)	-	-	$(mg/g(l/mg)^{1/n})$	-	-	(l/g)	-	-
KCAC	32.25	2.066	0.005	0.985	20.53	0.401	0.972	18.29	7.170	0.977
KFAC	29.42	1.542	0.006	0.985	16.78	0.340	0.910	16.67	6.112	0.937
MFSAC	21.74	0.467	0.021	0.997	10.37	0.214	0.996	16.65	3.370	0.994
AOPA	19.60	0.629	0.016	0.988	11.64	0.140	0.956	206.8	2.125	0.926

Table E-4 Langmuir, Freundlich and Temkin Isotherm at 70 °C Temperature for adsorption of Copper, Cu (II) onto KCAC, KFAC, MFSAC and AOPA

Activated sorbent	Linear Regression analysis of Isotherm									
	Langmuir Isotherm				Freundlich Isotherm			Temkin Isotherm		
	Maximum Monolayer adsorption capacity	Langmuir Constant	Separation Factor	Correlation Coefficient	Affinity Factor	Freundlich Exponent	Correlation Coefficient	Binding Constant	Temkin Constant	Correlation Coefficient
	q_{max}	K_L	R_L	R^2	K_F	1/n	R^2	K_T	B	R^2
	(mg/g)	(l/mg)	-	-	$(mg/g(l/mg)^{1/n})$	-	-	(l/g)	-	-
KCAC	33.34	2.500	0.004	0.977	23.27	0.426	0.970	20.73	7.523	0.967
KFAC	30.30	1.837	0.005	0.911	18.44	0.464	0.899	10.28	8.121	0.864
MFSAC	22.21	0.512	0.019	0.984	10.59	0.122	0.917	28.30	3.084	0.914
AOPA	20.00	0.075	0.118	0.981	18.08	0.138	0.912	7.596	1.622	0.988

Table E-5 Langmuir, Freundlich and Temkin Isotherm at 50 °C Temperature for adsorption of Manganese, Mn (II) onto KCAC, KFAC, MFSAC and AOPA

Activated sorbent	Linear Regression Analysis of Isotherm									
	Langmuir Isotherm				Freundlich Isotherm			Temkin Isotherm		
	Maximum Monolayer adsorption capacity	Langmuir Constant	Separation Factor	Correlation Coefficient	Affinity Factor	Freundlich Exponent	Correlation Coefficient	Binding Constant	Temkin Constant	Correlation Coefficient
	q_{max}	K_L	R_L	R^2	K_F	1/n	R^2	K_T	B	R^2
	(mg/g)	(l/mg)	-	-	(mg/g(l/mg)$^{1/n}$)	-	-	(l/g)	-	-
KCAC	32.26	0.263	0.037	0.951	8.819	0.426	0.974	0.919	7.088	0.937
KFAC	31.25	0.260	0.037	0.957	8.508	0.426	0.941	2.308	7.071	0.926
MFSAC	27.02	0.077	0.097	0.949	4.145	0.453	0.937	0.635	6.393	0.935
AOPA	18.18	0.047	0.175	0.968	2.472	0.422	0.929	0.472	3.930	0.873

Table E-6 Langmuir, Freundlich and Temkin Isotherm at 70 °C Temperature for adsorption of Manganese, Mn (II) onto KCAC, KFAC, MFSAC and AOPA

Activated sorbent	Linear Regression Analysis of Isotherm									
	Langmuir Isotherm				Freundlich Isotherm			Temkin Isotherm		
	Maximum Monolayer adsorption capacity	Langmuir Constant	Separation Factor	Correlation Coefficient	Affinity Factor	Freundlich Exponent	Correlation Coefficient	Binding Constant	Temkin Constant	Correlation Coefficient
	q_{max}	K_L	R_L	R^2	K_F	1/n	R^2	K_T	B	R^2
	(mg/g)	(l/mg)	-	-	(mg/g(l/mg)$^{1/n}$)	-	-	(l/g)	-	-
KCAC	37.03	0.296	0.033	0.942	9.708	0.503	0.973	2.504	8.596	0.950
KFAC	32.26	0.287	0.034	0.994	8.864	0.450	0.964	2.293	7.661	0.984
MFSAC	28.57	0.096	0.094	0.962	4.898	0.445	0.951	1.675	4.328	0.972
AOPA	17.54	0.039	0.203	0.896	2.083	0.441	0.831	0.274	4.464	0.859

APPENDIX F

Breakthrough Curve modeling for column dynamics studies for mangostene fruit shell based activated carbon (MFSAC)

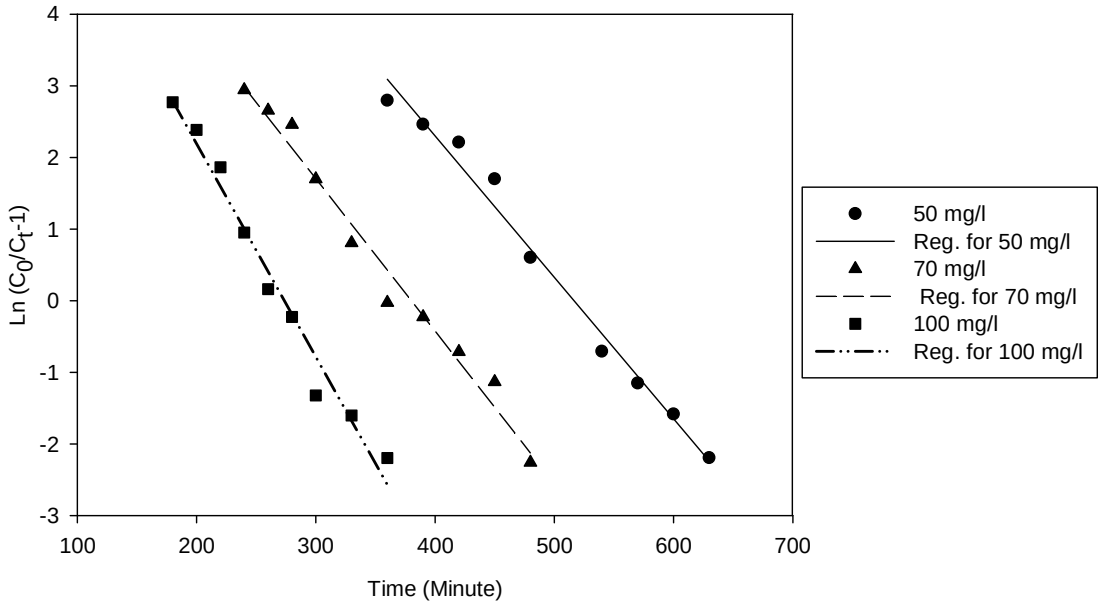

Figure F-1 (a) Linear Regression Analysis for breakthrough curve modeling by Thomas model for Lead, Pb (II) onto MFSAC at different influent/inlet concentration

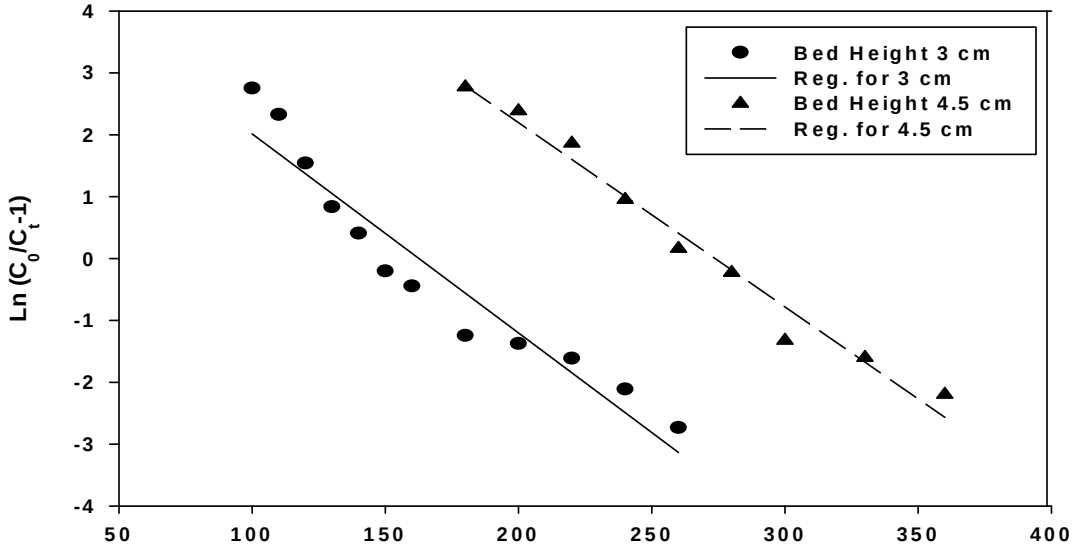

Figure F-1 (b) Linear Regression Analysis for breakthrough curve modeling by Thomas model for Lead, Pb (II) onto MFSAC at different bed height

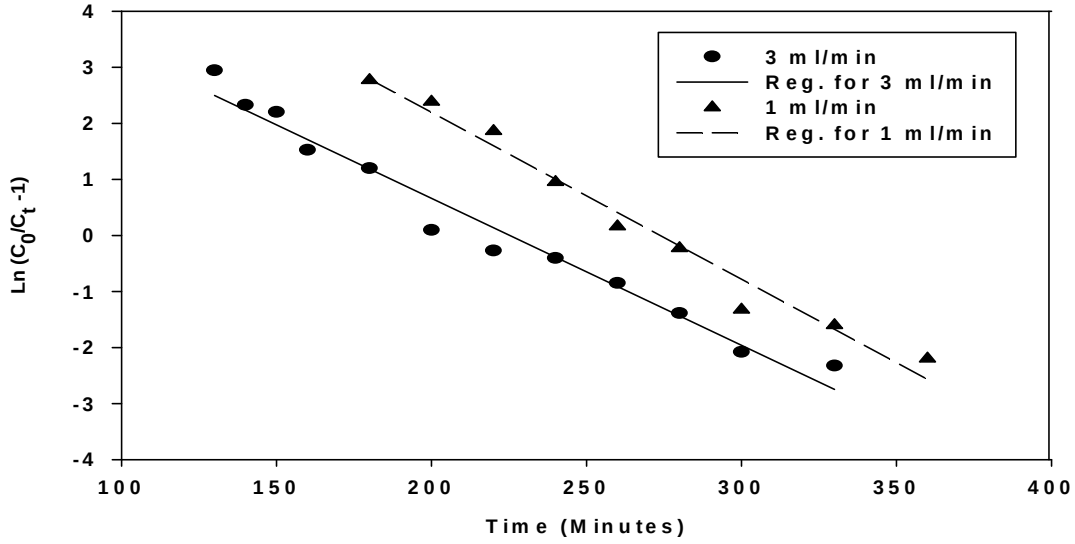

Figure F-1 (c) Linear Regression Analysis for breakthrough curve modeling by Thomas model for Lead, Pb (II) onto MFSAC at different flow rate

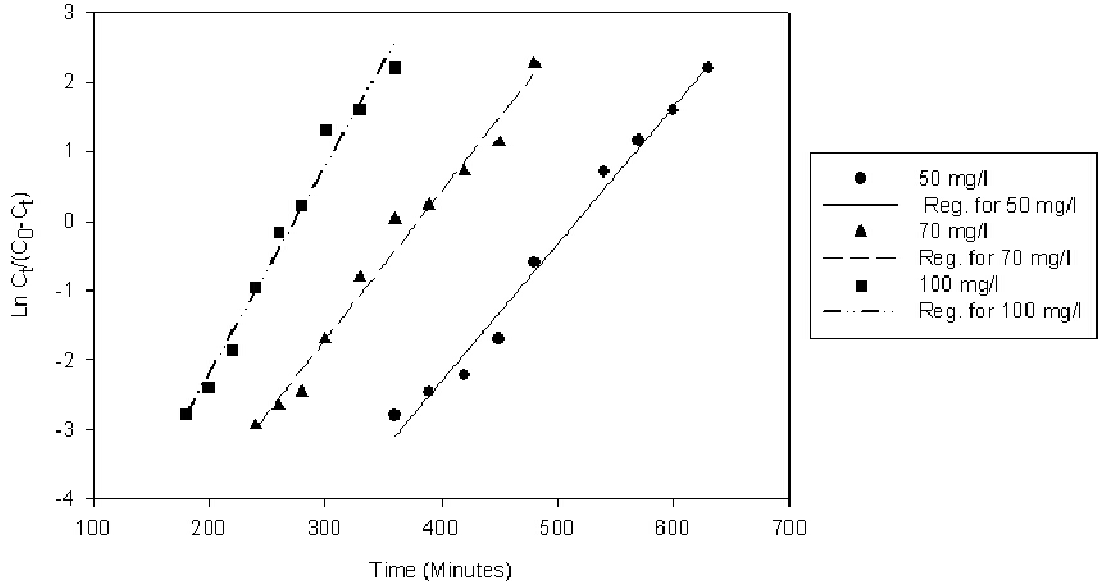

Figure F-2 (a) Linear Regression Analysis for breakthrough curve modeling by Yoon- Nelson model for Lead, Pb (II) onto MFSAC at different influent/inlet concentration

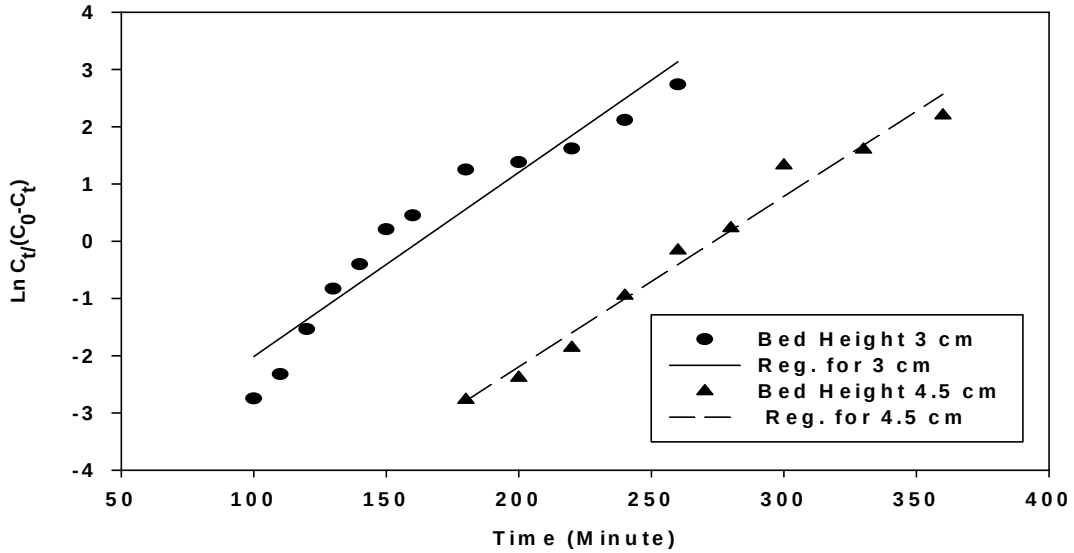

Figure F-2 (b) Linear Regression Analysis for breakthrough curve modeling by Yoon- Nelson model for Lead, Pb (II) onto MFSAC at different bed height

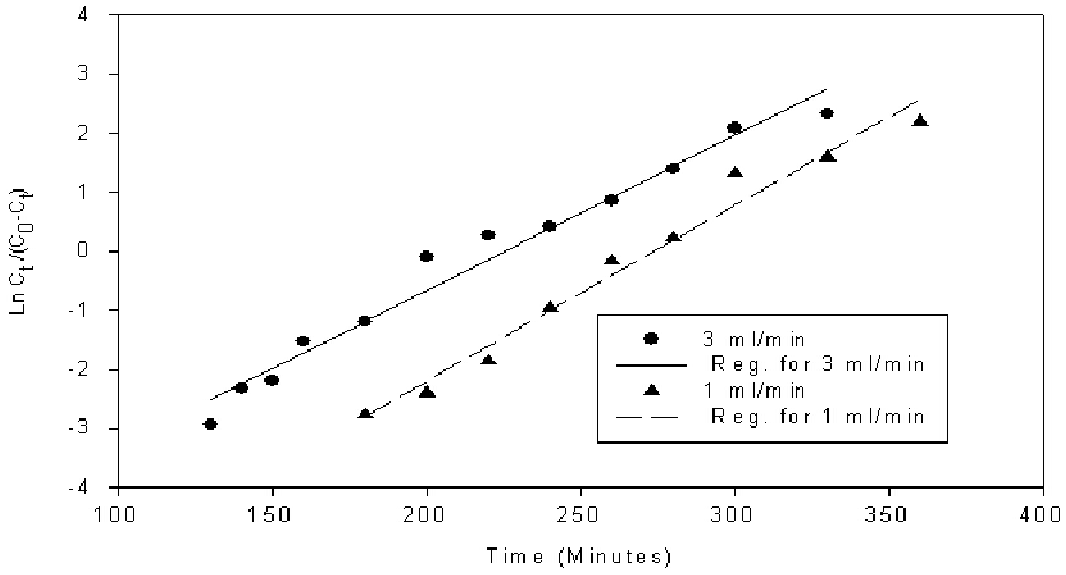

Figure F-2 (c) Linear Regression Analysis for breakthrough curve modeling by Yoon- Nelson model for Lead, Pb (II) onto MFSAC at different flow rate

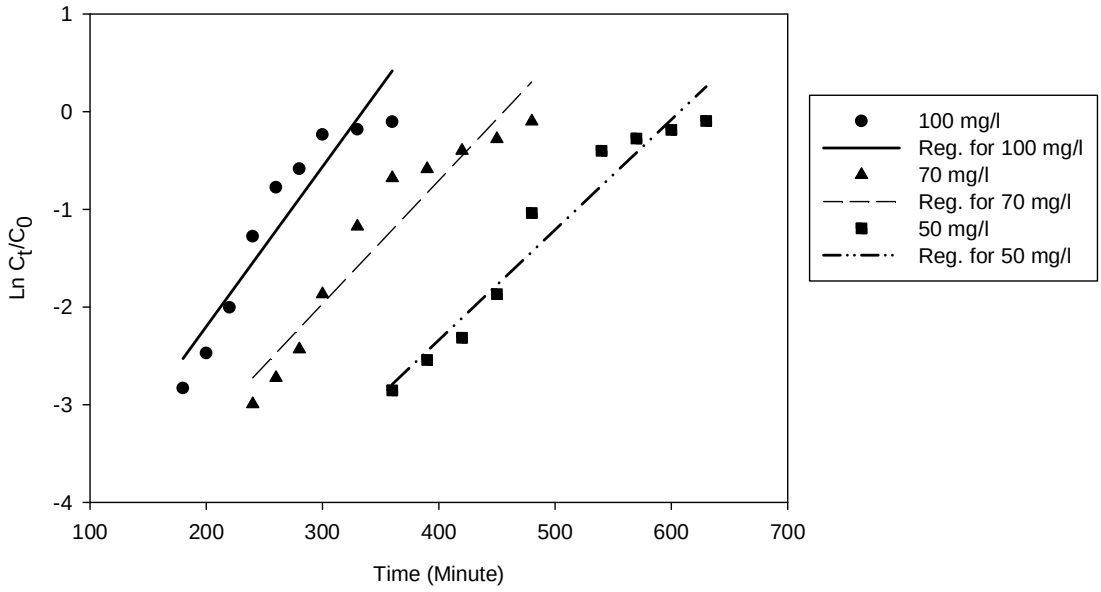

Figure F-3 (a) Linear Regression Analysis for breakthrough curve modeling by Bohart Adams model for Lead, Pb (II) onto MFSAC at different influent/inlet concentration

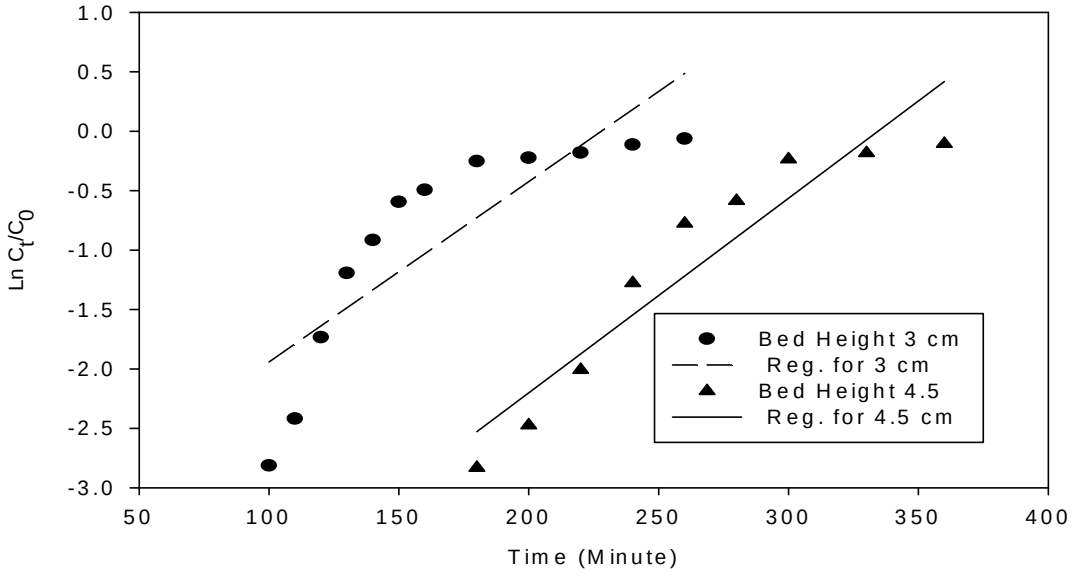

Figure F-3 (b) Linear Regression Analysis for breakthrough curve modeling by Bohart Adams model for Lead, Pb (II) onto MFSAC at different bed height

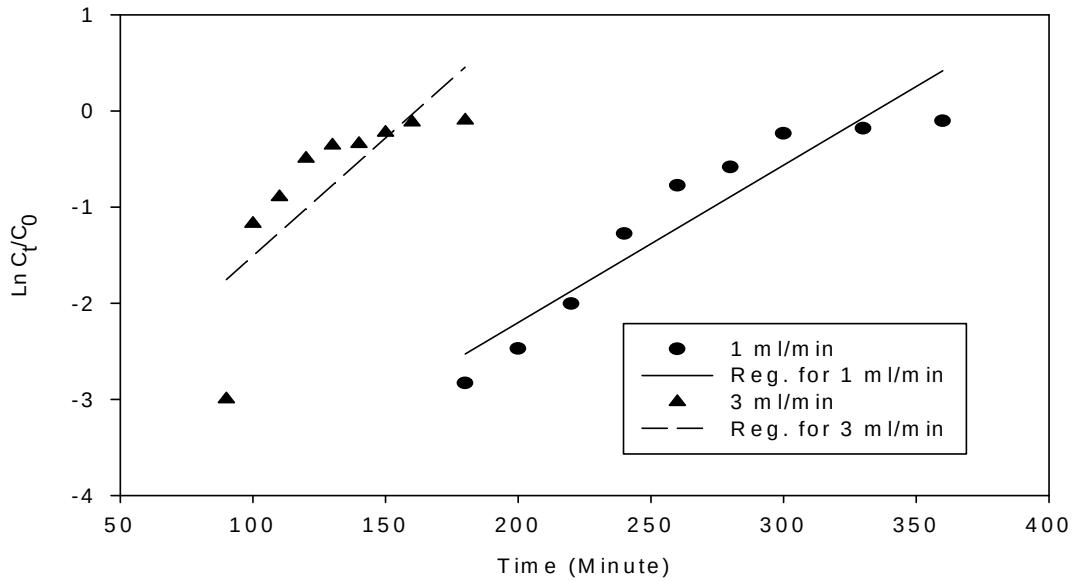

Figure F-3 (c) Linear Regression Analysis for breakthrough curve modeling by Bohart Adams model for Lead, Pb (II) onto MFSAC at different flow rate

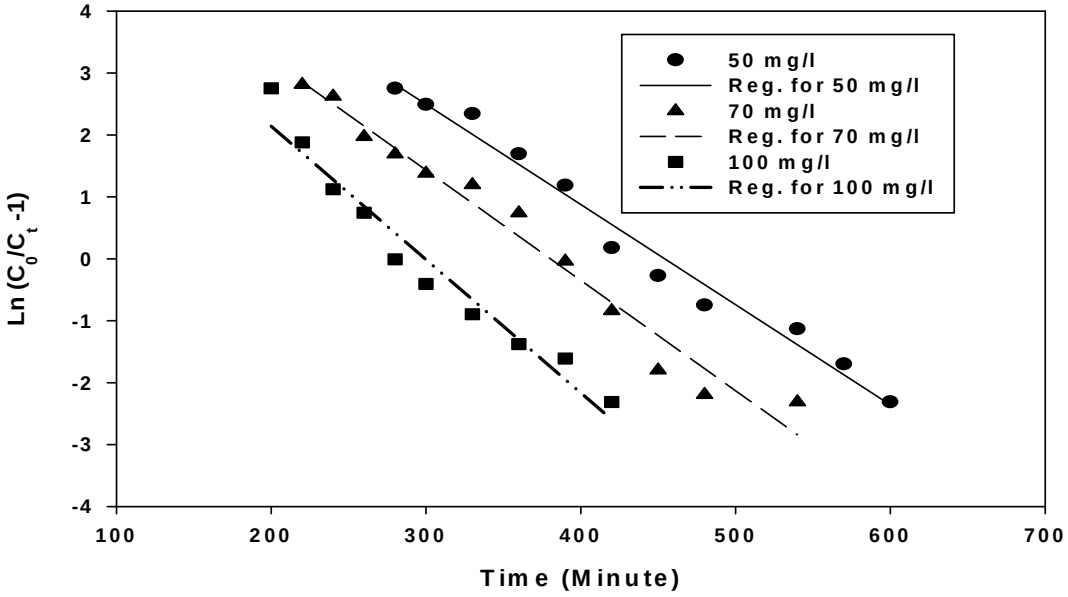

Figure F-4 (a) Linear Regression Analysis for breakthrough curve modeling by Thomas model for Copper, Cu (II) onto MFSAC at different influent/inlet concentration

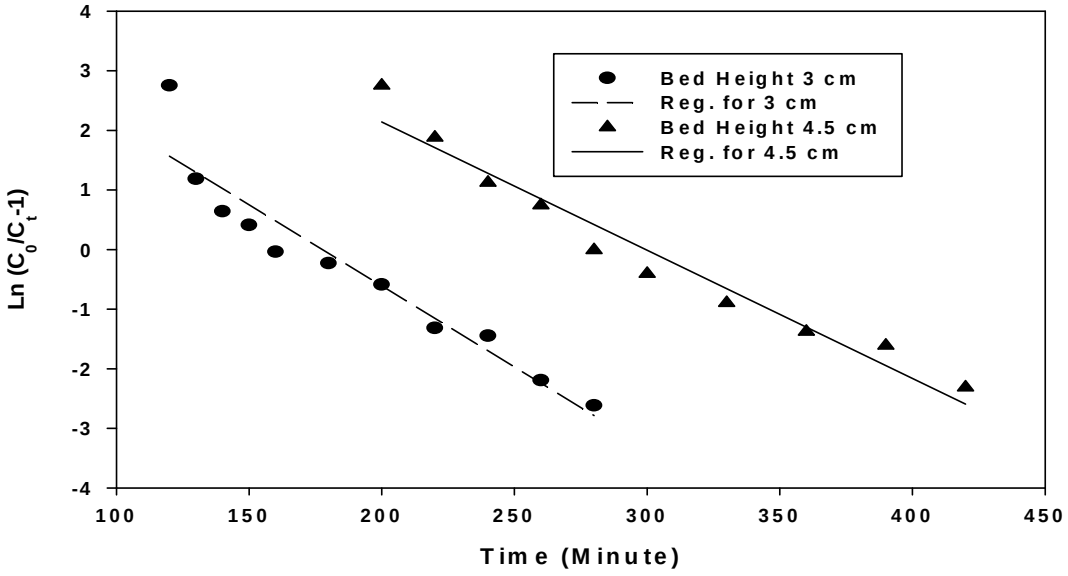

Figure F-4 (b) Linear Regression Analysis for breakthrough curve modeling by Thomas model for Copper, Cu (II) onto MFSAC at different bed height

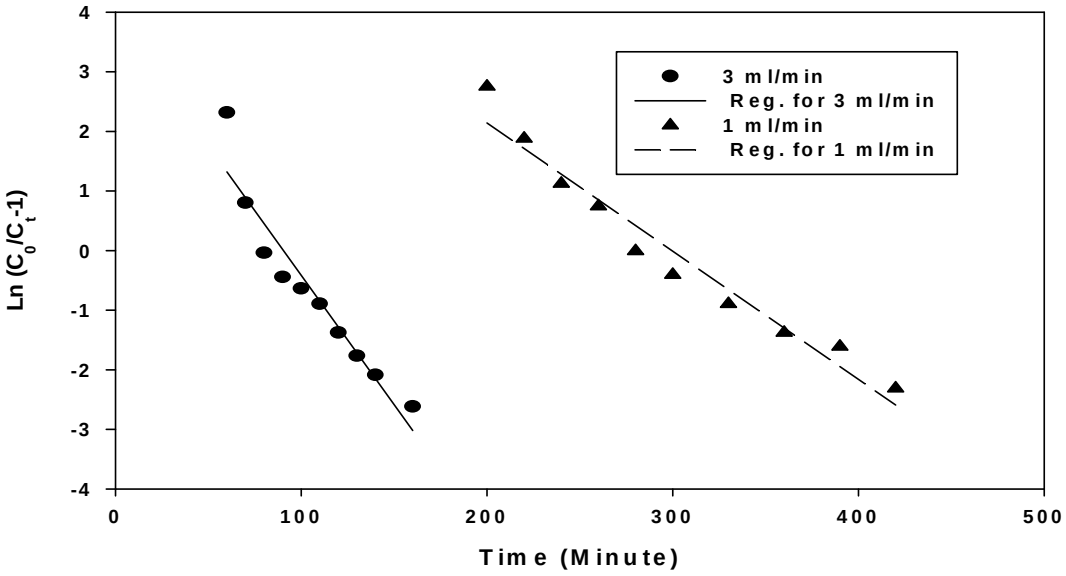

Figure F-4 (c) Linear Regression Analysis for breakthrough curve modeling by Thomas model for Copper, Cu (II) onto MFSAC at different flow rate

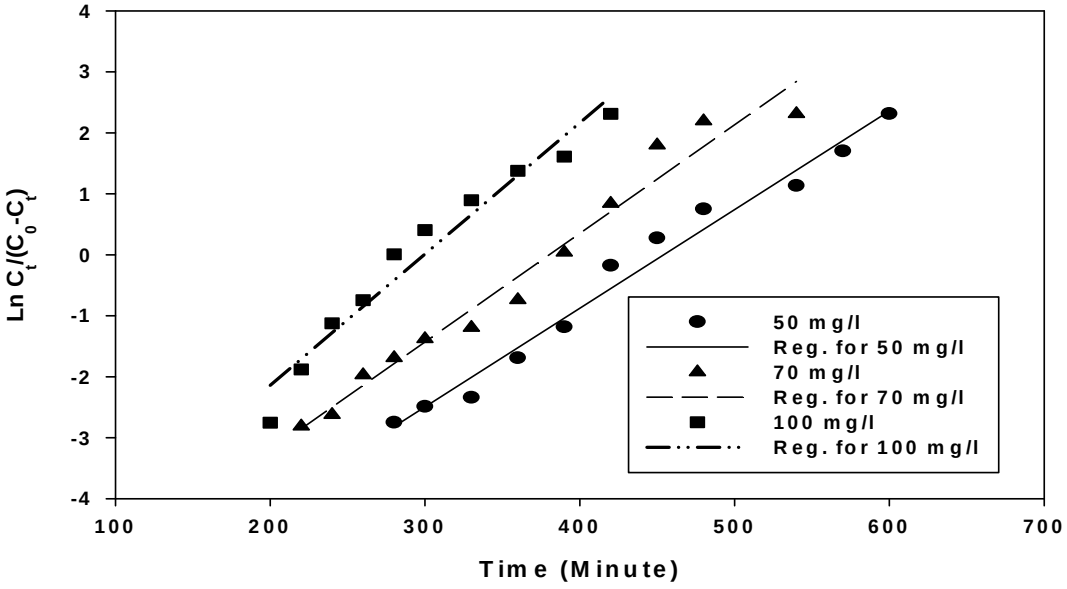

Figure F-5 (a) Linear Regression Analysis for breakthrough curve modeling by Yoon Nelson model for Copper, Cu (II) onto MFSAC at different influent/inlet concentration

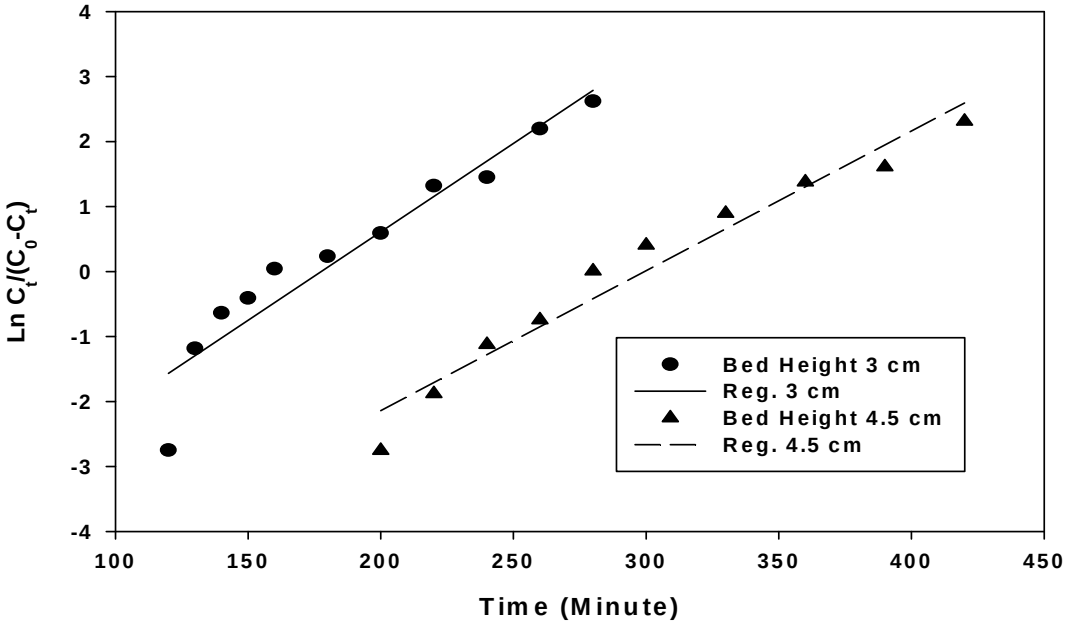

Figure F-5 (b) Linear Regression Analysis for breakthrough curve modeling by Yoon Nelson model for Copper, Cu (II) onto MFSAC at different bed height

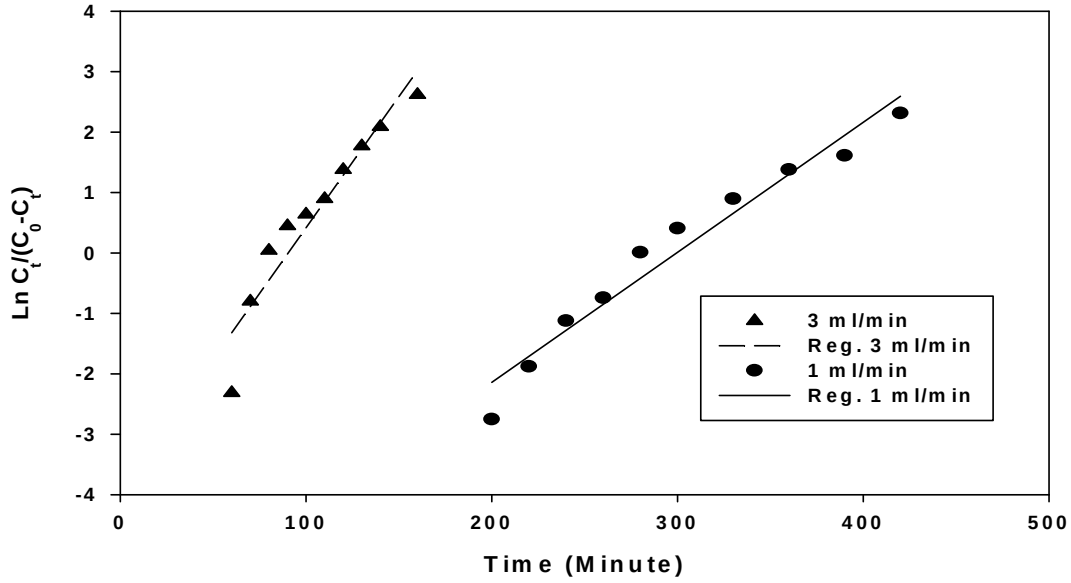

Figure F-5 (c) Linear Regression Analysis for breakthrough curve modeling by Yoon Nelson model for Copper, Cu (II) onto MFSAC at different flow rate

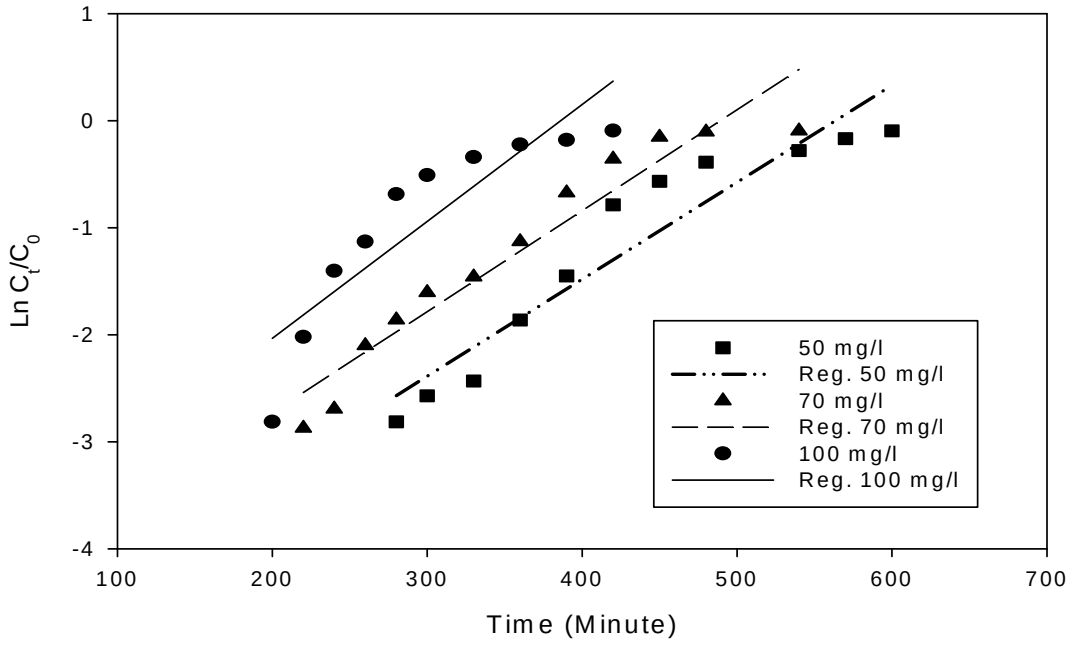

Figure F-6 (a) Linear Regression Analysis for breakthrough curve modeling by Bohart Adams model for Copper, Cu (II) onto MFSAC at different concentration

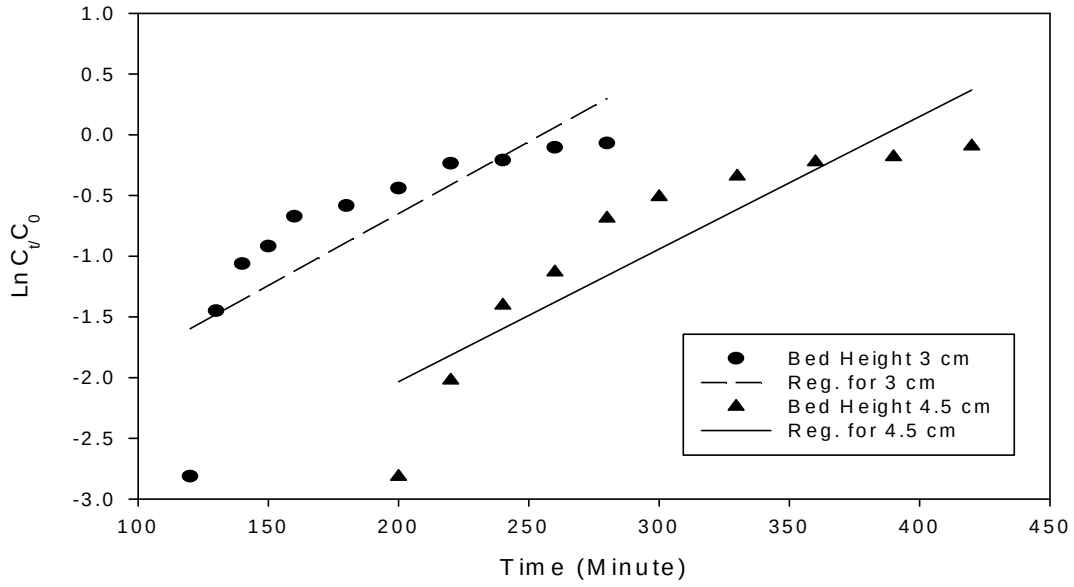

Figure F-6 (b) Linear Regression Analysis for breakthrough curve modeling by Bohart Adams model for Copper, Cu (II) onto MFSAC at different bed height

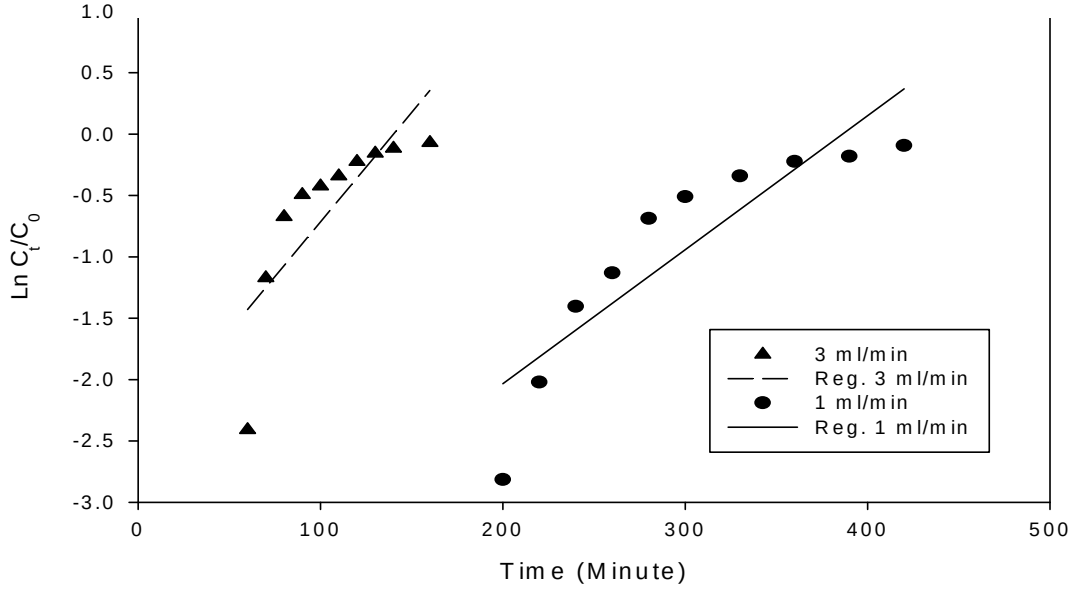

Figure F-6 (c) Linear Regression Analysis for breakthrough curve modeling by Bohart Adams model for Copper, Cu (II) onto MFSAC at different flow rate

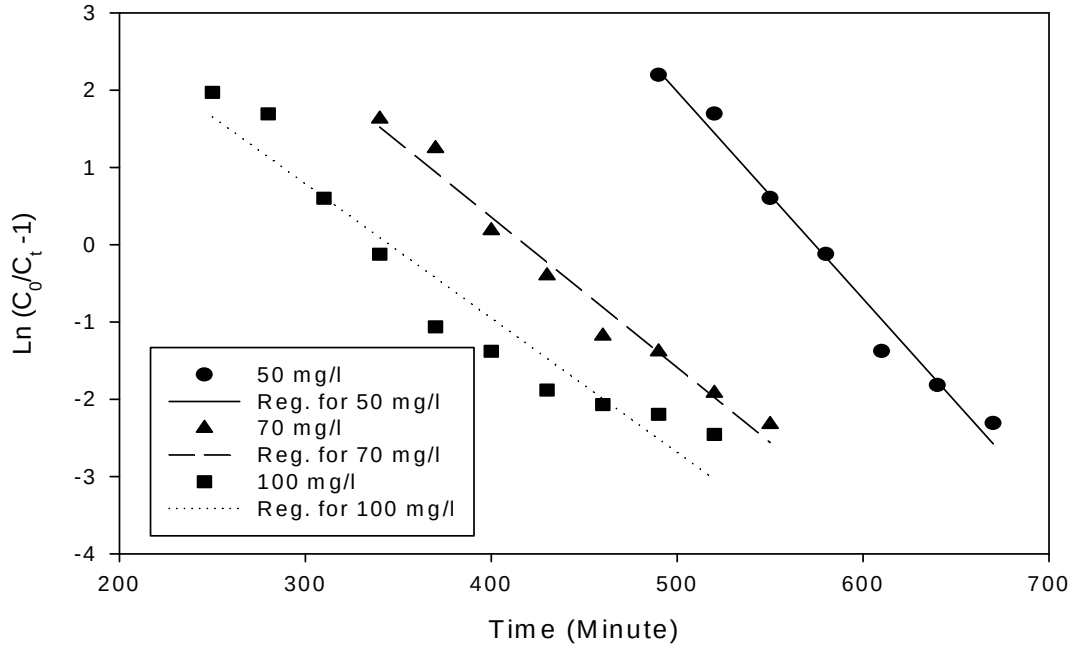

Figure F-7 (a) Linear Regression Analysis for breakthrough curve modeling by Thomas model for Manganese, Mn (II) onto MFSAC at different concentration

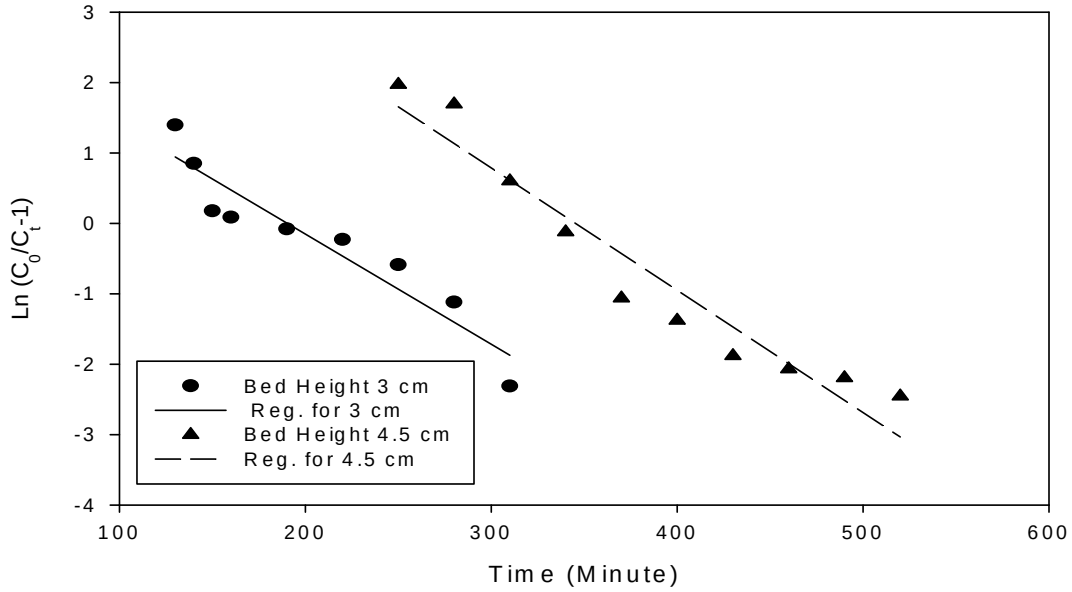

Figure F-7 (b) Linear Regression Analysis for breakthrough curve modeling by Thomas model for Manganese, Mn (II) onto MFSAC at different bed height

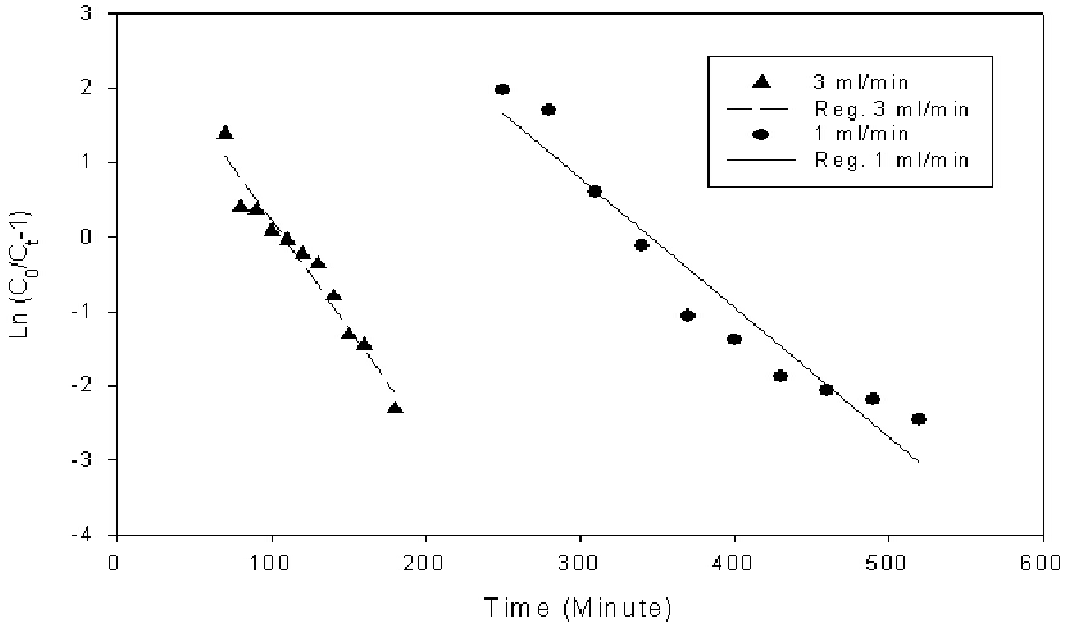

Figure F-7 (c) Linear Regression Analysis for breakthrough curve modeling by Thomas model for Manganese, Mn (II) onto MFSAC at different flow rate

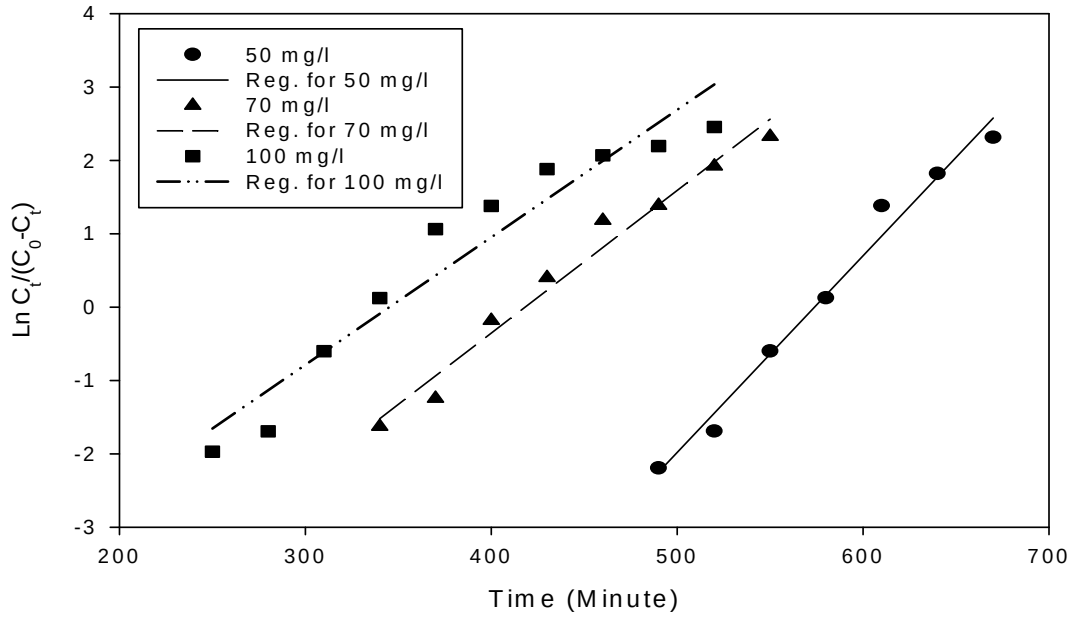

Figure F-8 (a) Linear Regression Analysis for breakthrough curve modeling by Yoon Nelson model for Manganese, Mn (II) onto MFSAC at different concentration

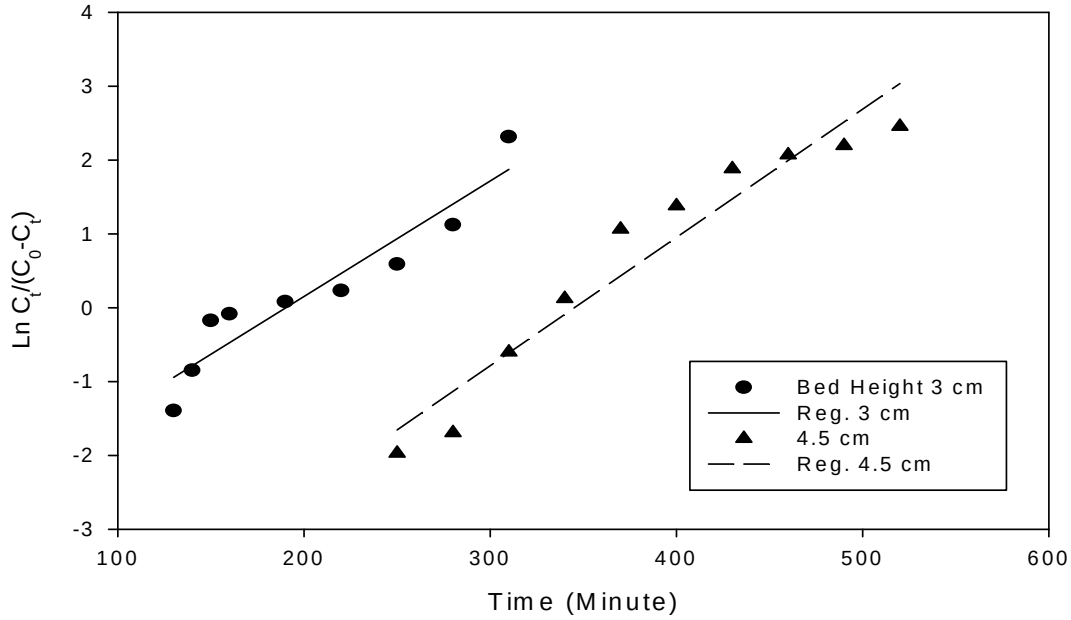

Figure F-8 (b) Linear Regression Analysis for breakthrough curve modeling by Yoon Nelson model for Manganese, Mn (II) onto MFSAC at different bed height

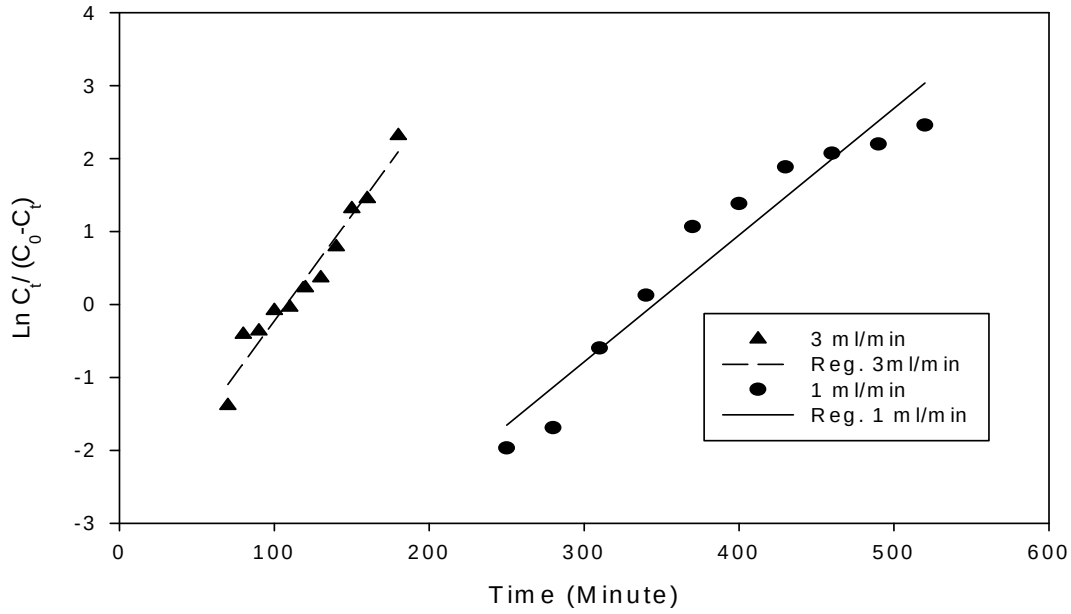

Figure F-8 (c) Linear Regression Analysis for breakthrough curve modeling by Yoon Nelson model for Manganese, Mn (II) onto MFSAC at different flow rate

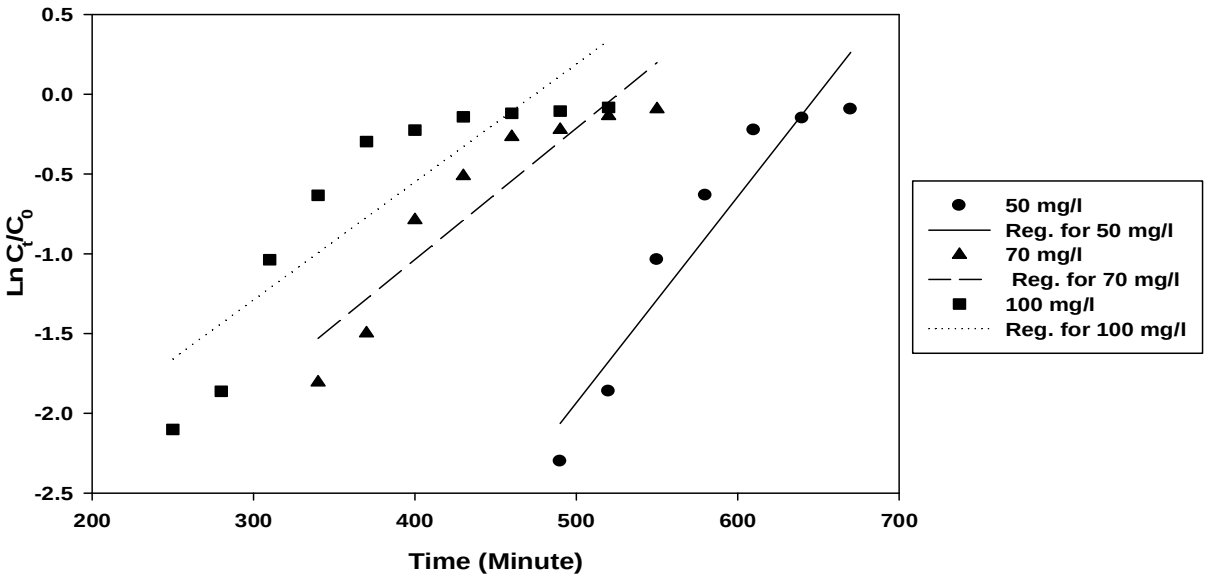

Figure F-9 (a) Linear Regression Analysis for breakthrough curve modeling by Bohart Adams model for Manganese, Mn (II) onto MFSAC at different concentration

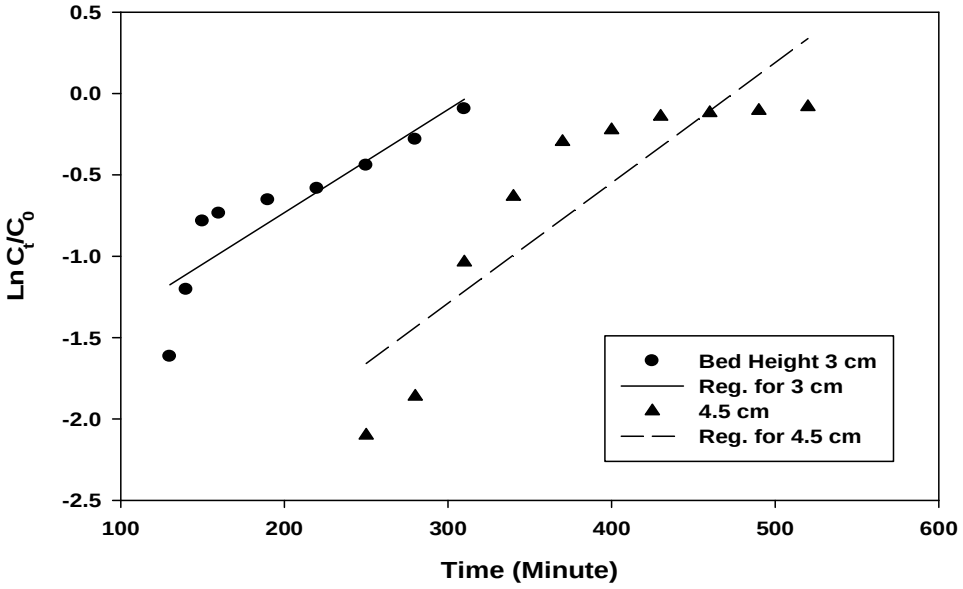

Figure F-9 (b) Linear Regression Analysis for breakthrough curve modeling by Bohart Adams model for Manganese, Mn (II) onto MFSAC at different bed height

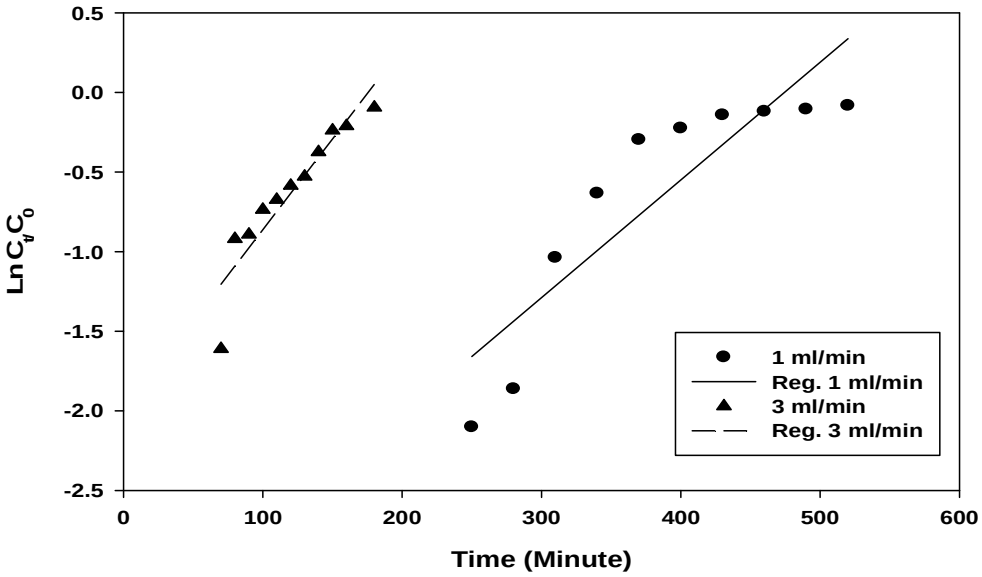

Figure F-9 (c) Linear Regression Analysis for breakthrough curve modeling by Bohart Adams model for Manganese, Mn (II) onto MFSAC at different flow rate

List of Publications

1. Process Variables Optimization for Preparation and Characterization of Novel Adsorbent from Lignocellulosic Waste, *Zaira Zaman Chowdhury*, Sharifuddin Mohd. Zain, Rashid Atta Khan and Khalid Khalisanni,* B*ioresourses*, 2012, 7(3), 3732-3754 ***(PUBLISHED)*** **ISI/Scopus cited publication.**

2. Batch and Fixed bed Adsorption Studies of Lead (II) cations from aqueous solutions onto granular activated carbon derived from *Mangostana garcinia* shell, *Zaira Zaman Chowdhury*, Sharifuddin Mohd. Zain, Rashid Atta Khan and Khalid Khalisanni Bioresourses*, 2012, 7(3), 2895-2915. ***(PUBLISHED)*** **ISI/Scopus cited publication.**

3. Preparation and characterizations of fibrous activated carbon from Kenaf for equilibrium adsorption studies of copper from waste water, *Zaira Zaman Chowdhury*, Sharifuddin Mohd. Zain, Rashid Atta Khan and Md. Sakinul Islam, Korean Journal of Chemical Engineering*,2012, *KiChE,DOI:10.1007/s11814-011-02979.****(PUBLISHED)*** **ISI/SCOPUS cited publication.**

4. Application of Central Composite Design for preparation of kenaf fiber based activated carbon for adsorption of Manganese (II) ion, *Zaira Zaman Chowdhury*, Sharifuddin Mohd. Zain & Rashid Atta Khan, International Journal of Physical Science* (IJPS), 2011 Volume 6(31), pg.7191-7202, ***(PUBLISHED)*** **ISI /SCOPUS cited publication.**

5. Preparation, Characterization and adsorption performance of the KOH-activated carbons derived from kenaf fiber to remove lead (II) from waste water, *Zaira Zaman Chowdhury*, Sharifuddin Mohd. Zain & Rashid Atta Khan, Scientific Research and Essays*, 2011, Volume 6(29), pg. 6185-6196 ***(PUBLISHED)***. **ISI /SCOPUS cited publication.**

6. Application of Response Surface Methodology (RSM) for optimizing production condition for removal of Pb (II) and Cu (II) onto kenaf fiber based activated carbon, *Zaira Zaman Chowdhury*, Sharifuddin Mohd. Zain & Rashid Atta Khan, and Khalid Khalisanni. Research Journal of Applied science, Engineering and Technology (RJASET),* 2012, Volume 4(5), pg. 458-465. ***(PUBLISHED)*** **ISI /SCOPUS cited publication.**

7. Equilibrium Kinetics and Isotherm Studies of Cu (II) Adsorption from Waste Water onto Alkali Activated Oil Palm Ash, *Zaira Zaman Chowdhury*, Sharifuddin Mohd. Zain & Rashid Atta Khan, American Journal of Basic and Applied Science* 2011,Volume 8(3), pg. 230-237 ***(PUBLISHED).*** **ISI/SCOPUS cited publication.**

8. Linear Regression Analysis for Kinetics and Isotherm Studies of Sorption of Manganese (II) Ions Onto Activated Palm ash from Waste Water, *Zaira Zaman Chowdhury*, Sharifuddin Mohd. Zain, Rashid Atta Khan and Khalid Khalisanni*. *Oriental Journal of Chemistry (OJCHEM)*, 2011, Vol. 27, No. (2): Pg. 405-415. ***(PUBLISHED)*** **ISI/SCOPUS cited publication.**

9. Breakthrough Curve Analysis for Column Dynamics Sorption of Mn (II) Ions from Waste Water by using *Mangostana garcinia* peel based Granular Activated Carbon (GAC), *Zaira Zaman Chowdhury*, Sharifuddin Mohd. Zain, Rashid Atta Khan and Khalid Khalisanni Journal of Chemistry*, 2013, *doi:10.1155/2013/959761*. ***(PUBLISHED)*** **ISI/Scopus cited publication.**

10. Equilibrium Isotherm Modeling, Kinetics and Thermodynamics Study for Removal of Lead from Waste Water, Zaira Zaman Chowdhury*, Sharifuddin Mohd. Zain & Rashid Atta Khan, *E Journal of Chemistry*, 2011, Voloume 8(1), (**PUBLISHED). ISI/ SCOPUS cited publication.**

11. Preparation of a novel adsorbent from ash residues: statistical analysis. *Zaira Zaman Chowdhury*, Sharifuddin Mohd. Zain, Rashid Atta Khan and Khalid Khalisanni, Bioresources,* ***(Submitted).*** **ISI/Scopus cited publication.**

12. Batch sorption modeling and error analysis for kinetic evaluation of Mn (II) onto kenaf core. *Zaira Zaman Chowdhury*, Sharifuddin Mohd. Zain, Rashid Atta Khan and Khalid Khalisanni, Brazilian Journal of Chemical Engineering,* ***(Submitted).*** **ISI/Scopus cited publication.**

13. Preparation of activated adsorbent from low cost agricultural residues: A Review. *Zaira Zaman Chowdhury*, Sharifuddin Mohd. Zain, Rashid Atta Khan and Khalid Khalisanni, Korean Journal of Chemical Engineering,* ***(Submitted).*** **ISI/Scopus cited publication.**

List of Conferences

1. Column Mode Adsorption Study of Pb (II) ions onto Granular Activated Carbon prepared from Mangostene fruit shell from Waste Water, *Zaira Zaman Chowdhury, and Sharifuddin Mohd. Zain & Rashid Atta Khan,* The 11th Asian Conference of Analytical Science *(Asianalysis XI),* 23rd -26th August, 2011, China.

2. Preparation, Characterization and Equilibrium Kinetics, Isotherm and Thermodynamics Study for Removal of Lead and Copper from Waste Water by Using Kenaf Core Based Activated Carbon, *Zaira Zaman Chowdhury, Sharifuddin Mohd. Zain & Rashid Atta Khan,* 14th Asian Chemical Congress, 5th -8th September, 2011, Thailand.

3. Removal of Mn (II) from aqueous solution using activated carbon derived from Kenaf Fiber by using Response Surface Methodology (RSM) Methodology, *Zaira Zaman Chowdhury, Sharifuddin Mohd. Zain & Rashid Atta Khan,* The 11th Asian Conference of Analytical Science *(Asianalysis XI),* August 23-26, 2011, China.

4. Preparation, Characterization and Removal of Cu (II) ions from aqueous solution using activated carbon derived from jute stick by using Response Surface Methodology (RSM), *Zaira Zaman Chowdhury, Sharifuddin Mohd Zain, Rashid Atta Khan,* The Seventh Mathematics and Physical Science Graduate Congress, Thailand, 13th- 15th Dec. 2011.

5. Batch adsorption and Thermodynamics study of copper (II) from synthetic waste water: Optimization of Kinetic and two parameter Isotherm models in a single solute system, *Zaira Zaman Chowdhury, Sharifuddin Mohd Zain, Rashid Atta Khan,* International Symposium of Forensic Science & Environmental Health 2009, 10-11th November 2009, Malaysia.

6. Effect of Temperature on adsorption process for treatment of waste water, *Zaira Zaman Chowdhury, Sharifuddin Mohd Zain, Rashid Atta Khan,* International Bangladesh Environmental Network (ICBEN-2010), 2nd Jan-3rd Jan 2010, Bangladesh.

7. Removal of Lead from waste water by activated Palm oil fuel ash, *Zaira Zaman Chowdhury, Sharifuddin Mohd Zain, Rashid Atta Khan,* International Bangladesh Environmental Network (ICBEN-2010), Bangladesh, 2nd Jan-3rd Jan 2010, Bangladesh.

List of Awards

Achieved Best Scientific Journal Article Winning Award from the journal Bioresource, ISI/Scopus cited, Q-1 journal, New California State University, America, ***Title:*** **Process Variables Optimization for Preparation and Characterization of Novel Adsorbent from Lignocellulosic Waste**